

SCHOOL OF CIVIL ENGINEERING



JOINT HIGHWAY  
RESEARCH PROJECT

JHRP-75-2

HIGHWAY BRIDGE VIBRATION STUDIES

Trakool Aramraks

i i  
i i  
i i  
C I L



PURDUE UNIVERSITY  
INDIANA STATE HIGHWAY COMMISSION



## Interim Report

TO: J. F. McLaughlin, Director February 4, 1975  
Joint Highway Research Project Project: C-36-56S

FROM: H. L. Michael, Associate Director File: 7-4-19  
Joint Highway Research Project

Attached is the first Interim Report on the HPR Part II research study titled "Bridge Vibration Studies". It has been authored by Mr. Trakool Aramraks, Graduate Instructor in Research on our staff, under the direction of Professors M. J. Gutzwiler and R. H. Lee. The report is titled "Highway Bridge Vibration Studies".

This Interim Report is of some of the activity which has been in progress on this research in the Joint Highway Research Project at Purdue University. It is an investigation of those parameters which affect bridge accelerations and human response. The findings indicate that the parameters which affect the human pedestrian are predominately span length, weight and speed of the vehicle, and surface roughness.

The Report is presented to the Board for acceptance as partial fulfillment of the objectives of the research. It will also be forwarded to ISHC and FHWA for their review, comment and approval.

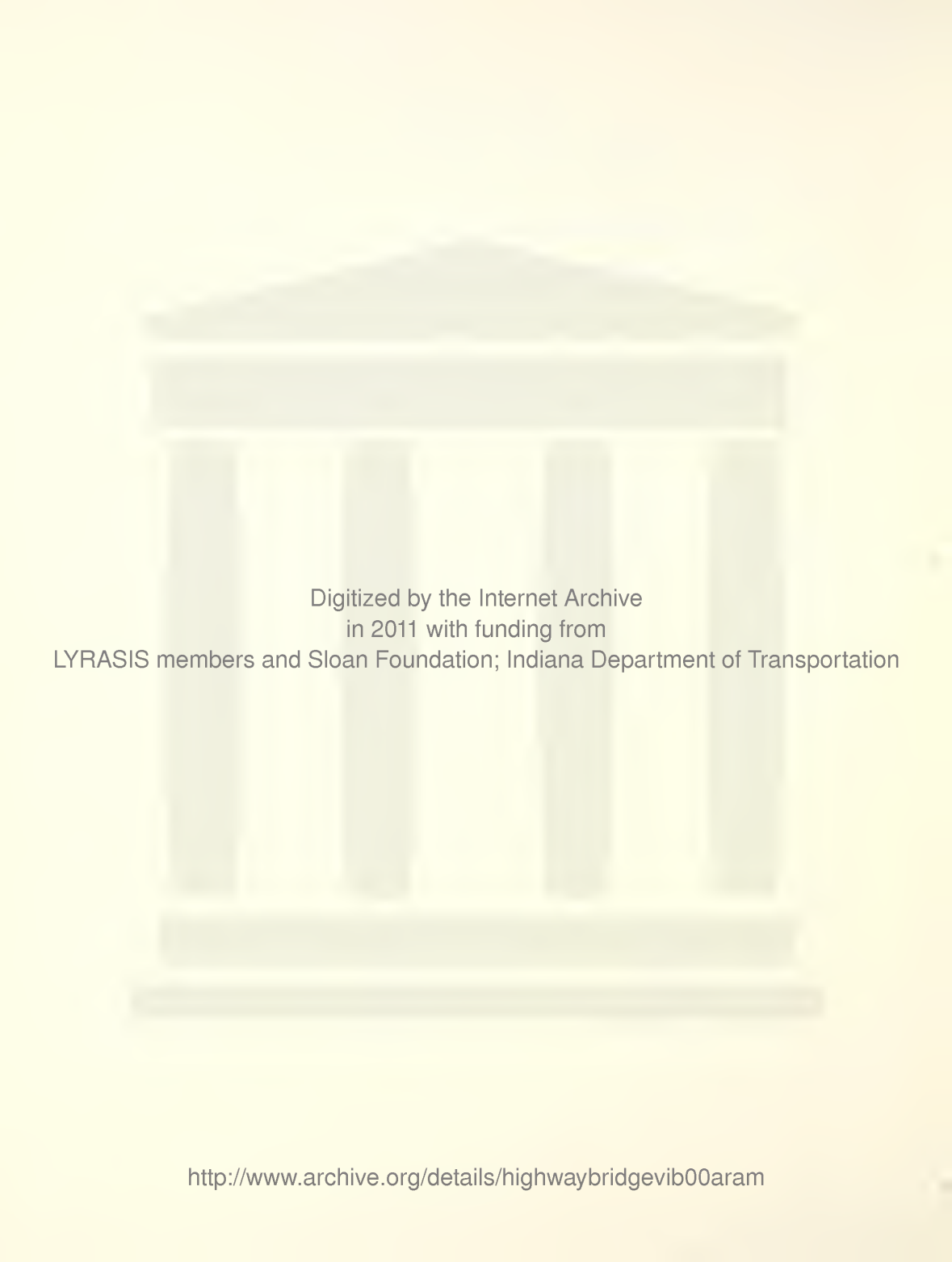
Respectfully submitted,

Panel 2 The last

Harold L. Michael  
Associate Director

HLM:mf

cc:	W. L. Dolch	M. L. Hayes	C. F. Scholer
	R. L. Eskew	C. W. Lovell	M. B. Scott
	G. D. Gibson	G. W. Marks	K. C. Sinha
	W. H. Goetz	R. F. Marsh	H. R. J. Walsh
	M. J. Gutzwiller	R. D. Miles	L. E. Wood
	G. K. Hallock	G. T. Satterly	E. J. Yoder
			S. R. Yoder

A very faint, large watermark-like image of a bridge structure is visible in the background of the page. It appears to be a suspension bridge with multiple towers and cables.

Digitized by the Internet Archive  
in 2011 with funding from

LYRASIS members and Sloan Foundation; Indiana Department of Transportation

## TECHNICAL REPORT STANDARD TITLE PAGE

1. Report No.	2. Government Accession No.	3. Recipient's Catalog No.	
4. Title and Subtitle  Highway Bridge Vibration Studies		5. Report Date  February 1975	
7. Author(s)  Trakool Aramraks		6. Performing Organization Code  C-36-56S	
9. Performing Organization Name and Address  Joint Highway Research Project Purdue University Civil Engineering Building West Lafayette, Indiana 47907		8. Performing Organization Report No.  JHRP-75-2	
12. Sponsoring Agency Name and Address  Indiana State Highway Commission 100 North Senate Avenue Indianapolis, Indiana 46204		10. Work Unit No.  11. Contract or Grant No.  HPR-1(12) Part II	
		13. Type of Report and Period Covered  Interim Report	
15. Supplementary Notes  Conducted in cooperation with the United States Department of Transportation, Federal Highway Administration. Research Study titled "Bridge Vibration Studies"		14. Sponsoring Agency Code  CA 362	
16. Abstract  The research presented herein is concerned with acceleration studies of highway bridges. The effects of the major parameters on the bridge accelerations were investigated and compared to the acceleration criteria for human response. Three different types of highway bridges were investigated: simple span, two span continuous and three span continuous bridges. Major parameters selected included the parameters related to the bridge, to the vehicle and the initial conditions of bridge and vehicle.			
The results of the investigation indicated that, for simple span bridges, the amplitudes of accelerations which psychologically disturbed the pedestrian were predominately affected by the span length of the bridge, the weight and speed of the vehicle, and the surface roughness. The parameters that provided the minor effects were the girder flexibilities and the transverse position of load. For two and three span continuous bridges, the magnitudes of acceleration were larger than the recommended limit of comfort only when the surface roughness of the bridges was taken into account.			
17. Key Words Bridge Vibration; Bridge Design; Bridge Accelerations; Human Response to Bridge Vibration	18. Distribution Statement		
19. Security Classif. (of this report)  Unclassified	20. Security Classif. (of this page)  Unclassified	21. No. of Pages 251	22. Price

## Highlight Summary

### HIGHWAY BRIDGE VIBRATION STUDIES

The research presented herein is concerned with acceleration studies of highway bridges. The effects of the major parameters on the bridge accelerations were investigated and compared to the acceleration criteria for human response. Three different types of highway bridges were investigated: simple span, two span continuous and three span continuous bridges. Major parameters selected included the parameters related to the bridge, to the vehicle and the initial conditions of bridge and vehicle. The numerical data presented were derived from theory in which the bridge was idealized as a plate continuous over flexible beams for simple span bridges and as a continuous beam with concentrated point masses for multi-span bridges. The vehicle was represented as a sprung single load consisting of two wheels for the simple span bridge model and as a sprung load unit having one, two or three axles with a suspension system for multi-span bridges.

The results of the investigation indicated that, for simple span bridges, the amplitudes of accelerations which psychologically disturbed the pedestrian were predominately affected by the span length of the bridge, the weight and speed of the vehicle, and the surface roughness. The parameters that provided the minor effects were the girder flexibilities and the transverse position of load. For two and three span continuous bridges, the magnitudes of acceleration were larger than the recommended limit of comfort only when the surface roughness of the bridges was taken into account.

Deflection limitations and maximum girder span-depth ratios used in present bridge design codes do not assure the bridge users' comfort. Present bridge design criteria have limited the use of high strength steel although the dynamic characteristics of the bridge may be satisfactory. Some reports indicate that bridge acceleration was significant in producing psychological effects. The results of this study indicate high strength steel girders could be used for highway bridges since the effect on bridge accelerations of flexibility of the steel was relatively insignificant.

Interim Report  
HIGHWAY BRIDGE VIBRATION STUDIES

by

Trakool Aramraks  
Graduate Instructor in Research

Joint Highway Research Project

Project No.: C-36-56S

File: 7-4-19

Prepared as Part of an Investigation

Conducted by

Joint Highway Research Project  
Engineering Experiment Station  
Purdue University

in cooperation with the

Indiana State Highway Commission

and the

U.S. Department of Transportation  
Federal Highway Administration

The contents of this report reflect the views of the author who is responsible for the facts and the accuracy of the data presented herein. The contents do not necessarily reflect the official views or policies of the Federal Highway Administration. This report does not constitute a standard, specification, or regulation.

Purdue University  
West Lafayette, Indiana  
February 4, 1975

#### ACKNOWLEDGMENTS

The author wishes to express his deep sense of gratitude to Professors Martin J. Gutzwiller and Robert H. Lee, major professors, for their patient guidance and advice during the entire course of the research. To Professor John T. Gaunt for his generous assistance and helpful suggestions, the author is very grateful. Special thanks are also given to Professor Robert E. Lynch for serving on the author's advisory committees.

The financial assistance granted by the Joint Highway Research Project is gratefully acknowledged.

## TABLE OF CONTENTS

	Page
<b>LIST OF TABLES . . . . .</b>	<b>vii</b>
<b>LIST OF FIGURES . . . . .</b>	<b>xi</b>
<b>LIST OF SYMBOLS . . . . .</b>	<b>xvi</b>
<b>CHAPTER I - INTRODUCTION . . . . .</b>	<b>1</b>
<b>CHAPTER II - METHODS OF ANALYSIS AND COMPUTER PROGRAMS . . . . .</b>	<b>7</b>
2.1 General . . . . .	7
2.2 Analysis of Static and Dynamic Response of Simple-Span, Multigirder Highway Bridges . . . . .	8
2.2.1 General . . . . .	8
2.2.2 Analysis of Static Problem . . . . .	9
2.2.3 Analysis of Dynamic Problem . . . . .	16
2.2.4 Computer Program . . . . .	32
2.3 Analysis of Static and Dynamic Response of Continuous Highway Bridges . . . . .	40
2.3.1 General . . . . .	40
2.3.2 Analysis of Three Span Continuous Highway Bridges . . . . .	41
2.3.3 Analysis of Two-Span Continuous Highway Bridges . . . . .	68
2.3.4 Computer Programs . . . . .	68
<b>CHAPTER III - ACCELERATION STUDIES OF SIMPLE SPAN HIGHWAY BRIDGES . . . . .</b>	<b>79</b>
3.1 General . . . . .	79
3.2 Solution Parameters . . . . .	80
3.3 Bridge Parameters . . . . .	84
3.3.1 Effect of Span Length . . . . .	84
3.3.2 Effect of Width . . . . .	95
3.3.3 Effect of Flexibility of Girder . . . . .	98
3.4 Vehicle Parameters . . . . .	103
3.4.1 Effect of Transverse Position of Wheels . . . . .	103
3.4.2 Effect of Number of Wheels . . . . .	108

## TABLE OF CONTENTS, cont.

	Page
3.4.3 Effect of Transverse Position of Single Load and Flexibility of Girder . . . . .	111
3.4.4 Effect of Speed . . . . .	116
3.5 Surface Roughness Parameter . . . . .	124
 CHAPTER IV - ACCELERATION STUDIES OF THREE SPAN CONTINUOUS HIGHWAY BRIDGES . . . . .	137
4.1 General . . . . .	137
4.2 Solution Parameters . . . . .	140
4.3 Bridge Parameters . . . . .	144
4.3.1 Accelerations of B.P.R. Bridges . . . . .	144
4.3.2 Effect of Span Ratio . . . . .	151
4.3.3 Effect of Girder Flexibility . . . . .	153
4.4 Vehicle Parameters . . . . .	157
4.4.1 Effect of Vehicle Loads . . . . .	157
4.4.2 Effect of Number of Axles and Axle Spacing . . . . .	162
4.4.3 Effect of Vehicle Speed . . . . .	165
4.4.4 Effect of Frequency Ratio . . . . .	170
4.5 Initial Conditions of Vehicle and Bridge . . . . .	173
4.5.1 Effect of Initially Oscillating Vehicle . . . . .	173
4.5.1.1 Effect of Amplitude of Initial Oscillation . . . . .	174
4.5.1.2 Effect of Initial Phase Angle Difference . . . . .	175
4.5.1.3 Effect of Coefficient of Interleaf Friction . . . . .	182
4.5.2 Effect of Bridge Surface Roughness . . . . .	186
 CHAPTER V - ACCELERATION STUDIES OF TWO SPAN CONTINUOUS HIGHWAY BRIDGES . . . . .	199
5.1 General . . . . .	199
5.2 Solution Parameters . . . . .	200
5.3 Bridge Parameters . . . . .	202
5.3.1 Effect of Span Length . . . . .	202
5.3.2 Effect of Girder Flexibility . . . . .	207
5.4 Vehicle Parameters . . . . .	210
5.4.1 Effect of Number of Axles and Axle Spacing . . . . .	210
5.4.2 Effect of Vehicle Speed . . . . .	216
5.4.3 Effect of Frequency Ratio . . . . .	219

## TABLE OF CONTENT, cont.

	Page
5.5 Initial Conditions of Vehicle and Bridge . . . . .	219
5.5.1 Effect of Initially Oscillating Vehicle . . . . .	219
5.5.2 Effect of Surface Roughness of Bridge: . . . . .	225
CHAPTER VI - SUMMARY AND CONCLUSIONS . . . . .	238
6.1 Summary . . . . .	238
6.2 Conclusions . . . . .	243
BIBLIOGRAPHY . . . . .	248

## LIST OF TABLES

Table		Page
1.1	Acceleration Criteria for Human Response to Harmonic Vertical Vibration . . . . .	5
3.1	Comparison of Accelerations Obtained by Using Different Numbers of Integration Step . . . . .	81
3.2	Comparison of Accelerations Obtained by Using Different Numbers of $n_1$ with Wheels Over Center Beam . . . . .	83
3.3	Comparison of Accelerations Obtained by Using Different Numbers of $n_1$ with Wheels Over Edge Beam . . . . .	85
3.4	Natural Frequencies of Simple Span B.P.R. Bridges . . . . .	88
3.5	Maximum Accelerations of Simple Span B.P.R. Bridges . . . . .	90
3.6	Maximum Accelerations at Midspan of Simple Span Bridges with Different Widths . . . . .	99
3.7	Maximum Accelerations at Midspan of Simple Span Bridges Due to Different Girder Flexibilities . . . . .	104
3.8	Maximum Accelerations at Midspan of Simple Span Bridges Due to Transverse Positions of Wheels . . . . .	105
3.9	Comparison of Accelerations at Midspan of Simple Span Bridges Obtained by Using Different Number of Wheels of Vehicle . . . . .	109
3.10	Maximum Accelerations at Midspan of Simple Span Bridges Due to Transverse Positions of Single Load and Girder Flexibilities . . . . .	112
3.11	Maximum Accelerations at Midspan of Simple Span Bridges Due to Different Vehicle Speeds . . . . .	125

## LIST OF TABLES, cont.

Table		Page
3.12	Maximum Accelerations at Midspan of Simple Span Bridge Due to Different Numbers of Half Sine Waves . . . . .	128
3.13	Maximum Accelerations at Midspan of Simple Span Bridge Due to Different Amplitudes of Roughness . . . . .	135
4.1	Data for "Typical Vehicles" . . . . .	139
4.2	Comparison of Accelerations at Mid-Center Span Obtained by Using Different Numbers of Integration Steps . . . . .	142
4.3	Characteristics of Three Span Continuous B.P.R. Bridges . . . . .	147
4.4	Maximum Accelerations of Three Span Continuous B.P.R. Bridges . . . . .	148
4.5	Maximum Accelerations of Three Span Continuous Bridges Obtained by Using Different Span Ratio Coefficients . . . . .	154
4.6	Maximum Accelerations of Three Span Continuous Bridges Obtained by Using Different Girder Flexibilities . . . . .	158
4.7	Maximum Accelerations of Three Span Continuous Bridges Obtained by Using Different Types of Vehicle . . . . .	160
4.8	Maximum Accelerations of Three Span Continuous Bridges Subjected to Vehicles with Different Numbers of Axles . . . . .	163
4.9	Maximum Accelerations of Three Span Continuous Bridges Subjected to Vehicles With Different Axle Spacings . . . . .	166
4.10	Maximum Accelerations of Three Span Continuous Bridges Obtained by Using Different Vehicle Speeds . . . . .	169
4.11	Maximum Accelerations of Three Span Continuous Bridges Obtained by Using Different Frequency Ratios . . . . .	171

## LIST OF TABLES, cont.

Table		Page
4.12	Maximum Accelerations of Three Span Continuous Bridges Subjected to Vehicles with Different Amplitudes of Initial Oscillation . . . . .	176
4.13	Maximum Accelerations of Three Span Continuous Bridges Subjected to 15% Initially Oscillating Vehicle with Varied Phase Angle Differences . . . . .	179
4.14	Maximum Accelerations of Three Span Continuous Bridges Subjected to 50% Initially Oscillating Vehicle with Varied Phase Angle Differences . . . . .	183
4.15	Maximum Accelerations of Three Span Continuous Bridges Subjected to Initially Oscillating Vehicle with Different Coefficients of Friction of Suspension Spring . . . . .	185
4.16	Maximum Accelerations of Three Span Continuous Bridges Due to Different Numbers of Half Sine Waves . . . . .	189
4.17	Maximum Accelerations of Three Span Continuous Bridges Due to Different Amplitudes of Surface Roughness . . . . .	195
5.1	Accelerations at Mid-Right Span of Two Span Continuous Bridge Obtained by Using Different Numbers of Integration Steps . . . . .	201
5.2	Maximum Accelerations of Two Span Continuous Bridges with Different Span Lengths . . . . .	203
5.3	Maximum Accelerations of Two Span Continuous Bridge Obtained by Using Different Girder Flexibilities . . . . .	208
5.4	Maximum Accelerations of Two Span Continuous Bridges Subjected to Different Numbers of Axles of Vehicle . . . . .	211
5.5	Maximum Accelerations of Two Span Continuous Bridges Subjected to Vehicles with Different Axle Spacings . . . . .	211
5.6	Maximum Accelerations of Two Span Continuous Bridges Due to Different Vehicle Speeds . . . . .	217

## LIST OF TABLES, cont.

Table	Page
5.7 Maximum Accelerations of Two Span Continuous Bridges Obtained by Using Different Frequency Ratios . . . . .	220
5.8 Maximum Accelerations of Two Span Continuous Bridges Subjected to Vehicle with Different Initial Amplitudes of Oscillation . . . . .	223
5.9 Maximum Accelerations of Two Span Continuous Bridges Subjected to 50% Initially Oscillating Vehicle with Varied Phase Angle Differences . . .	226
5.10 Maximum Accelerations of Two Span Continuous Bridges Due to Different Numbers of Half Sine Waves . . . . .	230
5.11 Maximum Accelerations of Two Span Continuous Bridges Due to Different Amplitudes of Surface Roughness . . . . .	234

## LIST OF FIGURES

Figure	Page
2.1 Simple Span Bridge Model . . . . .	10
2.2 Vehicle Model for Simple Span Bridge . . . . .	17
2.3 General Flow Chart for Complete Program . . . . .	34
2.4 Flow Chart for Subroutine (QIMJ) to Compute Quantities $Q_{m,j}$ . . . . .	35
2.5 Flow Chart for Subroutine (DOMOIS) to Compute $D_{i,s}^o$ and $M_{i,s}^o$ . . . . .	36
2.6 Flow Chart for Subroutine (EQMON) to Solve the Governing Differential Equations . . . . .	37
2.7 Flow Chart for Subroutine (RESLT) to Compute the Response . . . . .	37
2.8 Flow Chart of Subroutine (INTEG) for Integration Over At . . . . .	38
2.9 Three Span Continuous Bridge Model . . . . .	43
2.10 Representation of a Tractor-Trailer Type Vehicle . . . . .	43
2.11 Vehicle Models . . . . .	47
2.12 Combination of Bridge and Vehicle Model - Any Type of Bridge . . . . .	49
2.13 Combination of a Three Span Continuous Bridge and Vehicle Models . . . . .	50
2.14 Force Deformation Relationships for Tire Suspension System for Vehicle . . . . .	59
2.15 Two Span Continuous Bridge Model . . . . .	69
2.16 General Flow Chart for Complete Program . . . . .	71
2.17 Flow Chart for Subroutine (SMD) to Compute Static Moment and Deflection at Any Specified Point . .	73

## LIST OF FIGURES, cont.

Figure	Page
2.18 Flow Chart for Subroutine (DINTE) to Integrate Equations of Motion for One Time Interval . . . . .	75
2.19 Flow Chart for Subroutine (DMD) to Calculate Dynamic Moment and Deflection at Any Specified Point . . . . .	76
3.1 Cross Section of B.P.R. Bridges and Position of Wheels . . . . .	87
3.2 Maximum Accelerations at Midspan of B.P.R. Bridges . . . . .	91
3.3 Distributions of Maximum Acceleration to Each Beam of 28 ft Roadway B.P.R. Bridges with Different Span Lengths . . . . .	93
3.4 Comparison of History Curves for Accelerations of Beam . . . . .	96
3.5 Effect of Span Length on Acceleration on Edge Beam . . . . .	97
3.6 Cross Section of Bridges Used in Study . . . . .	100
3.7 Effect of Bridge Width on Acceleration of Edge Beam . . . . .	101
3.8 Effect of EI of Beam on Maximum Acceleration . .	106
3.9 Transverse Position of Wheels on Bridge . . . .	107
3.10 Effect of Transverse Position of Wheels on Acceleration . . . . .	110
3.11 Transverse Position of Single Load on Bridge . .	115
3.12 Effect of EI of Beam and Transverse Position of Load . . . . .	117
3.13 Effect of Flexibility of Girder and Transverse Position of Load on Acceleration . . . . .	122
3.14 Effect of Speed of Vehicle on Acceleration of Beam . . . . .	126
3.15 Effect of Roadway Unevenness on Acceleration . .	130

## LIST OF FIGURES, cont.

Figure	Page
3.16 Effect of Roadway Unevenness on Interacting Force . . . . .	131
3.17 Effect of Roadway Unevenness on Acceleration of Beam 5 . . . . .	133
3.18 Effect of Amplitude of Roughness on Acceleration . . . . .	136
4.1 Frequency Coefficients for the First Three Natural Modes of Vibration of a 3-Span Continuous Beam . . . . .	141
4.2 Cross Section Near Mid-Center Span of B.P.R. Bridges . . . . .	145
4.3 Bridge and Vehicle Models for Study of B.P.R. Bridges . . . . .	145
4.4 Effect of Span Length on Acceleration . . . . .	149
4.5 History Curves for Acceleration of 64-80-64 B.P.R. Bridge . . . . .	150
4.6 Bridge and Vehicle Models Used in Study . . . . .	152
4.7 Effect of Span Ratio on Acceleration . . . . .	156
4.8 Effect of EI on Acceleration . . . . .	159
4.9 Vehicle Models Used in Study . . . . .	161
4.10 Effect of Number of Axles on Acceleration . . . . .	164
4.11 Effect of Axle Spacing on Acceleration . . . . .	167
4.12 Effect of Speed on Acceleration . . . . .	168
4.13 Effect of Frequency Ratio on Acceleration . . . . .	172
4.14 Effect of Initially Oscillating Vehicle on Acceleration . . . . .	177
4.15 Effect of Initial Phase Angle Difference on Acceleration . . . . .	180
4.16 Model of Three Span Bridges with Rough Surface .	187

## LIST OF FIGURES, cont.

Figure		Page
4.17	Effect of Surface Roughness on Acceleration . . .	191
4.18-1	History Curves for Interacting Force Due to Surface Roughness . . . . .	192
4.18-2	History Curves for Acceleration as Affected by Surface Roughness . . . . .	193
4.19	Effect of Amplitude of Roughness on Acceleration . . . . .	197
5.1	Two Span Bridge and Vehicle Models . . . . .	204
5.2	Effect of Span Length on Acceleration . . . . .	206
5.3	History Curves for Acceleration of 60-60 Span Bridge . . . . .	209
5.4	Effect of EI on Acceleration . . . . .	212
5.5	Vehicle Models with Different Numbers of Axles .	213
5.6	Effect of Number of Axles on Acceleration . . .	214
5.7	Effect of Axle Spacing on Acceleration . . . . .	215
5.8	Effect of Speed of Vehicle on Acceleration . . .	218
5.9	Effect of Frequency Ratio on Acceleration . . .	221
5.10	Effect of Initially Oscillating Vehicle on Acceleration . . . . .	224
5.11	Effect of Initial Phase Angle Difference on Acceleration . . . . .	227
5.12	Two Span Bridges with Rough Surface . . . . .	228
5.13	Effect of Surface Roughness on Acceleration . .	231
5.14-1	History Curves for Acceleration as Affected by Surface Roughness . . . . .	232
5.14-2	History Curves for Interacting Force Due to Surface Roughness . . . . .	233
5.15	Effect of Amplitude of Roughness on Acceleration . . . . .	236

## LIST OF FIGURES, cont.

Figure	Page
6.1 Acceleration of Simple Span Bridge with Level Surface . . . . .	246
6.2 Acceleration of Simple Span Bridge with Rough Surface . . . . .	247

## LIST OF SYMBOLS

a	ratio of the side span to the center span
$a_1$	ratio of the horizontal distance between the center of gravity of the tractor and its rear axle to the axle spacing of the tractor
$a_2$	$1 - a_1$
$a_3$	ratio of the horizontal distance between the center of gravity of the trailer and its rear axle to the horizontal distance between that axle and the "fifth wheel pivot"
$a_4$	$1 - a_3$
$a_5$	ratio of the "fifth wheel" offset to the axle spacing of the tractor
b	overall width of slab
$b_1$	one-half the distance between the wheels of the vehicle model
C	$b/a$ , ratio of sides of bridge
$C_d, C_m$	influence coefficients for deflection and moment
$C'_d, C'_m$	dimensionless coefficients for deflection and moment produced by truck loading
$C_{d,j}, C_{m,j}$	dimensionless coefficients for static values of deflection and moment produced by the interacting force at the $j^{\text{th}}$ wheel
$C_i$	dimensionless amplitude of initial interacting force at the approach
c	coefficient of viscous damping for beam
$c_r$	critical value of c corresponding to the fundamental mode of vibration
D	flexural rigidity of slab

$D_{i,j}$	deflection produced in the $i^{\text{th}}$ beam by the static value of the interacting force at the $j^{\text{th}}$ wheel
$D_{i,s}^o$	deflection produced in the $i^{\text{th}}$ beam by the $s^{\text{th}}$ component of the inertia forces
$D_1$	deflection at a prescribed point on the left hand span of the beam
$D_4$	deflection at a prescribed point on the right hand span of the beam
$D_c$	deflection of the center of the center span
$d_{Pi}$	deviation of bridge profile at the point of application of $P_i$ , measured from a horizontal line passing through the left hand abutment
$E$	modulus of elasticity of the bridge material
$e_j$	dimensionless amplitude of roadway unevenness
$(E_b I_b)_i$	flexural rigidity of the $i^{\text{th}}$ beam
$F_i$	frictional force in the suspension spring for the $i^{\text{th}}$ axle
$F'_i$	maximum value of $F_i$
$f_b$	fundamental natural frequency of the bridge
$f_n$	generalized coordinates for the bridge
$f_{t,i}$	pseudo-frequency of the $i^{\text{th}}$ axle if only the tire spring acts
$f_{ts,i}$	pseudo-frequency of the $i^{\text{th}}$ axle if both the tire and the suspension springs act in series
$f_v$	frequency of the vehicle for verticle motion
$g$	gravitational acceleration
$(G_b J_b)_i$	torsional rigidity of the $i^{\text{th}}$ beam
$h$	length of a panel in the center span
$h_r$	length of the $r^{\text{th}}$ panel
$I$	moment of inertia of the bridge cross section
$i_1, i_2$	dynamic indexes of the tractor and trailer, respectively

$J$	polar moment of inertia of the sprung mass about an axis through its center of gravity and normal to the transverse vertical plane
$J_r^j$	moment-deflection coefficient
$k$	spring constant for one spring
$k_i$	spring constant for the $i^{\text{th}}$ axle
$k'_r$	modified carry-over factor
$k_{t,i}$	effective stiffness of tires for the $i^{\text{th}}$ axle
$k_{ts,i}$	effective stiffness for the $i^{\text{th}}$ axle when the suspension spring and tire spring act in series
$L$	length of the overall span for simple span bridge, of the center span for three span bridge and of either span for two span bridge
$L_b$	total length of bridge
$l_1, l_2$	axle spacings
$M_1, M_4$	moments at the sections where $D_1$ and $D_4$ are evaluated
$M_2, M_3$	moments over the first and second interior support, respectively
$M_c$	moment at the center of the center span
$M_{i,j}$	moment corresponding to $D_{i,j}$
$M_{i,s}^o$	moment corresponding to $D_{i,s}^o$
$m$	number of panels in the center span
$m_r$	mass concentration at the $r^{\text{th}}$ node
$m_o$	number of terms used in the longitudinal direction in the computation of the static effects
$m_1$	a positive integer
$N$	total number of integration steps for time required for the vehicle to cross the length of the bridge
$n$	number of panels in either side span of three span bridge or number of panels in either span of two span bridge

$n_o, n_1, n_2$	numbers of $Y_n$ functions used for various purposes
$P_i$	interacting force between the $i^{\text{th}}$ axle and the bridge or approach
$P_{i,s}$	value of $P_i$ at the end of the $s^{\text{th}}$ time interval
$P_{st,i}$	static reaction for the $i^{\text{th}}$ axle
$p$	number of beam spacings
$\bar{P}_m$	the $m^{\text{th}}$ term in the Fourier series expansion of the load
$P_m$	a function of $\eta$
$Q_r^i$	reaction-load coefficient
$q_n$	generalized coordinate for bridge and vehicle
$R_i$	reaction at the $i^{\text{th}}$ abutment
$R_r^j$	reaction-deflection coefficient
$s_1, s_2$	$l_1/L$ and $l_2/L$ , respectively
$T$	kinetic energy
$T_b$	fundamental natural period of the bridge
$T_v$	natural period of the vehicle for vertical motion
$t$	time, measured from the instant the first axle enters the bridge
$U$	potential energy of the gravity forces
$u$	dynamic rotation of the sprung mass in the transverse vertical plane
$u_i$	shortening of the suspension-tire system of the $i^{\text{th}}$ axle
$V$	strain energy
$v$	speed of the vehicle
$W$	total weight of the vehicle model
$W_b$	weight of the center span of three span bridge or of either span of two span bridge

- $w_1, w_2$  sprung weight of the tractor or trailer, respectively
- $w$  static or dynamic deflection function for simple span bridge
- $w_1, w_2, w_3$  unsprung weights of vehicle
- $x$  distance between the first abutment and the first axle
- $y_n$  dimensionless functions of  $n$
- $y_r$  displacement of  $r^{\text{th}}$  node, measured from the position of static equilibrium of the bridge when the load is off the bridge
- $y_{r,s}$  value of  $y_r$  at  $t_s$
- $y_{p,i}$  deflection of the bridge under the  $i^{\text{th}}$  axle, measured from the static equilibrium position of the bridge under the action of its own weight
- $y_{p_i,s}$  value of  $y_{p_i}$  at  $t_s$
- $z$  dynamic vertical displacement of the center of gravity of the sprung mass, measured from the static position of equilibrium
- $z_i$  generalized coordinate for the  $i^{\text{th}}$  axle
- $z_{i,s}$  value of  $z_i$  at  $t_s$
- $\alpha$   $\frac{vT_b}{2L}$ , dimensionless speed parameter
- $\theta_r$  angle coefficient for the  $r^{\text{th}}$  node
- $\theta_i$  initial phase angle of the  $i^{\text{th}}$  axle
- $\phi$  dimensionless generalized coordinate for the vehicle
- $\delta_n$  dimensionless coefficients
- $\zeta$  dimensionless generalized coordinate for the vehicle
- $\lambda_n$  dimensionless coefficient in the expression for  $w_n$
- $\nu$   $(f_v/f_b)^2$
- $\mu_i$   $F_i'/P_{st,i}$ , coefficient of interleaf friction of  $i^{\text{th}}$  axle
- $\xi$   $x/L_b$ , a measurement of time or of the position of the first axle on the bridge

- $\eta_j$  transverse position of  $j^{\text{th}}$  wheel on the simple span bridge
- $\tau$   $\frac{vt}{L}$ , dimensionless time parameter
- $\psi_n$  dimensionless generalized coordinate for bridge
- $\omega_n$   $n^{\text{th}}$  natural circular frequency of the bridge

CHAPTER I  
INTRODUCTION

The purpose of this investigation is to develop concepts and simple approximate relations that may be used to estimate the magnitude of the dynamic response of highway bridges having significance in producing adverse psychological effects to bridge users. The investigation is aimed at a better understanding of bridge vibrations and ultimately establishing a basis for inclusion in bridge specifications of design criteria which will directly regulate dynamic response characteristics.

Dynamic response is not specifically referenced in present bridge design codes<sup>(1)\*</sup>. Deflection limitations and maximum girder span-depth ratios have been used in the hope that such limitations will lead to structures that have satisfactory vibration characteristics. These code provisions do not attack the problem directly and the results obtained by their observance seem to reflect this fact. It is probable that other phenomena, for example acceleration, are at least as significant as deflection amplitudes in

---

\* Numbers in parentheses, unless otherwise identified, are reference numbers.

producing adverse psychological effects. Complaints of disturbing bridge motions have come from pedestrians and from persons in halted vehicles.

The economical use of modern high-strength steels in bridge construction has been hindered somewhat by present code limitations. In order to obtain stiffnesses which meet AASHO deflection and/or span-depth ratios an increase in the quantity of steel is required. The increment of human comfort thus gained is of questionable significance for bridges not located in urban areas, i.e., for bridges not serving pedestrians or stopped vehicles. Significant savings would result if the design of high strength steel girders could be freed from arbitrary restrictions which do not guarantee relevant improvement in bridge performance.

Although the response of simple span and multi-span continuous highway bridges to the influence of moving vehicles has been studied at some length<sup>(7)-(34)</sup>, there has been comparatively little attention given to the control of dynamic response of bridge structures which will assure human comfort. The design of bridge structures at the present time, which is based on deflection limitations and limiting span-depth ratio, still does not guarantee satisfactory vibration characteristics within acceptable limits, since the proper parameters influencing the vibration have not been recognized appropriately.

The dynamic response of three kinds of highway bridges will be investigated in this study: the simple span, two span continuous and three span continuous highway bridges. It is necessary that the method of analysis which is required to determine the response of these bridges should allow consideration of the major parameters which affect the response. The most successful analytic studies in recent years have been presented by Oran<sup>(28)</sup> for simple span highway bridges and by Veletsos and Huang<sup>(4)(29)</sup> for multi-span continuous highway bridges. Parameters which may be considered in the analysis include bridge damping, roadway unevenness and initial vertical oscillation of the vehicle. The theory was verified by comparisons with the results of laboratory studies on simply supported beams and with results of the AASHO Road Test bridge studies.<sup>(22)</sup> The bridges tested in the AASHO study were simple-span single lane structures conforming rather closely to the assumptions of the theory.

There have been a few reports available<sup>(5)(6)(38)(39)</sup> discussing criteria for human response to vertical vibration. A recent paper by Wright and Walker<sup>(5)</sup> summarizes the effects of bridge flexibility on human response and presents a summary and discussion of the previous studies of the criteria. It is suggested in the paper that acceleration of the bridge is more important than the velocity or jerk in producing psychological effects since the natural

frequencies of highway bridges range between 1 to 10 cps. The report further suggests that the amplitude of the dynamic component of acceleration in the fundamental mode of vibration should be limited to 100 in/sec<sup>2</sup> to assure the human comfort. Acceleration criteria for human response presented by the paper are shown in Table 1.1.

The primary purpose of this investigation is to study the behavior of highway bridges under a moving vehicle, as affected by major parameters and to obtain the maximum accelerations. By comparison with the available acceleration criteria, conclusions about the significance of each parameter can be made and finally, the accelerations of given bridge structures can be predicted analytically. All parameters considered in this study are kept within a realistic range of expected values.

The method of analysis and a description of computer programs to compute the response of simple span and multi-span highway bridges are presented in Chapter II. All computer programs used in this study were originally developed at the University of Illinois and contributed by Prof. W. H. Walker of the Civil Engineering Department of the University of Illinois. His contribution is gratefully acknowledged. The programs are modified to handle dimensional input parameters and to compute the accelerations at any specified point on the bridges. In Chapter III the effects of major parameters on accelerations of multi-girder

Table 1.1 Acceleration Criteria for Human Response to Harmonic Vertical Vibration<sup>(5)</sup>

Human Response	Amplitude of Acceleration (in/sec <sup>2</sup> )	
	Transient	Sustained
Imperceptible	5	0.5
Perceptible to few	10	1
Perceptible to some	20	2
Perceptible	50	5
Unpleasant to few	100	10
Unpleasant to some	200	20
Unpleasant	500	50
Intolerable to few	1000	100
Intolerable to some	2000	200
Intolerable		

simple span bridges are studied. Chapter IV is devoted to a study of the accelerations of three span continuous highway bridges as affected by major parameters and the initial conditions of the vehicle. The effect of the same parameters are studied in Chapter V for two span continuous bridges. A summary of the important findings and conclusions are given in Chapter VI.

## CHAPTER II

### METHODS OF ANALYSIS AND COMPUTER PROGRAMS

#### 2.1 General

The purpose of this chapter is to review the analyses of simple span and of continuous highway bridges under moving vehicles. General theories for both analyses have been summarized and the methods to compute the accelerations at any specified points on the bridges have been added. The methods of analysis for simple span and continuous highway bridges were developed by Oran<sup>(28)</sup> and Huang<sup>(29)</sup>, respectively. The descriptions of computer programs for both analyses are also presented in this chapter. Both original computer programs<sup>(28)(29)</sup> have been modified to compute the accelerations of the bridges in addition to the original response which includes the static and dynamic deflections, the static and dynamic moments and the interacting forces between the vehicle and the bridge. The input and output form of both programs have also been revised so that the programs can handle either the dimensional or non-dimensional data input and provide printed and plotted results. Most of the symbols used in the analyses are defined where they are first introduced.

## 2.2 Analysis of Static and Dynamic Response of Simple-Span, Multigirder Highway Bridges

### 2.2.1 General

In this analysis, the bridge is represented as a plate continuous over flexible beams, and the bending and torsional stiffnesses of the beams are taken into account. The analysis involves two major steps:

(a) The determination of the instantaneous values of the dynamic forces acting on the bridge; these include the interacting forces between the vehicle and the bridge, and the inertia forces of the bridge itself.

(b) The evaluation of the deflections and moments produced in the bridge by these forces.

The second step, which is strictly a problem of statics, is solved by an application of the Rayleigh-Ritz energy procedure. The deflection of the structure is expressed as a series combination of functions that is capable of approximating any deflection configuration in both the longitudinal and transverse directions.

The method used to evaluate the dynamic forces is essentially an extension of that used for the static problem. In contrast to the expression used to represent the static deflection, however, the dynamic deflection of the bridge is assumed to be half-sine wave in the direction of the span.

The vehicle is represented by a single-axle loading consisting of a sprung mass and two equal unsprung masses, or wheels. The so-called rolling effect of the vehicle is thus taken into account. The springs are assumed to be linearly elastic. No damping is considered for either the vehicle or the bridge.

### 2.2.2 Analysis of Static Problem

The structure considered is shown in Figure 2.1. It consists of a reinforced concrete slab continuous over parallel steel or reinforced concrete beams spanning in the direction of traffic and simply supported at the ends. The beam spacing may be arbitrary. The dimensions of the beams may vary from one beam to the next, but all beams are assumed to be prismatic. The slab is considered to be isotropic, of constant thickness, and simply supported at the abutments.

The assumptions made in the analysis are those embodied in the ordinary theory of medium-thick, elastic plates and in the ordinary theory of flexure of beams. In addition, it is assumed that

- (1) A beam and the slab over it deflect and rotate alike.
- (2) There is no transfer of horizontal shear between the beams and the slab.

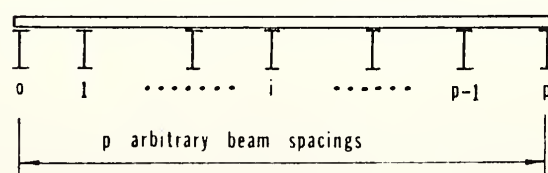
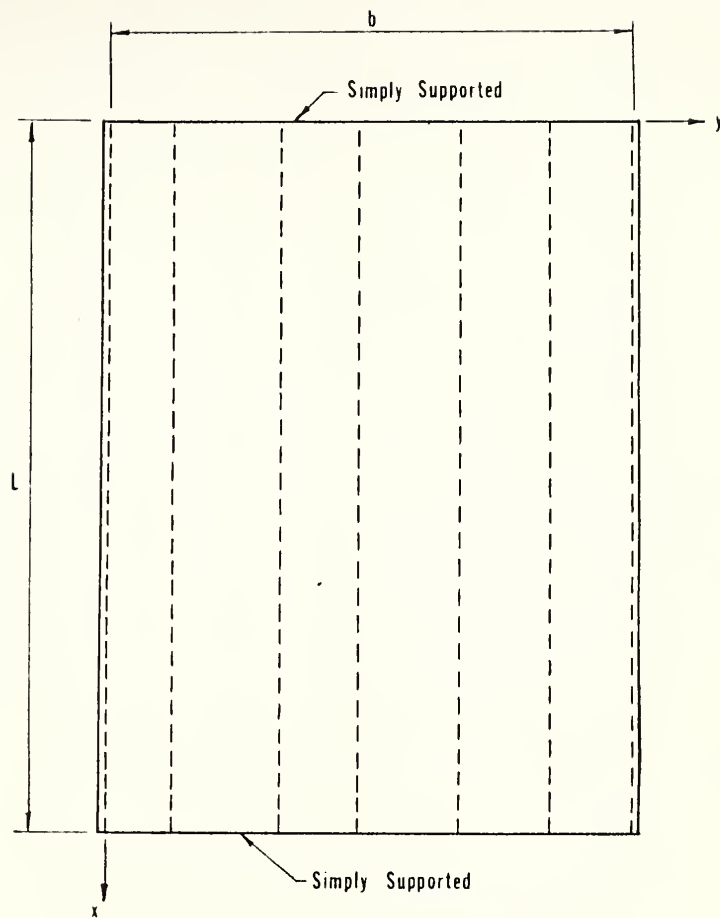


Figure 2.1 Simple Span Bridge Model

The span length of the bridge, center to center of supports, is denoted by  $L$ , and the overall width of the slab by  $b$ . The position of a point on the bridge is specified in terms of dimensionless cartesian coordinates  $\xi$  and  $\eta$ , defined by the equations

$$\begin{aligned}\xi &= x/L \\ \eta &= y/b\end{aligned}\quad (2-1)$$

#### Method of Analysis

The method used is a combination of the Rayleigh-Ritz energy method, and the Levy method of analysis for rectangular plates simply supported along two opposite edges. Let the vertical load on the structure,  $p(\xi, \eta)$ , be represented by a single trigonometric series of the form

$$p(\xi, \eta) = \sum_{m=1}^{\infty} \bar{p}_m = \sum_{m=1}^{\infty} p_m \sin m\pi\xi \quad (2-2)$$

in which  $p_m$  is a function of  $\eta$  only. The deflection of the structure,  $w(\xi, \eta)$ , can then be expressed as

$$w(\xi, \eta) = \sum_{m=1}^{\infty} \bar{w}_m = \sum_{m=1}^{\infty} w_m \sin m\pi\xi \quad (2-3)$$

where  $\bar{w}_m = w_m \sin m\pi\xi$  is the deflection component corresponding to the load component  $\bar{p}_m$ , and  $w_m$  is a function of  $\eta$  only. Let the deflection functions  $w_m$  be expressed in the form

$$w_m = \sum_n \alpha_{mn} Y_n \quad (2-4)$$

where  $Y_n$  are known functions of the  $n$ -coordinate, and  $\alpha_{mn}$  are coefficients which will be evaluated by minimizing the total energy of the system. Let the functions  $Y_n$  be dimensionless; then the coefficients  $\alpha_{mn}$  have the dimension of length.

Let the  $Y_n$  functions be taken as follows:

$$Y_n = \begin{cases} 1 & \text{for } n = -1 \\ 0.5 - n & \text{for } n = 0 \\ \sin n\pi \eta & \text{for } n \geq 1 \end{cases} \quad (2-5)$$

Note that,  $Y_{-1}, Y_1, Y_3, \dots$  are symmetric and  $Y_0, Y_2, Y_4, \dots$  are antisymmetric with respect to the longitudinal center-line of the structure,  $\eta = 0.5$ .

#### Energy of the System

The energy of the system consists of the strain energy of the slab, the strain energy of the beams and the potential energy of external forces. The energy expressions correspond to the deflection component  $\bar{w}_m = w_m \sin m\pi \xi$  and the associated load component  $\bar{p}_m = p_m \sin m\pi \xi$ .

Let the strain energy of the system,  $V_m$ , be written in the form

$$V_m = (V_m)_s + (V_m)_b \quad (2-6)$$

where  $(V_m)_s$  is the strain energy of the slab, and  $(V_m)_b$  is the strain energy of the beams.  $(V_m)_s$  and  $(V_m)_b$  are given by the equation

$$(V_m)_s = \frac{DLb}{2L^4} \int_0^1 \int_0^1 \left[ \left( \frac{\partial^2 \bar{w}_m}{\partial \xi^2} \right)^2 + \frac{2}{c^2} \left( \frac{\partial^2 \bar{w}_m}{\partial \xi \partial \eta} \right)^2 + \frac{1}{c^4} \left( \frac{\partial^2 \bar{w}_m}{\partial \eta^2} \right)^2 \right] d\xi d\eta \quad (2-7)$$

$$\begin{aligned} &= \frac{m^4 n^4 D}{L^4} \frac{bL}{4} \left[ \sum_n \sum_s \alpha_{mn} \alpha_{ms} \int_0^1 Y_n' Y_s' d\eta \right. \\ &\quad \left. + \frac{2}{\pi^2 (mc)^2} \sum_n \sum_s \alpha_{mn} \alpha_{ms} \int_0^1 Y_n'' Y_s'' d\eta \right. \\ &\quad \left. + \frac{1}{\pi^4 (mc)^4} \sum_n \sum_s \alpha_{mn} \alpha_{ms} \int_0^1 Y_n''' Y_s''' d\eta \right] \end{aligned} \quad (2-8)$$

$$(V_m)_b = \sum_{i=0}^p \left[ \frac{(E_b I_b)_i}{2L^3} \int_0^1 \left( \frac{\partial^2 \bar{w}_m}{\partial \xi^2} \right)_i^2 d\xi + \frac{(G_b J_b)_i}{2Lb^2} \int_0^1 \left( \frac{\partial^2 \bar{w}_m}{\partial \xi \partial \eta} \right)_i^2 d\xi \right] \quad (2-9)$$

$$\begin{aligned} &= \frac{m^4 n^4 D}{L^4} \frac{bL}{4} \sum_{i=0}^p \left[ \lambda_i \sum_n \sum_s \alpha_{mn} \alpha_{ms} (Y_n)_i (Y_s)_i \right. \\ &\quad \left. + \frac{k_i}{\pi^2 (mc)^2} \sum_n \sum_s \alpha_{mn} \alpha_{ms} (Y_n')_i (Y_s')_i \right] \end{aligned} \quad (2-10)$$

where  $c = b/L$

$D$  = the flexural rigidity per unit width of the slab

$(E_b I_b)_i$  = the flexural rigidity of the  $i^{th}$  beam

$(G_b J_b)_i$  = the torsional rigidity of the  $i^{th}$  beam

and a prime denotes and differentiation with respect to  $\eta$ .

The strain energy of the system,  $V_m$ , can be rewritten in the form,

$$V_m = \frac{m^4 \pi^4 D}{4} \frac{bL}{4} \bar{F}_m (\alpha_{mn} \alpha_{ms}) \quad (2-11)$$

where  $\bar{F}_m (\alpha_{mn} \alpha_{ms})$  is a quadratic form of the unknown coefficients  $\alpha_{mn}$ .

The potential energy,  $U_m$ , of the load component  $\bar{p}_m$  is given by the equation

$$U_m = -bL \int_0^1 \int_0^1 \bar{w}_m \bar{p}_m d\xi d\eta \quad (2-12)$$

$$= -bL \int_0^1 \int_0^1 (w_m \sin m\pi\xi) (p_m \sin m\pi\xi) d\xi d\eta \quad (2-13)$$

$$= -\frac{bL}{2} \sum_n \alpha_{mn} \int_0^1 p_m Y_n d\eta \quad (2-14)$$

The total energy of the system,  $I_m$ , is the sum of Eqs. (2-11) and (2-14)

$$I_m = \frac{m^4 \pi^4 D}{4} \frac{bL}{4} \bar{F}_m (\alpha_{mn} \alpha_{ms}) - \frac{bL}{2} \sum_n \alpha_{mn} \int_0^1 p_m Y_n d\eta \quad (2-15)$$

The condition that  $I_m$  be a minimum yields a system of linear algebraic equations of the form

$$[F_m] [A_m] = [B_m] \quad (2-16)$$

in which  $[A_m]$  is a column matrix of the unknown coefficients  $\alpha_{mn}$ ,  $[B_m]$  is a column matrix of known load terms, and  $[F_m]$  is a symmetric matrix, the order of which is equal to the number of  $Y_n$  functions used in Eq. (2-4). The element  $f_{m,ns}$  in the  $n^{\text{th}}$  row and  $s^{\text{th}}$  column of the  $[F_m]$  matrix is given by the equation

$$f_{m,ns} = \left[ \int_0^1 Y_n Y_s d\eta + \frac{2}{\pi^2 (mc)^2} \int_0^1 Y_n' Y_s' d\eta + \frac{1}{\pi^4 (mc)^4} \int_0^1 Y_n'' Y_s'' d\eta \right] \\ + \sum_{i=0}^p \left[ \lambda_i (Y_n)_i (Y_s)_i + \frac{k_i}{\pi^2 (mc)^2} (Y_n')_i (Y_s')_i \right] \quad (2-17)$$

The element  $b_{mn}$  in the  $n^{\text{th}}$  row of the  $[B_m]$  matrix is

$$b_{mn} = \frac{2PL^3}{\pi^4 Db} \frac{\sin m\pi\xi_1}{m^4} Y_n(\eta_1) \quad (2-18)$$

The solution of the system of Equations (2-16) gives the value of  $\alpha_{mn}$ , which are then used to determine the deflection component  $\bar{w}_m = w_m \sin m\pi\xi$ . In general, Eqs. (2-16) are solved for as many values of  $m$  as may be necessary in a particular application. The total deflection,  $w$ , of the structure is then determined from Eq. (2-3) by superposing the component deflections. The latter equation may be rewritten in one of the following forms

$$w = \sum_m \left( \sum_n \alpha_{mn} Y_n \right) \sin m\pi\xi = \sum_m [A_m] \cdot [Y_n(\eta)] \sin m\pi\xi \quad (2-19)$$

where  $Y_n(n)$  is a column matrix of the values of the  $Y_n$  functions evaluated at the point under consideration, and a dot denotes a scalar product.

### 2.2.3 Analysis of Dynamic Problem

The structure analyzed is the same as that considered in the static analysis. In addition to the assumptions made previously, it is assumed that the mass of the slab is uniformly distributed, and that the mass per unit of length of the beams, although it may vary from one beam to the next, is constant for any one beam.

The vehicle is represented by a single-axle, two wheel loading consisting of a sprung mass and two equal unsprung masses, as shown in Figure 2.2. The center of gravity of the sprung mass is assumed to be located halfway between the supporting springs. The springs are considered to be linearly elastic and to have identical stiffnesses. Damping for both the vehicle and the bridge has been neglected.

The analysis of the problem involves

- (a) The determination of the instantaneous values of the interacting forces between the vehicle and the structure, and of the inertia forces due to the mass of the structure, and
- (b) The computation of the deflections and bending moments produced in the structure by these forces.

The dynamic deflection configuration of the structure in the longitudinal direction ( $\xi$ -direction) is assumed to be a half-sine wave and is expressed as

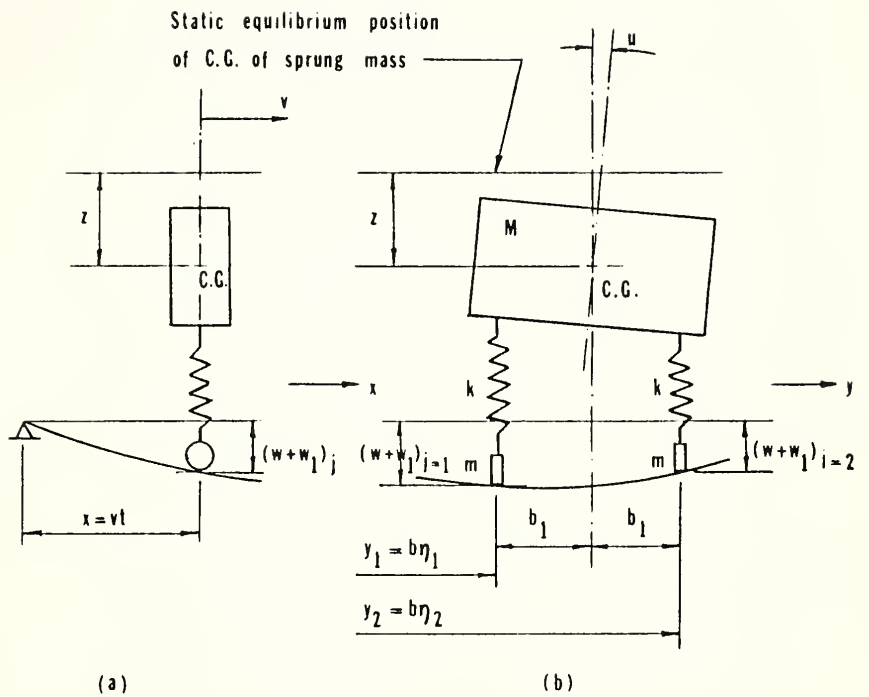


Figure 2.2 Vehicle Model for Simple Span Bridge

$$w = w_0 \sin \pi \xi \sum_n f_n(t) Y_n(n) \quad (2-20)$$

where  $w$  = the deflection of any point of the bridge at any time, due to the static and dynamic effects of the vehicle

$w_0$  = a quantity with the dimension of deflection, chosen arbitrarily as  $WL^3/(E_b I_b)_{io}$

$W$  = total static weight of the vehicle

$(E_b I_b)_{io}$  = flexural rigidity of a reference beam

$f_n(t)$  = dimensionless coefficients that are functions of time; these are the generalized coordinates for the bridge

$Y_n(n)$  = dimensionless functions of  $n$ , as previously discussed.

The coordinates used to specify the configuration of the sprung mass are the vertical displacement of the center of gravity of the mass,  $z$ , and the rotation of the mass about an axis normal to the transverse vertical plane,  $u$ , (see Figure 2.2). The vertical positions of the unsprung masses are determined by the configuration of the bridge. Thus the total number of generalized coordinates of the bridge-vehicle system is equal to the number of  $f_n(t)$  functions used in Eq. (2-20) plus the two coordinates  $z$  and  $u$  used for the vehicle.

The vehicle is assumed to move along the bridge with a constant velocity,  $v$ , and the wheels of the vehicle

are assumed to be attached to the surface of the bridge at all times. The system under consideration possesses a time-dependent potential energy function, and it is possible to formulate the equations of motion by application of Lagrange's equation

$$\frac{d}{dt} \left( \frac{\partial T}{\partial \dot{q}_n} \right) - \frac{\partial T}{\partial q_n} + \frac{\partial (U + V)}{\partial q_n} = 0 \quad (2-21)$$

in which  $V$  = the strain energy of the system

$U$  = the potential energy of the gravity forces

$T$  = the kinetic energy of the system

$q_n$  = the  $n^{\text{th}}$  generalized coordinate of the system

$$\dot{q}_n = \frac{dq_n}{dt}$$

#### Energy of the System

The datum of zero energy level for the system is defined by the following conditions: the structure is in an unstressed position, and the springs of the vehicle are undeformed.

Let  $w_2$  represent the deflection configuration of the bridge when loaded with its own weight: this deflection is measured from the unstressed configuration of the bridge. Then the total deflection of the bridge, measured from its unstressed position, is  $(w + w_2)$ . The dead load deflection configuration,  $w_2$ , can be represented in a form

$$w_2 = w_o \sum_m \left( \sum_n \delta_{mn} Y_n \right) \sin m\pi\xi \quad (2-22)$$

$$= w_o \sin \pi\xi \sum_n \delta_n Y_n(n) \quad (2-23)$$

where  $\delta_{mn}$  and  $\delta_n$  are constant dimensionless coefficients.

Let  $w_1$  be a deflection function representing the deviation of the deck of the bridge, when loaded with its own weight, from the horizontal plane passing through the supports. It is positive when downward. This quantity is equal to the sum of the dead load deflection configuration and the configuration representing any possible unevenness of the unstressed bridge. The roadway surface unevenness function,  $w_1$ , appears only as  $(w_1)_j$ , i.e., with its ordinates evaluated at the transverse location of the wheels, can be represented in a form

$$(w_1)_j = w_o e_j \sin m_1 \pi \xi \quad (2-24)$$

where  $e_j$  ( $j = 1$  or  $2$ ) are dimensionless quantities and  $w_o e_j$  denotes the amplitude of the unevenness. The quantities  $e_1$  and  $e_2$  may or may not be equal; they may also be positive or negative. The quantity  $m_1$  is a positive integer.

The total strain energy of the system,  $V$ , is written in the form

$$V = V_s + V_b + V_{sp} \quad (2-25)$$

where  $V_s$ ,  $V_b$ , and  $V_{sp}$  are the strain energies of the slab, of the beams, and of the springs, respectively, and are given by the equations

$$V_s = \frac{D b L}{2 L^4} \int_0^1 \int_0^1 \left[ \left( \frac{\partial^2 (w+w_2)}{\partial \xi^2} \right)^2 + \frac{2}{c^2} \left( \frac{\partial^2 (w+w_2)}{\partial \xi \partial \eta} \right)^2 + \frac{1}{c^4} \left( \frac{\partial^2 (w+w_2)}{\partial \eta^2} \right)^2 \right] d\xi d\eta \quad (2-26)$$

$$V_b = \sum_{i=0}^p \left[ \frac{(E_b I_b)_i}{2 L^3} \int_0^1 \left( \frac{\partial^2 (w+w_2)}{\partial \xi^2} \right)_i^2 d\xi + \frac{(G_b J_b)_i}{2 L b^2} \int_0^1 \left( \frac{\partial^2 (w+w_2)}{\partial \xi \partial \eta} \right)_i^2 d\xi \right] \quad (2-27)$$

$$V_{sp} = \frac{1}{2} k \sum_{j=1}^2 [z + z_s - (w+w_1)_j + (-1)^j u_b]_1^2 \quad (2-28)$$

The complete forms of the equations, after substituting the values of  $w$ ,  $w_1$ ,  $w_2$  and evaluating the integrals, are given in Ref. (28).

The potential energy of the gravity forces is written in the form

$$U = U_s + U_b + U_{sp} + U_u \quad (2-29)$$

where  $U_s$ ,  $U_b$ ,  $U_{sp}$ , and  $U_u$  are the potential energies of the slab, of the beams, of the sprung mass, and of the unsprung masses, respectively, and are given by the equations

$$U_s = -\mu g I b \int_0^1 \int_0^1 (w + w_2) d\xi d\eta \quad (2-30)$$

$$U_b = -Lg \int_0^1 \left[ \sum_{i=0}^p (m_b)_i (w + w_2)_i \right] d\xi \quad (2-31)$$

$$U_{sp} = -Mg (z + z_s) \quad (2-32)$$

$$U_u = -mg \sum_{j=1}^2 (w + w_1)_j \quad (2-33)$$

The complete forms of the equations, after substituting the values of  $w$ ,  $w_1$ ,  $w_2$  and evaluating the integrals, are given in Ref. (28).

The total kinetic energy of the system is expressed in the form

$$T = T_s + T_b + T_{sp} + T_u \quad (2-34)$$

where  $T_s$ ,  $T_b$ ,  $T_{sp}$ , and  $T_u$  are the kinetic energies of the slab, of the beams, of the sprung mass, and of the unsprung masses, respectively, and are given in the forms

$$T_s = \frac{1}{2} \mu L b \int_0^1 \int_0^1 \left( \frac{\partial w}{\partial t} \right)_i^2 d\xi d\eta \quad (2-35)$$

$$T_b = \frac{L}{2} \sum_{i=0}^p \int_0^1 (m_b)_i \left( \frac{\partial w}{\partial t} \right)_i^2 d\xi \quad (2-36)$$

$$T_{sp} = \frac{1}{2} M \left( \frac{dz}{dt} \right)^2 + \frac{1}{2} J \left( \frac{du}{dt} \right)^2 \quad (2-37)$$

$$T_u = \frac{1}{2} m \sum_{j=1}^2 \left[ \frac{d}{dt} (w + w_1)_j \right]^2 \quad (2-38)$$

The complete forms of the equations, after substituting the values of  $w$ ,  $w_1$ , and evaluating the integrals, are given in Ref. (28).

### The Governing Differential Equations

The differential equations governing the motion of the bridge-vehicle system are obtained from Eq. (2-21) by substituting the energy expressions derived above. The number of equations obtained is equal to the number of generalized coordinates used to define the configuration of the system. The final derived equation corresponding to the  $n^{\text{th}}$  generalized coordinate of the bridge,  $f_n$ , is

$$\begin{aligned}
 & w_o \sum_s f_s'' \left[ \frac{\mu D}{2} \int_0^L Y_n Y_s dm + \frac{L}{2} \sum_{j=0}^p (m_b)_i (Y_n)_i (Y_s)_i + m \sin^2 \frac{\pi v t}{L} \sum_{j=1}^2 (Y_n)_j (Y_s)_j \right] \\
 & + w_o \sum_s f_s' \left[ 2m \left( \frac{\pi v}{L} \right) \sum_{j=1}^2 (Y_n)_j (Y_s)_j \right] \sin \frac{\pi v t}{L} \cos \frac{\pi v t}{L} \\
 & + w_o \sum_s f_s \left[ \frac{\pi^4 D}{L^4} \frac{ab}{2} \left[ A_{ns} + \sum_{i=0}^p \lambda_i (Y_n)_i (Y_s)_i + \sum_{i=0}^p \frac{k_i}{\pi^2 c^2} (Y'_n)_i (Y'_s)_i \right] \right. \\
 & \quad \left. + k \sin^2 \frac{\pi v t}{L} \sum_{j=1}^2 (Y_n)_j (Y_s)_j - m \left( \frac{\pi v}{L} \right)^2 \sin^2 \frac{\pi v t}{L} \sum_{j=1}^2 (Y_n)_j (Y_s)_j \right] \\
 & - \sin \frac{\pi v t}{L} \sum_{j=1}^2 (Y_n)_j \left[ \frac{qM}{2} + k \left[ z - (w_1)_j + (-1)^j ub_1 \right] \right]
 \end{aligned}$$

$$-mg \sin \frac{\pi vt}{L} \sum_{j=1}^2 (Y_n)_j + m \left(\frac{v}{L}\right)^2 \sin \frac{\pi vt}{L} \sum_{j=1}^2 (Y_n)_j \left( \frac{\partial^2 w_1}{\partial x^2} \right)_j = 0 \quad (2-39)$$

The summations on s should extend from  $s = -1$ , to  $s = n_1$ , the maximum value of n used in Eq. (2-20). There will be a total of  $n_1 + 2$  equations.

The equation corresponding to the z coordinate of the vehicle is

$$Mz'' + k \sum_{j=1}^2 \left[ z - (w_1)_j - w_o \sin \frac{\pi vt}{L} \sum_s f_s (Y_s)_j \right] = 0 \quad (2-40)$$

and the one corresponding to the u coordinate is

$$Ju'' + kb_1 \sum_{j=1}^2 (-1)^j \left[ (-1)^j ub_1 - (w_1)_j - w_o \sin \frac{\pi vt}{L} \sum_s f_s (Y_s)_j \right] = 0 \quad (2-41)$$

$$\text{where } A_{ns} = \left[ \int_0^1 Y_n Y_s d\eta + \frac{2}{\pi^2 c^2} \int_0^1 Y_n' Y_s' d\eta + \frac{1}{\pi^4 c^4} \int_0^1 Y_n'' Y_s'' d\eta \right] \quad (2-42)$$

The dimensionless form of the governing equations can be obtained by assuming the following parameters

$$v = \frac{2m + M}{L [kb + \sum_{i=0}^p (m_b)_i]} = \frac{\text{Total weight of vehicle}}{\text{Total weight of bridge}}$$

$$\omega = \frac{2m}{2m + M} = \frac{\text{Unsprung weight of vehicle}}{\text{Total weight of vehicle}} \quad (2-43)$$

$$\gamma_i = \frac{(m_b)_i}{b + \sum_{i=0}^p (m_b)_i} = \frac{\text{Weight of } i^{\text{th}} \text{ beam}}{\text{Total weight of bridge}}$$

$$\alpha = \frac{v T_b}{2L}$$

$$\kappa = \left(\frac{f_v}{f_b}\right)^2 = \left(\frac{T_b}{T_v}\right)^2$$

in which

$f_b$  = the fundamental natural frequency of the bridge evaluated on the assumption that it acts as a one dimensional beam.

$f_v$  = the natural frequency of the vehicle for vertical motion on its springs.

These frequencies are given by the equations

$$f_b^2 = \frac{1}{T_b^2} = \frac{\pi^2}{4L^4} \frac{D_b + \sum_{i=0}^p (E_b I_b)_i}{\mu_b + \sum_{i=0}^p (m_b)_i}$$

(2-44)

$$f_v^2 = \frac{1}{T_v^2} = \frac{1}{4\pi^2} \frac{2k}{M}$$

In addition, let

$$\tau = \frac{vt}{L}$$

$$\psi_s(\tau) = f_s(t)$$

(2-45)

$$\zeta(\tau) = \frac{z(t)}{w_0}$$

$$u(\tau) = \frac{u(t)b_1}{w_0}$$

Now by multiplying Eq. (2-39) by  $\frac{T_b^2}{2w_o} \frac{1}{\mu bL + L \sum_{i=0}^p (m_b)_i}$

and substituting the dimensionless quantities defined by Eqs. (2-43) and (2-44), the governing differential equations can be reduced to the forms

$$\begin{aligned} & \sum_s \psi_s'' (B_{ns} + C_{ns} \sin^2 \pi \tau) + \sum_s \psi_s' D_{ns} \sin \pi \tau \cos \pi \tau \\ & + \sum_s \psi_s (E_{ns} + F_{ns} \sin^2 \pi \tau) + H_n \sin \pi \tau \\ & + L_n (\zeta, 0, \tau) + R_n \sin \pi \tau \sin m_1 \pi \tau = 0 \end{aligned} \quad (2-46)$$

$$2\alpha^2 \zeta'' + \pi^2 \kappa \left[ 2\zeta - \sin m_1 \pi \tau \sum_{j=1}^2 e_j - \sin \pi \tau \sum_s \psi_s \sum_{j=1}^2 (Y_s)_j \right] = 0 \quad (2-47)$$

$$\begin{aligned} & 2\alpha^2 \rho \theta'' + \pi^2 \kappa \left[ 2\theta - \sin m_1 \pi \tau \sum_{j=1}^2 (-1)^j e_j \right. \\ & \left. - \sin \pi \tau \sum_s \psi_s \sum_{j=1}^2 (-1)^j (Y_s)_j \right] = 0 \end{aligned} \quad (2-48)$$

where

$$B_{ns} = \alpha^2 \left[ \left( 1 - \sum_{i=0}^p \gamma_i \right) \int_0^1 Y_n Y_s d_n + \sum_{j=0}^p \gamma_j (Y_n)_j (Y_s)_j \right]$$

$$C_{ns} = \alpha^2 v \omega \sum_{j=1}^2 (Y_n)_j (Y_s)_j$$

$$D_{ns} = 2\alpha^2 \pi v \omega \sum_{j=1}^2 (Y_n)_j (Y_s)_j$$

$$E_{ns} = \frac{\pi^2}{\frac{p}{1 + \sum_{i=0}^p \lambda_i}} \left[ A_{ns} + \sum_{i=0}^p \lambda_i (Y_n)_i (Y_s)_i \right]$$

$$+ \frac{1}{\pi^2 c^2} \sum_{i=0}^p k_i (Y'_n)_i (Y'_s)_i \right]$$

$$F_{ns} = \pi^2 v [\kappa(1 - \omega) - \alpha^2 \omega] \sum_{j=1}^2 (Y_n)_j (Y_s)_j$$

$$H_n = -\frac{1}{\pi^2} \frac{\lambda_{io}}{1 + \sum_{i=0}^p \lambda_i} \sum_{j=1}^2 (Y_n)_j$$

$$L_n = -\pi^2 \kappa v (1 - \omega) \sin \pi \tau \sum_{j=1}^2 (Y_n)_j [\zeta + (-1)^j \theta]$$

$$R_n = \pi^2 v [\kappa(1 - \omega) - \alpha^2 \omega m_1^2] \sum_{j=1}^2 e_j (Y_n)_j$$

$$\rho = \frac{J}{M b_1^2}$$

#### Computation of Response

The procedure used to evaluate the dynamic response of the bridge-vehicle system may be summarized briefly as follows:

(a) The governing differential equations of motion are solved, by means of a step-by-step method of numerical integration, to determine the values of the generalized coordinates and of their first two derivatives.

(b) The interacting forces between the vehicle and the bridge and the inertia forces of the bridge are evaluated.

(c) The dynamic deflections and bending moments induced in the bridge are determined from the dynamic forces acting on the bridge, instead of directly from the generalized coordinates computed in the first step, and the accelerations of the bridge are evaluated.

The system of Eqs. (2-46) through (2-48) are solved by means of a step-by-step method of numerical integration. The time required for the vehicle to cross the span,  $0 < \tau < 1$ , is divided into a number of small intervals, and the governing equations are "satisfied" only at the ends of these intervals.

Let  $q_{n,r}$  represent a dimensionless generalized coordinate - it may refer to the bridge or the vehicle -, and  $\dot{q}_{n,r}$  and  $\ddot{q}_{n,r}$  represent its first and second derivatives with respect to  $\tau_r$ . Let it be assumed that the values of  $q_{n,r}$ ,  $\dot{q}_{n,r}$  and  $\ddot{q}_{n,r}$  are known for each generalized coordinate of the system, and that it is desired to find the corresponding values at  $\tau = \tau_{r+1} = \tau_r + \Delta\tau$  in which  $\Delta\tau$  is a short interval.

The variation of  $\ddot{q}_n$  within the time interval  $\Delta\tau$  was considered to be linear; with this assumption, the expressions for  $\dot{q}_{n,r+1}$  and  $q_{n,r+1}$  become

$$\dot{q}_{n,r+1} = \dot{q}_{n,r} + \frac{1}{2}(\Delta\tau)(\ddot{q}_{n,r} + \ddot{q}_{n,r+1}) \quad (2-49)$$

$$q_{n,r+1} = q_{n,r} + (\Delta\tau)\dot{q}_{n,r} + \frac{1}{3}(\Delta\tau)^2\ddot{q}_{n,r} + \frac{1}{6}(\Delta\tau)^2\ddot{q}_{n,r+1} \quad (2-50)$$

The iterative procedure may be summarized as follows:

1. Assume that the second derivatives of the generalized coordinates at the end of the time interval are the same as those at the beginning of the interval, i.e. take  $\ddot{q}_{n,r+1} = \ddot{q}_{n,r}$  and by application of Eqs. (2-49) and (2-50) evaluate  $\dot{q}_{n,r+1}$  and  $q_{n,r+1}$ .

2. Substitute the values of  $\dot{q}_{n,r+1}$  and  $q_{n,r+1}$  thus obtained into the governing differential equations, and by solving the resulting system of algebraic equations, obtain improved values for  $\dot{q}_{n,r+1}$ .

3. From Eqs. (2-49) and (2-50) calculate the values of  $\dot{q}_{n,r+1}$  and  $q_{n,r+1}$  corresponding to the values of  $\ddot{q}_{n,r+1}$  just determined.

4. Repeat Step 2 by using the latest available values of  $\dot{q}_{n,r+1}$  and  $q_{n,r+1}$ .

5. For each generalized coordinate compare the newly derived values of  $\ddot{q}_{n,r+1}$  with the previously available value. If the difference between the two values for each coordinate exceeds a prescribed tolerance, repeat Steps 3 through 5, until all differences are less than the prescribed tolerance. The algebraic equations are then considered to be solved, and the integration for the time interval  $\tau_r$  to  $\tau_{r+1}$  completed.

The next step, to obtain the dynamic response of the system, is to evaluate the interacting forces between the vehicle and the bridge. The static value of the interacting force for each wheel is one-half the total weight of the vehicle or  $W/2$ . The dynamic increment of the interacting force for the  $j^{\text{th}}$  wheel may conveniently be stated in the form  $\Delta_j \frac{W}{2}$  where  $\Delta_j$  is a dimensionless factor. Now let

$$\Delta_j = (\Delta_1)_j + (\Delta_2)_j \quad (2-51)$$

where  $(\Delta_1)_j$  = the component of  $\Delta_j$  due to the dynamic increment of the compression in the spring.

$(\Delta_2)_j$  = the component of  $\Delta_j$  due to the vertical acceleration of the unsprung mass  $j$ .

These quantities may be determined as follows:

$$(\Delta_1)_j \frac{W}{2} = k [z + (-1)^j ub_1 - (w_1 + w)_j] \quad (2-52)$$

$$(\Delta_2)_j \frac{W}{2} = -m \left[ \left( \frac{d^2 w}{dt^2} \right)_j + \left( \frac{v}{L} \right)^2 \left( \frac{d^2 w_1}{dx^2} \right)_j \right] \quad (2-53)$$

The dynamic increments of deflection  $(\Delta D)_i$  and of moment  $(\Delta M)_i$  can now be expressed in the form

$$(\Delta D)_i = \sum_{j=1}^2 D_{i,j} \Delta_j + \sum_s D_{i,s}^o \psi_s'' \quad (2-54)$$

$$(\Delta M)_i = \sum_{j=1}^2 M_{i,j} \Delta_j + \sum_s M_{i,s}^o \psi_s'' \quad (2-55)$$

where  $D_{i,j}$  = the deflection produced at a specified point of the  $i^{\text{th}}$  beam by a concentrated force  $W/2$  applied at the position of the  $j^{\text{th}}$  wheel.

$M_{i,j}$  = the bending moment corresponding to  $D_{i,j}$ .

$D_{i,s}^O$  = the deflection produced at a given point of beam  $i$  by a static load which is distributed as a sine wave in the longitudinal direction.

$M_{i,s}^O$  = the bending moment corresponding to  $D_{i,s}^O$ .

The expression for the accelerations of the bridge at midspan can be derived directly from Eq. (2-20) and appears in the form

$$\ddot{w} = w_0 \sum_n \ddot{f}_n(t) Y_n(\eta) \quad (2-56)$$

Substituting the second derivative dimensionless function  $\ddot{\psi}_n(\eta)$  defined by Eq. (2-45), gives

$$\ddot{w} = w_0 \left(\frac{v}{L}\right)^2 \sum_n \ddot{\psi}_n(\tau) Y_n(\eta) \quad (2-57)$$

where  $w_0 \left(\frac{v}{L}\right)^2$  is a quantity with the dimension of acceleration. The accelerations of the beams can be evaluated at the transverse location of the beams in the  $\eta$ -direction.

#### 2.2.4 Computer Program

The method described in the preceding sections has been programmed<sup>(28)</sup> to analyze simple-span bridges having from one to fifteen uniformly spaced prismatic beams. The beams are assumed to be arranged symmetrically with respect to the longitudinal centerline of the structure. All interior beams are considered to be identical. The exterior beams on either side of the bridge are assumed to be located along the edge of the slab and, while identical to one another, they may be different from the interior beams. The program is limited only to non-composite sections and the effect of side curbs is not considered. The vehicle is a single-axle load, consisting of one or two wheels. The roadway surface unevenness is represented by a trigonometric function in the longitudinal direction.

The input parameters of the program can be either dimensionless or dimensional. The dimensionless parameters have been defined by Eqs. (2-1), (2-24) and (2-43). The dimensional parameters are divided into three major groups, i.e., bridge parameters, vehicle parameters and solution parameters. After the dimensional parameters are entered, the frequencies of bridge and of vehicle are computed. Then all parameters are converted to a dimensionless form by the program before the start of static and dynamic computations.

The program provides results for the complete history of the response of the system, by printing and plotting out the crawl or static values of deflections and moments in the beam at midspan, the corresponding dynamic increments, the dynamic increment of the wheel reactions, and the accelerations in the beams at midspan.

#### Flow Diagram

A general flow diagram for the complete program is shown in Figure 2.3, and the flow diagrams for the subroutines (QIMJ), (DOMOIS), (EQMON), (RESLT), (INTEG) are shown in Figures 2.4, 2.5, 2.6, 2.7, 2.8 respectively.

The program starts with the reading of the parameters specifying the characteristics of the vehicle and bridge, and necessary parameters to carry out the solutions.

Next the subroutine (QIMJ) is entered to evaluate the quantities  $Q_{m,j}$  which are used to evaluate the deflections and bending moments in the beams at midspan. These are defined by the equations

$$Q_{m,j} = \frac{1}{m^2} \sin \frac{m\pi}{2} \sum_{n=-1}^{n_o} a'_{mn,j} Y_n(n_i)$$

$$D_{i,j} = (C_d)_j \frac{WL^3}{(E_b I_b)_o} \quad (2-58)$$

$$M_{i,j} = (C_m)_j WL$$

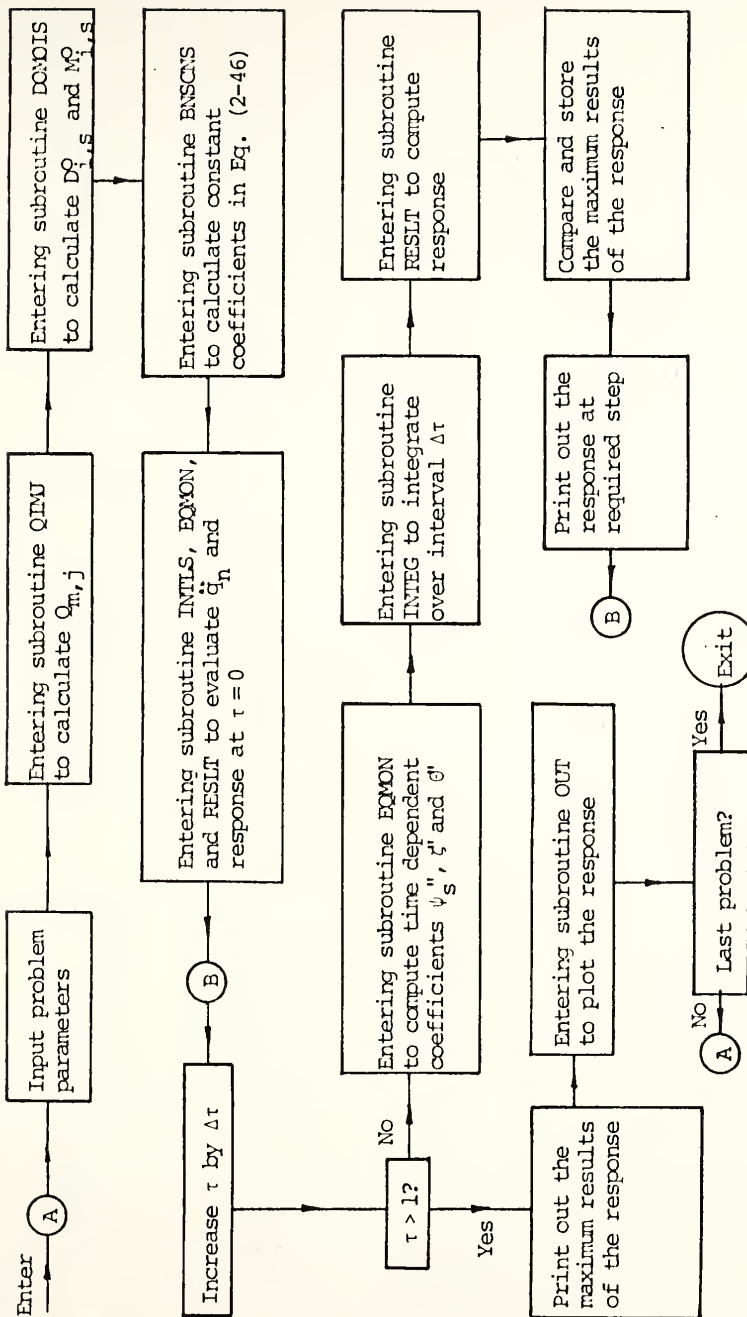


Figure 2.3 General Flow Chart for Complete Program

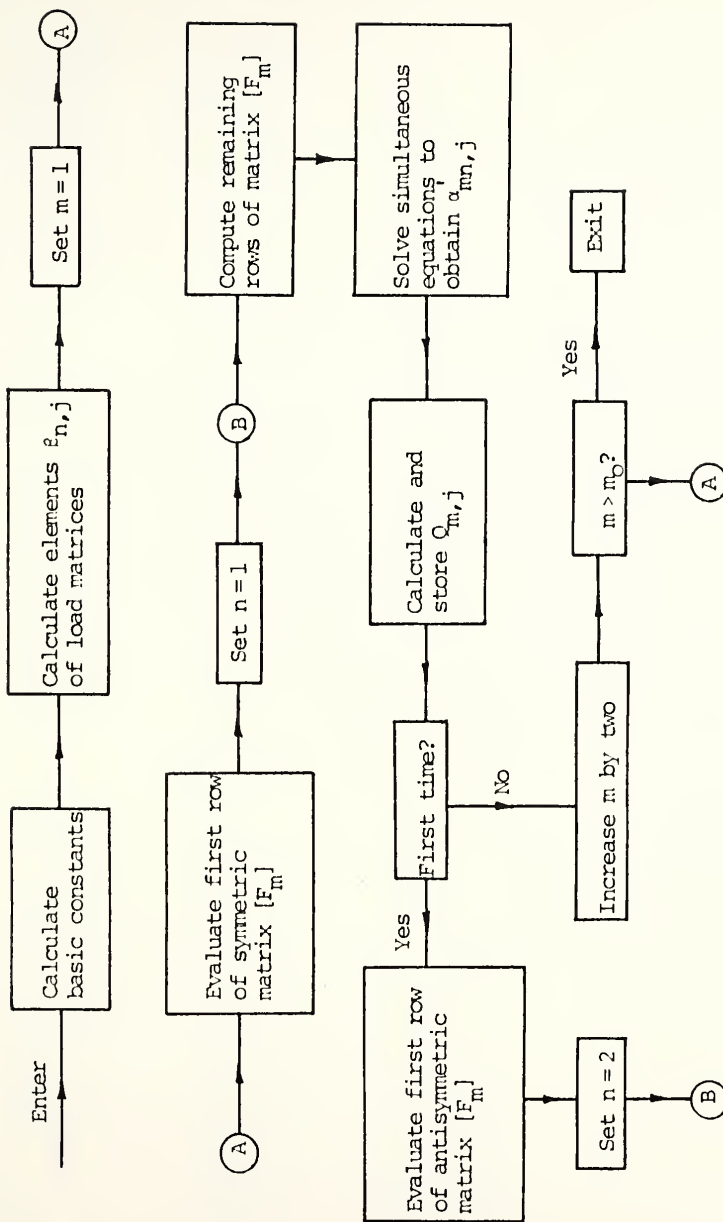


Figure 2.4 Flow Chart for Subroutine (QIMJ) to Compute Quantities  $Q_{m,j}$

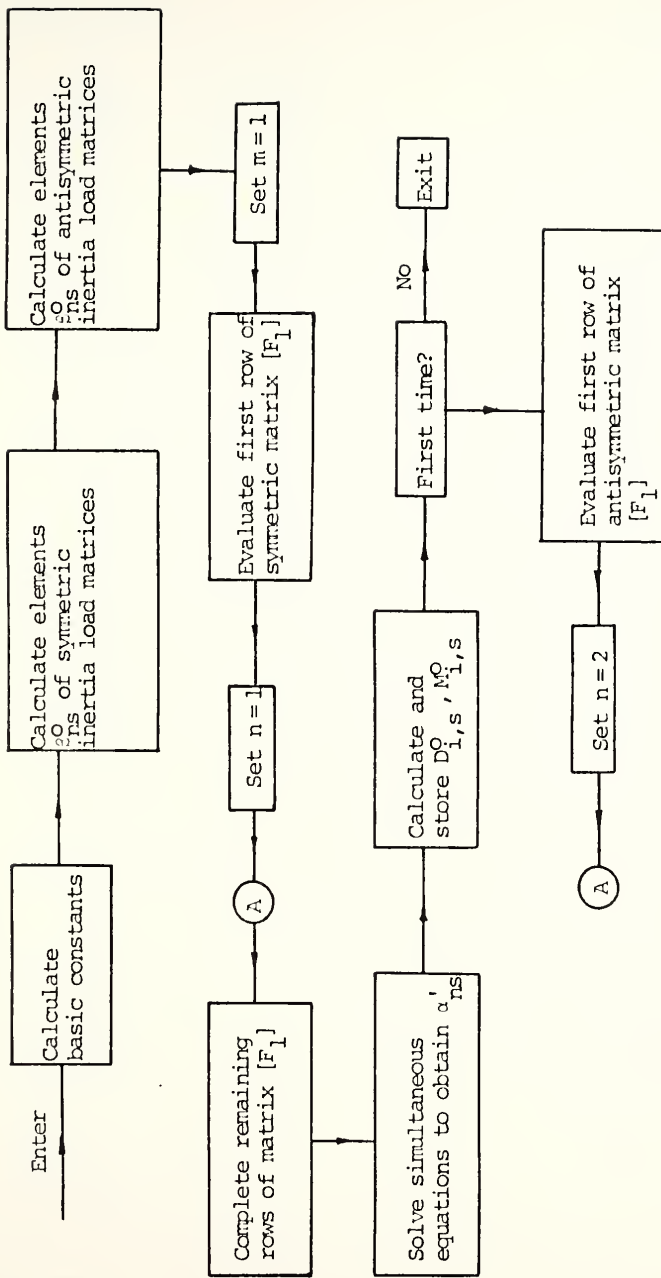


Figure 2.5 Flow Chart for Subroutine (DOMOIS) to Compute  $D_{i,s}^O$  and  $M_{i,s}^O$

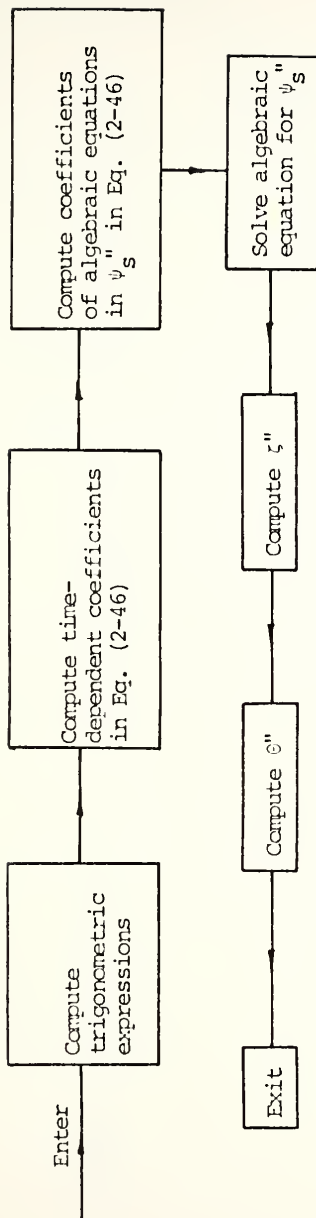


Figure 2.6 Flow Chart for Subroutine (EQMON) to Solve the Governing Differential Equations

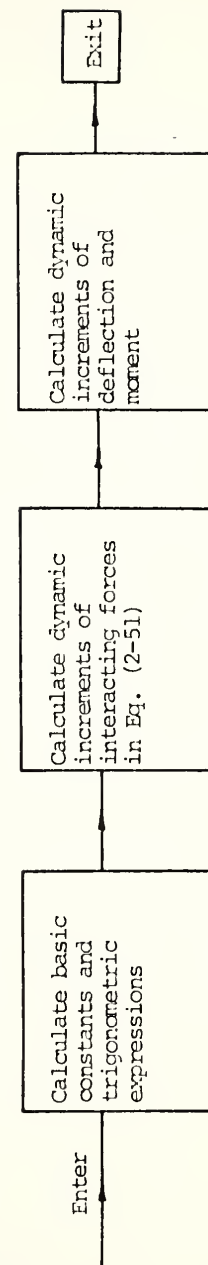


Figure 2.7 Flow Chart for Subroutine (PESLT) to Compute the Response

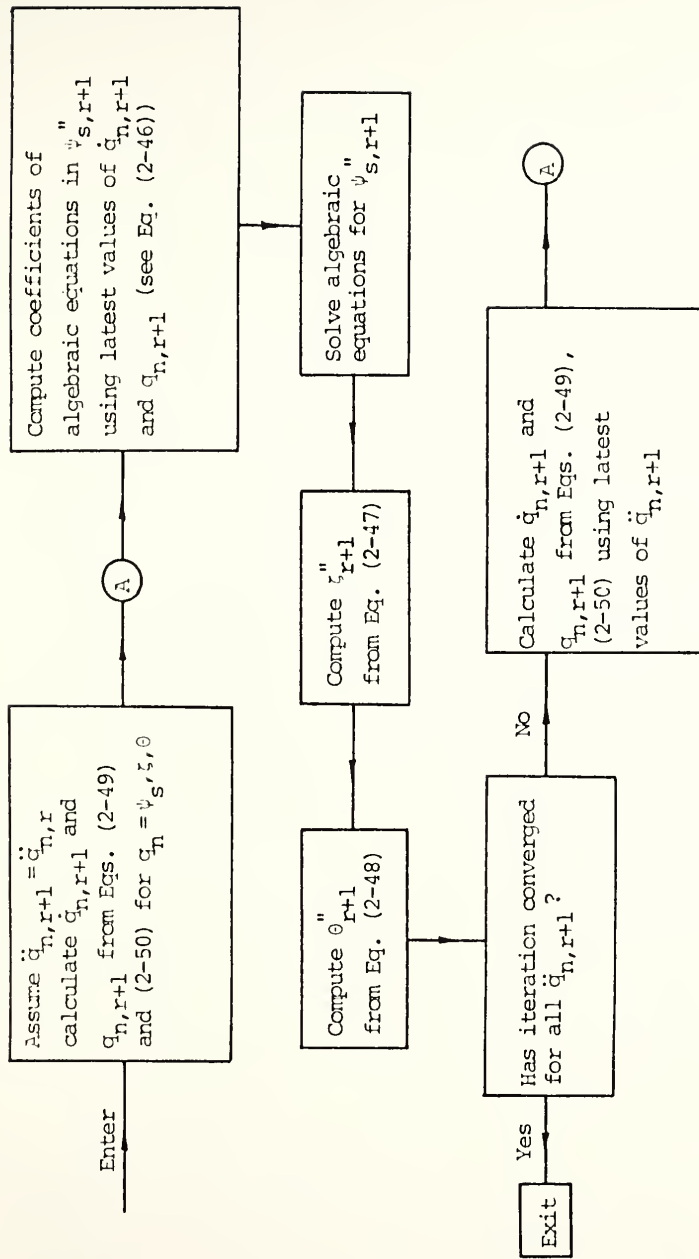


Figure 2.8 Flow Chart of Subroutine (INTEG) for Integration Over Interval  $\Delta t$

where  $D_{i,j}$  = the deflection at midspan of beam  $i$  due to load  $j$ .

$M_{i,j}$  = the moment at midspan corresponding to  $D_{i,j}$ .

$$(C_d)_j = \frac{1}{\pi^2} \sum_{m=1,3,\dots}^{m_o} \frac{1}{m^2} Q_{m,j} \sin m\pi\tau \quad (2-59)$$

$$(C_m)_j = \frac{\lambda_i}{\lambda_o} \sum_{m=1,3,\dots}^{m_o} Q_{m,j} \sin m\pi\tau \quad (2-60)$$

Following this, the subroutines (DOMOIS) and (BNSCNS) are entered to compute and store the values of  $D_{i,s}^o$  and  $M_{i,s}^o$ , and the values of constant coefficients in Eq. (2-46), respectively.

Before starting the integration of the differential equations, the second derivatives of the generalized coordinates  $\ddot{q}_n$  (i.e.,  $\psi''_s$ ,  $\zeta''$ , and  $\theta''$ ), the interacting forces, and the deflections and moments in the bridge are evaluated for  $\tau = 0$  by entering subroutines (INTLS) and (EQMON). The next part of the program is to integrate the governing differential equations numerically and to compute the interacting forces, the deflections, the moments, and the accelerations in the bridge at  $\tau = \tau_r$ . The procedure is done at each time interval,  $\tau_r$ , by use of subroutines (EQMON), (INTEG) and (RESLT), until  $\tau_r = 1$ , or the vehicle leaves the bridge. During the integration procedure, the maximum results of the response are chosen and stored, in order to be printed out afterward. The

response of the bridge can be printed out at the desired step of integration by using the print-out parameter which is read in at the beginning of the program.

The interacting forces, the deflections, the moments and the accelerations of the bridge at each step of time interval can be plotted by using the subroutine (OUT).

The machine time required to obtain a solution depends on the particular problem considered. The total time consists of the following major parts; the time required to read in parameters, the time required to calculate the necessary constants and functions, the time required for the integration procedure and the response computations, and the time required for printing and plotting out the results. The total time required to obtain the response of 60 ft. span bridge with 400 integration steps is approximately 2 minutes and 30 seconds.

## 2.3 Analysis of Static and Dynamic Response of Continuous Highway Bridges

### 2.3.1 General

In this analysis, the bridge is idealized as a single continuous beam and the resulting infinite number of degrees of freedom is replaced by a discrete system having a finite number of degrees of freedom. This discretization is effected by concentrating the distributed mass of the beam into a series of point masses, but considering the flexibility

of the beam to be distributed in the actual system. A vehicle of the tractor-trailer type is represented by a three-axle load unit consisting of two interconnected rigid masses. Each axle is represented by two springs in series and a frictional mechanism which simulates the effect of friction in the suspension spring of the vehicle.

The equations governing the motion of the bridge-vehicle system are formulated in general terms. They can be applied to continuous bridges of any number of spans as well as to simple span bridges or cantilever bridges.

The computer program has been developed for three-span bridges<sup>(29)</sup> having a uniform cross section and equal side spans and for a load unit having a maximum of three axles. This program has been modified for two-span bridges having equal spans for the same load unit. The programs can handle various parameters defining the characteristics of the bridge and the vehicle, the initial conditions of the vehicle, and the roughness surface of the bridge. The programs provide the printed-out and plotted results including the interacting forces, the reactions, the deflections, the moments and the accelerations.

### 2.3.2 Analysis of Three Span Continuous Highway Bridges

#### Idealization of Bridge

The beam used to represent the actual bridge is

analyzed as a system having a finite number of degrees of freedom. The discretization is effected by replacing the distributed mass by a series of concentrated point masses and considering the beam flexibility to be distributed as in the original structure. Bridge damping is assumed to be of the absolute viscous type, and is approximated by a series of dashpots arranged as shown in Figure 2.9.

The magnitude of the concentrated mass at a node is taken equal to the total distributed mass for the portion of the actual beam between midpoints of the panels on either side of that node. Similarly, the coefficient of damping for the associated dashpot is taken equal to the product of the average coefficient of damping per unit of length of the original beam multiplied by the length of the tributary section for the node under consideration. Masses and dashpots attached to rigid supports have no influence on the response of the system and may be neglected. The number of degrees of freedom for the substitute beam is thus equal to the number of deflecting masses involved.

The analysis is based on the ordinary theory of flexure of beams which assumes the material is linearly elastic and the effects of shearing deformation are negligible. Furthermore, as the distributed mass of beam is replaced by concentrated point masses, the rotary inertia effects are not considered.

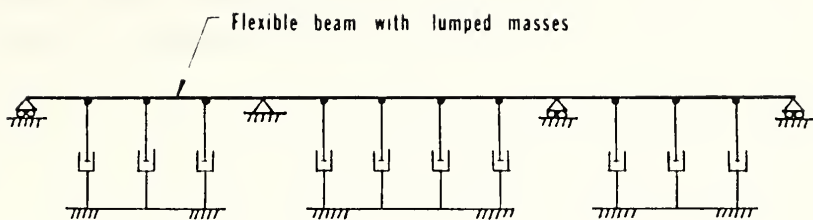


Figure 2.9 Three Span Continuous Bridge Model

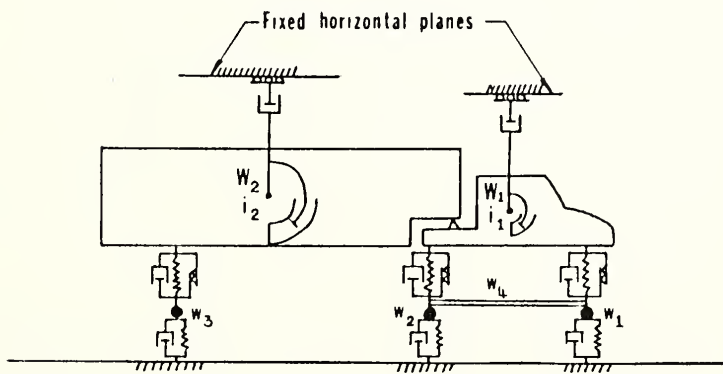


Figure 2.10 Representation of a Tractor-Trailer Type Vehicle

### Idealization of Vehicle

Since the bridge has been idealized as a beam, the width of the vehicle and consequently, the rolling effect cannot be considered in the analysis. Even when treated as a plane system, a vehicle is a very complex mechanical system. Figure 2.10 shows diagrammatically the detailed features of what is believed to be a complete representation of a tractor-trailer combination. The quantity  $w_1$  represents the weight of the tractor mounted on its suspension system. The quantity  $i_1$ , is the dynamic index<sup>(2)</sup> of the tractor. This is a measure of the rotary moment of inertia of the weight  $w_1$ , and it is defined as the ratio of the radius of gyration squared to the product of the horizontal distances between the two supports and the center of gravity of the weight. The dashpots at the center of gravity of  $w_1$  represent damping resistances against vertical motion and rotary motion. The rigid bar represents the chassis of the tractor and its weight is designated as  $w_4$ . The point masses, with weights  $w_1$  and  $w_2$ , represent the mass of the axles, springs, and tires for the two axles. The quantities  $w_2$ ,  $i_2$ , and  $w_3$  refer to the trailer and have the same meaning as that of the corresponding quantities for the tractor. For convenience in presentation, the weights  $w_1$  and  $w_2$  are referred to as "sprung" weights and the remaining weights are referred to as "unsprung" weights.

The dynamic characteristics of the tires for each axle of the vehicle are represented by a spring and a dashpot. The suspension system for each axle is represented by a massless spring, a dashpot, and a frictional device. The dashpot accounts for the effects of shock absorbers or air suspension, and the frictional device accounts for any frictional force that may develop in the suspension system, particularly in the leaf springs. The value of the frictional force developed at any time is designated by  $F$  and the limiting or maximum possible value is designated by  $F'$ . As long as  $-F' < F < F'$  for a particular axle, the suspension spring for that axle is inactive (i.e. only the tire springs deflects), and the effective stiffness of that axle is equal to the stiffness of the tires. On the other hand, if  $F = \pm F'$ , both springs are active and the effective stiffness is that of the two springs acting in series.

In the present analysis the above system is further simplified by (a) neglecting all sources of viscous damping and (b) replacing the "unsprung" weights by concentrated "sprung" weights as shown in Figure 2.11a. In this replacement the weight of the chassis, designated as  $w_4$  in Figure 2.10, is incorporated into the weights  $w_1$  and  $w_2$ . This replacement is justified by the fact that the "unsprung" weights are quite small in comparison to the "sprung" weights. For a representative tractor the ratio

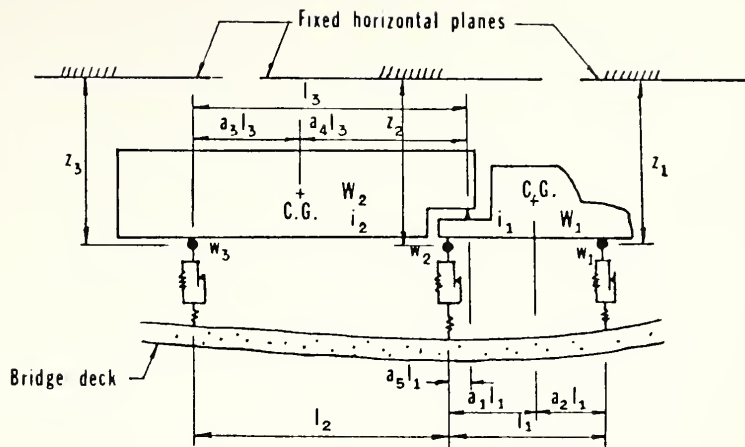
of the total "unsprung" weights to the "sprung" weight is about 1/7, and for a trailer it is for all practical purposes negligible. In addition to the three-axle load unit, in Figure 2.11 are shown specialized models for a two-axle and a single-axle load unit.

With its velocity specified, the three axle load unit shown in Figure 2.11a has three degrees of freedom. The parameters which define its characteristics are:

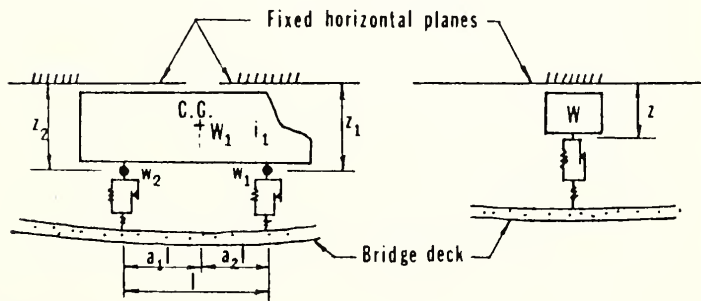
- (a) the weight distribution parameters which include the weights  $w_1$ ,  $w_2$ ,  $w_1'$ ,  $w_2'$  and  $w_3$ , and the dynamic indices  $i_1$  and  $i_2$ ;
- (b) the geometrical parameters which include the axle spacings  $l_1$  and  $l_2$ , and the ratios  $a_1$  through  $a_5$  as defined in Figure 2.11a;
- (c) the stiffness parameters for the tires and the suspension springs; for the  $i^{\text{th}}$  axle ( $i = 1, 2, 3$ ), the stiffness of the tires is denoted by  $k_{t,i}$  and the stiffness of the tires and the suspension springs when acting in series is denoted by  $k_{ts,i}$ ;
- (d) the friction parameters, for the suspension systems of the vehicle. For the  $i^{\text{th}}$  axle this is the limiting frictional force,  $F_i'$ .

#### The Assumptions for the Analysis

The analysis is based on the ordinary beam theory, which neglects the effects of shearing deformation and



(a) Model for Three Axle Vehicle



(b) Model for Two Axle Vehicle

(c) Model for Single Axle Load

Figure 2.11 Vehicle Models

axial forces. In addition, since the distributed mass is treated as a series of point masses, the effect of rotary moment of inertia does not enter in the solution. The vehicle travels with constant speed and is assumed to remain in contact with the bridge at all times, and its angular displacements are considered to be small. It is further assumed that no longitudinal force can develop at the junction of the tractor and trailer. This junction is known as the "fifth wheel pivot". Finally, all springs of the vehicle are considered to be elastic.

#### Equations of Motion for Bridge Model

The motion of the vehicle-bridge system is expressed in terms of the coordinates  $z_i$  and  $y_r$  shown in Figure 2.12. The coordinate  $z_i$  denotes the vertical displacement, measured from a fixed horizontal plane, of the point of support of the vehicle mass for the  $i^{\text{th}}$  axle. The coordinate  $y_r$  denotes the deflection of the  $r^{\text{th}}$  node point of the beam. This deflection is measured from the static equilibrium position when the bridge is subjected to its own weight alone. Both coordinates  $z$  and  $y$  are considered to be positive when downward.

Figure 2.13 shows a three-span continuous bridge model of equal side spans and uniform flexural rigidity,  $EI$ . The length of the center span is denoted by  $L$  and the length of a side span by  $aL$ . The center span is divided into  $m$  equal panels of length  $h$ , and each side span is

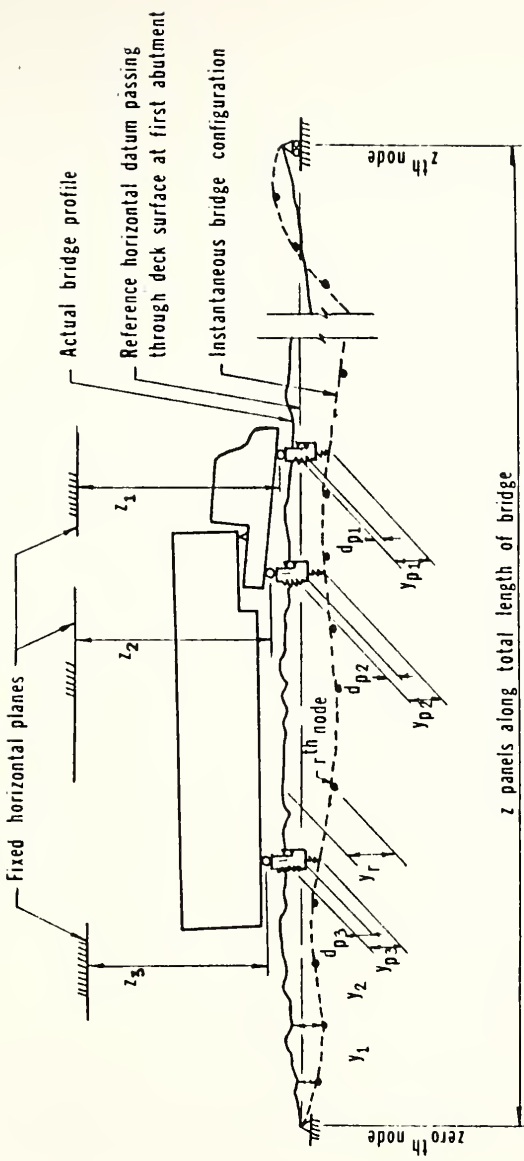


Figure 2.12 Combination of Bridge and Vehicle Model – Any Type of Bridge

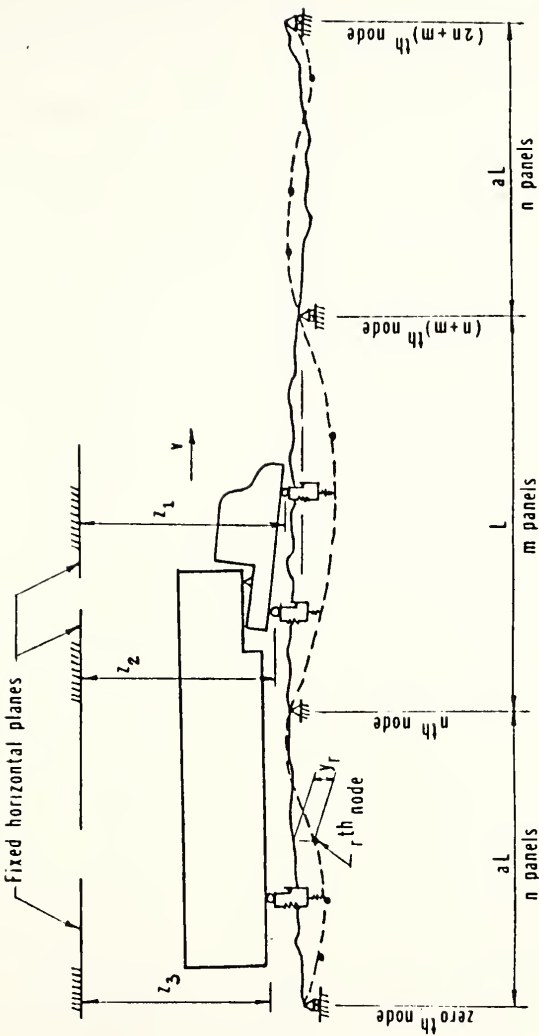


Figure 2.13 Combination of a Three Span Continuous Bridge and Vehicle Models

divided into  $n$  equal panels of length  $\frac{m}{n}ah$ . The nodes are numbered consecutively starting with zero at the left abutment and terminating with  $(2n + m)$  at the right abutment. The panel between nodes  $r$  and  $r - 1$  is designated as the  $r^{\text{th}}$  panel. As before, the mass is considered to be concentrated at the node points.

Let  $P_i$  be the interacting force between the bridge surface and the  $i^{\text{th}}$  axle of the vehicle. Then the equation of motion for the concentrated mass at the  $r^{\text{th}}$  node of the beam,  $m_r$ , may be expressed as follows:

$$m_r \ddot{y}_r + c_r \dot{y}_r - \sum_{j=1}^{2n+m} R_r^j y_j - \sum_{i=1}^3 Q_r^i P_i = 0 \quad (2-61)$$

where  $y_r$  is the deflection of the  $r^{\text{th}}$  node, as previously defined, and a dot superscript denotes one differentiation with respect to time;  $c_r$  is the damping coefficient for the damper at the  $r^{\text{th}}$  node. The quantity  $R_r^j$  is defined as the reaction-deflection coefficient and represents the static reaction at the  $r^{\text{th}}$  node point induced by a unit deflection of the  $j^{\text{th}}$  node point, when all other nodes are supported against deflection. A reaction is considered as positive when directed upward. In an analogous manner,  $Q_r^i$  is defined as the reaction-load coefficient and represents the reaction at the  $r^{\text{th}}$  node point induced by a concentrated unit load at the point of application of  $P_i$  when all nodes are supported

against deflection. Obviously, when the unit load is off the bridge,  $Q_x^i = 0$ . It should be noted that the interacting forces  $P_i$  are not known at this stage. By application of Eq. (2-61) to each mass, one obtains as many equations as there are degrees of freedom for the bridge model.

The reaction-deflection coefficients,  $R_r^j$  are constants for a given bridge model and can be evaluated by a modified moment distribution procedure introduced by T. Y. Lin<sup>(37)</sup>. The procedure makes use of the concept of the effective stiffness and effective carry-over factors which are defined as follows: Consider a bar ab resting on non-deflecting supports and elastically restrained against rotation at end b by a coil spring having a stiffness  $\bar{R}$ . The moment at end a necessary to produce a unit rotation at that end is defined as the effective stiffness of that end of the bar. Denoted by  $K_a'$ , this stiffness is given by the equation,

$$K_a' = [1 - \frac{k_{a,b} k_{b,a} K_b}{K_b + \bar{R}}] K_a \quad (2-62)$$

where  $K_a$  and  $K_b$  are the Hardy-Cross stiffnesses of the bar for the ends a and b respectively. Similarly  $k_{a,b}$  and  $k_{b,a}$  are the Hardy-Cross carry-over factors from ends a to b and from b to a, respectively. The ratio of the moment produced at end b to the applied moment at a is defined as the effective carry-over factor,  $k_{a,b}'$ , and is given by the equation:

$$k'_{a,b} = \frac{\bar{R}}{(1 - k_{a,b} k_{b,a}) K_b + \bar{R}} k_{a,b} \quad (2-63)$$

For a prismatic bar,  $K_a = K_b = K$ ,  $k_{a,b} = k_{b,a} = -1/2$ , and the above equations become

$$K' = [1 - \frac{1}{4} \frac{K}{K + \bar{R}}] K \quad (2-64)$$

and

$$k'_{a,b} = \frac{\bar{R}}{\frac{3}{2} K + 2\bar{R}} \quad (2-65)$$

For a continuous beam the coil spring symbolizes the continuity of a particular span with the adjacent spans.

In the course of calculating the coefficients  $R_r^j$  by this procedure, one calculates also the moments at the nodes due to a unit displacement at the  $j^{th}$  node. These moments are termed as moment-deflection coefficients and are designated by  $J_r^j$ . In evaluating the coefficients  $R_r^j$  and  $J_r^j$ , the following quantities are used. In all cases, it is assumed that the bridge model is supported against deflection at the node points.

(a) Effective Stiffness Coefficients. Consider the portion of the bridge model between the left hand abutment and the  $r^{th}$  node as a beam continuous over non-deflective supports at the nodes. Then the effective stiffness of the beam at end  $r$  may be stated as the product of a

dimensionless stiffness coefficient  $C_r$  and the quantity  $4EI/h$ , where  $h$  refers to the length of a panel in the center span of the bridge model. By application of Eq. (2-64) it can be shown that the coefficient  $C_r$  is given by the following recurrence formula:

$$C_r = \frac{h}{h_r} \left[ 1 - \frac{1}{4} \frac{\frac{h}{h_r}}{\frac{h}{h_r} + C_{r-1}} \right] \quad (2-66)$$

where  $h_r$  is the length of the  $r^{\text{th}}$  panel. For a panel on the center span,  $h_r = h$ ; and for a panel on a side span,  $h_r = \frac{m}{n}ah$ .

It should be noted that, because of symmetry, the dimensionless coefficient for the stiffness at node  $r$  for the portion of the beam between the  $r^{\text{th}}$  node and the right hand support is equal to  $C_{2n+m-r}$ .

(b) Effective Distribution Factors. The effective distribution factor for the right hand side of the  $r^{\text{th}}$  node, designated as  $d_r$ , is given by the expression,

$$d_r = \frac{C_{2n+m-r}}{C_r + C_{2n+m-r}} \quad (2-67)$$

The distribution factor for the left hand side of the  $r^{\text{th}}$  node is  $1 - d_r$ .

(c) Effective Carry-Over Factors. The effective carry-over factor from node  $r$  to node  $r-1$  is designated

as  $k'_{r,r-1}$ . By application of Eq. (2-65), one finds that

$$k'_{r,r-1} = \frac{-C_{r-1}}{\frac{3}{2} \frac{h_r}{h_r} + 2C_{r-1}} \quad (2-68)$$

Since the beam is symmetrical about the center line, it follows that

$$k'_{r,r+1} = k'_{2n+m-r, 2n+m-r-1}$$

For the sake of brevity, in the following discussion the quantity  $k'_{r,r-1}$  is designated as  $k'_r$ .

To determine the moment-deflection coefficients  $J_r^j$  and the reaction-deflection coefficients  $R_r^j$ , the  $j^{th}$  node of the model is first displaced by a unit amount, and by keeping all nodes fixed against rotation the fixed-end moments produced at the nodes  $(j-1)$ ,  $j$  and  $(j+1)$  are evaluated. The resulting unbalanced moments (if  $h_j = h_{j+1}$ , there is no unbalanced moment at the  $j^{th}$  node) are then distributed and carried over by use of the quantities given in Eqs. (2-67) and (2-68). The final moments at the nodes yield the coefficients  $J_r^j$ . The reaction-deflection coefficients  $R_r^j$  are next evaluated from the equation

$$R_r^j = \frac{J_{r-1}^j - J_r^j}{h_r} - \frac{J_r^j - J_{r+1}^j}{h_{r+1}} \quad (2-69)$$

The quantities  $C_r$  and  $d_r$  are used only to evaluate the coefficients  $R_r^j$  and  $J_r^j$ , whereas the carry-over factors

$k'$  and the quantities  $R_r^j$  and  $J_r^j$  are used repeatedly in later stages of the solution.

Another quantity needed in subsequent computation is the total angle change produced at the  $r^{th}$  node when the beam is cut at the  $r^{th}$  node and a unit bending moment is applied on the two sides of that node. As before, all nodes are assumed to be held against deflection. This angle change is denoted by  $\theta_2$  and is given by the expression,

$$\theta_r = \left[ \frac{1}{C_r} + \frac{1}{C_{2n+m-r}} \right] \frac{h}{4EI}$$

By use of Eq. (2-68), the above expression may be written as

$$\theta_r = \frac{h}{EI} \left[ \frac{h_r}{h} \left( \frac{2}{3} + \frac{1}{3} k_r' \right) + \frac{h_{r-1}}{h} \left( \frac{2}{3} + \frac{1}{3} k_{2n+m-r}' \right) \right] \quad (2-70)$$

It should be emphasized that the quantities defined above depend only on the characteristics of the bridge model.

#### Equations of Motion for a Vehicle

Let  $P_{st,i}$  be the reaction at the  $i^{th}$  axle when the vehicle is in a position of static equilibrium. With  $P_i$  denoting the dynamic reaction at any time  $t$ , the disturbing force for the  $i^{th}$  axle is  $P_i - P_{st,i}$  and the equation of motion for a three-axle vehicle can be stated in the form:

$$\begin{bmatrix} a_{11} & a_{12} & a_{13} \\ a_{12} & a_{22} & a_{23} \\ a_{13} & a_{23} & a_{33} \end{bmatrix} \begin{bmatrix} \ddot{z}_1 \\ \ddot{z}_2 \\ \ddot{z}_3 \end{bmatrix} = -\frac{g}{W} \begin{bmatrix} p_1 - p_{st,1} \\ p_2 - p_{st,2} \\ p_3 - p_{st,3} \end{bmatrix} \quad (2-71)$$

where  $g$  is the gravitational acceleration,  $W$  is the total weight of the vehicle, and  $a_{11}$  through  $a_{33}$  are dimensionless coefficients given by the following expressions:

$$\begin{aligned} a_{11} &= (a_1^2 + a_1 a_2 i_1) \frac{w_1}{W} + a_5^2 (a_3^2 + a_3 a_4 i_2) \frac{w_2}{W} + \frac{w_1}{W} \\ a_{12} &= a_1 a_2 (1 - i_1) \frac{w_1}{W} + a_5 (1 - a_5) (a_3^2 + a_3 a_4 i_2) \frac{w_2}{W} \\ a_{13} &= a_3 a_4 a_5 (1 - i_2) \frac{w_2}{W} \\ a_{22} &= (a_2^2 + a_1 a_2 i_1) \frac{w_1}{W} + (1 - a_5)^2 (a_3^2 + a_3 a_4 i_2) \frac{w_2}{W} + \frac{w_2}{W} \\ a_{23} &= a_3 a_4 (1 - a_5) (1 - i_2) \frac{w_2}{W} \\ a_{33} &= (a_4^2 + a_3 a_4 i_2) \frac{w_2}{W} + \frac{w_3}{W} \end{aligned} \quad (2-72)$$

The details of derivation are presented in Ref. (29).

Premultiplication of Eq. (2-71) by the inverse of matrix  $\Lambda$  yields,

$$\begin{bmatrix} \ddot{z}_1 \\ \ddot{z}_2 \\ \ddot{z}_3 \end{bmatrix} = \frac{q}{W} \begin{bmatrix} b_{11} & b_{12} & b_{13} \\ b_{12} & b_{22} & b_{23} \\ b_{13} & b_{23} & b_{33} \end{bmatrix} \begin{bmatrix} P_1 - P_{st,1} \\ P_2 - P_{st,2} \\ P_3 - P_{st,3} \end{bmatrix}. \quad (2-73)$$

Let  $u_i$  be the shortening of the suspension-tire system of the  $i^{\text{th}}$  axle. The relationship between the interacting force,  $P_i$ , and the shortening,  $u_i$ , of the combined suspension-tire system is shown in Figure 2.14. Also included in this figure is a diagram showing the relationship between  $u_i$  and the frictional force,  $F_i$ .

As the load,  $P$ , is increased above its initial value,  $P_{st}$ , the deformation of the tire spring increases linearly, but the suspension spring does not deform at first, the initial increase in the load of the suspension system being resisted entirely by friction. The initial paths, oa, of the  $P-u$  diagram and the  $F-u$  diagram in Figure 2.14 are, therefore, parallel, and the slope of these paths is equal to the stiffness of the tire spring,  $k_t$ . This relationship continues until the frictional force attains its limiting value,  $F'$ . At that stage, the suspension spring engages, and the effective stiffness of the tire-suspension system becomes equal to the stiffness,  $k_{ts}$ , of the two springs acting in series, in which

$$\frac{1}{k_{ts}} = \frac{1}{k_t} + \frac{1}{k_s} \quad (2-74)$$

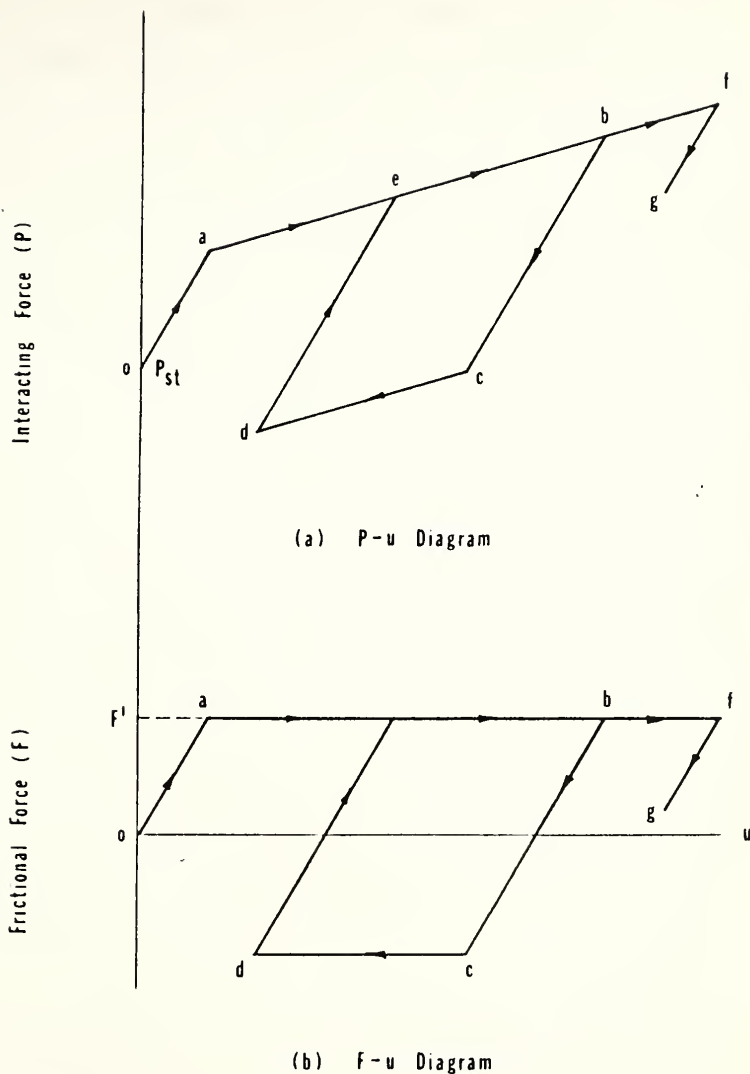


Figure 2.14 Force Deformation Relationships for Tire Suspension System for Vehicle

and  $k_s$  is the stiffness of the suspension spring. It follows that, along the segments ab, the slope of the P-u<sub>s</sub> diagram is  $k_s$ , the slope of the P-u diagram is  $k_{ts}$ , and the frictional force has its limiting value,  $F'$ . Now, if at the load corresponding to points b of the diagrams the direction of loading were reversed, the tire spring would rebound elastically, but the deformation of the suspension spring would not change, as the decrease in load would be resisted entirely by friction. The force in the frictional device would decrease at the same rate as the load, and the unloading paths, bc, on both the P-u diagram and the F-u diagram would be parallel to each other and to the initial loading path, oa. This condition would continue until the load is reduced by  $2F'$ , at which time the frictional force would attain its limiting value in the negative direction, and the suspension spring would once again engage. A possible path on these diagrams beyond this point is represented by the segments ed - de - ef - fg. This behavior is in good agreement with available test data (25) (26).

To summarize, the parameters that define the behavior of a tire-suspension system are the stiffness of the two springs,  $k_t$  and  $k_s$ , and the limiting value of the frictional force,  $F'$ . The latter force may conveniently be expressed in the form

$$F' = \mu P_{st} \quad (2-75)$$

in which  $\mu$  = a dimensionless coefficient, referred to as the "coefficient of interleaf friction".

#### Evaluation of Interacting Forces

Equations (2-61) and (2-71) are coupled through the interacting forces  $P_i$ , which remain to be evaluated. Let time,  $t$ , be measured from the instant the first axle enters the bridge. Then the interacting force at time  $t$  is given by the equation

$$P_i = P_i \Big|_{t=0} + \int_0^t k_i \frac{du_i}{d\tau} d\tau \quad (2-76)$$

where  $P_i \Big|_{t=0}$  is the initial value of  $P_i$ ,  $k_i$  is the instantaneous effective stiffness of the suspension-tire system for the  $i^{th}$  axle at any time,  $\tau$ , and  $u_i$  is the corresponding shortening of the suspension-tire system. If at the instant it enters the bridge, the vehicle is at the position of static equilibrium, the initial force  $P_i \Big|_{t=0} = P_{st,i}$ . The instantaneous stiffness  $k_i$  depends on the history of the shortening  $u_i$  as shown in Figure 2.14.

The shortening  $u_i$  can be expressed in the form

$$u_i = z_i + d_{pi} - y_{pi} \quad (2-77)$$

where  $z_i$  is the coordinate for the  $i^{th}$  axle, as previously

defined, and  $d_{Pi}$  is the deviation of the bridge profile at the point of application  $P_i$ . This deviation is measured from a horizontal line passing through the first abutment of the bridge, as shown in Figure 2.12. The quantity  $y_{Pi}$  represents the deflection of the bridge at the point where  $P_i$  acts.

The term "bridge deviation" includes the dead load deflection, initial camber, grade, vertical curve and roadway unevenness. For a given bridge, these quantities may be presumed to be known. This deviation is considered to be positive when upward. The deflection  $y_{Pi}$  is measured from the static equilibrium position of the beam, when acted upon by its own weight, and it is positive when downward.

#### Computation of the Response

Application of Eqs. (2-61) and (2-73) to each concentrated mass of the bridge model and to each axle of the vehicle yields a set of simultaneous, second order differential equations, equal in number to the number of degrees of freedom of the bridge-vehicle system. These equations can be solved by a numerical integration method in which the evaluation of the interacting forces  $P_i$  is a major intermediate step.

As the integration of the differential equations is carried out, the values of all the coordinates, of all

accelerations at nodes, and of the interacting forces are determined. From these quantities the values of the corresponding deflections, moments and reactions at any desired section may then be evaluated by statics.

#### Integration of Equations of Motion

The differential equations of motion defined by Eqs. (2-61) and (2-73) have been integrated numerically using an iterative procedure within each integration step. To describe the method, assume at some time,  $t_s$ , the values of all displacements and of their first two derivatives are known, and it is desired to determine the corresponding quantities at time:

$$t_{s+1} = t_s + \Delta t \quad (2-78)$$

in which  $\Delta t$  is a small time interval. In the method used, an assumption must first be made concerning the manner in which the accelerations vary within the interval,  $\Delta t$ . This variation is assumed to be linear in the present study. The velocities and displacements at  $t_{s+1}$  can then be determined in terms of the known quantities at  $t_s$  and the unknown acceleration at  $t_{s+1}$  by use of the following recurrence formulas:

$$\dot{q}_{r,s+1} = \dot{q}_{r,s} + \frac{1}{2} \Delta t \ddot{q}_{r,s} + \frac{1}{2} \Delta t \ddot{q}_{r,s+1} \quad (2-79)$$

$$q_{r,s+1} = q_{r,s} + \Delta t \dot{q}_{r,s} + \frac{1}{3} (\Delta t)^2 \ddot{q}_{r,s} + \frac{1}{6} (\Delta t)^2 \ddot{q}_{r,s+1} \quad (2-80)$$

in which  $q_r$  is either the displacement of a node,  $y_j$ , or the displacement of a point of support of the vehicle,  $z_i$ ; a dot subscript denotes differentiation with respect to time; and the subscripts  $s$  and  $s+1$  following a comma identify quantities corresponding to times  $t_s$  and  $t_{s+1}$  respectively. Next, the unknown accelerations at  $t_{s+1}$  are evaluated by satisfying the equations of motion at that instant. The details of the iterative procedure used are as follows:

1. Define the longitudinal position of each axle of the vehicle at time  $t_{s+1}$ .
2. Assume the accelerations  $\ddot{y}_j$  and  $\ddot{z}_i$  at  $t_{s+1}$  are the same as those at  $t_s$ , and, by application of Eqs. (2-79) and (2-80) determine approximate values for the velocities,  $\dot{y}_{j,s+1}$  and  $\dot{z}_{i,s+1}$  and for the displacements,  $y_{j,s+1}$  and  $z_{i,s+1}$ .
3. Determine improved values for  $\ddot{y}_{j,s+1}$ ,  $\dot{y}_{j,s+1}$  and  $y_{j,s+1}$  by proceeding as follows:

a) By application of Eq. (2-61) to the first node,  $r = 1$ , obtain an improved estimate for  $\ddot{y}_{1,s+1}$ . The major operation in this step is the computation of the quantities  $\sum_j R_1^j Y_j$  and  $\sum_i Q_1^i P_i$ . The values of  $P_i$  used in this step are those corresponding to the beginning of the time interval, i.e.,  $P_{i,s}$ , and the values of  $y_j$  and  $\dot{y}_j$  are the approximate values determined in Step 2.

b) From Eqs. (2-79) and (2-80) calculate the values of  $\dot{y}_{1,s+1}$  and  $y_{1,s+1}$  corresponding to the acceleration

$\ddot{y}_{1,s+1}$  determined in Step 3a.

c) Repeat Steps 3a and 3b for the remaining nodes ( $r = 2, 3, \dots, 2n+m$ ), considering successively one node at a time. In each computation, use the latest available values of  $y_i$ ,  $z_i$  and their derivatives.

4. Determine improved values for  $\ddot{z}_{i,s+1}$ ,  $\dot{z}_{i,s+1}$  and  $z_{i,s+1}$  proceeding as follows:

a) Compute a first approximation for  $P_{1,s+1}$ , the value of the first interacting force at the end of the time interval. The various steps involved in this computation are described in detail in the following section.

b) Evaluate  $\ddot{z}_{1,s+1}$  from Eq. (2-73), using the latest available values of  $P_i$ . The value of  $P_1$  used is that determined in Step 4a, and the values of  $P_2$  and  $P_3$  are those corresponding to the beginning of the time interval.

c) From Eqs. (2-79) and (2-80) determine the values of  $\dot{z}_{1,s+1}$  and  $z_{1,s+1}$  corresponding to the acceleration computed in Step 4b.

d) Repeat Steps 4a and 4c for the remaining axles, considering one axle at a time and always using the latest available values of  $P_i$  and  $z_i$ .

5. Compare the derived accelerations with the previously available values. If the difference between the initial and derived values for any one coordinate exceeds a prescribed tolerance, repeat Steps 3 through 5,

always using the latest available values of  $P_i$ ,  $z_i$ ,  $y_j$  and their derivatives. When all differences are less than the prescribed tolerance, the integration for the time interval under consideration is completed. One then proceeds to the next time interval and repeats the process.

In the computation of  $P_{i,s+1}$  needed in Steps 4a and 4d, it is assumed that the effective stiffness of the suspension-tire system remains constant within a time interval of integration. Under this assumption, Eq. (2-76) may be rewritten in the form

$$P_{i,s+1} = P_{i,s} + (\Delta u_i) k_i$$

or

$$P_{i,s+1} = P_{i,s} + (u_{i,s+1} - u_{i,s}) k_i \quad (2-81)$$

The value of  $u_{i,s+1}$  is determined by Eq. (2-77). The value of  $y_{Pi}$  in this equation is evaluated by superimposing the following three components: (i) deflection due to the moments acting at the two ends of the panel; (ii) deflection due to the force or forces  $P_i$  acting on the panel; and (iii) deflection due to a rigid body displacement of the panel. The deflection  $y_{Pi}$  must be evaluated for each cycle of iteration in the integration process, since the values of  $y_j$  and  $P_i$  vary from one cycle to the next.

The value of  $k_i$  in Eq. (2-81) is determined by making use of the F-u diagram for that axle, as shown in Figure 2.14.

Let the frictional force corresponding to  $u_{i,s}$  be denoted by  $F_{i,s}$ . In the F-u diagram, imagine a straight line which passes through the point  $(u_{i,s}, F_{i,s})$  and is parallel to the initial line oa. Let  $u_{i,s}^u$  be the abscissa of the point of intersection of this inclined line and a horizontal line corresponding to the positive value of  $F'$ . Similarly, let  $u_{i,s}^l$  represent the point of intersection of this inclined line with a horizontal line corresponding to the negative value of  $F'$ . Then the value of  $k_i$  is determined from the following criteria:

$$\begin{array}{llll} \text{case 1} & u_{i,s} + \Delta u_i \leq u_{i,s}^u & k_i = k_{t,i} \\ \text{case 2} & u_{i,s} + \Delta u_i > u_{i,s}^u & k_i = k_{ts,i} \\ \\ \text{case 3} & u_{i,s} + \Delta u_i > u_{i,s}^l & k_i = k_{t,i} \\ \text{case 4} & u_{i,s} + \Delta u_i \leq u_{i,s}^l & k_i = k_{ts,i} \end{array}$$

It follows that the selection of  $k_i$  depends only on the value of  $\Delta u$ ,  $u^u$  and  $u^l$ . The value of  $F$  need not be computed. For cases 1 and 3 the values of  $u^u$  and  $u^l$  at time  $t_{s+1}$  are the same as those at time  $t_s$ , whereas for cases 2 and 4 they differ by the amount  $\Delta u$ .

The time interval or integration employed should be sufficiently small so that successive cycles of iteration converge and the resulting solution is stable and accurate. For a linear system, it has been shown<sup>(35)</sup> the method used is convergent if the integration step

$$\Delta t \leq 0.389 T$$

(2-82)

in which  $T$  is the shortest natural period of vibration of the system. The total time between the instant the front axle enters the bridge and the instant the last axle leaves the bridge is  $(1 + 2a + S_1 + S_2)L/v$ . Let  $N$  be the number of steps used for a complete solution, then

$$N > \frac{(1 + 2a + S_1 + S_2)L}{0.389 VT} \quad (2-83)$$

### 2.3.3 Analysis of Two-Span Continuous Highway Bridges

The method of analysis is the same as that used to solve the three span continuous bridges. The only difference between the two methods is the bridge model used in the analysis. The bridge model in this case is a two span continuous beam of equal spans and uniform flexural rigidity,  $EI$ , as shown in Figure 2.15. The length of either span is denoted by  $L$ . Both spans are divided into  $n$  equal panels of length  $h$  and the total number of nodes is  $2n$ . As before, the mass is considered to be concentrated at the node points. The total time for the vehicle to cross the bridge is  $(2 + S_1 + S_2)L/v$ .

### 2.3.4 Computer Programs

The method described in the preceding articles has been programmed<sup>(29)</sup> for digital computation of the dynamic response of uniform continuous bridges. Two different

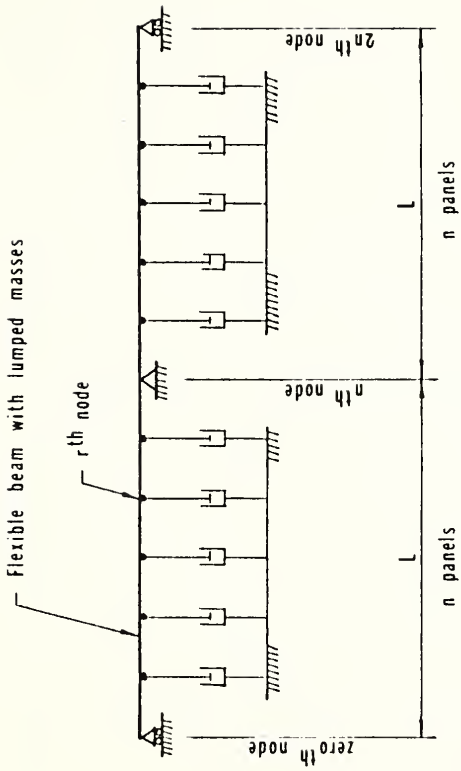


Figure 2.15 Two Span Continuous Bridge Model

programs have been prepared. The first program was developed to compute the static and dynamic histories of uniform three-span continuous bridges with equal side spans when traversed by a single vehicle load having either one, two or three axles, while the other has been modified to compute the dynamic response of uniform two-span continuous bridges with equal span lengths when traversed by the same characteristics of a vehicle load.

Both programs can handle either the dimensional or non-dimensional input and provide the output of static and dynamic histories including the reactions at the supports, the moments over the interior piers, the moments and deflections at selected points on the spans, the interacting forces between the axles of the vehicle and the bridge, and the accelerations of the bridge at node points. The programs also provide the maximum values of these results and can plot out the static and dynamic histories by using a suitable plotting device.

#### Description of Three-Span Program

A general flow diagram for the complete program is shown in Figure 2.16. The program can be divided into three major parts. The function of each part and the sequence of operations involved are described in the following.

(a) Part I The program starts with input of the parameters specifying the characteristics of the vehicle and bridge, excluding those parameters which specify the

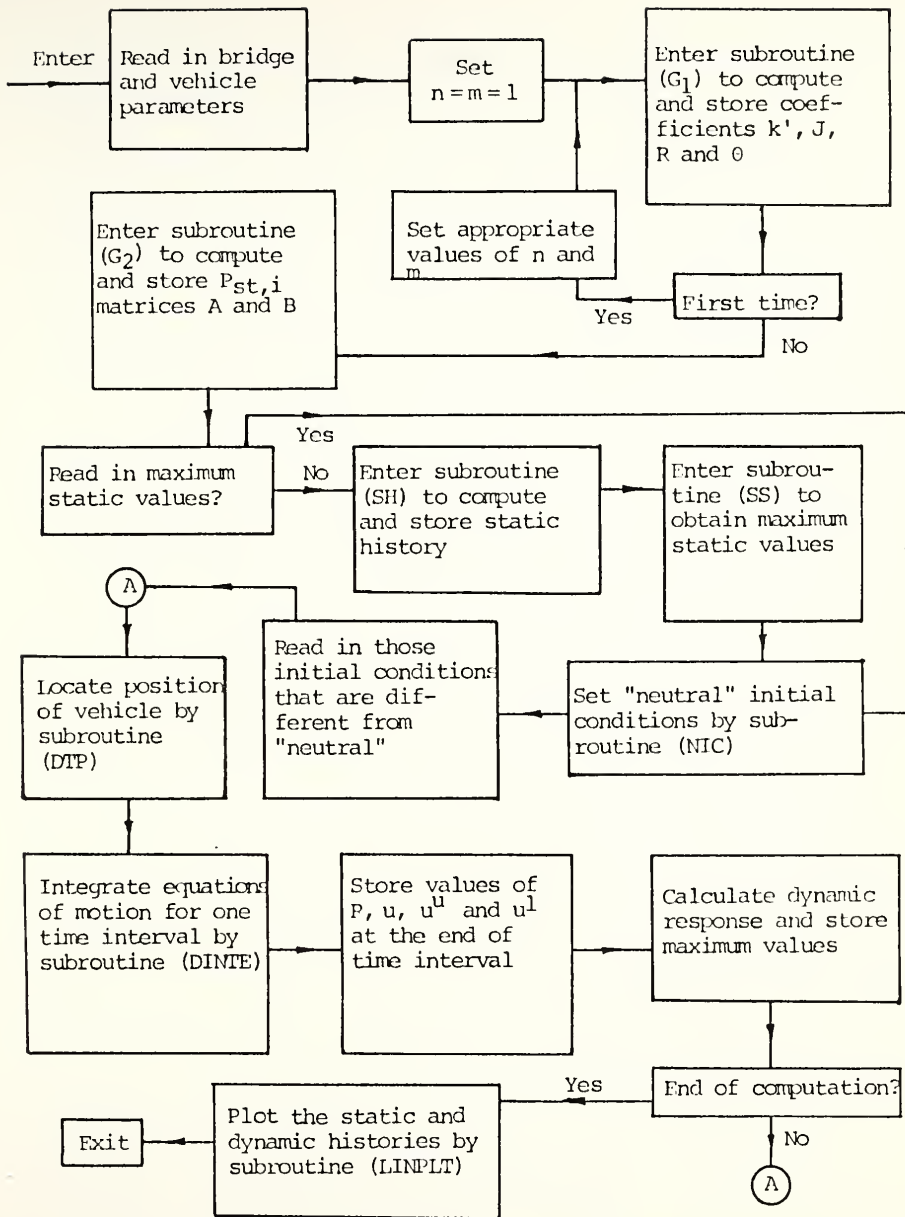


Figure 2.16 General Flow Chart for Complete Program

initial conditions of the system. Next the subroutine ( $G_1$ ) is entered, and the constants including the effective carry-over factors,  $k_r^j$ , the moment-deflection coefficients,  $J_r^j$ , the reaction-deflection coefficients,  $R_r^j$ , and the angle coefficients,  $\theta_r$ , are computed and stored. The coefficients required for the static computation are determined by taking  $n=m=1$ . Following this, subroutine ( $G_2$ ) is entered to compute the value of  $P_{st}$  and the elements of the matrix B in Eq. (2-73). The values of  $P_{st}$  are determined in terms of the parameters specifying the geometry and weight distribution of the vehicle. The matrix B is determined by first forming matrix A in Eq. (2-71) and then inverting it.

(b) Part II This part performs three major tasks. The first step is the determination of the maximum static effects using subroutines (SH) and (SS). Subroutine (SH) determines the static history and subroutine (SS) selects the maximum static values. Both subroutines make use of a number of subroutines, of which the most important are (a) subroutine (DTP), which defines the position of the axles on the bridge, (b) subroutine (SMD), as shown in Figure 2.17, which calculates the static moments and deflections at any specified point on the bridge by use of subroutines (SCM), (SDCP), (STMOME), (STAREA), (SMRP) and (STREAC).

In this part of the computation the characteristic coefficients corresponding to  $n=m=1$  are used. If the

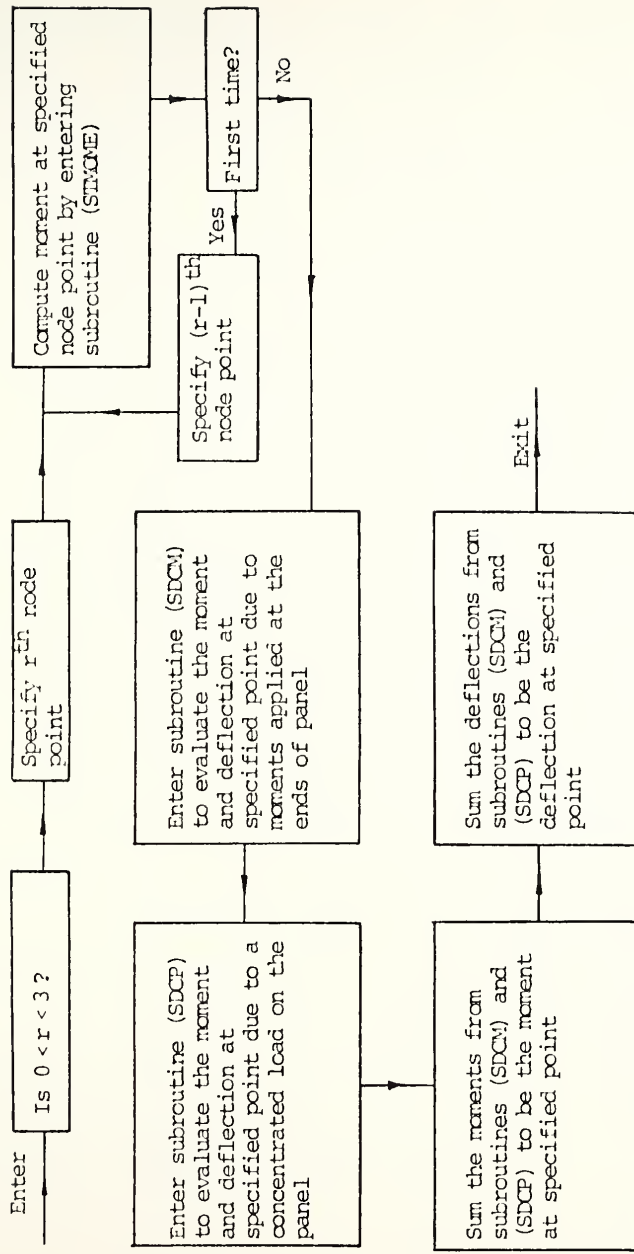


Figure 2.17 Flow Chart for Subroutine (SMD) to Compute Static Moment and Deflection at Any Specified Point

maximum static effects are known, they may be fed into the machine at the beginning of the problem and the calculation of the maximum static values is bypassed by transferring control directly to the next operation.

The second function of this part of the program is to set the initial conditions of the problem at the so-called "neutral condition". This is done by subroutine (NIC). If the initial conditions are different from these, the appropriate parameters are read in at this stage.

The third function is performed by subroutine ( $G_3$ ) to establish for each axle the values of  $u^u$  and  $u^\ell$  which are consistent with the initial values of  $F_i$ . Three values are required to determine the value of the effective stiffness of the suspension-tire system.

(c) Third Part The principal functions of the third part are to integrate Eqs. (2-61) and (2-73) numerically and to compute dynamic deflections, moments, reactions and accelerations. The major operations involved are:

(i) To determine the position of the vehicle at the end of each time interval by use of subroutine (DTP).

(ii) To integrate the equations of motion for this time interval, and to store the values of  $P$ ,  $u$ ,  $u^u$  and  $u^\ell$  at the end of this time interval. This operation is carried out by subroutine (DINTE) as shown in Figure 2.18.

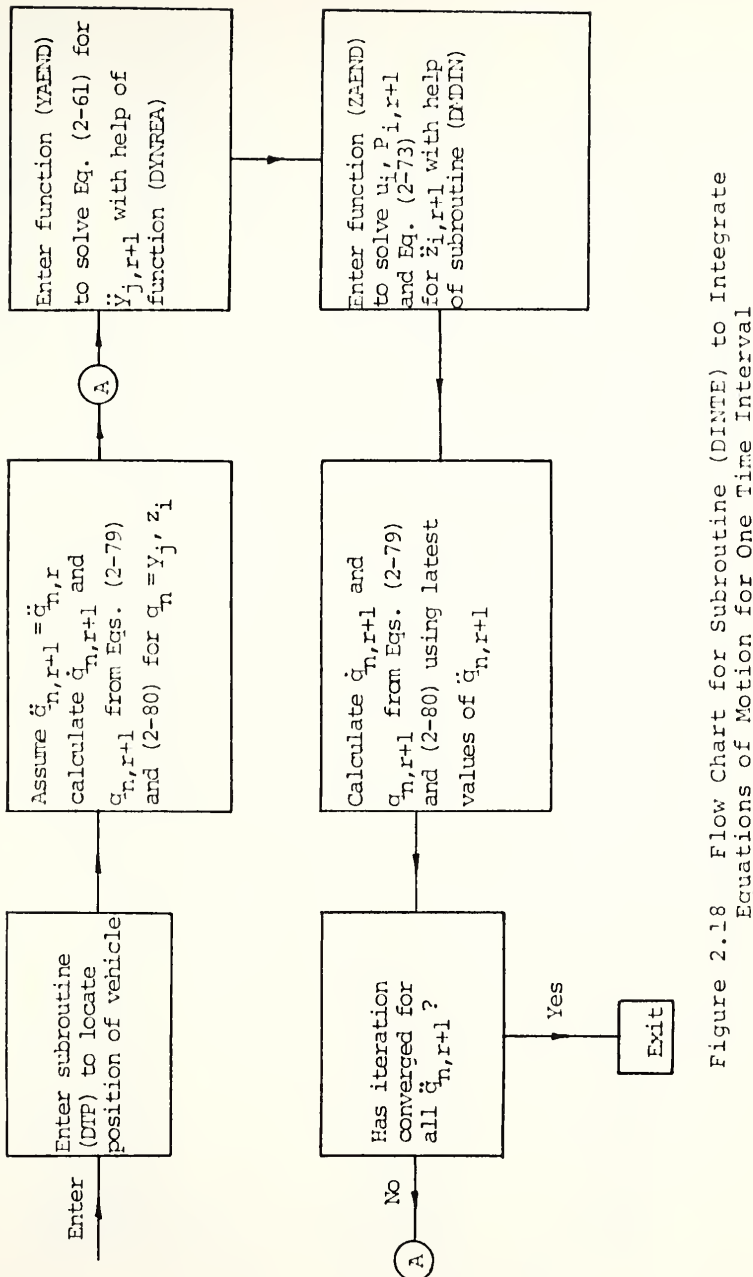
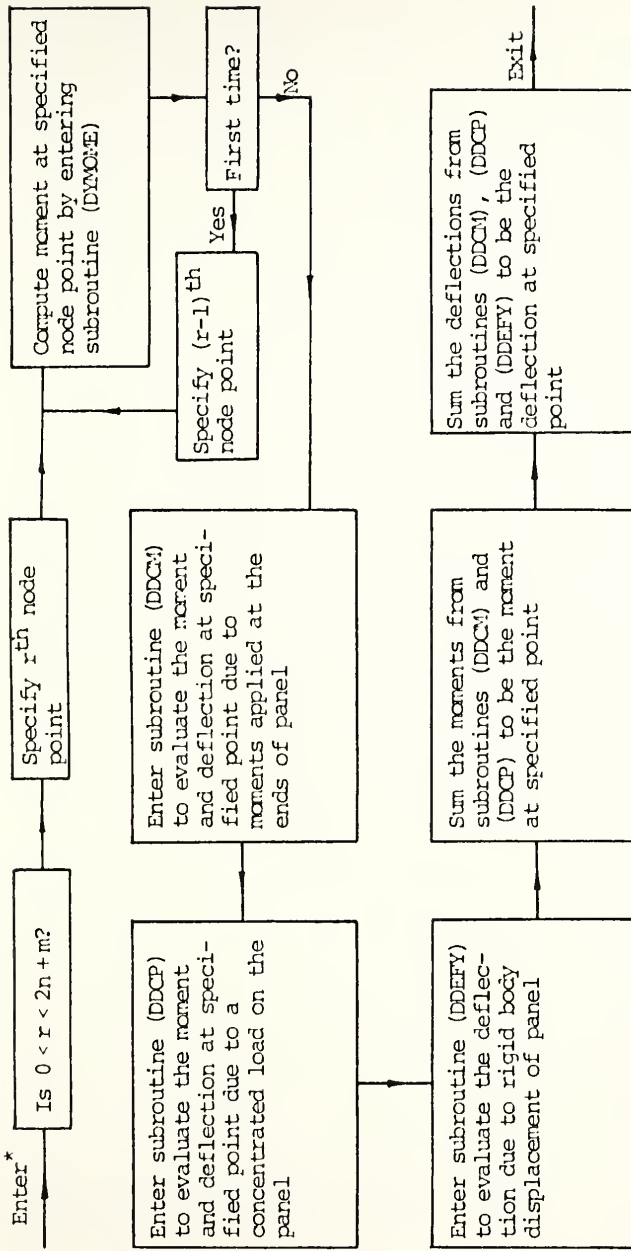


Figure 2.18 Flow Chart for Subroutine (DINTE) to Integrate Equations of Motion for One Time Interval



\* Before entering this subroutine, the coordinate of the point is specified where the deflection and moment are to be evaluated, let this point be on the  $r^{\text{th}}$  panel, and the value of  $r$  is ( $0 < r < 2n + m$ ).

Figure 2.19 Flow Chart for Subroutine (DMD) to Calculate Dynamic Moment and Deflection at Any Specified Point

(iii) To evaluate dynamic deflections, moments and reactions by use of subroutine (DMD) as shown in Figure 2.19. Subroutine (DMD) makes use of subroutines (DMMDM), (DMDP), (DDCM), (DDCP), (DYMOME), (DYNREA), (DYREAC), (DMRP), (DMDIN) and (DDEFY). Since these quantities are computed at the end of each time interval and are compared with the previous values, the maximum values can then be obtained. The foregoing steps are repeated until the last interval is reached.

#### Description of the Two-Span Program

The three-span program was modified to be used to compute the dynamic response of two span continuous bridges by changing some subroutines in the following way:

a) The stiffness properties of the two span bridge are obtained by using subroutine ( $G_1$ ) of the three-span program using as input three equal spans, the third of which has a moment of inertia of zero. The modified moment distribution is used and the coefficients including the effective carry-over factors,  $k_r'$ , the moment-deflection coefficients,  $J_r^j$ , the reaction-deflection coefficients,  $R_r^j$ , and the angle coefficients,  $\theta_r$ , are computed and stored for use in the rest of the program. Those coefficients calculated for the second span are moved into the third span position, therefore the second span is skipped.

b) All subprograms are altered so the truck moves off of the first span to the third span and the stiffness properties calculated as above are for the first span joined directly to the third span. By creating the two-span program in this way, the bookkeeping required for getting a truck on or off the bridge does not need to be altered.

## CHAPTER III

### ACCELERATION STUDIES OF SIMPLE SPAN HIGHWAY BRIDGES

#### 3.1 General

The purpose of this chapter is to study the major parameters which affect the accelerations of the simple-span highway bridges under a moving single-axle vehicle. The study is based on the method of analysis and computer program described in Art. 2.2. The sources of information used in this chapter include the Standard Plans of Highway Bridge Superstructures of the U.S. Bureau of Public Roads (hereafter abbreviated as B.P.R.)<sup>(41)</sup>. The study is restricted to bridges of I-beam type composed of steel girders and a reinforced concrete deck with non-composite action, and the side curbs of the bridge are not taken into account. All frequencies of the bridges in this chapter are natural fundamental frequencies and no damping is considered for either the vehicle or the bridge. Throughout this chapter, the acceleration under discussion is at midspan.

The major parameters that affect the acceleration of the bridge can be classified into the following four groups:

- a) Solution parameters to assure the convergence and stability of the solutions.
- b) Bridge parameters including the span length, the width and the flexibility of the girder.
- c) Vehicle parameters including the number of wheels, the velocity and the transverse position of wheels on the bridge.
- d) Parameters expressing the initial conditions of the bridge including the surface roughness.

### 3.2 Solution Parameters

In the analysis of simple span bridges described in previous chapter, the following parameters are needed to assure the convergence and stability of the solutions:

- a) The number of integration steps ( $N$ ).
- b) The maximum number of terms used in the longitudinal direction in the computation of the static effects ( $m_o$ ).
- c) The maximum number of  $Y_n$  functions used in static computation ( $n_o$ ).
- d) The maximum number of  $Y_n$  functions used in the equations of motion ( $n_1$ ).

In a previous study by Oran<sup>(28)</sup>, it was shown that convergence of the static results was satisfied by using fifteen terms in the trigonometric series expression ( $m_o = 15$ ) and eight  $Y_n$  functions ( $n_o = 8$ ). Table 3.1

Table 3.1 Comparison of Accelerations Obtained by Using Different Numbers of Integration Step

x/I <sub>c</sub>	N	Accelerations at Midspan		
		Edge Beam	Beam No. 2	Center Beam
0.20	200	-0.255277	-0.297954	-0.315632
	300	-0.253380	-0.298322	-0.316935
	400	-0.252714	-0.298451	-0.317395
	500	-0.252405	-0.298511	-0.317608
	600	-0.252237	-0.298543	-0.317723
	200	-0.159955	-0.410796	-0.514699
0.50	300	-0.159984	-0.411008	-0.514935
	400	-0.160029	-0.411076	-0.515064
	500	-0.160055	-0.411107	-0.515096
	600	-0.160072	-0.411124	-0.515113
	200	-0.258546	-0.331062	-0.361099
0.80	300	-0.266470	-0.329931	-0.356219
	400	-0.269257	-0.329532	-0.354500
	500	-0.270549	-0.329347	-0.353702
	600	-0.271251	-0.329246	-0.353269
	200	0.103452	0.159115	0.182171
1.00	300	0.112092	0.156269	0.174567
	400	0.115142	0.155268	0.171888
	500	0.116558	0.154804	0.170645
	600	0.117327	0.154551	0.169969

shows the solutions for the accelerations at midspan considering different numbers of integration steps. The accelerations are obtained at the different vehicle positions on the bridge. The vehicle is a single-axle loading consisting of two wheels and moves in the longitudinal direction of the bridge. The vehicle enters and leaves the bridge when the values of  $x/L$  are equal to zero and one, respectively. The characteristics of the bridge and vehicle are defined by the following non-dimensional parameters:  $c = 0.4$ ,  $\lambda = 12.5$ ,  $k = 0$ ,  $\gamma = 0.05$ ,  $\rho = 0.5$ ,  $\omega = 0$ ,  $\alpha = 0.15$ ,  $\mu = 0.2$ ,  $\kappa = 0.25$ ,  $n_1 = 0.35$ ,  $n_2 = 0.65$ ,  $m_o = 15$ ,  $n_o = 8$ ,  $n_1 = 4$ ,  $n_2 = 4$  and the bridge model is a five girder bridge. Both the bridge and the vehicle are assumed to be initially in their static positions of the equilibrium, and the bridge has a level surface. It can be seen from Table 3.1 that the accelerations converge with the increasing values of  $N$ . Since the computer cost is higher when  $N$  is larger, and there are small differences of the acceleration values between 400 and 600 steps of integration, 400 integration steps were used.

Table 3.2 shows the results for the accelerations at midspan which are computed by using different numbers of  $Y_n$  functions. Since the  $Y_n$  functions have been used to specify the transverse configuration of the bridge, the larger number of  $n_1$  should provide better results. The parameters defining the bridge and vehicle system are the same as before. It can be seen that the

Table 3.2 Comparison of Accelerations Obtained by Using Different Numbers of  $n_1$  with Wheels Over Center Beam

Vehicle at center beam of the bridge,  $N = 400$

$x/L$	$n_1$	Accelerations at Midspan		
		Edge Beam	Beam No. 2	Center Beam
0.20	2	-0.274466	-0.274466	-0.274466
	4	-0.252714	-0.298451	-0.217295
	6	-0.269274	-0.294369	-0.210257
0.50	2	-0.348272	-0.348272	-0.348272
	4	-0.160029	-0.411076	-0.515064
	6	-0.167445	-0.406655	-0.517048
0.80	2	-0.293332	-0.293332	-0.293332
	4	-0.269257	-0.329532	-0.354500
	6	-0.262305	-0.338745	-0.363971
1.00	2	0.090615	0.090615	0.090615
	4	0.115142	0.155268	0.171888
	6	0.118075	0.161762	0.176689

accelerations converge when six terms of the  $Y_n$  functions are used ( $n_1 = 6$ ). Table 3.3 is similar to Table 3.2 by showing the accelerations at midspan converge with the increasing values of  $n_1$ , except that, at this time, the vehicle travels over the edge beam of the bridge and the positions of wheels are defined by the parameters:

$$n_1 = 0.10, n_2 = 0.40.$$

For the numerical results presented in this chapter, the following values of solution parameters are used:  
 $N = 400, m_0 = 15, n_0 = 8, n_1 = 6$ , and  $n_2 = 6$ .

### 3.3 Bridge Parameters

#### 3.3.1 Effect of Span Length

Several previous field tests have indicated that the span length is one of the major variables affecting the vibration of the bridge. In this study, the simple-span bridge models with different span lengths are used in the computation to evaluate the accelerations of each beam at midspan while keeping the vehicle parameters constant.

In order to obtain practical values for bridge parameters, the Bureau of Public Roads bridges<sup>(41)</sup> with span lengths in the range between 20 and 70 ft. are considered. These bridges are of the I-beam type and are designed either for H 15-44 loading or for HS 20-44 loading. The bridges designed for H 15-44 loading have a

Table 3.3 Comparison of Accelerations Obtained by Using Different Numbers of  $n_1$  with Wheels Over Edge Beam

Vehicle at left edge beam of the bridge,  $N = 400$

$x/L$	$n_1$	Accelerations at Midspan		
		Left Edge Beam	Right Edge Beam	Center Beam
0.20	2	-0.566199	0.011037	-0.277580
	4	-0.556376	0.090094	-0.303591
	6	-0.558713	0.087076	-0.305147
0.50	2	-0.125344	-0.499783	-0.312563
	4	-0.118537	-0.424207	-0.340399
	6	-0.112022	-0.430594	-0.340199
0.80	2	0.011045	-0.616277	-0.252910
	4	0.208124	-0.643312	-0.272986
	6	0.207292	-0.634261	-0.269409
1.00	2	0.481108	-0.234304	0.123401
	4	0.466486	-0.164051	0.192613
	6	0.473863	-0.169914	0.195106

roadway width of 28 ft. and a concrete slab 7 in. thick. The entire deck is supported on four wide-flange steel girders. For the bridges designed for the HS 20-44 loading, the roadway width is 44 ft., and the slab thickness is 7-1/2 in., and a total of six wide-flange steel girders are used to support the deck. The cross-section of both bridge types are shown in Figure 3.1. It should be noted that the effects of side curbs are not considered in this study.

The weight per unit of length of bridge was evaluated by computing the weight per unit of length of an interior girder and its tributary slab and multiplying the result by the number of girders. The fundamental frequency of vibration of each bridge was computed by using Eq. (2-44) in Article 2.2, and the period of vibration was obtained by inverting the corresponding frequency. These results for both bridge types are presented in Table 3.4. It was assumed that the roadway surface was horizontal and smooth.

The vehicle is represented by a single axle loading consisting of two wheels and has total sprung load of 30 kips for H 15-44 loading and of 72 kips for HS 20-44 loading. The stiffness of each tire spring for both vehicle types is 6 kips per inch<sup>(22)</sup> and the weight of unsprung loads or wheels are neglected. From this information, the frequency of vehicle can be computed by using Eq. (2-44)

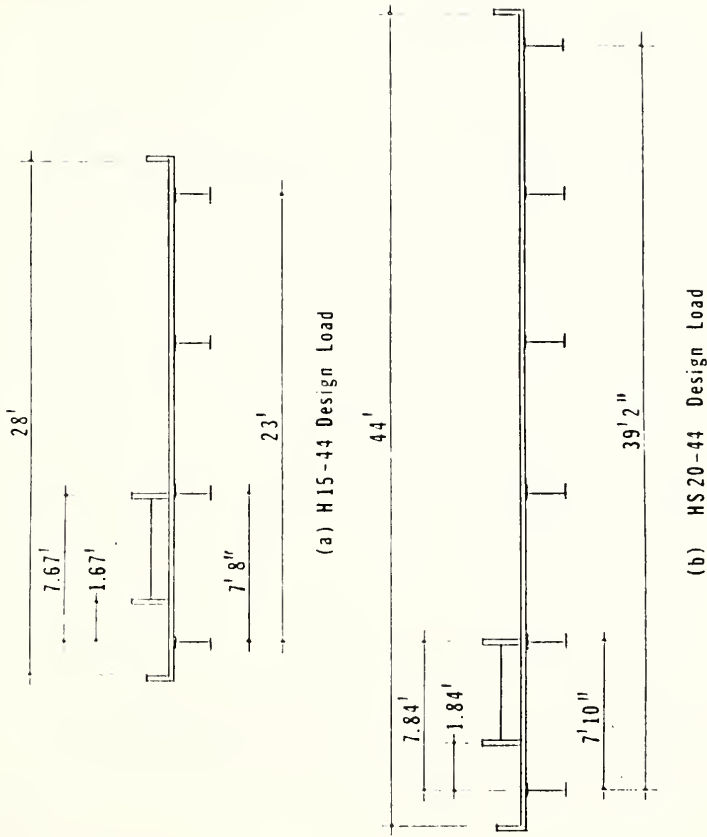


Figure 3.1 Cross Section of B.P.R. Bridges and Position of Wheels

Table 3.4 Natural Frequencies of Simple Span B.P.R. Bridges  
 28 ft. Roadway for H 15-44 loading

Span (ft)	I-Beam	Weight (kips)	Freq. (cps)	Period (sec)
20	21WF55	44.65	16.05	0.06
25	24WF68	57.11	12.32	0.08
30	24EF76	69.49	9.04	0.11
35	27WF94	83.60	7.98	0.13
40	30WF108	97.78	6.98	0.14
45	33WF118	111.80	6.24	0.16
50	33WF130	126.62	5.32	0.19
60	36WF160	159.15	4.33	0.23
70	36WF230	205.27	3.73	0.27

44 ft. Roadway for HS 20-44 loading

Span (ft)	I-Beam	Weight (kips)	Freq. (cps)	Period (sec)
20	21WF62	80.56	16.12	0.06
25	24WF76	102.81	12.26	0.08
30	27WF94	126.61	10.17	0.10
35	30WF116	152.33	8.86	0.11
40	33WF130	177.45	7.76	0.13
45	36WF150	205.03	6.96	0.14
50	36WF170	233.81	5.98	0.17
60	36WF230	302.17	4.76	0.21
70	36WF300	381.94	3.89	0.26

in Article 2.2. The positions of both wheels while the vehicle travels on the bridge are shown in Figure 3.1, where the right wheel is over beam no. 2 and the transverse spacing of the wheels is 6 feet.

The maximum acceleration results at midspan of both B.P.R. bridge types with varying span lengths are evaluated and shown in Table 3.5. The maximum acceleration of each beam is shown and the corresponding value of  $x/L_b$  defines the longitudinal position of the wheels at that time. Figure 3.2 shows graphically the results corresponding to Table 3.5, each curve representing the maximum acceleration of one beam. It can be seen that the acceleration increases with shortening span and the rate of increase for span lengths between 20 ft. and 40 ft. is higher than that for span lengths between 40 ft. and 70 ft. In other words, the acceleration of the bridge decreases if the span length of the bridge increases. It should also be noted that, in Figure 3.2, the maximum accelerations of the B.P.R. bridges with 44 ft. roadway width are greater than those with 28 ft. roadway width. It can then be concluded that the acceleration increases for heavier vehicle loads on the bridge.

Figure 3.3 shows the distributions of maximum acceleration to each beam corresponding to the results shown in Table 3.5 and Figure 3.2. For both B.P.R. bridge types, the right wheel is over the second beam from the left (beam 2). This

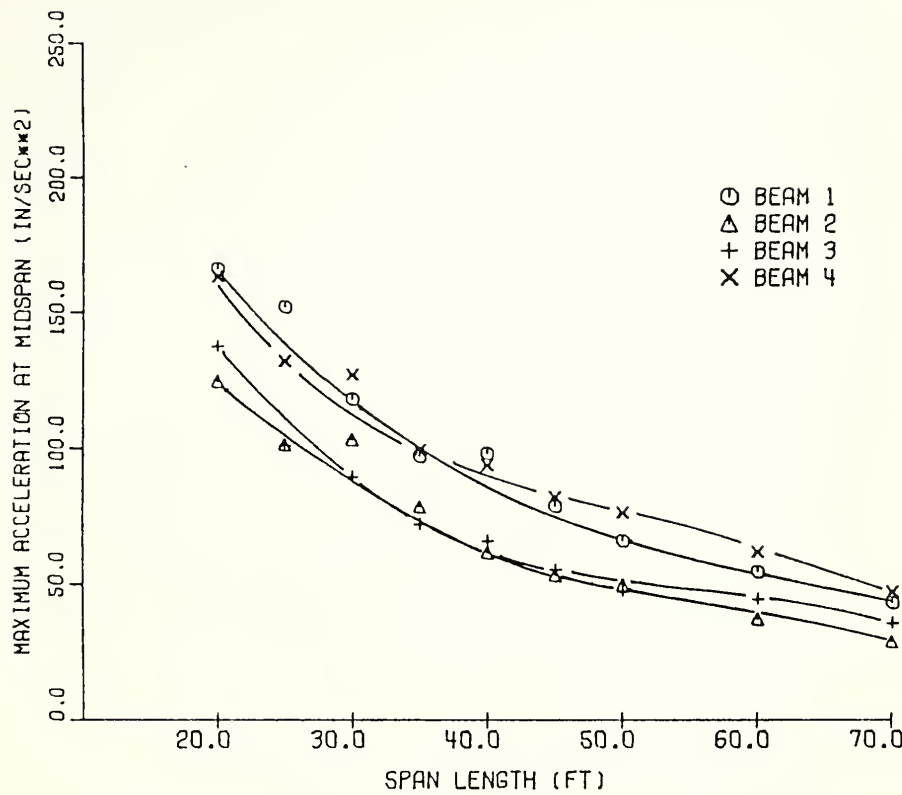
Table 3.5 Maximum Accelerations of Simple Span B.P.R. Bridges

28 ft. Roadway H-15-44 Loading Velocity 60 m.p.h. Level Surface

Span (ft)	Maximum Accelerations at Midspan (in/sec <sup>2</sup> )					
	Beam 1	x/L	Beam 2	x/L	Beam 3	x/L
20	-166.27	0.82	-124.87	0.18	-137.67	0.49
25	-152.21	0.82	101.44	0.97	101.21	0.38
30	118.41	0.06	-103.44	0.90	89.60	0.41
35	97.23	1.00	-78.65	0.87	-72.12	0.55
40	-98.43	0.88	-61.57	0.86	-66.23	0.55
45	-78.87	0.86	53.38	1.00	-55.53	0.55
50	-66.14	0.20	-49.88	0.90	-47.49	0.56
60	-54.70	0.21	37.22	0.07	-44.70	0.58
70	-43.40	0.20	-28.90	0.23	-35.92	0.58

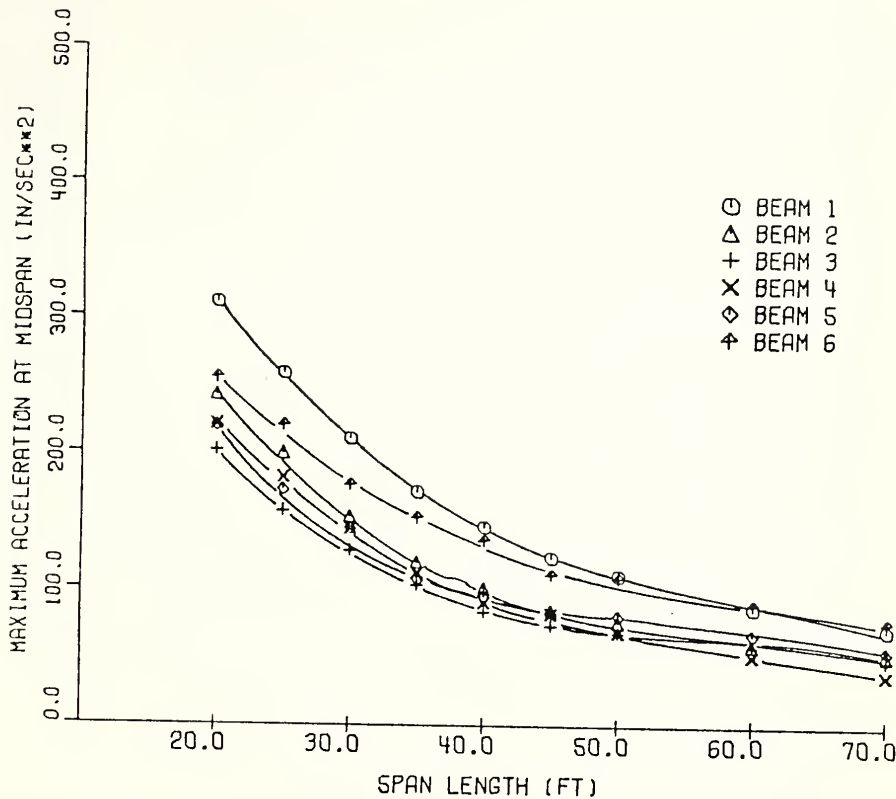
44 ft. Roadway HS 20-44 Loading Velocity 60 m.p.h. Level Surface

Span (ft)	Maximum Accelerations at Midspan (in/sec <sup>2</sup> )					
	Beam 1	x/L	Beam 2	x/L	Beam 3	x/L
20	310.53	0.05	-242.07	0.19	-201.76	0.47
25	258.20	0.05	-199.71	0.19	-157.47	0.22
30	210.60	0.05	-153.52	0.18	-128.21	0.22
35	171.90	0.05	119.84	0.07	103.48	0.34
40	146.09	0.05	101.32	0.07	-84.06	0.23
45	123.81	0.05	85.03	0.07	-73.90	0.22
50	110.87	0.05	76.42	0.07	-68.91	0.24
60	87.01	0.06	-60.10	0.20	-59.39	0.22
70	71.46	0.06	-53.91	0.22	-49.09	0.24



28 FT ROADWAY    H15-44 LOADING    VELOCITY 60 MPH    LEVEL SURFACE  
 TWO WHEELS    6 FT WHEEL SPACING    RIGHT WHEEL OVER SECOND BEAM

Figure 3.2 Maximum Accelerations at Midspan of B.P.R.  
 Bridges



44 FT ROADWAY    HS20-44 LOADING    VELOCITY 60 MPH    LEVEL SURFACE  
 TWO WHEELS    6 FT WHEEL SPACING    RIGHT WHEEL OVER SECOND BEAM

Figure 3.2, cont.

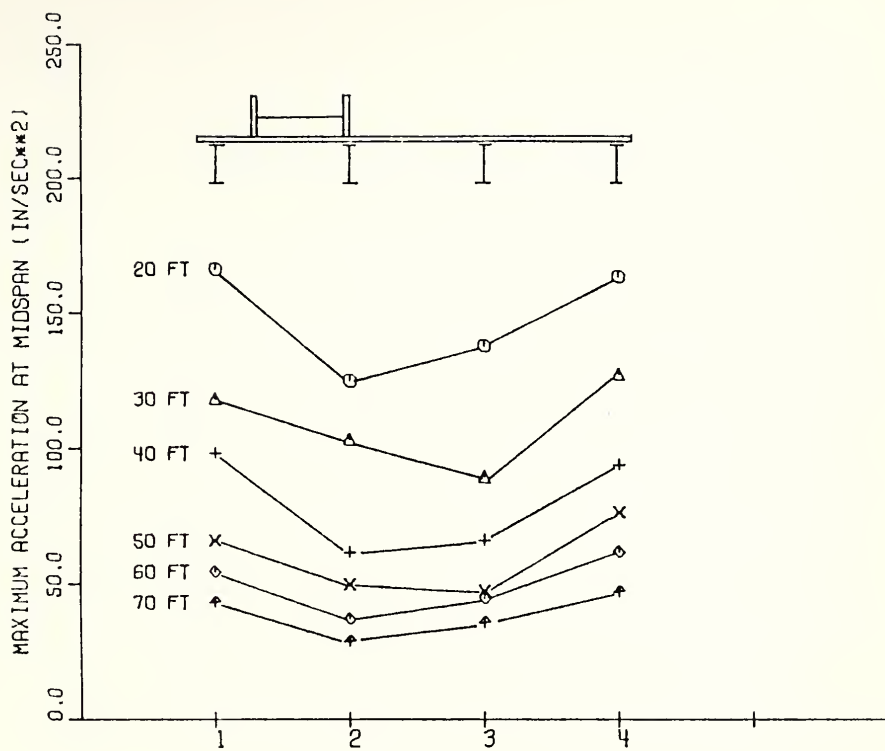


Figure 3.3 Distributions of Maximum Acceleration to Each Beam of 28 ft Roadway B.P.R. Bridges with Different Span Lengths

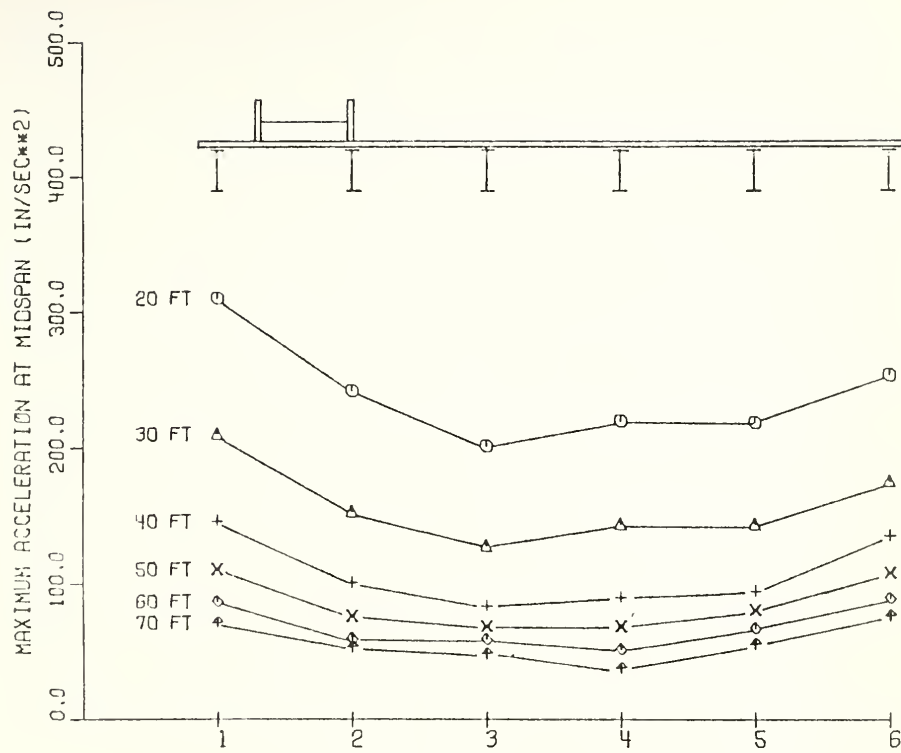


Figure 3.3, cont.

causes the accelerations of the exterior beams to be larger than those of the interior beams. The differences in accelerations between these beams decrease as the bridge span increases.

Figure 3.4 shows the acceleration of each beam in the form of history curves for a bridge having a 60 ft. span and a 44 ft. roadway width with the right wheel of the vehicle over beam 2. A history curve is a plot of acceleration as a function of time, or in terms of longitudinal position of the load on the bridge. It can be seen that accelerations of beam 1 and beam 6 are out of phase all the time. It is of some interest to note also that the maximum acceleration of beam 1 occurs when the vehicle enters the bridge but the maximum acceleration of beam 6 occurs when the vehicle is at the midspan or is leaving the bridge.

Figure 3.5 shows the history curves of acceleration of beam 6 with varying span lengths corresponding to the results presented in Table 3.5. It can be seen that the curves are similar except that larger ordinate of the curve for the shorter span lengths.

### 3.3.2 Effect of Width

In order to investigate the effect of bridge width on acceleration, three bridge models as shown in Figure 3.6(a) have been assumed. All three bridges have the same parameters

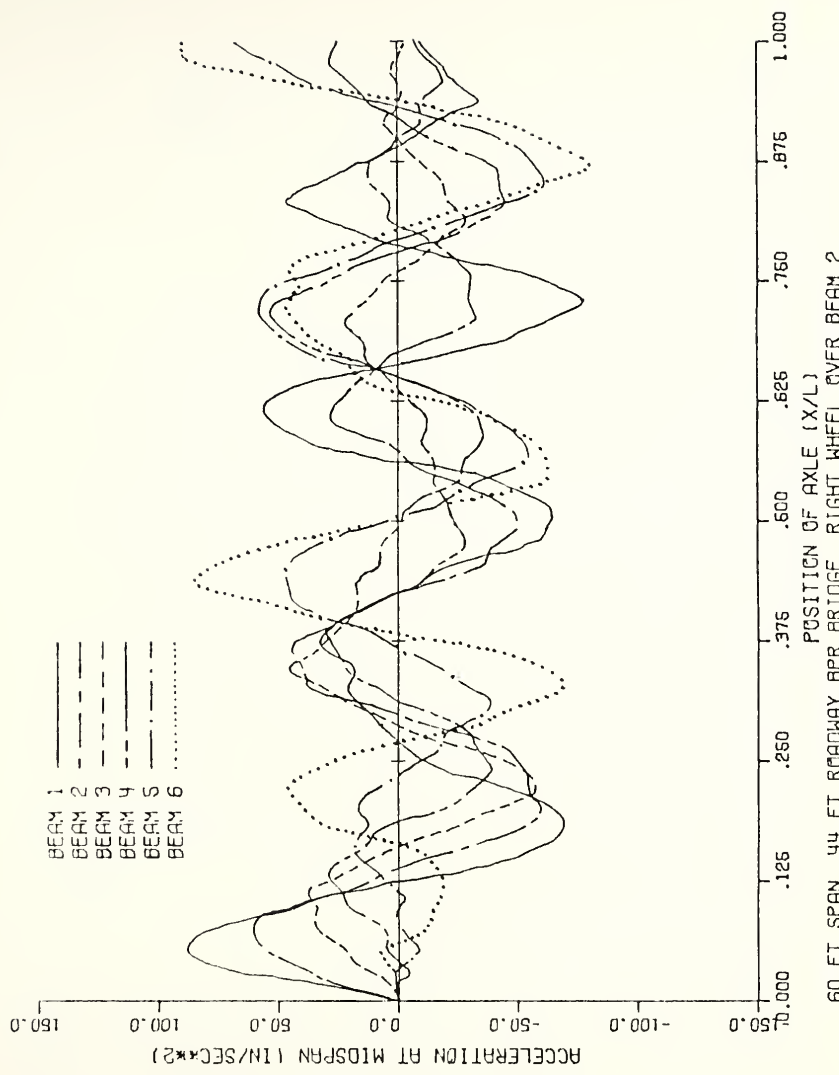


Figure 3.4 Comparison of History Curves for Accelerations of Beam

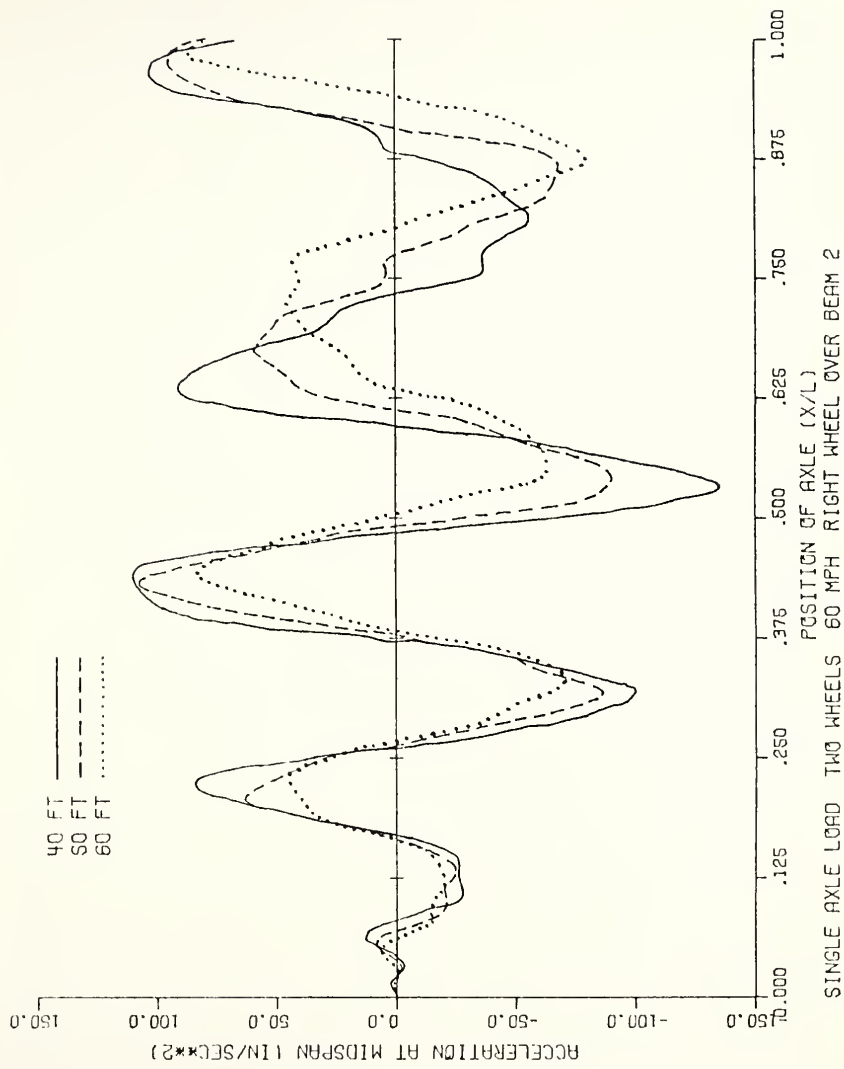


Figure 3.5 Effect of Span Length on Acceleration on Edge Beam

except the width and the number of beams. Beam 1 and beam 4 are designated as the exterior beams and beams 2, 3, 5 and 6 as the interior beams. Vehicle parameters are constant for this comparison. The study is divided into two cases. In case A, the vehicle travels at the center line of the bridges as shown in Figure 3.6(a), while the left wheel is over beam 1 for case B. The results of the study and descriptions of all parameters are summarized in Table 3.6 and the corresponding history curves of beam 1 are shown in Figure 3.7. It can be seen from these results that there is not much difference in beam acceleration with increasing bridge widths although the accelerations of narrower bridges tend to be slightly higher than those of the wider bridges.

### 3.3.3 Effect of Flexibility of Girder

Figure 3.6(b) shows the bridge model used for a study to obtain the accelerations for varying girder flexibilities while keeping other parameters constant. The transverse vehicle position is arranged so that its left wheel is over beam 1 at all times. The details of necessary parameters used in this study, including six different girders, are presented in Table 3.7. It should be remembered that all five girders of the bridge have the same section. The 36 WF 230 wide flange girders would be the normal design for this bridge.

Table 3.6 Maximum Accelerations at Midspan of Simple Span Bridges with Different Widths

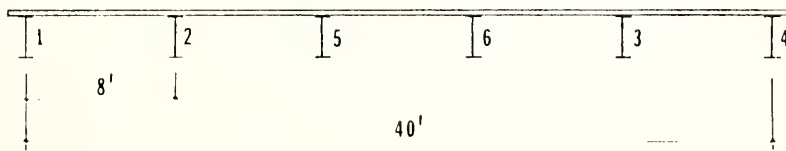
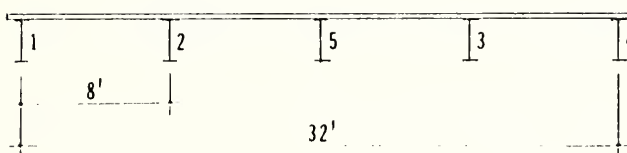
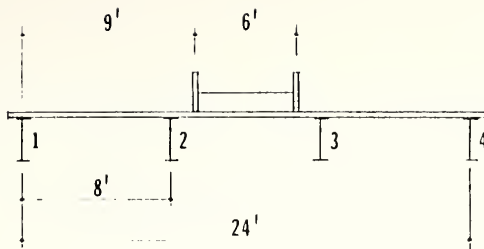
Girder Bridge 60 ft. span 7.5 in. Deck Thickness  
 36WF230 Girder 8 ft. Spacing HS 20-44 Loading  
 60 m.p.h. Level Surface

Case A Load at Center Line

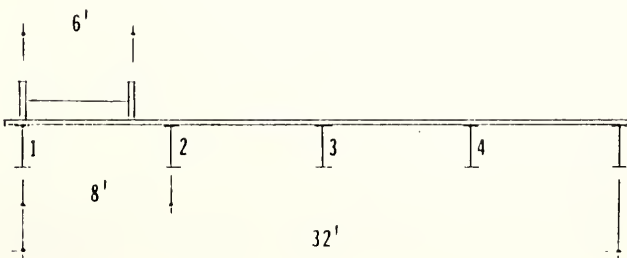
Beam	Maximum Accelerations at Midspan (in/sec <sup>2</sup> )					
	24 ft Width	x/L	32 ft Width	x/L	40 ft Width	x/L
1	-71.47	0.50	-69.76	0.84	-64.18	0.25
4	-71.47	0.50	-69.76	0.84	-64.18	0.25
2	-66.69	0.81	-49.79	0.25	-47.70	0.23
3	-66.69	0.81	-49.79	0.25	-47.70	0.23
5			70.65	1.00	-65.50	0.54
6					-65.50	0.54

Case B Left Wheel Over Beam 1

Beam	Maximum Accelerations at Midspan (in/sec <sup>2</sup> )					
	24 ft Width	x/L	32 ft Width	x/L	40 ft Width	x/L
1	125.84	0.98	100.81	0.05	100.67	0.05
4	120.15	0.39	119.14	0.68	107.20	0.44
2	-80.53	0.84	-72.18	0.20	65.11	0.07
3	-76.92	0.51	-69.97	0.56	62.89	0.73
5			-56.91	0.85	-62.70	0.24
6					59.82	0.73



(a) Effect of Width on Acceleration



(b) Effect of EI on Acceleration

Figure 3.6 Cross Section of Bridges Used in Study

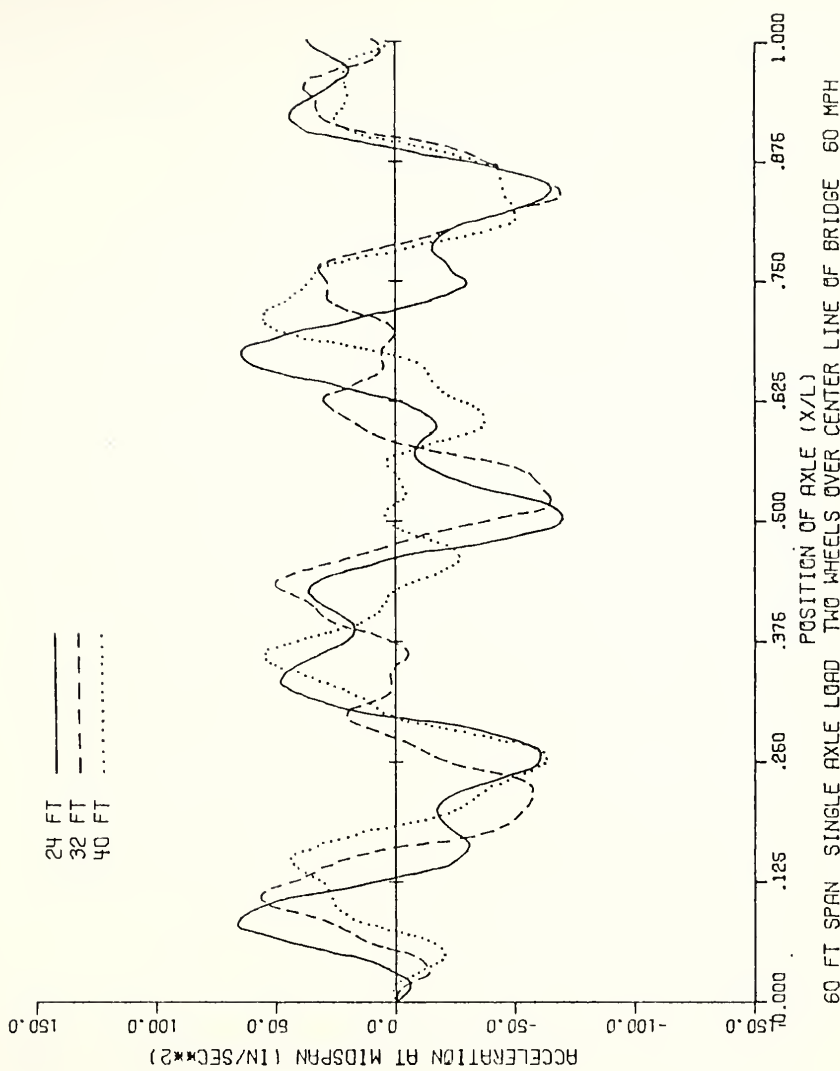


Figure 3.7 Effect of Bridge Width on Acceleration of Edge Beam

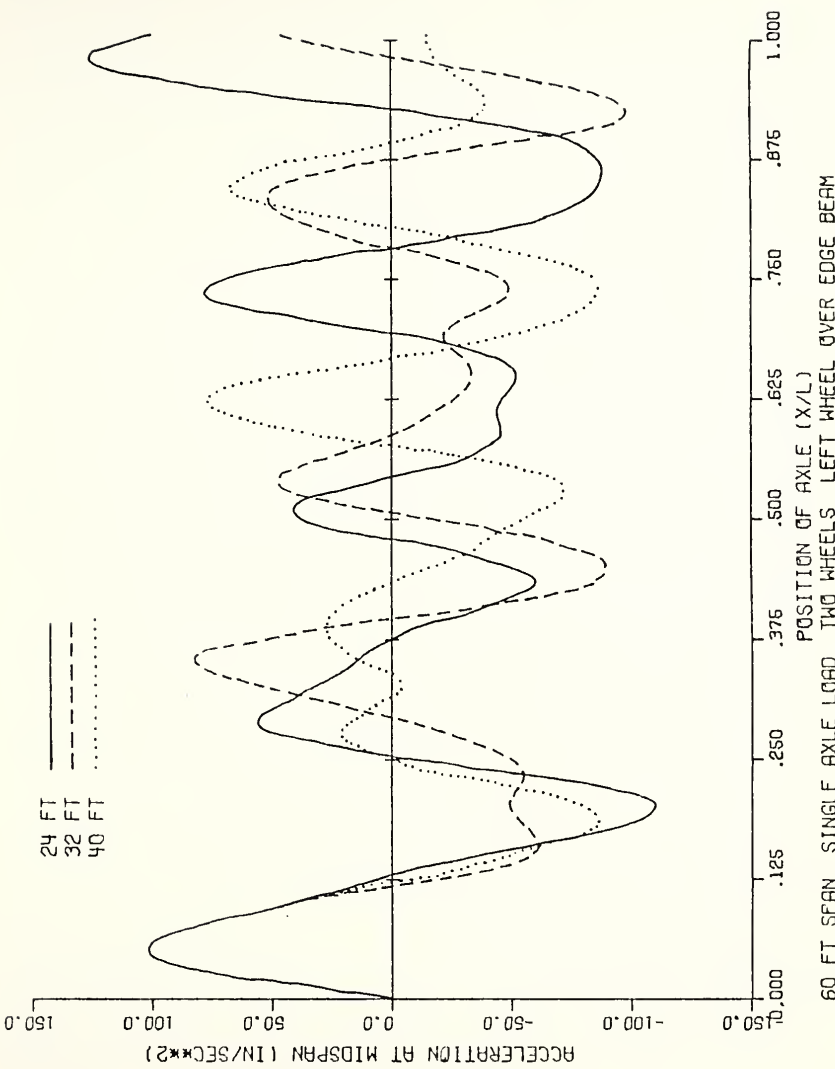


Figure 3.7, cont.

Five girder sections smaller than the 36 WF 230 section are used and the smallest section (36 WF 135) has a moment of inertia nearly half that of 36 WF 230 section. The results of the study are tabulated in Table 3.7 and the relationships between the acceleration of each beam and the moment of inertia of beam are plotted in Figure 3.8. The fundamental frequency and the total weight of the bridge for each type of girder are also calculated and presented in Table 3.7. From these results, as might be expected, the acceleration is lowest when the largest size of section has been used and it is higher when the size has been reduced. It can be seen that the accelerations increase approximately only 20 percent while the moment of inertia of section is reduced nearly 40 percent.

### 3.4 Vehicle Parameters

#### 3.4.1 Effect of Transverse Position of Wheels

The bridge model used for this comparison is the same as that used in Article 3.3.3 and shown in Figure 3.6(b). A 36 WF 230 girder section is used. Figure 3.9 shows the transverse position of the wheels on the bridge in six different cases. Case A has the leftmost position of wheels on the bridge while, in case F, the wheels are symmetrically arranged over the center beam.

Table 3.8 shows the acceleration results for each case, giving the maximum acceleration of each beam and the

Table 3.7 Maximum Accelerations at Midspan of Simple Span Bridges Due to Different Girder Flexibilities

5 Girder Bridge 60 ft. Span 7.5 in. Deck Thickness  
 8 ft. Spacing of Girder HS 20-44 Loading Two Wheels  
 Left Wheel Over Beam 1 60 m.p.h. Level Surface

Type of Girder	Moment of Inertia (in. <sup>4</sup> )	Weight (k./ft.)	Area (in. <sup>2</sup> )
36WF230	15000	0.230	67.7
36WF194	12100	0.194	57.2
36WF182	11300	0.182	53.6
36WF170	10500	0.170	50.0
36WF160	9760	0.160	47.1
36WF135	7820	0.135	39.8

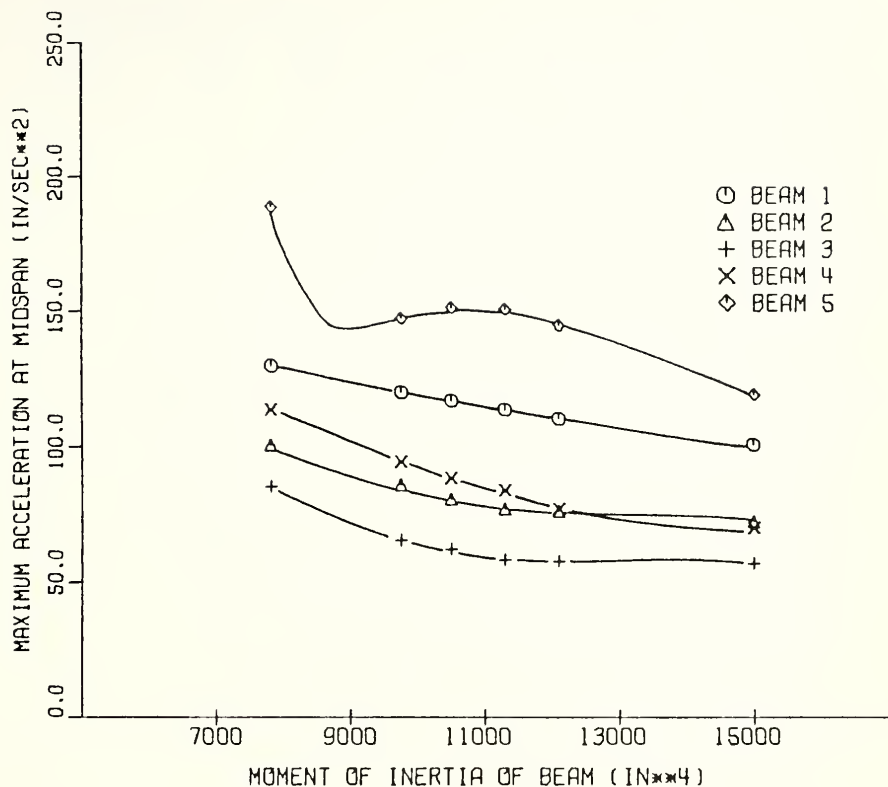
Girder	Freq (cps)	W (kips)	Maximum Accelerations at Midspan (in/sec <sup>2</sup> )				
			Beam 1	Beam 2	Beam 3	Beam 4	Beam 5
36WF230	4.79	249.0	100.81	-72.18	-56.91	-69.97	119.14
36WF194	4.41	238.2	110.36	-76.06	-57.78	77.02	-144.60
36WF182	4.30	234.6	113.51	-76.84	58.30	83.85	-150.66
36WF170	4.18	231.0	116.86	-80.49	62.18	-88.31	-151.01
36WF160	4.06	228.0	120.04	-85.88	65.47	-94.53	-147.29
36WF135	3.72	220.5	129.84	-100.51	-85.37	-113.69	188.64

Table 3.8 Maximum Accelerations at Midspan of Simple Span Bridges  
Due to Transverse Positions of Wheels

5 Girder Bridge 60 ft. Span 7.5 in. Deck Thickness  
Girder 36WF230 8 ft. Spacing 72 kips Single Axle Load Two Wheels  
60 m.p.h. Level Surface

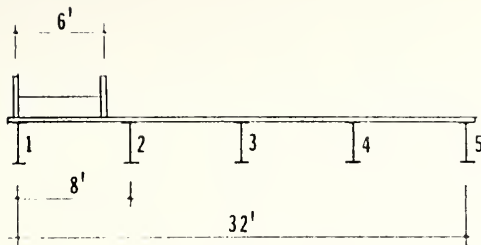
Case	Maximum Accelerations at Midspan (in/sec <sup>2</sup> )									
	Beam 1	x/L	Beam 2	x/L	Beam 3	x/L	Beam 4	x/L	Beam 5	x/L
A	100.73	0.05	-72.13	0.20	-56.90	0.85	-70.07	0.56	118.48	0.68
B	85.64	0.05	-68.75	0.22	-53.32	0.53	-67.65	0.55	109.24	0.69
C	-83.40	0.20	-69.01	0.23	-48.69	0.25	-63.81	0.55	87.63	0.70
D	-83.44	0.20	-63.52	0.23	57.50	1.00	61.01	0.54	-87.35	0.83
E	-74.78	0.20	-56.90	0.24	66.65	1.00	-58.38	0.53	-82.64	0.83
F	-69.76	0.84	-49.66	0.25	72.42	1.00	-49.66	0.25	-69.76	0.84

Case A Left Wheel Over Edge Beam  
 Case B Right Wheel Over Beam 2  
 Case C Symmetrical Wheels Over Beam 2  
 Case D Left Wheel Over Beam 2  
 Case E Right Wheel Over Center Beam  
 Case F Symmetrical Wheels Over Center Beam



5 GIRDER BRIDGE 60 FT SPAN HS20-44 LOADING LEVEL SURFACE  
TWO WHEELS LEFT WHEEL OVER BEAM 1 VELOCITY 60 MPH

Figure 3.8 Effect of EI of Beam on Maximum Acceleration



Case A Left wheel over  
edge beam



Case B Right wheel over  
beam 2



Case C Symmetrical wheels  
over beam 2



Case D Left wheel over  
beam 2



Case E Right wheel over  
center beam



Case F Symmetrical wheels  
over center beam

Figure 3.9 Transverse Position of Wheels on Bridge

longitudinal position of the vehicle at that time. The details of all necessary parameters are also provided in Table 3.8. The relationships between the acceleration of beam and wheel position are plotted in Figure 3.10. There are three important things to be noted from these results. First, the accelerations of edge beams are the greatest when the vehicle travels over the edge beam and tend to decrease when the vehicle travels near the center line of the bridge. Second, in contrast, the acceleration of the center beam is the least when the vehicle travels over the edge beam and the greatest when the vehicle is over the center line of the bridge. Center beam accelerations are slightly greater than the accelerations of edge beams. Third, practically, most vehicles travel on the bridge with a wheel position corresponding to case C or case D and the accelerations of the edge beams are then greater than those of interior beams.

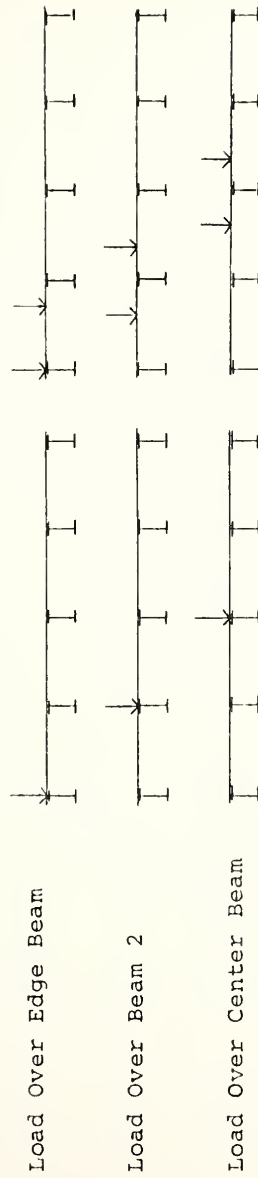
### 3.4.2 Effect of Number of Wheels

Table 3.9 presents the results of acceleration comparison obtained by using a single axle having one or two wheels. Both vehicle models have the same total load of 72 kips. As shown in Table 3.9, there are three different transverse positions of load on the bridge: first, the load is over the edge beam, second, the load is over beam 2 and third, the load is over the center beam. The bridge

Table 3.9 Comparison of Accelerations at Midspan of Simple Span Bridges  
Obtained by Using Different Number of Wheels of Vehicle

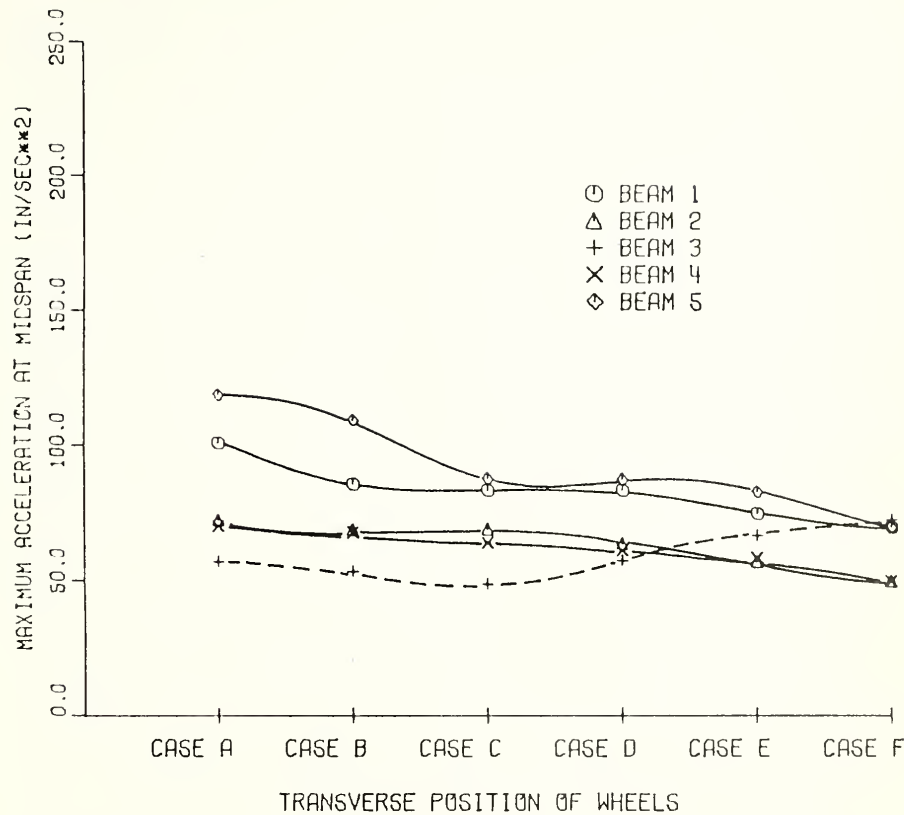
5 Girder Bridge 60 ft. Span 7.5 in. Deck Thickness Girder 36WF230 8 in. Spacing  
72 kips Single Axle Load Velocity 60 m.p.h. Level Surface

One Wheel (72 kips)      Two Wheels (72 kips)



Maximum Accelerations at Midspan (in/sec<sup>2</sup>)

Beam	Load Over Edge Beam		Load Over Beam 2		Load Over Center Beam	
	One Wheel	Two Wheels	One Wheel	Two Wheels	One Wheel	Two Wheels
1	-148.41	100.73	-93.77	-83.40	-78.53	-69.76
2	-94.54	-72.13	-77.27	-69.01	-53.94	-49.66
3	-74.88	-56.90	-53.49	-48.69	80.18	72.42
4	88.65	-70.07	-66.73	-63.81	-53.94	-49.66
5	155.95	118.48	95.57	87.63	-78.53	-69.76



5 GIRDER BRIDGE 60 FT SPAN 36WF230 HS20-44 LOADING 60 MPH

Figure 3.10 Effect of Transverse Position of Wheels on Acceleration

parameters are kept constant and are described in Table 3.9. It can be seen from the results that the accelerations obtained by using the single wheel vehicle are greater than those obtained by using the two wheel vehicle. It may be noted that the difference in accelerations is approximately 10 percent when the load is over beam 2 and over the center beam but the acceleration difference ranges from 25 to 48 percent when the load is over edge beam. This can be explained in that the center of gravity of two wheel vehicle is not actually over the edge beam as in the case of one wheel vehicle. The 10 percent difference may be expected if the two wheel vehicle has its center of gravity over the edge beam.

#### 3.4.3 Effect of Transverse Position of Single Load and Flexibility of Girder

In Article 3.3.3, the effect of girder flexibility on accelerations was studied for a constant position of wheels over the edge beam and it was shown that reduced girder section had relatively small effects on acceleration. In this study, the transverse position of single load on the bridge is varied and it is classified into five different cases as shown in Figure 3.11. In each case, the comparisons are made for the same six girder sections as in Article 3.3.3 (properties of these sections are shown in Table 3.7). In Table 3.10, the remaining

Table 3.10 Maximum Accelerations at Midspan of Simple Span Bridges Due to Transverse Positions of Single Load and Girder Flexibilities

5 Girder Bridge 60 ft. Span 7.5 in. Deck Thickness 72 kips Load  
Single Axle One Wheel 60 m.p.h. Level Surface

Case A Single Load Over Beam 1 (Edge Beam)

Moment of Inertia (in <sup>4</sup> )	Maximum Accelerations at Midspan (in/sec <sup>2</sup> )						
	Beam 1 x/L	Beam 2 x/L	Beam 3 x/L	Beam 4 x/L	Beam 5 x/L		
15000	-148.41	0.92	-94.54	0.20	-74.88	0.84	88.65
12100	149.02	0.89	-97.66	0.20	-77.86	0.22	99.89
11300	153.49	0.36	-96.55	0.19	-78.92	0.22	110.29
10500	-164.53	0.77	95.87	0.07	-78.89	0.21	109.26
9760	-201.38	0.77	99.14	0.07	85.93	0.45	-113.89
7820	-245.49	0.77	-116.61	0.26	-105.11	0.68	-127.47

Table 3.10, cont.

## Case B Single Load Halfway Between Beam 1 and Beam 2

Moment of Inertia (in <sup>4</sup> )	Maximum Accelerations at Midspan (in/sec <sup>2</sup> )									
	Beam 1	x/L	Beam 2	x/L	Beam 3	x/L	Beam 4	x/L	Beam 5	x/L
15000	98.69	0.20	-71.99	0.22	-58.00	0.53	-71.57	0.55	123.76	0.70
12100	106.77	0.07	-84.31	0.22	-57.14	0.24	-82.49	0.59	-134.19	0.60
11300	111.33	0.07	-86.08	0.22	60.32	0.44	-81.77	0.62	-140.56	0.60
10500	116.17	0.07	-87.08	0.22	64.13	0.44	-88.99	0.62	-140.05	0.62
9760	120.82	0.07	-86.96	0.22	64.52	0.44	-92.79	0.65	-147.35	0.62
7820	-144.17	0.80	-99.16	0.25	-86.52	0.70	-114.19	0.68	165.83	0.52

## Case C Single Load Over Beam 2

Moment of Inertia (in <sup>4</sup> )	Maximum Accelerations at Midspan (in/sec <sup>2</sup> )									
	Beam 1	x/L	Beam 2	x/L	Beam 3	x/L	Beam 4	x/L	Beam 5	x/L
15000	-93.77	0.20	-77.27	0.22	-53.49	0.25	-66.73	0.55	95.57	0.70
12100	-95.81	0.20	-86.29	0.22	-60.21	0.24	-89.98	0.59	109.14	0.76
11300	-94.24	0.19	-86.93	0.22	-66.53	0.60	-87.31	0.59	122.25	0.76
10500	96.01	0.07	-86.77	0.22	-67.54	0.28	85.88	0.46	116.57	0.76
9760	99.29	0.07	-85.31	0.22	-72.13	0.63	-99.20	0.65	-119.91	0.63
7820	-115.50	0.26	95.82	0.05	-77.13	0.27	-100.88	0.67	-145.43	0.69

Table 3.10, cont.

## Case D Single Load Halfway Between Beam 2 and Beam 3

Moment of Inertia (in <sup>4</sup> )	Maximum Accelerations at Midspan (in/sec <sup>2</sup> )									
	Beam 1	x/L	Beam 2	x/L	Beam 3	x/L	Beam 4	x/L	Beam 5	x/L
15000	-90.26	0.20	-64.09	0.24	66.82	1.00	-64.92	0.53	-95.20	0.83
12100	-88.55	0.20	-73.11	0.24	-75.35	0.59	-82.62	0.60	106.15	0.75
11300	-86.67	0.20	-74.33	0.23	-79.47	0.61	-87.28	0.60	108.14	0.75
10500	-84.39	0.20	-74.58	0.23	-87.87	0.61	-84.41	0.60	109.25	0.77
9760	82.35	0.13	-73.67	0.23	-90.04	0.61	-80.17	0.65	97.64	0.77
7820	103.98	0.45	-86.56	0.29	-97.03	0.29	-98.89	0.66	-147.83	0.70

## Case E Single Load Over Beam 3 (Center Beam)

Moment of Inertia (in <sup>4</sup> )	Maximum Accelerations at Midspan (in/sec <sup>2</sup> )									
	Beam 1	x/L	Beam 2	x/L	Beam 3	x/L	Beam 4	x/L	Beam 5	x/L
15000	-78.53	0.84	-53.94	0.25	80.18	1.00	-53.94	0.25	-78.53	0.84
12100	76.04	0.43	-63.67	0.60	-87.88	0.59	-63.37	0.60	76.04	0.43
11300	80.55	0.78	-71.12	0.60	-90.85	0.62	-71.12	0.60	80.55	0.78
10500	88.03	0.45	-72.14	0.60	-102.58	0.62	-72.14	0.60	88.03	0.45
9760	96.35	0.45	-76.35	0.64	-105.27	0.61	-76.35	0.64	96.35	0.45
7820	-115.36	0.68	-81.43	0.66	-111.50	0.29	-81.43	0.66	-115.36	0.68

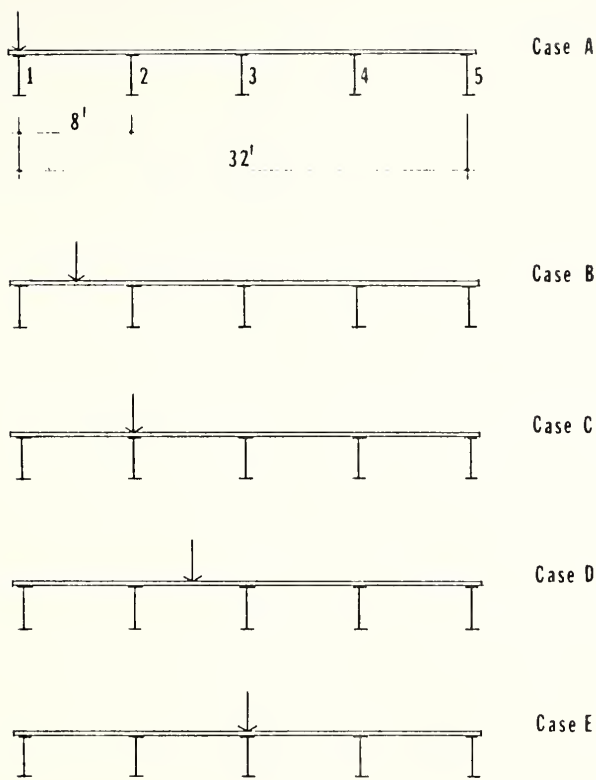


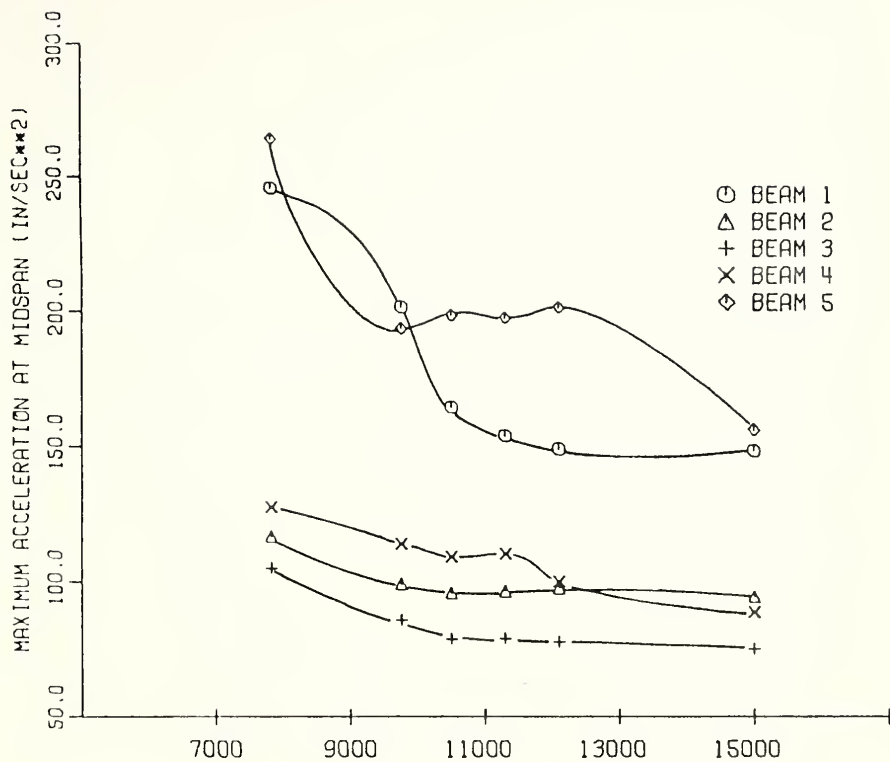
Figure 3.11 Transverse Position of Single Load  
on Bridge

parameters are summarized and the results of the study in each case are presented. Figure 3.12 shows the relationship between maximum acceleration of each beam and the variation of moment of inertia of the section for all five different load positions on the bridge. It can be seen graphically that, in all cases except case A, the acceleration is slightly increased when the section of beam is reduced. To be specific, the acceleration is not increased more than 15 percent while the moment of inertia of section is reduced over 30 percent. In case A, where the load is over the edge beam, the accelerations of the edge beams increase significantly when the section is reduced. However, vehicles travelling at 60 m.p.h. tend to be in the lanes near the center line of bridge.

The curves in Figure 3.13 show graphically the variation of the maximum accelerations of edge beams for different transverse load positions with the relative flexibility of beam. For a position of 60 m.p.h. vehicle, the increased beam flexibility affects the maximum acceleration slightly if the moment of inertia of the section is not reduced more than 35 percent from the normal size.

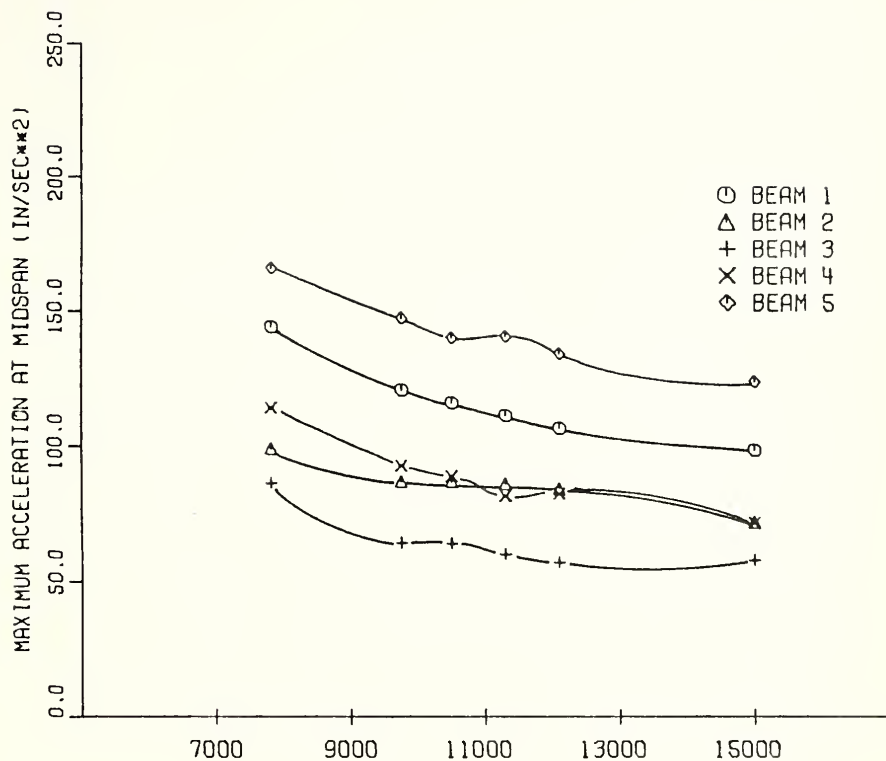
#### 3.4.4 Effect of Speed

The bridge-vehicle system used in this article is the same as that used in Article 3.3.3 and has been shown in Figure 3.6. The maximum acceleration of each beam is



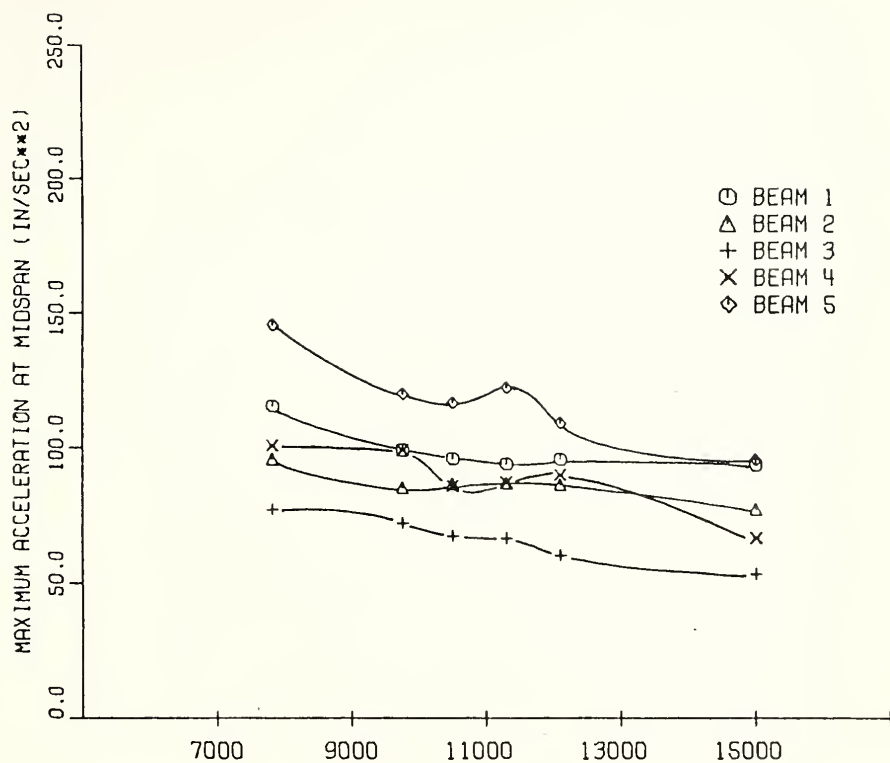
5 GIRDER BRIDGE 60 FT SPAN 72 KIPS SINGLE LOAD LEVEL SURFACE  
CASE A) SINGLE LOAD OVER BEAM 1 (EDGE BEAM)

Figure 3.12 Effect of EI of Beam and Transverse Position of Load



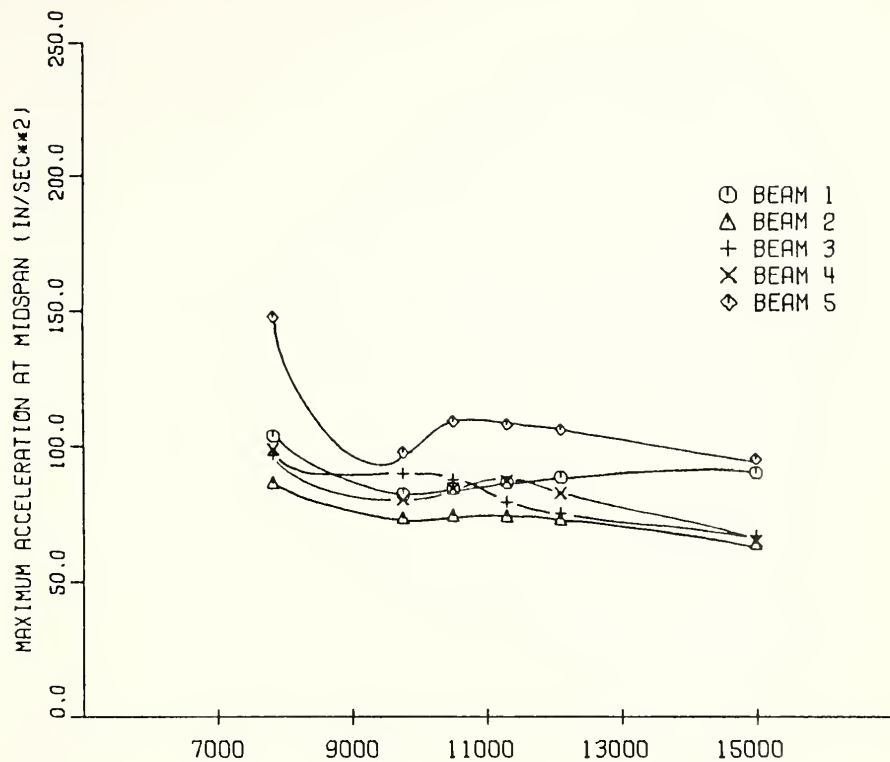
5 GIRDER BRIDGE 60 FT SPAN 72 KIPS SINGLE LOAD LEVEL SURFACE  
CASE B) SINGLE LOAD HALFWAY BETWEEN BEAM 1 AND BEAM 2

Figure 3.12, cont.



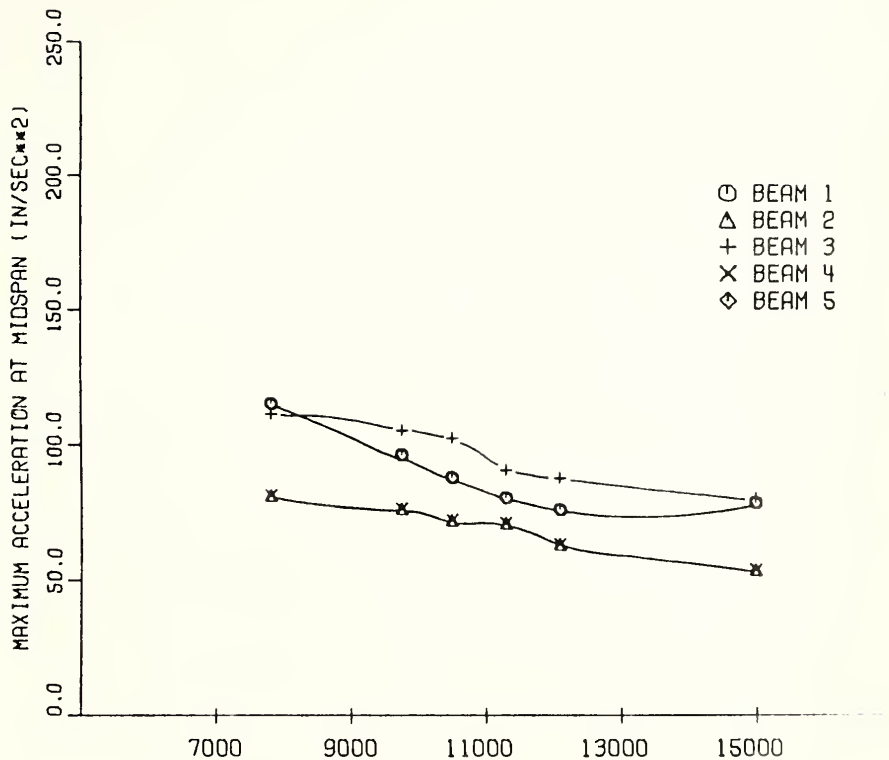
5 GIRDER BRIDGE 60 FT SPAN 72 KIPS SINGLE LOAD LEVEL SURFACE  
CASE C) SINGLE LOAD OVER BEAM 2

Figure 3.12, cont.



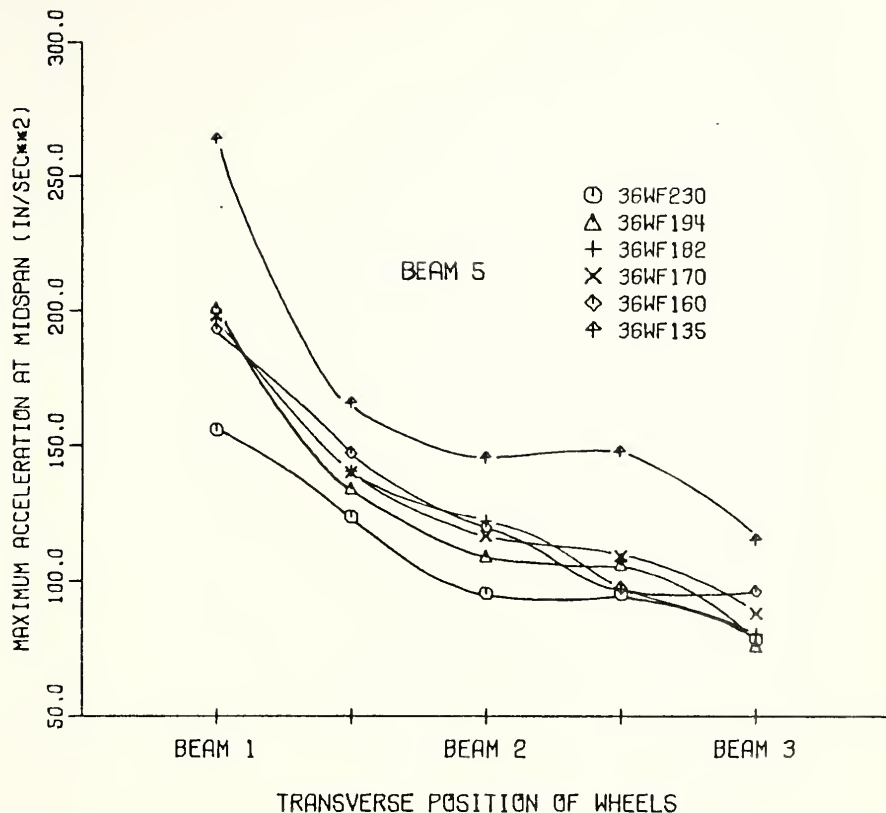
5 GIRDER BRIDGE 60 FT SPAN 72 KIPS SINGLE LOAD LEVEL SURFACE  
CASE D) SINGLE LOAD HALFWAY BETWEEN BEAM 2 AND BEAM 3

Figure 3.12, cont.



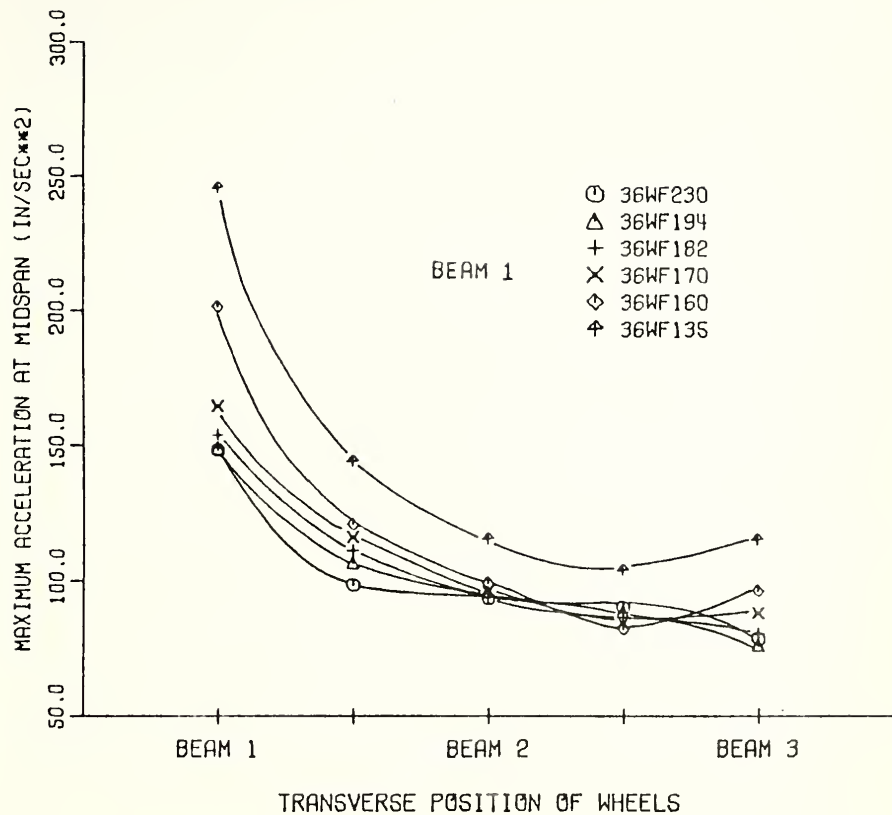
5 GIRDER BRIDGE 60 FT SPAN 72 KIPS SINGLE LOAD LEVEL SURFACE  
CASE E) SINGLE LOAD OVER BEAM 3 (CENTER BEAM)

Figure 3.12, cont.



5 GIRDER BRIDGE 60 FT SPAN SINGLE LOAD 72 KIPS 60 MPH  
LEVEL SURFACE

Figure 3.13 Effect of Flexibility of Girder and Transverse Position of Load on Acceleration



5 GIRDER BRIDGE 60 FT SPAN SINGLE LOAD 72 KIPS 60 MPH  
LEVEL SURFACE

Figure 3.13, cont.

evaluated for vehicle speeds ranging from 20 mph to 70 mph. The values of the remaining parameters are the same as previously and are presented in Table 3.11. The numerical acceleration results with varied speeds of vehicle are also presented in Table 3.11 and the corresponding curves are plotted in Figure 3.14. As might be expected, the values of the maximum accelerations increase for vehicles with higher speeds. It should be noted also that the rate of change of acceleration in each beam is approximately the same as that of the vehicle speed.

### 3.5 Surface Roughness Parameter

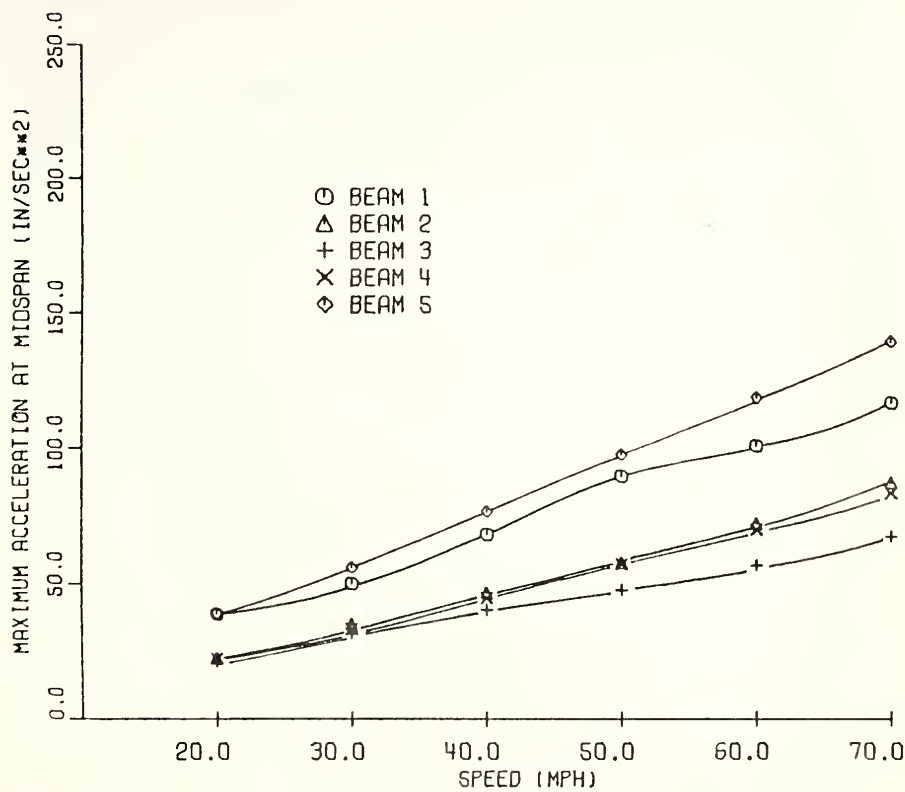
Several previous test reports<sup>(14)(25)(32)</sup> have indicated that the surface roughness is one of the most important parameters which affect the vibration of highway bridges. These reports have recommended that the bridge surface should be as smooth as possible. In this study, the effect of the surface roughness on accelerations is investigated and the corresponding numerical results are presented.

The bridge models used in the previous articles in this chapter, Article 3.2 through Article 3.4, were assumed to have a level surface. In this article, the same bridge and vehicle models as used in Article 3.3 and shown in Figure 3.6 are used but, this time, the initial bridge surface is rough. The parameters representing

Table 3.11 Maximum Accelerations at Midspan of Simple Span Bridges Due to Different Vehicle Speeds

5 Girder Bridge 60 ft. Span 7.5 in. Deck Thickness Girder 36WF230  
 8 ft. Spacing 72 kips Load Single Axle Two Wheels Level Surface  
 Left Wheel Over Beam 1

Speed (mph)	Maximum Accelerations at Midspan (in/sec <sup>2</sup> )									
	Beam 1	x/L	Beam 2	x/L	Beam 3	x/L	Beam 4			
20	-38.89	0.90	-22.51	0.49	-20.74	0.39	-22.33	0.28	-39.05	0.69
30	-50.30	0.71	-34.99	0.59	-31.61	0.58	-33.40	0.28	56.11	0.37
40	-68.33	0.62	-46.59	0.79	-40.43	0.78	-44.66	0.36	76.70	0.48
50	-89.81	0.77	-57.67	0.17	-47.87	0.71	-57.13	0.47	97.43	0.57
60	100.73	0.05	-72.13	0.20	-56.90	0.85	-70.07	0.56	118.48	0.68
70	116.73	0.06	-87.16	0.23	-67.40	0.25	-83.26	0.65	139.30	0.80



5 GIRDER BRIDGE 60 FT SPAN HS20-44 LOADING LEVEL SURFACE  
36WF230 GIRDER TWO WHEELS LEFT WHEEL OVER EDGE BEAM

Figure 3.14 Effect of Speed of Vehicle on Acceleration of Beam

the surface roughness have been designated as  $w_1$ ,  $w_o$ ,  $m_o$  and  $e_j$  which are defined in Article 2.2.3. The term  $w_1$  represents the deviation of the deck of the bridge and has been defined by Eq. (2-24), the term  $w_o e_j$  denotes the amplitude of unevenness and the term  $m_1$  indicates the number of half sine waves. It should be noted that the shape of bridge surface is idealized as a number of half sine waves with amplitudes at both supports of the bridge equal to zero. The amplitude of roughness can be upward or downward depending on the sign of the  $w_o e_j$  quantities.

Throughout the study, it is assumed that the shape of the bridge roughness surface and its amplitude under both wheels of vehicle are the same. The study of the effect of the roadway unevenness parameters on accelerations can be classified into two cases. First, varying numbers of half sine waves were studied while keeping the amplitudes constant, and second, roughness amplitudes were varied while keeping the numbers of half sine waves constant. The remaining parameters of the bridge and vehicle are considered to be the same as before.

Table 3.12 shows the numerical results for accelerations obtained by using different numbers of half sine waves to represent the roadway unevenness of the bridge. A number of half sine waves equal to zero indicates that the bridge has a level surface and the larger number of half sine waves indicates that the bridge surface is rougher. The

Table 3.12 Maximum Accelerations at Midspan of Simple Span Bridge Due to Different Numbers of Half Sine Waves

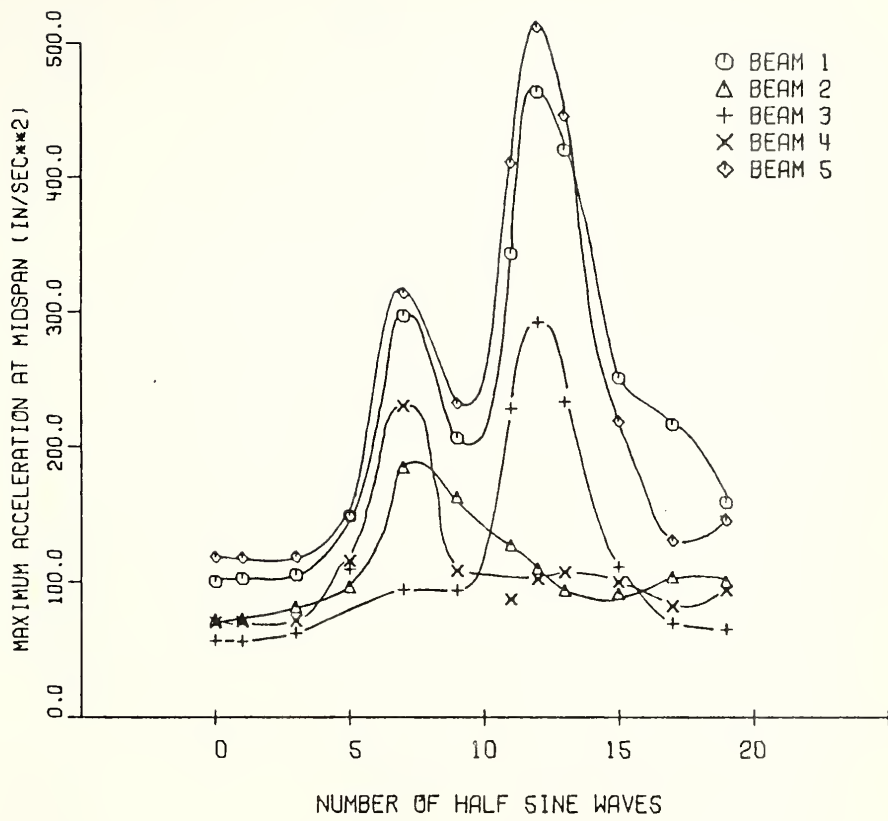
5 Girder Bridge 60 ft. Span 36WF230 HS 20-44 Loading 60 m.p.h.  
Left Wheel Over Beam 1 0.5 inch Amplitude of Roughness

Number of Half Sine Waves	Maximum Accelerations at Midspan (in/sec <sup>2</sup> )									
	Beam 1	x/L	Beam 2	x/L	Beam 3	x/L	Beam 4	x/L	Beam 5	x/L
0	100.73	0.05	-72.13	0.20	-56.90	0.85	-70.07	0.56	118.48	0.68
1	102.58	0.05	-72.67	0.20	-56.30	0.21	-70.36	0.56	117.92	0.68
3	105.70	0.05	-81.46	0.20	-62.26	0.85	-71.41	0.83	118.66	0.69
5	148.85	0.35	-96.50	0.20	-109.69	0.86	115.47	0.71	149.09	0.70
7	-297.12	0.93	-184.86	0.69	-94.53	0.61	229.97	0.93	-314.03	0.79
9	-206.71	0.81	-162.64	0.83	-93.68	0.84	-108.21	0.92	-232.19	0.93
11	-343.34	0.94	-127.34	0.50	-228.25	0.86	-87.22	0.84	410.57	0.69
12	-463.25	0.90	-110.18	0.46	-292.32	0.82	-102.11	0.83	511.47	0.98
13	-419.78	0.71	94.01	0.34	-233.30	0.94	107.31	0.70	445.53	0.96
15	251.22	0.56	-91.73	0.22	-111.10	0.56	-100.20	0.56	218.82	0.70
17	-216.88	0.44	-103.95	0.20	-69.61	0.85	82.14	0.44	-130.43	0.56
19	158.97	0.86	-100.77	0.19	-64.91	0.56	-94.00	0.55	145.81	0.67

amplitude of roughness measured at the top of the waves is assumed to be constant and has the value of 0.5 inches. The number of half sine waves used ranged from 0 to 19 and the corresponding maximum accelerations together with the longitudinal position of vehicle when it happens are listed. These results are also plotted in Figure 3.15.

It can be seen from these results that the accelerations were not influenced by the effect of the surface roughness for less than three half sine waves. This effect increases markedly when the number of half sine waves is greater than five and reaches its peak when the bridge surface consists of twelve half sine waves. The maximum results affected by the number of half sine waves are as much as five times the values of bridge with level surface. It should also be noted that the accelerations of edge beams, designated as beam 1 and beam 5, are greatest for every number of half sine waves.

Figure 3.16 shows the comparison of the history curves of interacting force between the bridge and the vehicle with three different number of half sine waves, the level surface, seven and twelve. The results of the interacting forces are in the terms of static wheel force and correspond to the results in Table 3.12. It can be seen that the interacting forces on the level surface bridge are very much different from the rough surface bridge. The periods of the interacting forces with seven



5 GIRDER BRIDGE 60 FT SPAN 36WF230 HS20-44 LOADING 60 MPH  
LEFT WHEEL OVER BEAM 1 0.5 INCH AMPLITUDE OF ROUGHNESS

Figure 3.15 Effect of Roadway Unevenness on Acceleration

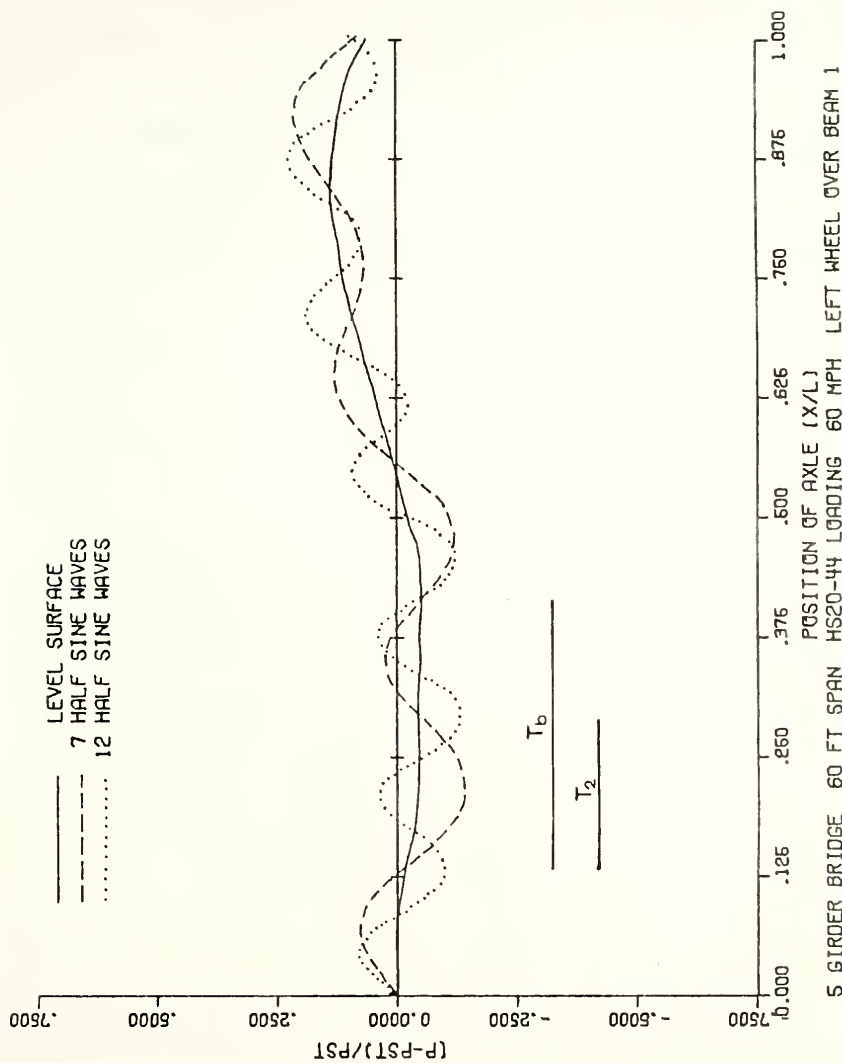


Figure 3.16 Effect of Roadway Unevenness on Interacting Force

and twelve half sine waves are equal to the first and second natural periods of bridge vibration respectively.

Figure 3.17 shows the comparison of the history curves representing the acceleration of beam 5 with three different numbers of half sine waves corresponding to the results shown in Figure 3.16 and Table 3.12. All curves are very similar when the longitudinal position of the vehicle is in the first quarter of the bridge length. It is then seen that, for the rest of the bridge length, the curves representing the rougher bridge will have more cycles and greater amplitudes of acceleration. This is caused by the resonance between the bridge and the vehicle.

The remaining parameter which also represents the roadway unevenness is the amplitude of roughness. The practical range of this parameter is between zero to one inch. The study of the acceleration affected by the varied amplitudes of roughness is classified into two different cases. In case A, a bridge profile consisting of three half sine waves which had little effect on the acceleration is used, while in case B, twelve half sine waves having the most effect are used. In each case, five different amplitudes of roughness have been used to evaluate the results. These five amplitudes have the values of 0., 0.25, 0.50, 0.75 and 1.0 inches. The remaining parameters are considered to be the same as before.

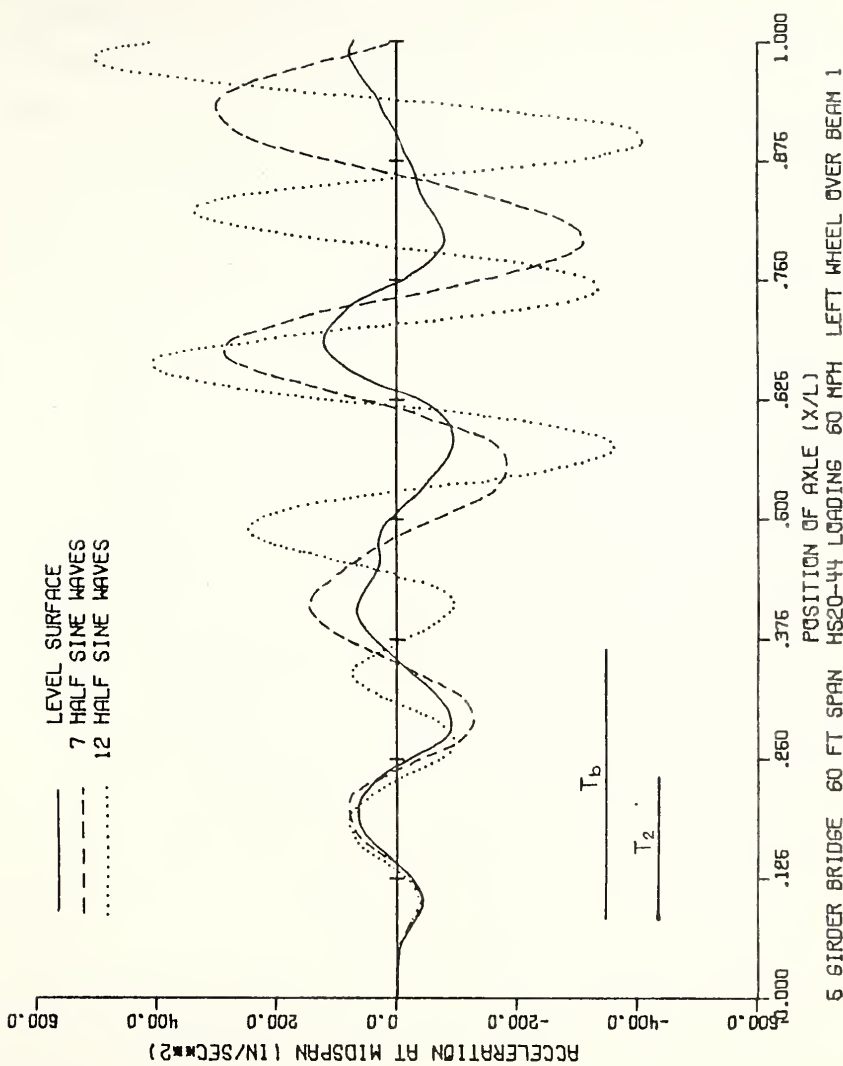


Figure 3.17 Effect of Roadway Unevenness on Acceleration of Beam 5

The numerical results in both cases are presented in Table 3.13 and the corresponding curves are plotted in Figure 3.18. From these results, it can be seen clearly that the effect of the amplitude depends on the number of half sine waves. For the increased values of roughness amplitude, the acceleration of each beam does not change at all in case A but it increases as much as ten times from the original value with the level surface in case B.

Table 3.13 Maximum Accelerations at Midspan of Simple Span Bridge Due to Different Amplitudes of Roughness

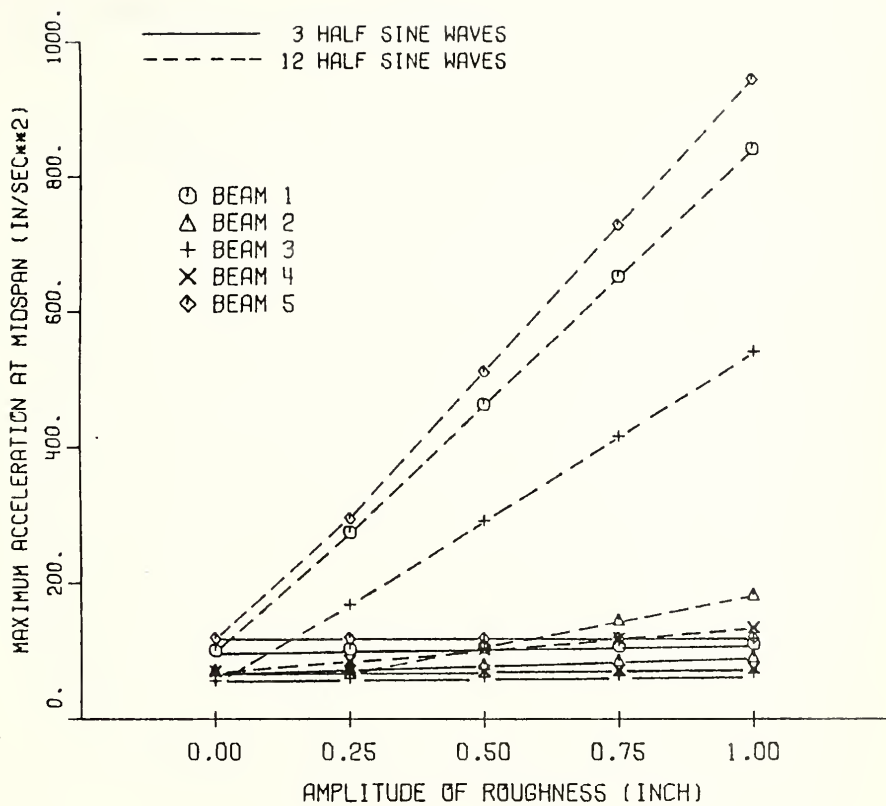
5 Girder Bridge 60 ft. Span 36WF230 HS 20-44 Loading  
Velocity 60 m.p.h. Left Wheel Over Beam 1

Case A Three Half Sine Waves

Amplitude (inch)	Maximum Accelerations at Midspan (in/sec <sup>2</sup> )						
	Beam 1	x/L	Beam 2	x/L	Beam 3	x/L	Beam 4
0.00	100.73	0.05	-72.13	0.20	-56.90	0.85	-70.07
0.25	103.29	0.05	-76.67	0.20	-59.59	0.85	-70.60
0.50	105.70	0.05	-81.46	0.20	-62.26	0.85	-71.41
0.75	108.18	0.05	-86.50	0.20	-64.95	0.85	-72.59
1.00	110.67	0.05	-91.81	0.21	-67.66	0.85	-74.01

Case B Twelve Half Sine Waves

Amplitude (inch)	Maximum Accelerations at Midspan (in/sec <sup>2</sup> )						
	Beam 1	x/L	Beam 2	x/L	Beam 3	x/L	Beam 4
0.00	100.73	0.05	-72.13	0.20	-56.90	0.85	-70.07
0.25	-275.84	0.90	-73.36	0.46	-168.76	0.82	-85.78
0.50	-463.25	0.90	-110.18	0.46	-292.32	0.82	-102.11
0.75	-652.20	0.90	-147.00	0.46	-416.59	0.82	-118.43
1.00	-841.44	0.90	-183.82	0.46	-540.85	0.82	-134.75



5 GIRDER BRIDGE 60 FT SPAN 36WF230 HS20-44 LOADING 60 MPH

Figure 3.18 Effect of Amplitude of Roughness on Acceleration

## CHAPTER IV

## ACCELERATION STUDIES OF THREE SPAN CONTINUOUS HIGHWAY BRIDGES

4.1 General

The purpose of this chapter is to study the major parameters which affect the accelerations of three-span continuous highway bridges subjected to moving vehicles. The method of analysis and the description of the computer program used in this study have been presented in Articles 2.3.2 and 2.3.4 respectively. In order to be able to compare the investigated accelerations of the bridge model with the available acceleration criterion for human response, all input data and output results are in dimensional form and in a practical range of bridge parameters. The parameters can be classified into the following four groups:

- a) Solution parameters to satisfy the convergence and stability of the solution.
- b) Bridge parameters including the span length, the ratio of side span to center span and the flexibility of girder.
- c) Vehicle parameters including the vehicle load, the axle spacing and the speed of vehicle.

- d) Initial conditions of vehicle and bridge including the initial oscillation of vehicle and the surface roughness of the bridge deck.

Throughout this chapter, the bridge is assumed to be an I-beam type composed of steel girders and a reinforced concrete deck with non-composite action. It has a prismatic cross-section and equal side spans. Damping is considered in both bridge and vehicle. The bridge and vehicle models are referred to Figures 2.9 and 2.11 respectively. Most of the vehicle parameters such as the coefficients of friction and frequencies of the tire-suspension system, weight ratios of tire to the vehicle load were obtained from the information presented in Table 4.1. (29) Table 4.1 shows the characteristics of "typical" vehicles including three axle vehicles, two axle vehicles and single axle loading. These characteristics are average values and were obtained from information given in Reference 2 and from manufacturers' data. The vehicle is assumed to travel from left to right with constant velocity. The calculated acceleration of the bridge occur at specified node points of the prismatic beam as shown in Figure 2.9. The maximum values of acceleration together with the corresponding position of axle at that time are considered.

The natural frequencies of the continuous beam used to approximate the actual bridge can be evaluated by obtaining the value of the dimensionless parameter  $\lambda_j$

Table 4.1 Data for "Typical Vehicles" (29)

Quantity	Unit	Three-axle Vehicle	Two-axle Vehicle	Single-axle Vehicle
W	kips	72	64	64
L <sub>1</sub>	ft.	12	14-35	-
L <sub>2</sub>	ft.	14-35	-	-
w <sub>1</sub> /W		0.08	0.90	-
w <sub>2</sub> /W		0.80	-	-
w <sub>1</sub> /W		0.03	0.05	-
w <sub>2</sub> /W		0.05	0.05	-
w <sub>3</sub> /W		0.04	-	-
i <sub>1</sub>		0.5-1.0	0.9-1.7	-
i <sub>2</sub>		0.9-1.7	-	-
a <sub>1</sub>		0.602	0.5	-
a <sub>3</sub>		0.494	-	-
a <sub>5</sub>		0.083	-	-
$\mu_1$		0.05-0.10	0.12-0.28	0.12-0.28
$\mu_2$		0.12-0.28	0.12-0.28	-
$\mu_3$		0.12-0.28	-	-
f <sub>t,1</sub>	cps	3.13-3.72	3.13-3.72	3.13-3.72
f <sub>t,2</sub>	cps	3.13-3.72	3.13-3.72	-
f <sub>t,3</sub>	cps	3.13-3.72	-	-
f <sub>ts,1</sub>	cps	1.57-1.65	1.99-2.14	1.74-2.36
f <sub>ts,2</sub>	cps	1.99-2.14	1.74-2.36	-
f <sub>ts,3</sub>	cps	1.74-2.36	-	-
P <sub>st,1</sub>	kips	8	32	64
P <sub>st,2</sub>	kips	32	32	-
P <sub>st,3</sub>	kips	32	-	-

which is plotted as a function of span ratio "a", in Figure 4.1. The subscript j is an integer denoting the order of the natural frequency under consideration. These data were evaluated by application of the method described briefly in Reference 36. The natural frequency in cycles per second can then be calculated by the equation

$$(f_b)_j = \frac{\lambda_j^2}{2\pi L^2} \sqrt{\frac{EI}{m_b}} \quad (4-1)$$

where EI is the flexural rigidity of the beam cross section,  $m_b$  is its mass per unit of length and L is the length of the center span.

#### 4.2 Solution Parameters

Solution parameters which are necessary to assure that successive cycles of iteration converge and the solution is stable consist of the number of integration steps for a complete solution and the number of mass concentrations which affects the accuracy of the results. Table 4.2 shows the convergence of the acceleration at mid-center span due to the variations in the number of integration steps. These accelerations are evaluated at the different positions of the front axle of the vehicle on the bridge. The bridge model used is a 64 ft.- 80 ft.- 64 ft. span, I-beam girder type with a bridge damping factor of 0.02. The damping factor is the ratio of the viscous damping of

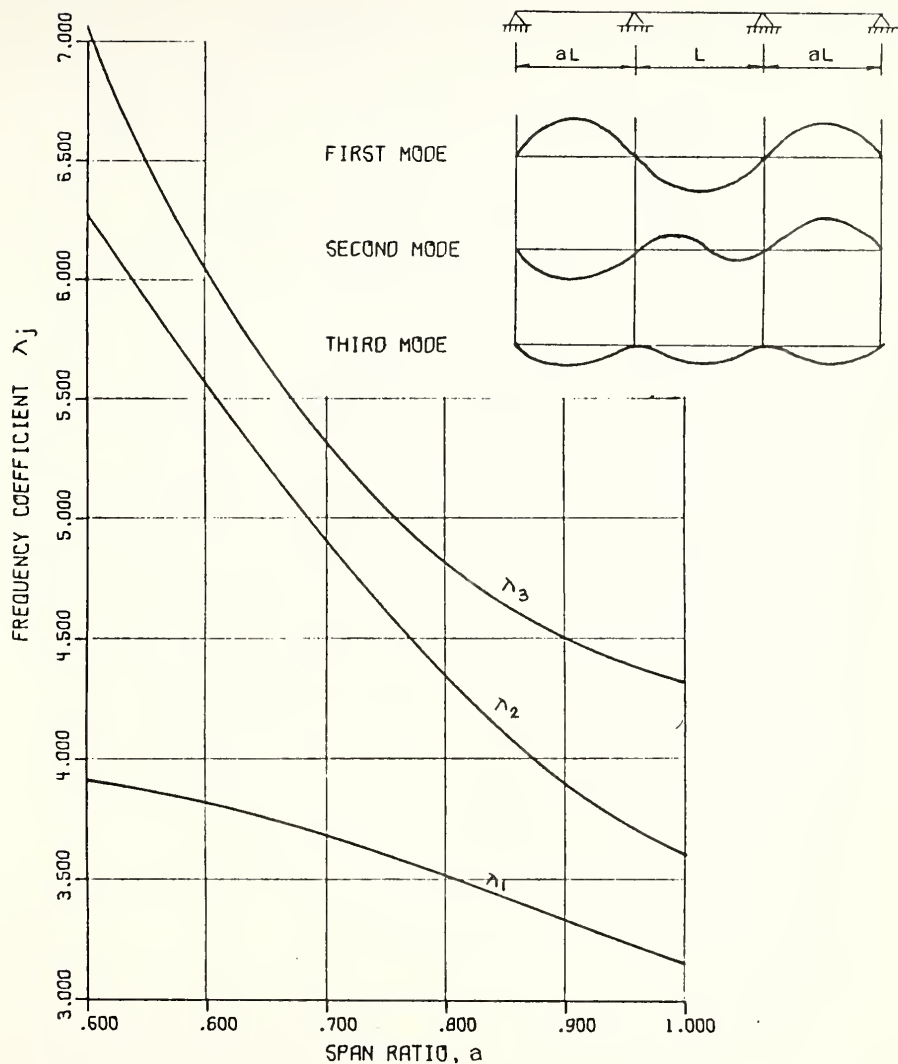


Figure 4.1 Frequency Coefficients for the First Three Natural Modes of Vibration of a 3-Span Continuous Beam (30)

Table 4.2 Comparison of Accelerations at Mid-Center Span Obtained by Using Different Numbers of Integration Steps

64-80-64 ft. Continuous Span 36WF170 Girders  
 $n = 4$   $m = 4$   $c/c_r = .02$  HS 20-44 Loading  
 Smooth Vehicle 60 m.p.h. Level Surface

$x/L_b$	Accelerations at Mid-Center Span (in/sec <sup>2</sup> )				
	N = 600	N = 1000	N = 1600	N = 2000	N = 2200
0.1	-1.616	-1.510	-1.483	-1.479	-1.476
0.2	-0.591	-0.716	-0.813	-0.830	-0.829
0.3	11.543	11.375	11.347	11.343	11.338
0.4	-8.525	-9.300	-9.237	-9.230	-9.205
0.5	-1.581	-0.831	-1.009	-0.980	-1.036
0.6	-3.499	-3.187	-2.986	-3.017	-2.993
0.7	-7.970	-8.251	-8.083	-8.122	-8.041
0.8	5.922	5.945	5.517	5.548	5.473
0.9	0.073	-0.459	-0.227	-0.305	-0.297
1.0	-2.740	-2.760	-2.552	-2.490	-2.457
1.1	-0.169	0.184	-0.017	-0.044	-0.021
1.2	-1.289	-1.636	-1.499	-1.730	-1.661

bridge to the critical damping value. The value of 0.02 is a practical value for most three span continuous highway bridges, according to References 14, 16, 19, 22 and 25. The vehicle model is a three axle vehicle with HS 20-44 loading type and has a velocity of 60 m.p.h. The initial conditions are that the vehicle has no initial vertical oscillation before entering the bridge (hereafter referred to as smooth vehicle) and the bridge has a smooth and level surface.

Observation of the calculated accelerations obtained by using from 600 to 2200 integration steps indicates that 2000 integration steps are sufficient for the stability of the solutions. Since the cost of the computer solution increases as N increases, the "minimum" number should be chosen for economy.

It was shown in Reference 29 that the results obtained from the bridge model with  $n = 4$  and  $m = 4$  (where  $n$  and  $m$  represent the number of divisions of end spans and center span, respectively) were sufficiently accurate and the natural periods of this model were close to those of the continuous beam. The cost of the computer solution is increased for a larger number of mass concentrations. Since a large number of solutions were to be made for the complete parameter study, the bridge model with  $n = 4$  and  $m = 4$  was considered to be satisfactory and was used throughout this study.

#### 4.3 Bridge Parameters

##### 4.3.1 Accelerations of B.P.R. Bridges

The characteristics of the Bureau of Public Roads bridges presented in Reference 41 are for I-beam type bridges which are designed either for H 15-44 loading or for HS 20-44 loading. The lengths of the individual spans are in the ratio of 4:5:4, and the overall length ranges from 130 ft. to 260 ft. Thus the shortest bridge has spans of 40 ft. - 50 ft. - 40 ft. and the longest bridge has spans of 80 ft. - 100 ft. - 80 ft. The bridges designed for the H 15-44 and HS 20-44 loadings have roadway widths of 28 ft. and 44 ft., respectively. Since it was shown in Article 3.3.1 that the accelerations of simple span B.P.R. bridges with roadway width of 44 ft. were greater than those with roadway width of 28 ft. because of the heavier moving vehicle load, the three span continuous B.P.R. bridges with roadway widths of 44 ft. are the only type to be studied in this article.

The cross section of the B.P.R. bridge is shown in Figure 4.2 and the single beam with the mass concentrations used to represent the bridge in the analysis is idealized as shown in Figure 4.3. Also shown in this figure is the HS 20-44 vehicle load which is assumed to be smooth vehicle. It should be remembered that the bridge and vehicle models shown in Figure 4.3 are not the complete

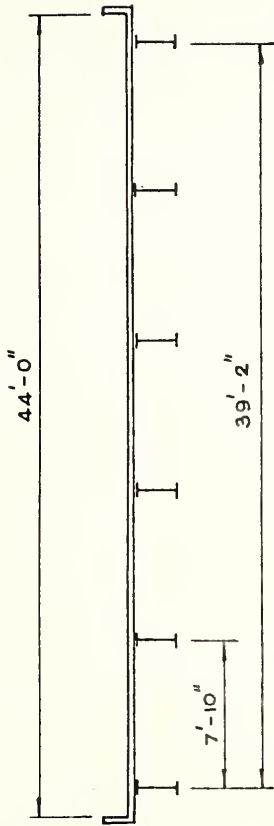


Figure 4.2 Cross Section Near Mid-Center Span of B.P.R. Bridges

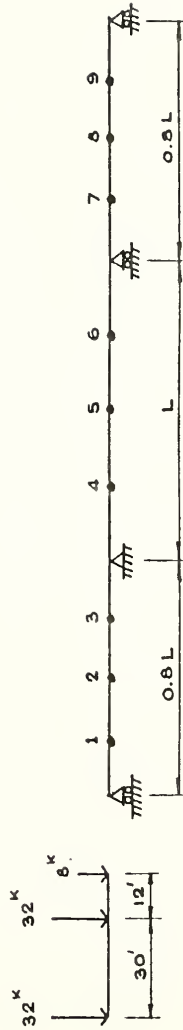


Figure 4.3 Bridge and Vehicle Models for Study of B.P.R. Bridges

models used in the analysis. Figures 2.9 and 2.11 show the complete models.

Table 4.3 shows the characteristics of the three span continuous B.P.R. bridges including the weight per unit length, the fundamental natural frequency and the corresponding period of vibration of the bridges. The quantities shown are necessary as input data to evaluate the corresponding accelerations at nodes 1 to 9. The parameters of three-axle vehicle are considered to be the same as in Article 4.2 and the roadway surface is horizontal and smooth. The bridge is assumed to have a damping factor of 0.02 and this value is used for all bridge models throughout this chapter.

Table 4.4 shows the maximum accelerations at each node obtained by using B.P.R. bridge models with different span lengths. The corresponding position of front axle as the maximum acceleration occurs is also shown. These results are plotted graphically and shown in Figure 4.4. It can be seen that these accelerations increase with decreasing values of span length. In other words, the accelerations are larger for shorter spans. This is in agreement with the results from simple span bridges presented in Article 3.3.1 except that the accelerations of simple span bridges are four times greater than those for the three span bridges. It should be also noted that, for most of the span lengths, the acceleration of node 2

Table 4.3 Characteristics of Three Span Continuous B.P.R. Bridges

Span Length (ft)	Girder Section	$I^*$ (in <sup>4</sup> )	$W_b^+$ (k/ft <sup>2</sup> )	Frequency $\tilde{\omega}^{++}$ (cps)	Period $\tilde{T}$ (sec)
40-50-40	30WF99	43800	5.34	5.81	0.17
48-60-48	33WF118	55200	5.46	4.48	0.22
56-70-56	36WF150	73980	5.65	3.75	0.27
64-80-64	36WF170	82800	5.77	3.00	0.33
72-90-72	36WF230	109800	6.13	2.65	0.38
80-100-80	36WF245	116400	6.22	2.20	0.46

\*  $I$  is the total moment of inertia of cross-section

+  $W_b$  is weight per linear length of center span

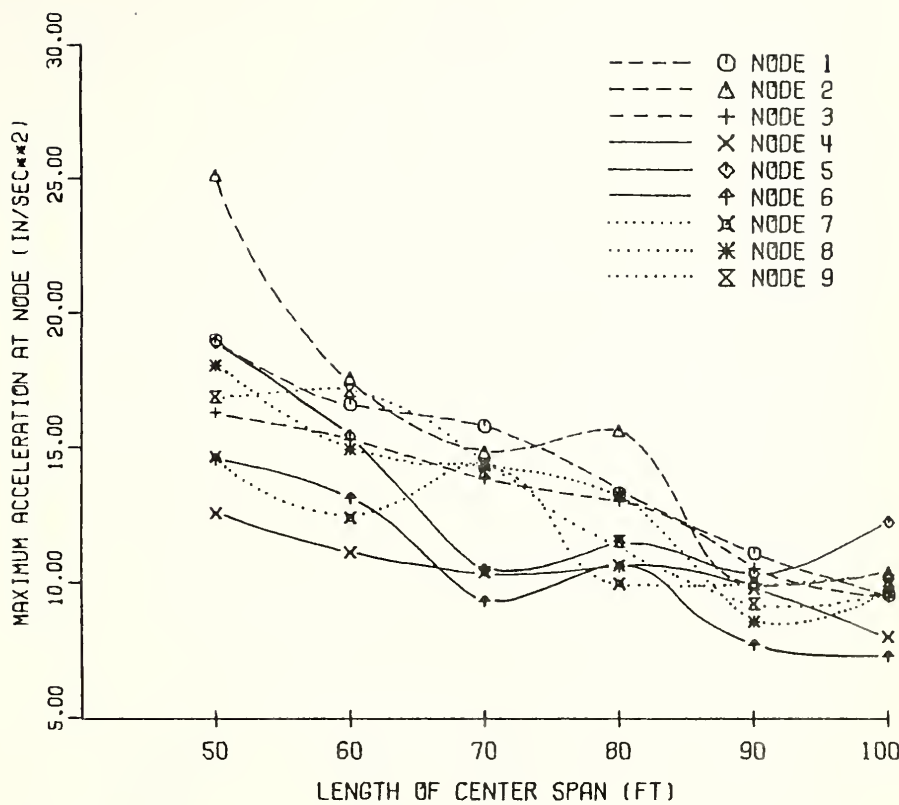
++ Frequency is the fundamental natural frequency

Table 4.4 Maximum Accelerations of Three Span  
Continuous B.P.R. Bridges

HS 20-44 Loading    60 m.p.h.    Level Surface  
 $n = 4$      $m = 4$      $a = 0.8$      $c/c_r = 0.02$

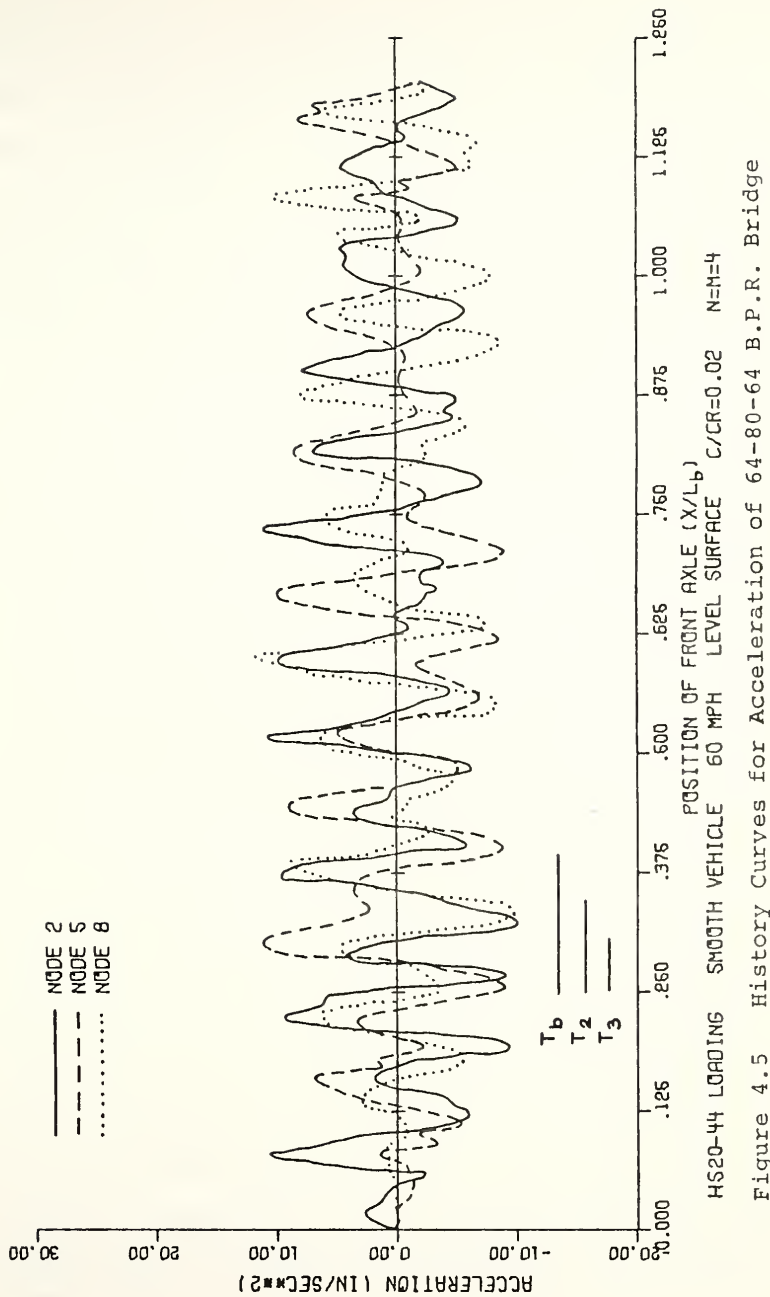
Node	Maximum Acceleration (in/sec <sup>2</sup> )					
	40-50-40	x/L <sub>b</sub>	48-60-48	x/L <sub>b</sub>	56-70-56	x/L <sub>b</sub>
1	19.00	0.34	-16.59	0.33	-15.79	0.46
2	25.12	0.34	-17.57	0.38	14.82	0.51
3	16.28	0.10	-15.27	0.32	-13.83	0.45
4	-12.56	1.13	11.11	0.48	-10.38	0.63
5	18.90	0.40	-15.42	1.12	-10.46	0.62
6	14.53	0.40	13.12	0.36	09.30	0.62
7	-14.63	0.41	12.38	1.09	-14.38	0.33
8	18.03	0.46	14.92	0.55	-14.30	0.32
9	16.86	0.46	-17.08	0.51	-14.12	0.34

Node	Maximum Acceleration (in/sec <sup>2</sup> )					
	64-80-64	x/L <sub>b</sub>	72-90-72	x/L <sub>b</sub>	80-100-80	x/L <sub>b</sub>
1	13.30	0.23	11.10	0.21	-9.55	0.44
2	15.61	0.22	9.98	0.07	-10.38	0.64
3	-13.00	0.32	10.52	0.06	-9.48	0.45
4	10.65	0.29	9.77	0.29	8.00	0.29
5	11.49	0.30	10.36	0.28	12.25	0.29
6	10.59	0.30	7.69	0.42	7.28	0.31
7	9.96	1.07	-10.10	0.31	-9.91	0.31
8	13.24	0.59	-8.55	1.05	-9.70	0.95
9	-11.53	0.33	-9.23	0.30	-10.07	0.29



SPAN RATIO = 0.8    LEVEL SURFACE    C/CR=0.02    N=M=4  
HS 20-44    SMOOTH VEHICLE    60 MPH

Figure 4.4 Effect of Span Length on Acceleration

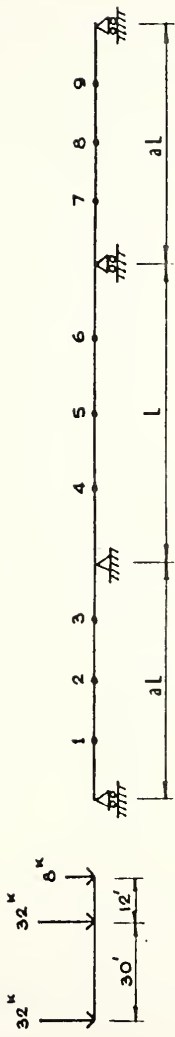


is greatest and the accelerations at the center of either end span or center span are greater than those at other points on that span.

Figure 4.5 shows the history curves of the accelerations of three midspan nodes. The accelerations of node 2 increase rapidly when the vehicle enters the bridge, while the accelerations of nodes 5 and 8 are not significant at this step. The same is true for the other two nodes, that is, the accelerations of node 5 and node 8 have their largest values when the vehicle is on the center span and third span respectively.

#### 4.3.2 Effect of Span Ratio

The bridge models in the previous articles had a span ratio of 0.8 which is commonly used for three span continuous highway bridges. In this article, the span ratios range from 0.6 to 1.0 and the resulting effects on acceleration are studied. The bridge model used as shown in Figure 4.6(a) has the center span L constant at 80 ft. while both end spans range from 48 ft. to 80 ft. The remaining parameters of the vehicle and bridge models are considered to be the same as before. The fundamental frequency and period of vibration of each bridge for the corresponding value of span ratio was evaluated from the plot shown in Figure 4.1. These frequencies and the maximum acceleration at each node as affected by the span ratio



(a) Effect of Span Ratio on Acceleration

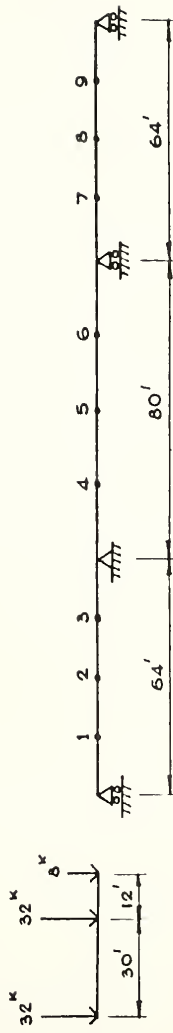
(b) Effect of  $|E|$  on Acceleration

Figure 4.6 Bridge and Vehicle Models Used in Study

parameter are presented in Table 4.5. These results are also shown graphically in Figure 4.7. It can be seen that the span ratio has no effect on the magnitudes of acceleration. It follows that the accelerations of the end spans are greater than that of the center span when the span ratio is less than 0.8 and these accelerations tend to be equal when the span ratio approaches the value of 1.0. This can be explained by the fact that the acceleration is larger for the shorter span.

#### 4.3.3 Effect of Girder Flexibility

Figure 4.6(b) shows the bridge model used for the study of the accelerations as affected by using different values of girder stiffness. The bridge has 64 ft. - 80 ft. - 64 ft. span lengths with a damping factor of 0.02 and a level surface. The remaining parameters are considered to be the same as before. Five different girder sections are used to evaluate the accelerations at each node. The 36WF170 is supposed to be the proper section for the design of this bridge. The section is reduced and four smaller sections are used to study the effect of girder flexibility. The smallest section used is the 33WF118 which has a moment of inertia nearly half that of the 36WF170. The properties of each section were obtained from the information given in Reference 42 and shown in Table 4.6.

Table 4.5 Maximum Accelerations of Three Span Continuous Bridges Obtained by Using Different Span Ratio Coefficients

HS 20-44 Loading 60 m.p.h. Smooth Vehicle Level Surface n = 4  
 $m = 4$   $c/c_r = 0.02$  L = 80 ft. 36WF170 Girders

a = ratio of side span to center span

$\lambda_i$  = dimensionless coefficient in the expression for fundamental frequency of oscillation of a continuous beam

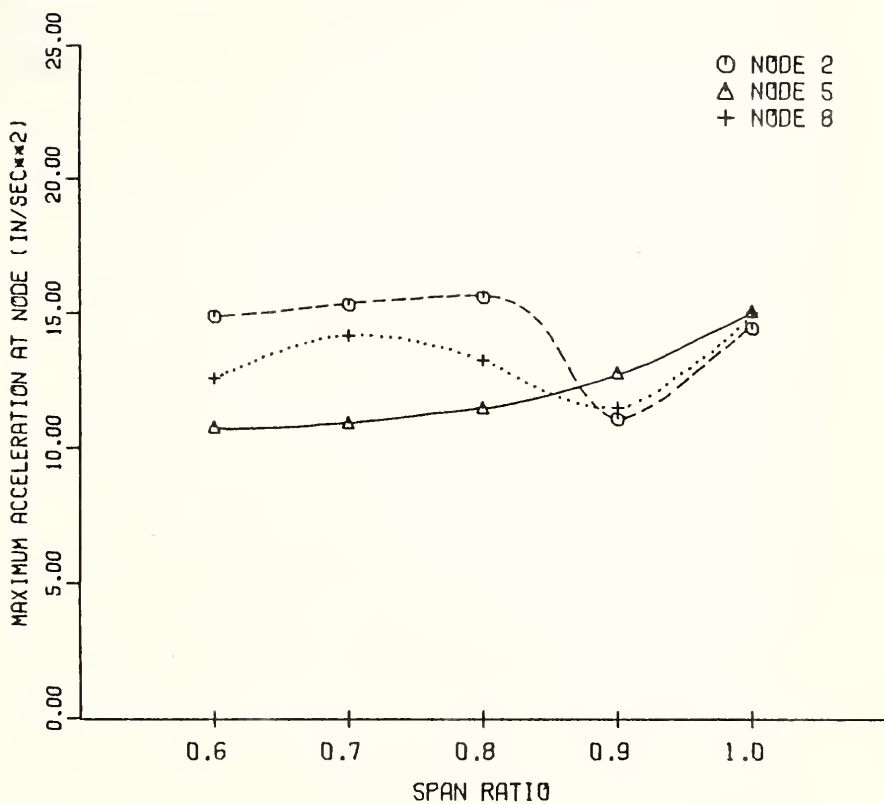
a	$\lambda_i$	$f_b$ (cps)	$T_b$ (sec)
0.6	3.84	3.54	0.25
0.7	3.70	3.28	0.30
0.8	3.54	3.00	0.33
0.9	3.35	2.69	0.37
1.0	3.16	2.39	0.42

Table 4.5, cont.

Node	Maximum Acceleration (in/sec <sup>2</sup> )					
	$a = 0.6$	$x/L_b$	$a = 0.7$	$x/L_b$	$a = 0.8$	$x/L_b$
1	-15.25	0.33	12.53	0.08	13.30	0.23
2	14.89	0.08	15.34	0.62	15.61	0.22
3	15.23	0.25	13.07	0.77	-13.00	0.32
4	-8.23	0.65	-12.41	0.63	10.65	0.29
5	-10.78	0.66	-10.95	0.25	11.49	0.30
6	-8.18	0.67	-9.59	0.26	10.59	0.30
7	14.27	1.08	12.21	1.07	9.96	1.07
8	-12.59	1.12	-14.18	0.31	13.24	0.58
9	17.37	1.08	-13.41	1.18	-11.53	0.33

Node	Maximum Acceleration (in/sec <sup>2</sup> )					
	$a = 0.9$	$x/L_b$	$a = 1.0$	$x/L_b$	$a = 1.0$	$x/L_b$
1	12.37	0.22	12.94	0.56	12.94	0.56
2	-11.09	0.31	14.48	0.55	14.48	0.55
3	-13.56	0.30	-14.12	0.29	-14.12	0.29
4	12.13	0.31	10.46	0.30	10.46	0.30
5	12.80	0.31	15.12	0.47	15.12	0.47
6	10.21	0.32	11.01	0.31	11.01	0.31
7	11.67	0.38	13.52	1.07	13.52	1.07
8	-11.49	0.97	-15.06	1.14	-15.06	1.14
9	11.65	0.40	14.37	0.39	14.37	0.39



6 GIRDER BRIDGE    LEVEL SURFACE    C/CR=0.02    N=M=4    L=80FT  
HS 20-44    SMOOTH VEHICLE    60 MPH

Figure 4.7    Effect of Span Ratio on Acceleration

Maximum accelerations at nodes are obtained by using these five different sections while keeping all other parameters constant. These results are shown in Table 4.6 and are plotted graphically as a function of girder moment of inertia in Figure 4.8. It can be seen from these results that the accelerations of the bridges analyzed are not materially affected by the increased girder flexibilities.

#### 4.4 Vehicle Parameters

##### 4.4.1 Effect of Vehicle Loads

Three different types of commercial trucks have been considered as the vehicle model used on the 64 ft. - 80 ft. - 64 ft. B.P.R. bridge at a speed of 60 m.p.h. These trucks are HS 20-44, HS 15-44 and H 20-44. The total load on each axle of each type was obtained from the information given in Reference 43. Since the bridge was idealized as a single beam in the analysis, these vehicle loads are also idealized as a single line and the resulting load on each axle is shown in Figure 4.9(a). The total vehicle loads for HS 20-44, HS 15-44 and H 20-44 are 72, 54 and 40 kips respectively.

Each truck was simulated to traverse the bridge model and the maximum accelerations at nodes were obtained as shown in Table 4.7. As might be expected, the accelerations of the bridge are greatest for the heaviest vehicle load.

Table 4.6 Maximum Accelerations of Three Span Continuous Bridges Obtained by Using Different Girder Flexibilities

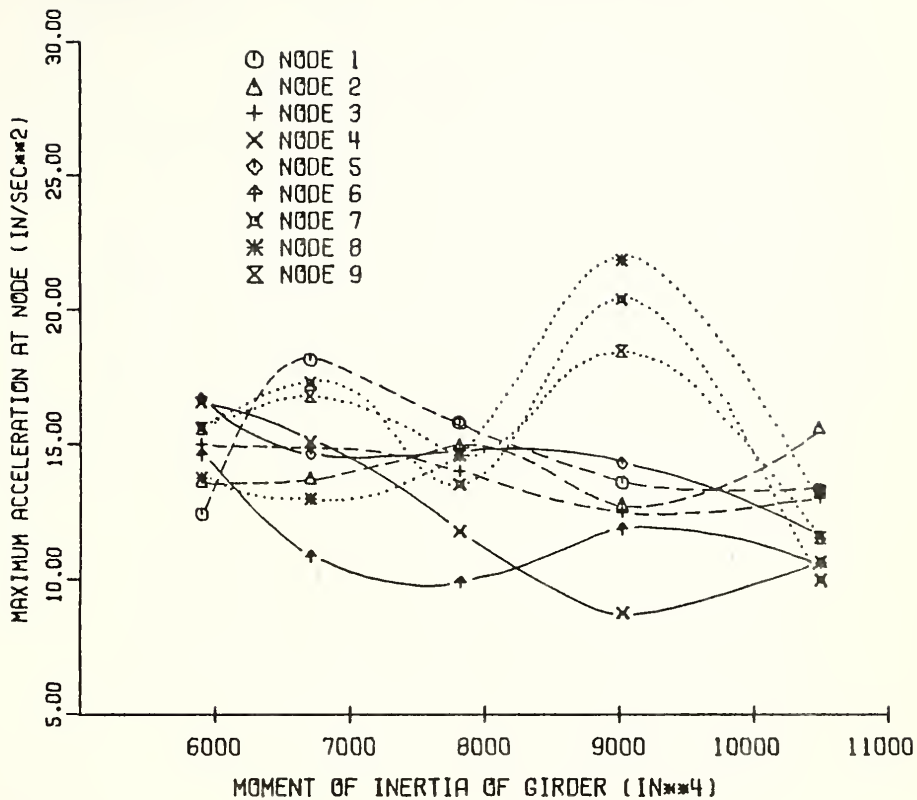
64-80-64 Continuous Span Bridge  $n = 4$   $m = 4$   $c/c_x = .02$  Level Surface  
 HS 20-44 Loading 60 m.p.h. Smooth Vehicle

Girder	$I_{xx}$ (in. <sup>2</sup> )	$W$ (k./ft.)	$\lambda$ (in. <sup>-1</sup> )	$\varepsilon_b$ (cps)	$\tau_b$ (sec)
36WF170	10500	.170	50.0	3.00	0.33
36WF150	9030	.150	44.2	2.87	0.35
36WF135	7820	.135	39.8	2.75	0.36
36NT130	6710	.120	38.3	2.61	0.38
36WF118	5900	.118	34.3	2.52	0.40

Node	Maximum Acceleration (in/sec <sup>2</sup> )					
	36WF170	$x/L_b$	36WF150	$x/L_b$	36WF135	$x/L_b$
1	13.30	0.23	13.59	0.23	15.79	0.23
2	15.61	0.22	-12.97	0.34	-14.98	1.18
3	-13.00	0.32	12.48	0.07	14.01	0.07
4	10.65	0.29	-8.76	1.10	11.78	0.22
5	11.49	0.30	14.29	0.30	15.83	0.31
6	10.59	0.30	11.85	0.31	9.90	0.32
7	9.96	1.07	20.36	1.07	-23.50	0.35
8	13.24	0.58	21.82	1.08	14.57	0.61
9	-11.53	0.33	18.44	1.08	14.64	0.61

Node	Maximum Acceleration (in/sec <sup>2</sup> )					
	36WF118	$x/L_b$	36WF118	$x/L_b$	36WF118	$x/L_b$
1	12.41	1.20	-18.14	1.20	12.41	0.59
2	13.65	0.08	13.74	0.08	13.65	0.08
3	14.99	0.07	14.86	0.07	14.99	0.07
4	16.56	0.33	15.09	0.33	16.56	0.34
5	16.68	0.34	14.64	0.34	16.68	0.34
6	14.60	0.34	10.87	0.34	14.60	0.35
7	15.62	1.07	17.27	1.07	15.62	1.08
8	-13.76	1.08	12.97	1.08	-13.76	1.12
9	-15.59	1.09	16.77	1.09	-15.59	1.14



64-80-64 SPAN BRIDGE LEVEL SURFACE C/CR=0.02 N=M=4  
HS 20-44 SMOOTH VEHICLE 60 MPH

Figure 4.8 Effect of EI on Acceleration

Table 4.7 Maximum Accelerations of Three Span Continuous Bridges Obtained by Using Different Types of Vehicle

64-80-64 B.P.R. Bridge    n = 4    m = 4    c/c<sub>r</sub> = .02  
 Level Surface    Smooth Vchicle    60 m.p.h.

Node	Maximum Acceleration (in/sec <sup>2</sup> )					
	HS 20-44	x/L <sub>b</sub>	HS 15-44	x/L <sub>b</sub>	H 20-44	x/L <sub>b</sub>
1	13.30	0.23	9.75	0.23	10.60	0.17
2	15.61	0.22	11.37	0.22	12.83	0.16
3	-13.00	0.32	-9.11	0.32	11.12	0.16
4	10.65	0.29	8.36	0.29	7.67	0.23
5	11.49	0.30	9.27	0.30	9.50	0.24
6	10.59	0.30	8.39	0.30	8.13	0.24
7	9.96	1.07	7.29	1.07	7.62	0.69
8	13.24	0.59	-9.13	0.92	-8.11	0.26
9	-11.53	0.33	-8.52	0.33	-9.62	0.27

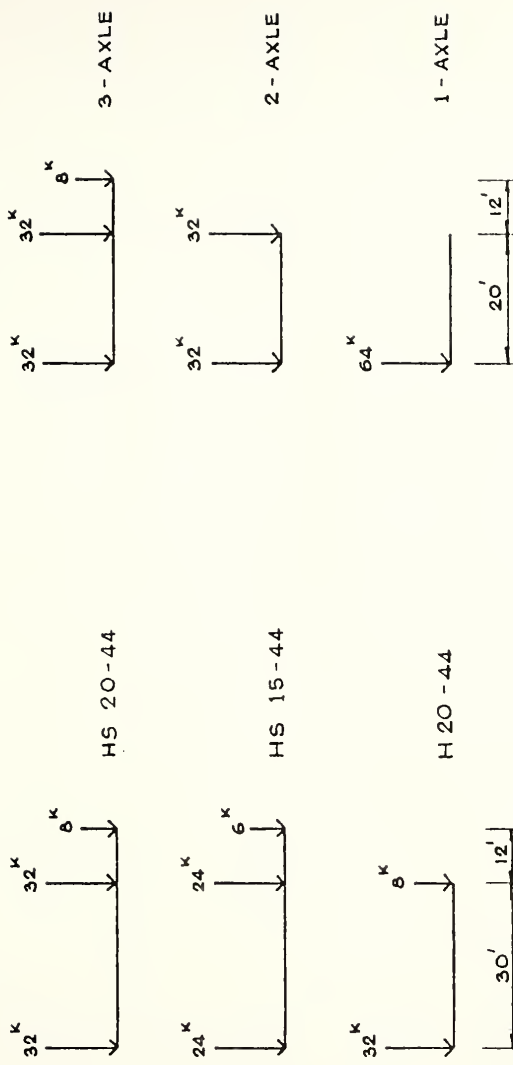


Figure 4.9 Vehicle Models Used in Study

(a) Effect of Vehicle Load on Acceleration  
(b) Effect of Number of Axles on Acceleration

It can be seen that the accelerations for HS 15-44 and H 20-44 are close although HS 15-44 has the larger total load. It can be explained that HS 15-44 has a larger number of axles than H 20-44 and the number of axles has an effect on acceleration. This will be discussed further in Article 4.4.2. Study results reported in this article indicate that the heavier vehicle load will cause greater accelerations of the bridge.

#### 4.4.2 Effect of Number of Axles and Axle Spacings

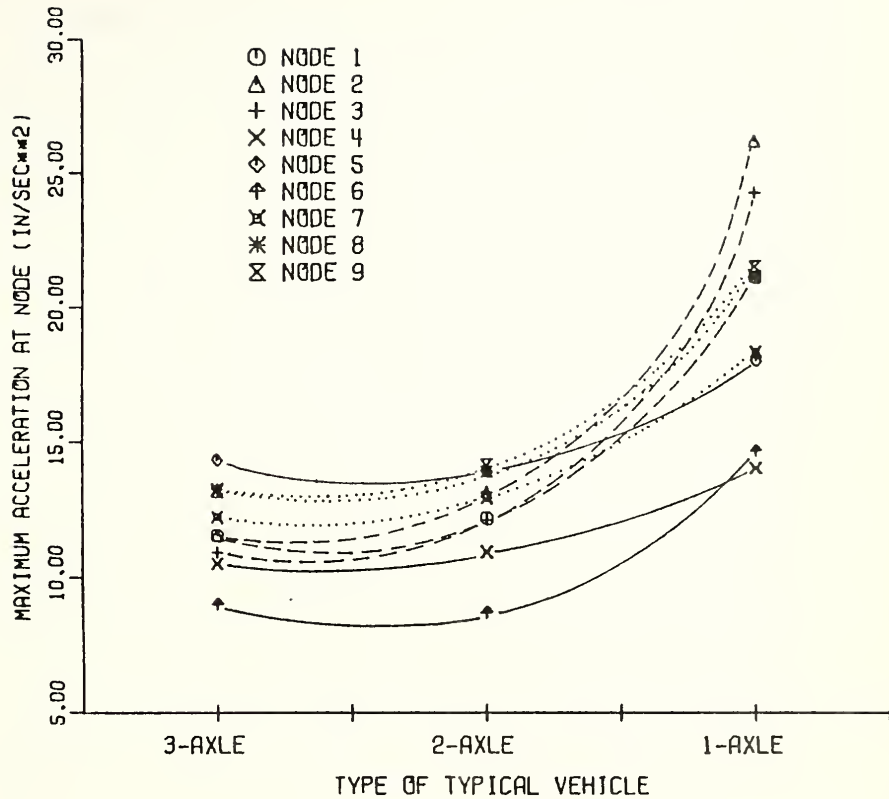
Figure 4.9(b) shows the typical vehicles with different number of axles. The parameters of typical vehicles were given in Table 4.1. The bridge model and the remaining parameters are the same as before. Although the values of the axle load for two-axle and single axle vehicle are not practical, the results of the accelerations of the bridge obtained will be useful for the further studies of design criteria. These results can also be compared with those for simple span bridges, for which the vehicle model was a single axle load.

The maximum accelerations at various nodes due to different moving typical vehicles are compared in Table 4.8 and shown graphically in Figure 4.10. It can be seen that there is not much difference between the acceleration magnitudes for three axle and two axle vehicles. The front axle load of 8 kips does not have much influence on

Table 4.8 Maximum Accelerations of Three Span  
Continuous Bridges Subjected to Vehicles  
with Different Numbers of Axles

64-80-64 B.P.R. Bridge  $n = 4$   $m = 4$   $c/c_r = .02$   
Level Surface Smooth Vehicle 60 m.p.h.

Node	Maximum Acceleration (in/sec <sup>2</sup> )					
	3-axle	x/L <sub>b</sub>	2-axle	x/L <sub>b</sub>	1-axle	x/L <sub>b</sub>
1	11.56	0.45	-12.18	0.14	21.12	0.03
2	-11.56	0.27	13.14	0.02	26.16	0.02
3	10.92	0.07	12.12	0.02	24.24	0.02
4	10.50	0.30	10.93	0.24	14.03	0.24
5	14.33	0.31	13.89	0.25	-17.99	0.43
6	9.01	0.30	8.69	0.24	-14.66	0.04
7	-12.21	0.27	-12.93	0.21	18.34	0.54
8	-13.26	0.42	-13.89	0.21	21.15	0.54
9	13.16	0.22	14.14	0.16	-21.51	0.50



64-80-64 BPR BRIDGE    LEVEL SURFACE    C/CR=0.02    N=M=4  
TYPICAL SMOOTH VEHICLES    60 MPH

Figure 4.10 Effect of Number of Axles on Acceleration

acceleration. As might be expected, the magnitudes of accelerations under single axle loads are almost double the values of two and three axle vehicles.

Table 4.9 and Figure 4.11 show the effect of vehicle axle spacing on bridge accelerations. The vehicle model is the HS 20-44 loading with trailer axle spacing varying from 20 ft. to 35 ft. the tractor axle spacing is kept constant at 12 ft. and the vehicle speed is 60 m.p.h. All remaining vehicle parameters are the same as in Article 4.3.3. The bridge model is the 64 ft. - 80 ft. - 64 ft. B.P.R. bridge with a damping factor of 0.02 and a level surface.

From the results, the magnitudes of the maximum accelerations are not affected by varied axle spacing although these values are slightly higher when the axle spacing is between 30 ft. and 35 ft. It should be noted that these results will be changed if different span lengths of the bridge model are used. In order to consider the results in a non-dimensional form, the ratio of the axle spacing of the vehicle to the length of the center span is introduced. It can be seen that for the three span continuous bridge, the accelerations slightly increase when the axle spacing ratio ranges between 0.37 to 0.43.

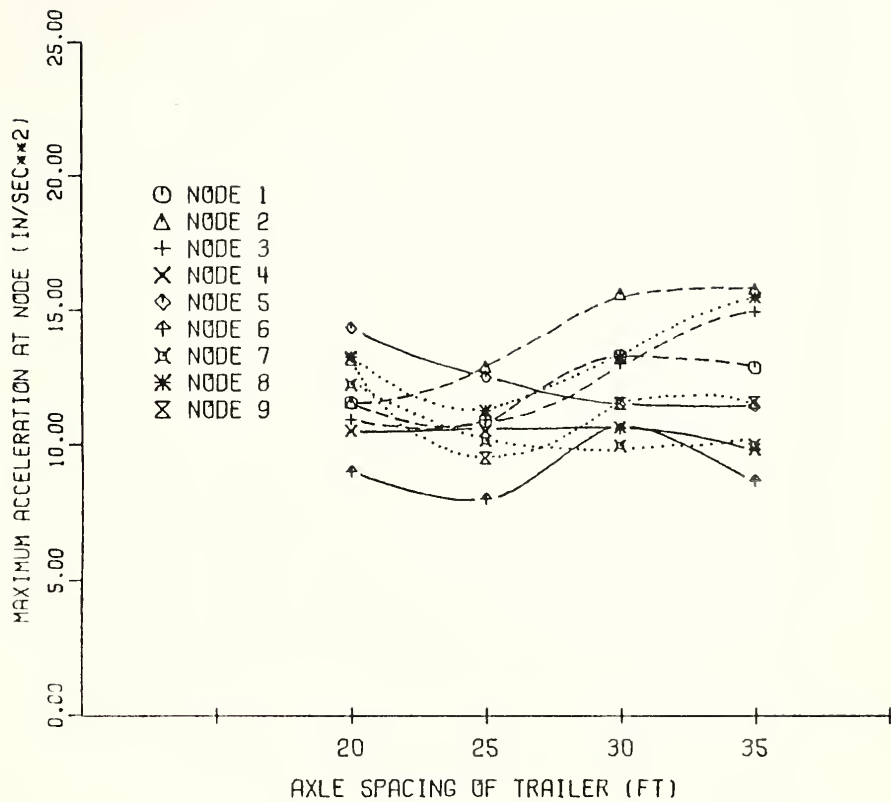
#### 4.4.3 Effect of Vehicle Speed

Table 4.10 and Figure 4.12 show the maximum accelerations

Table 4.9 Maximum Accelerations of Three Span Continuous Bridges  
Subjected to Vehicles with Different Axle Spacings

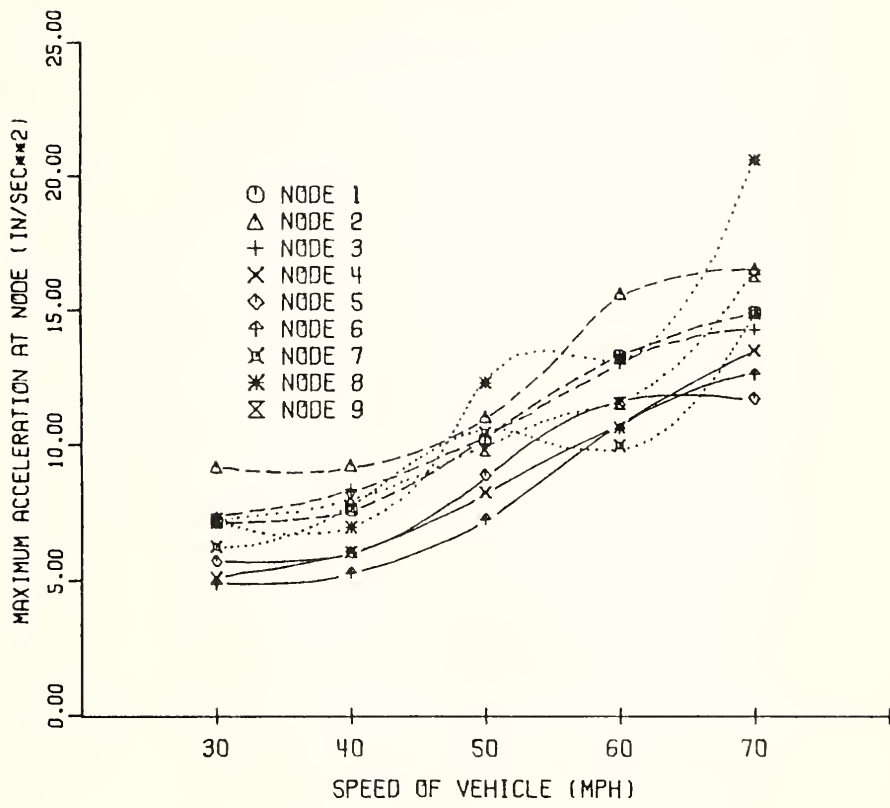
64-80-64 B.P.R. Bridge  $n = 4$   $m = 4$   $c/c_f = .02$  Level Surface  
72 kips Total Load 3-Axle Smooth Vehicle 60 m.p.h.

Node	Maximum Acceleration ( $\text{in/sec}^2$ )						
	$l_2 = 20 \text{ ft.}$	$x/L_b$	$l_2 = 25 \text{ ft.}$	$x/L_b$	$l_2 = 30 \text{ ft.}$	$x/L_b$	$l_2 = 35 \text{ ft.}$
1	11.45	0.45	-10.87	0.31	13.30	0.23	12.86
2	-11.56	0.27	-12.90	0.30	15.61	0.22	15.77
3	10.92	0.07	-10.93	0.30	-13.00	0.32	14.94
4	10.50	0.29	10.49	0.24	10.65	0.29	9.82
5	14.33	0.31	12.51	1.15	11.49	0.30	11.43
6	9.01	0.30	8.01	0.91	10.59	0.30	-8.66
7	-12.21	0.27	10.14	1.07	9.96	1.07	-10.00
8	-13.26	0.42	-11.24	1.11	13.24	0.58	-15.47
9	13.16	0.22	-9.49	0.18	-11.53	0.33	11.56



64-80-64 BPR BRIDGE    LEVEL SURFACE    C/CR=0.02    N=M=4  
 3-AXLE SMOOTH VEHICLE    60 MPH    AXLE SPACING OF TRACTOR = 12 FT

Figure 4.11 Effect of Axle Spacing on Acceleration



64-80-64 BPR BRIDGE LEVEL SURFACE C/CR=0.02 N=M=4  
HS 20-44 SMOOTH VEHICLE

Figure 4.12 Effect of Speed on Acceleration

Table 4.10 Maximum Accelerations of Three Span Continuous Bridges  
 Obtained by Using Different Vehicle Speeds  
 64-80-64 B.P.R. Bridge  $n = 4$   $m = 4$   $c/c_r = .02$  Level Surface  
 HS 20-44 Loading Smooth Vehicle

Node	Maximum Acceleration (in/sec <sup>2</sup> )						
	30 mph	x/L <sub>b</sub>	40 mph	x/L <sub>b</sub>	50 mph	x/L <sub>b</sub>	60 mph
1	-7.17	0.26	-7.62	0.28	10.18	0.45	13.30
2	-9.20	0.26	-9.24	0.29	11.02	0.07	15.61
3	7.33	0.21	-8.37	0.28	10.02	0.21	-13.00
4	5.11	0.32	6.05	0.36	8.25	0.27	10.65
5	5.72	0.25	-6.04	0.53	-8.89	0.23	11.49
6	4.87	0.25	5.27	0.22	-7.26	0.62	10.59
7	-6.26	0.33	7.63	1.07	-10.43	0.29	9.96
8	-7.14	0.33	-6.96	0.13	-12.29	0.29	13.24
9	-7.26	0.34	-8.04	0.38	-9.81	0.29	-11.53

of the three span continuous bridge affected by the vehicle speeds between 30 m.p.h. to 70 m.p.h. The bridge model is the 64 ft. - 80 ft. - 64 ft. B.P.R. bridge and has the remaining parameters the same as in Article 4.4.2. The vehicle model has HS 20-44 loading. As might be expected, the accelerations of the bridge increase as the vehicle speed increases.

#### 4.4.4 Effect of Frequency Ratio

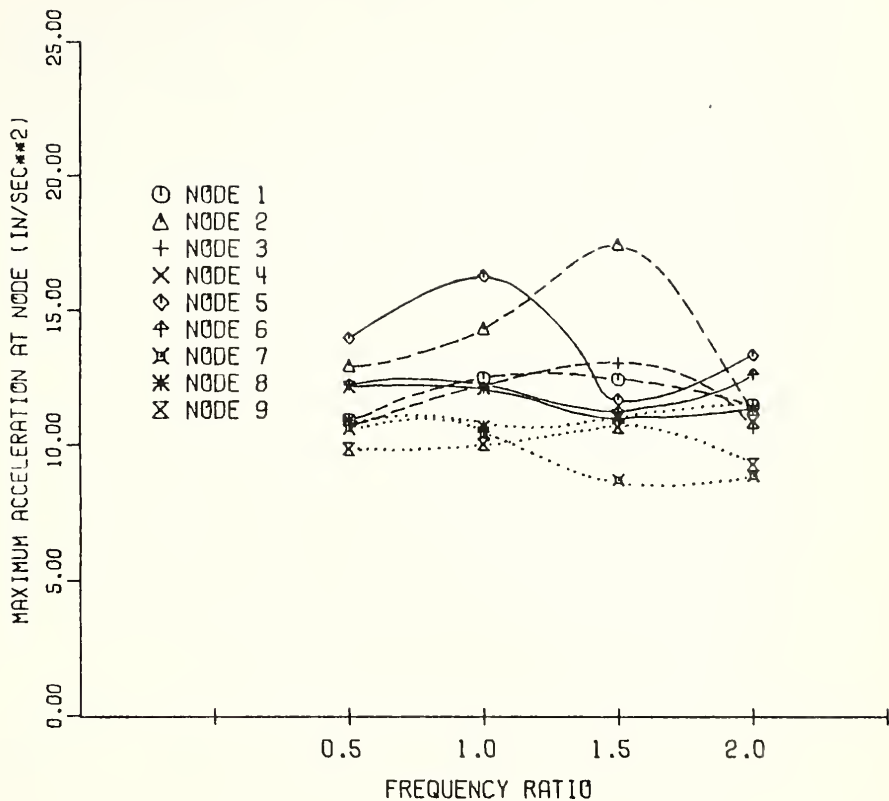
Table 4.11 and Figure 4.13 show the maximum bridge accelerations obtained by using the values of frequency ratio  $f_v/f_b$  in the range between 0.5 and 2.0. The bridge model used is 64 ft. - 80 ft. - 64 ft. B.P.R. bridge as used in Article 4.4.2 and has a fundamental natural frequency of 3.0 c.p.s. The vehicle has HS 20-44 loading and is assumed to oscillate on its tires only. The frequency of vehicle  $f_v$  used is the tire frequency of the rear axles and the corresponding coefficients of friction of the suspension spring have an infinite value.

It can be seen from the results shown that the frequency ratio has no appreciable effect on the bridge accelerations and the magnitudes of the accelerations in these curves are about the same for all values of frequency ratio. In particular, the accelerations for  $f_v/f_b = 1.0$  are no larger than those for the other frequency ratios.

Table 4.11 Maximum Accelerations of Three Span Continuous Bridges  
 Obtained by Using Different Frequency Ratios  
 64-80-64 B.P.R. Bridge     $m = \frac{4}{n}$      $c/c_s = .02$     Level Surface  
 HS 20-44 Loading    60 m.p.h.    Smooth Vehicle    The Tire Spring is Only Active  
 $\mu = \infty$

Node	Maximum Acceleration (in/sec <sup>2</sup> )					
	$f_v/f_b = 0.5$	$x/L_b$	$f_v/f_b = 1.0$	$x/L_b$	$f_v/f_b = 1.5$	$x/L_b$
1	10.94	0.23	-12.50	0.34	-12.45	0.32
2	12.96	0.22	-14.35	0.33	17.48	0.22
3	10.72	0.07	-12.11	0.32	13.05	0.21
4	12.13	0.29	-12.10	0.64	11.10	0.29
5	13.97	0.30	-16.29	0.63	11.69	0.30
6	12.22	0.30	-12.14	0.63	11.21	0.30
7	10.60	1.07	10.39	1.07	-8.72	0.31
8	10.92	0.37	-10.68	1.00	-10.99	0.31
9	9.85	0.36	-10.04	0.47	-10.68	0.32

 $f_v/f_b = 2.0$  $x/L_b$



64-80-64 BPR BRIDGE LEVEL SURFACE C/CR=0.02 N=M=4  
HS 20-44 SMOOTH VEHICLE 60 MPH  
TIRE SPRING IS ONLY ACTIVE

Figure 4.13 Effect of Frequency Ratio on Acceleration

## 4.5 Initial Conditions of Vehicle and Bridge

### 4.5.1 Effect of Initially Oscillating Vehicle

It is seldom that a vehicle enters the bridge with its suspended mass in equilibrium for vertical motion. It is therefore necessary to investigate the effect of initially oscillating vehicles on bridge motion. The initial oscillation of the vehicle may arise either from the ever present irregularities of the approach pavement or from a sharp discontinuity between the approach pavement and the entrance of the bridge.

The method of analysis assumes that, while the vehicle is on the approach pavement, the vertical oscillation of each axle is of the simple harmonic type. The initial value of the interacting force,  $P_i$ , between the  $i^{\text{th}}$  axle and the pavement is expressed as

$$P_i = (1 + C_i \cos \theta_i) P_{st,i} \quad (4-2)$$

where  $C_i$  is the amplitude of the initial force variation,  $\theta_i$  is the phase angle between the time at which the force attains its maximum value and the time at which the front axle enters the bridge, and  $P_{st,i}$  is the static reaction on the axle. For a two-axle loading, the phase angles  $\theta_1$  and  $\theta_2$  will in general be different. The quantity  $\Delta\theta = \theta_1 - \theta_2$  will be referred to as the phase angle difference of the vehicle.

The values of  $C_i$  and  $\theta_i$  depend upon such variables as the dimensions and location of the irregularities and discontinuity, and upon the speed of the vehicle. The initial value of the frictional force depends, in addition, on the past history of the deformation of the suspension spring, and may have any value between  $F'$  and  $-F'$ .

It was shown in Reference 30 that the height of discontinuity required to produce a variation of interacting force of  $0.15 P_{st}$ , or  $C_i = 0.15$ , is about 0.12 in. The value of  $C_i = 0.15$  is considered to represent the vehicle with an initial oscillation due to the roughness of the approach pavement. In addition, the value of  $C_i = 0.50$  is considered to define the effect of a large discontinuity at the abutment, or of a large irregularity on the approach pavement located close to the entrance of the bridge. The value of phase angle,  $\theta_i$ , was considered to vary between  $0^\circ$  and  $360^\circ$  and the initial value of interleaf friction was assigned the values of  $F'$ , zero and  $-F'$ .

#### 4.5.1.1 Effect of Amplitude of Initial Oscillation

Maximum accelerations of the bridge as affected by the different amplitudes of initial oscillation of vehicle are studied. The bridge model is considered to be the same as in Article 4.4.3. The vehicle model has an HS 20-44 loading with the initial oscillation at the approach pavement and travels at the constant speed of

60 m.p.h. The amplitudes of initial oscillation of vehicle,  $C_i$ , are assigned to have the values of 0.0, 0.15, 0.30 and 0.50. These four values represent the smoothly moving, the oscillation due to the surface roughness, the oscillation due to a larger amplitude of roughness and the oscillation due to a large discontinuity, all at the approach pavement, respectively. The values of  $C_i$  are considered to be the same for each axle. The initial values of the frictional force and phase angle for each axle are all taken equal to zero.

The maximum accelerations at nodes evaluated by using the different values of  $C_i$  are compared in Table 4.12 and also are shown graphically in Figure 4.14. It can be seen that the accelerations increase for the larger amplitude of initial oscillation. The magnitude of maximum acceleration of all nodes increases as much as 1.5 times the original value for a smooth vehicle. It can be noted that the acceleration of the mid-center span is the largest value when the initial oscillation of vehicle is taken into account.

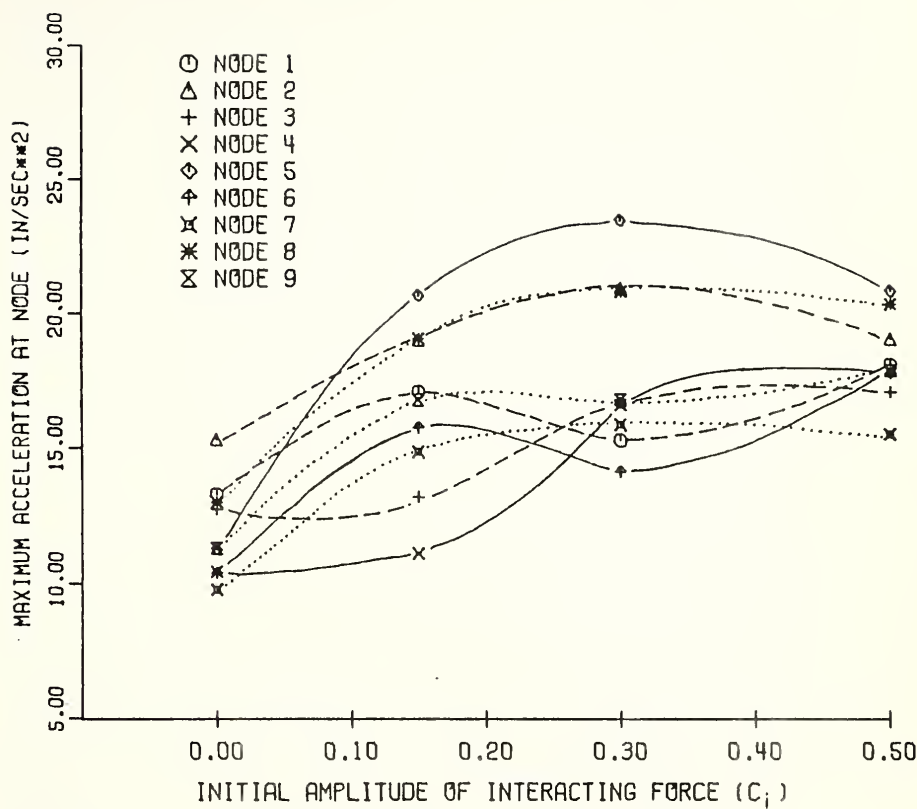
#### 4.5.1.2 Effect of Initial Phase Angle Difference

It is seldom that the initial oscillating three axle vehicle which passes over the irregularities at the approach will have the maximum initial forces for all axles. In other words, all axles would not have the same value of

Table 4.12 Maximum Accelerations of Three Span Continuous Bridges  
Subjected to Vehicles with Different Amplitudes of Initial  
Oscillation

64-80-64 B.P.R. Bridge    n = 4     $m = 4$      $c/c_r = .02$     Level Surface  
HS 20-44 Loading    60 m.p.h.    Oscillating Vehicle     $\theta_i = 0^\circ$      $u_i = 0$

Node	$C_i = 0$	$x/L_b$	$C_i = 0.15$	$x/L_b$	Maximum Acceleration (in/sec <sup>2</sup> )		
					$C_i = 0.30$	$x/L_b$	$C_i = 0.50$
1	13.30	0.23	17.08	0.23	15.29	0.28	18.08
2	15.32	0.22	18.99	0.22	-20.93	0.33	19.04
3	-12.76	0.32	-13.20	0.32	-16.67	0.32	17.05
4	10.45	0.29	-11.12	0.40	16.59	0.36	17.87
5	11.28	0.30	-20.66	0.40	23.46	0.35	-20.82
6	10.39	0.30	-15.74	0.39	14.12	0.35	-17.74
7	9.77	1.07	14.85	1.07	15.83	0.43	-15.50
8	12.99	0.58	-19.06	0.92	20.81	0.42	-20.34
9	-11.31	0.33	-16.78	0.33	-16.78	0.47	-17.87



64-80-64 BPR BRIDGE LEVEL SURFACE C/CR=0.02 N=M=4  
HS 20-44 OSCILLATING VEHICLE 60 MPH

Figure 4.14 Effect of Initially Oscillating Vehicle on Acceleration

initial phase angle of zero to obtain the maximum force referred to Equation (4-2). It can be explained that the vehicle has two axle spacings, the spacing between the first and second axles, and the spacing between the second and third axles. It will take quite a time between first and the following axles to pass the same irregularities at the approach. Assuming that the force of the first axle attains the maximum value at the approach or  $\theta_1 = 0^\circ$ , the forces of second and third axles will or will not attain their maximum values at the approach or  $\theta_2$  and  $\theta_3$  can vary from  $0^\circ$  to  $360^\circ$ .

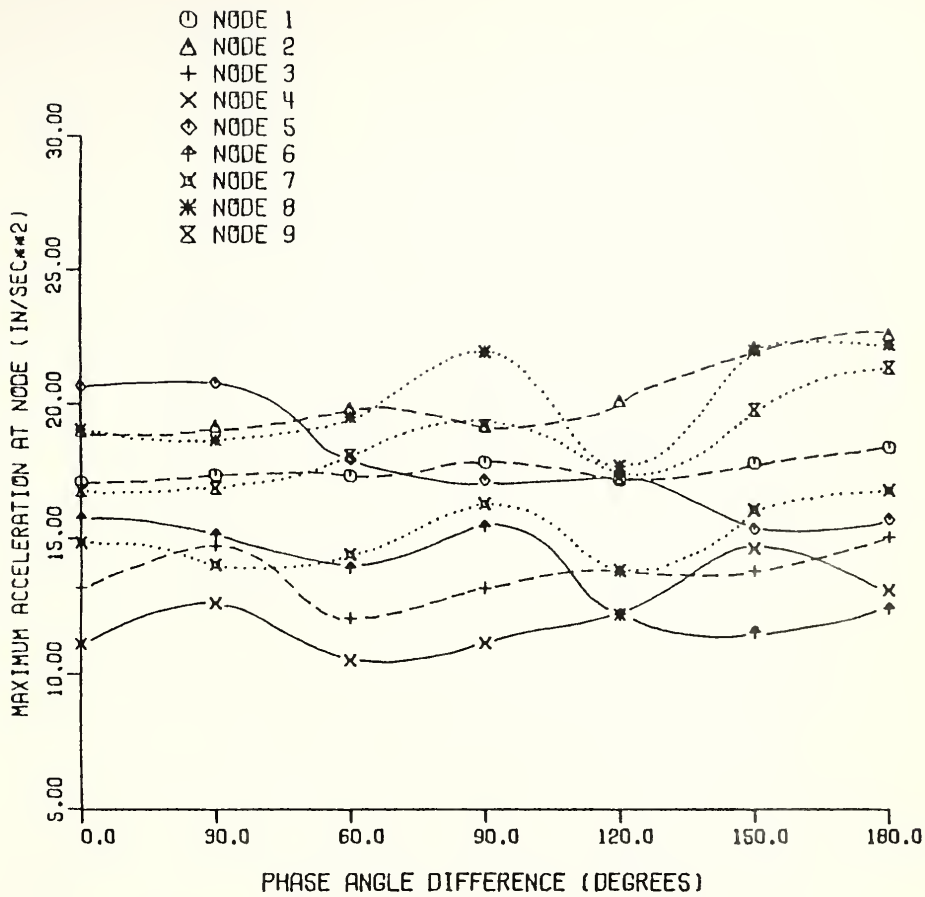
The effect of initial phase angle difference of the axles on accelerations was investigated and the results are shown in Table 4.13 and Figure 4.15. The bridge model is considered to be the same as in Article 4.5.1.1. The vehicle model has HS 20-44 loading with 15% initial oscillation for all axles. The value of initial coefficient of friction is taken equal to zero for each axle. The initial phase angles for first and second axles are kept constant at  $0^\circ$  while the initial phase angle of third axle is varied from  $0^\circ$  to  $180^\circ$ . The reason for keeping the phase angle of the first two axles at zero while studying the accelerations due to the difference between the second and third is that the first spacing is somewhat shorter than the second spacing, so the time required for the force to change its value is less.

Table 4.13 Maximum Accelerations of Three Span Continuous Bridges Subjected to 15% Initially Oscillating Vehicle with Varied Phase Angle Differences

64-80-64 B.P.R. Bridge     $n = 4$      $m = 4$      $c/c_i = .02$   
 Level Surface    HS 20-44 Loading    60 m.p.h.  
 Oscillating Vehicle     $C_i = 0.15$      $\mu_i = 0$   
 $\theta_1 = \theta_2 = 0^\circ$      $\Delta\theta = \theta_2 - \theta_3$

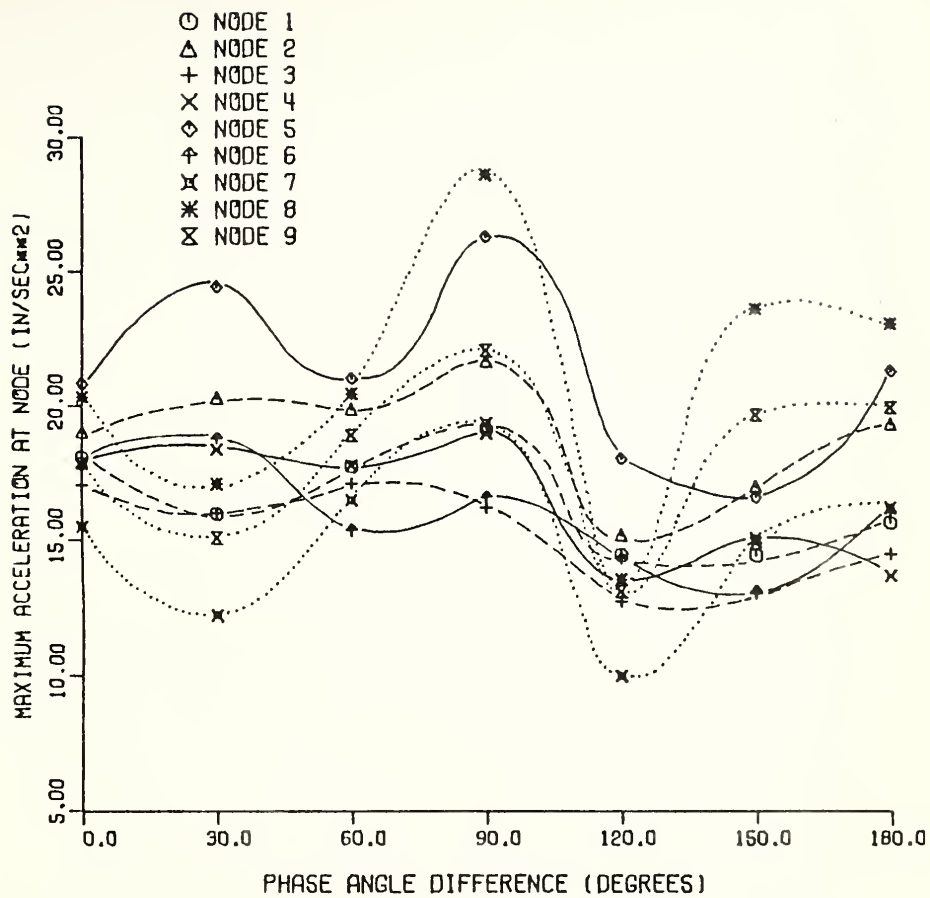
Node	Maximum Acceleration (in/sec <sup>2</sup> )							
	$\Delta\theta = 0^\circ$	$x/L_b$	$\Delta\theta = 30^\circ$	$x/L_b$	$\Delta\theta = 60^\circ$	$x/L_b$	$\Delta\theta = 90^\circ$	$x/L_b$
1	17.08	0.23	17.36	0.23	17.33	0.23	17.84	0.23
2	18.99	0.22	19.18	0.22	19.84	0.22	19.18	0.22
3	-13.20	0.32	-14.73	0.32	-12.05	0.32	-13.18	0.17
4	-11.12	0.40	-12.62	0.40	-10.51	0.40	11.15	0.32
5	-20.66	0.40	-20.78	0.40	-17.96	0.40	17.17	0.44
6	-15.74	0.39	-15.15	0.39	-13.92	0.39	15.44	0.45
7	14.85	1.07	-14.03	0.34	-14.42	0.34	-16.29	0.34
8	-19.06	0.92	-18.64	0.92	-19.51	0.33	-21.93	0.34
9	-16.77	0.33	-16.87	0.33	-18.09	0.33	-19.19	0.33

	$\Delta\theta = 120^\circ$	$x/L_b$	$\Delta\theta = 150^\circ$	$x/L_b$	$\Delta\theta = 180^\circ$	$x/L_b$
1	17.18	0.23	17.80	0.23	18.39	0.23
2	20.12	0.22	22.08	0.22	22.57	0.22
3	-13.79	0.32	13.81	0.51	-15.06	0.84
4	-12.19	0.40	14.64	0.36	13.09	0.36
5	-17.40	0.40	15.36	0.81	-15.72	0.36
6	-12.19	0.39	-11.54	0.55	-12.42	0.56
7	-13.82	0.34	16.07	0.74	16.79	0.74
8	-17.68	0.33	21.97	0.74	-22.19	0.33
9	-17.26	0.33	-19.78	0.33	-21.35	0.33



64-80-64 BPR BRIDGE LEVEL SURFACE C/CR=0.02 N=M=4  
HS 20-44 15 PERCENT INITIAL OSCILLATION

Figure 4.15 Effect of Initial Phase Angle Difference on Acceleration



64-80-64 BPR BRIDGE LEVEL SURFACE C/CR=0.02 N=M=4  
HS 20-44 50 PERCENT INITIAL OSCILLATION

Figure 4.15, cont.

From the results shown in Table 4.13 and Figure 4.15, the accelerations are not much affected by the initial phase angle difference ranging from 0° to 180°. The accelerations of midspan nodes are still the dominant values for whole range. It should be noted that the effect of the phase angle difference ranging from 180° to 360° is not shown because the values of initial forces were similar to those in 0° to 180° range.

The effects of initial phase angle difference were also investigated for a vehicle model having 50% initial oscillation due to a discontinuity at the approach. All remaining parameters are the same as before. The accelerations obtained are shown in Table 4.14 and Figure 4.15. Although these accelerations were markedly increased for the angle differences equal to 90° and 180°, it can be seen that the initial phase angle difference has no appreciable effect on acceleration.

#### 4.5.1.3 Effect of Coefficient of Interleaf Friction

In the previous studies of this chapter, the coefficient of friction of the suspension springs for the smoothly moving vehicle was assumed to have the value of 0.15 or  $\mu = 0.15$ , except when the effect of frequency ratio was studied, for which  $\mu$  was taken as infinite. In this study, the vehicle has an initial oscillation and initial coefficient of friction of suspension spring ( $\mu_i$ ). The

Table 4.14 Maximum Accelerations of Three Span Continuous Bridges Subjected to 50% Initially Oscillating Vehicle with Varied Phase Angle Differences

64-80-64 B.P.R. Bridge     $n = 4$      $m = 4$      $c/c_k = .02$   
 Level Surface    HS 20-44 Loading    60 m.p.h.  
 Oscillating Vehicle     $C_i = 0.50$      $\mu_i = 0$   
 $\theta_1 = \theta_2 = 0^\circ$      $\Delta\theta = \theta_2 - \theta_3$

Node	Maximum Acceleration (in/sec <sup>2</sup> )							
	$\Delta\theta = 0^\circ$	$x/L_b$	$\Delta\theta = 30^\circ$	$x/L_b$	$\Delta\theta = 60^\circ$	$x/L_b$	$\Delta\theta = 90^\circ$	$x/L_b$
1	18.08	0.28	15.97	0.28	17.73	0.23	19.12	0.28
2	19.04	0.28	-20.29	0.38	19.86	0.28	21.63	0.28
3	17.05	0.29	-16.01	0.38	17.09	0.29	-16.20	0.32
4	17.87	0.36	-18.36	0.45	17.74	0.36	18.94	0.36
5	-20.82	0.46	-24.41	0.46	-20.99	0.46	26.25	0.35
6	-17.74	0.46	-18.77	0.46	-15.35	0.46	16.58	0.35
7	-15.50	0.39	-12.21	0.38	-16.47	0.38	19.34	0.42
8	-20.34	0.39	-17.07	0.39	-20.43	0.39	28.57	0.42
9	-17.87	0.40	-15.07	0.40	-18.89	0.40	-22.04	0.47

	$\Delta\theta = 120^\circ$	$x/L_b$	$\Delta\theta = 150^\circ$	$x/L_b$	$\Delta\theta = 180^\circ$	$x/L_b$
1	-14.43	0.18	-14.43	0.18	-15.65	1.05
2	-15.18	0.25	-16.98	0.39	-19.31	1.06
3	12.72	0.29	-13.03	0.40	-14.48	0.32
4	13.53	0.36	14.88	0.88	13.66	0.35
5	-18.00	0.47	16.57	0.35	21.27	0.35
6	-14.31	0.46	13.07	1.01	16.03	0.35
7	-9.98	0.38	15.06	0.50	-16.18	0.46
8	-13.54	0.39	-23.58	0.55	23.04	0.71
9	-13.08	0.40	-19.63	0.55	19.92	0.51

numerical solutions of the accelerations of bridge are obtained for three different values of the coefficient of interleaf friction:  $\mu = \infty$ ,  $\mu = 0$  and  $\mu = 0.15$ . It is assumed that the initial coefficients of friction of suspension springs are infinite for  $\mu = \infty$  and equal to zero for  $\mu = 0$  and  $\mu = 0.15$ .

As previously explained, for  $\mu = \infty$  the suspension spring remains idle and the vehicle oscillates on its tires only. For  $\mu = 0$ , the suspension spring acts in series with the tire spring. Finally, for  $\mu = 0.15$  the frictional force exists and the energy dissipates in the suspension spring. The vehicle model is assumed to have 15 percent of initial interacting force and initial phase angle equal to zero for each axle. The vehicle has HS 20-44 loading and travels at 60 m.p.h. The bridge model and the remaining parameters are the same as in Article 4.5.1.2.

The results of investigations using three different values of  $\mu$  are obtained and shown in Table 4.15. It can be seen that the magnitudes of accelerations are not much different for the three different values of  $\mu$ . The accelerations for  $\mu = 0.15$  are slightly less than those for  $\mu = \infty$  because of the energy dissipated in the suspension spring and the amplitude of interacting force for  $\mu = 0.15$  was reduced, as described in Reference 30. The accelerations for  $\mu = 0$  are supposed to be higher than those for  $\mu = 0.15$ .

Table 4.15 Maximum Accelerations of Three Span  
Continuous Bridges Subjected to  
Initially Oscillating Vehicle  
with Different Coefficients of  
Friction of Suspension Spring

64-80-64 B.P.R. Bridge     $n = 4$      $m = 4$      $c/c_r = .02$   
Level Surface    HS 20-44 Loading    60 m.p.h.  
Initial Oscillating Vehicle     $C_i = 0.15$   
 $\theta_i = 0$      $\mu_i = \infty$  for  $\mu = \infty$      $\mu_i = 0$  for  $\mu = 0$  and  $\mu = 0.15$

Node	Maximum Acceleration (in/sec <sup>2</sup> )					
	$\mu = \infty$	$x/L_b$	$\mu = 0.15$	$x/L_b$	$\mu = 0$	$x/L_b$
1	16.07	0.89	18.08	0.23	-15.06	0.56
2	-20.94	0.94	19.04	0.22	-16.09	0.25
3	13.51	0.90	17.05	0.32	-13.34	0.51
4	15.62	0.29	17.87	0.40	-14.34	0.50
5	23.19	0.30	-20.82	0.40	-18.19	0.63
6	19.78	0.30	-17.74	0.39	-13.46	0.63
7	14.24	0.67	-15.50	1.07	-13.43	0.41
8	19.52	0.66	-20.34	0.92	-14.06	0.41
9	17.06	0.75	-17.87	0.33	-13.16	0.40

but they are the least. It can be explained that the vehicle frequency is different for each case.

#### 4.5.2 Effect of Bridge Surface Roughness

In the preceding study of three span continuous bridge, the surface of the bridge model is assumed to be smooth and level. Generally, this condition is seldom the case for most highway bridges. The surface roughness of the bridge specified in this study includes the initial camber, grade, vertical curve and roadway unevenness. It is designated as the term  $d_{pi}$  described in Article 2.3.2. For a given bridge, this quantity may be presumed to be known and its amplitude practically ranges from 0.0 to 1.0 inch.

The surface roughness can be of any shape due to factors described above. For this study, the profile of the surface roughness is idealized as a series of continuous half sine waves along the span length. The amplitude of the roughness is always equal to zero at the support and is maximum at the middle of the wave. For the three span continuous bridge, each span has an equal number of half sine waves. Figure 4.16 illustrates the examples of the profiles of bridge models having one, two and four half sine waves. The first wave of each span has a positive or upward amplitude. For a given bridge model, all peak amplitudes of half sine waves are

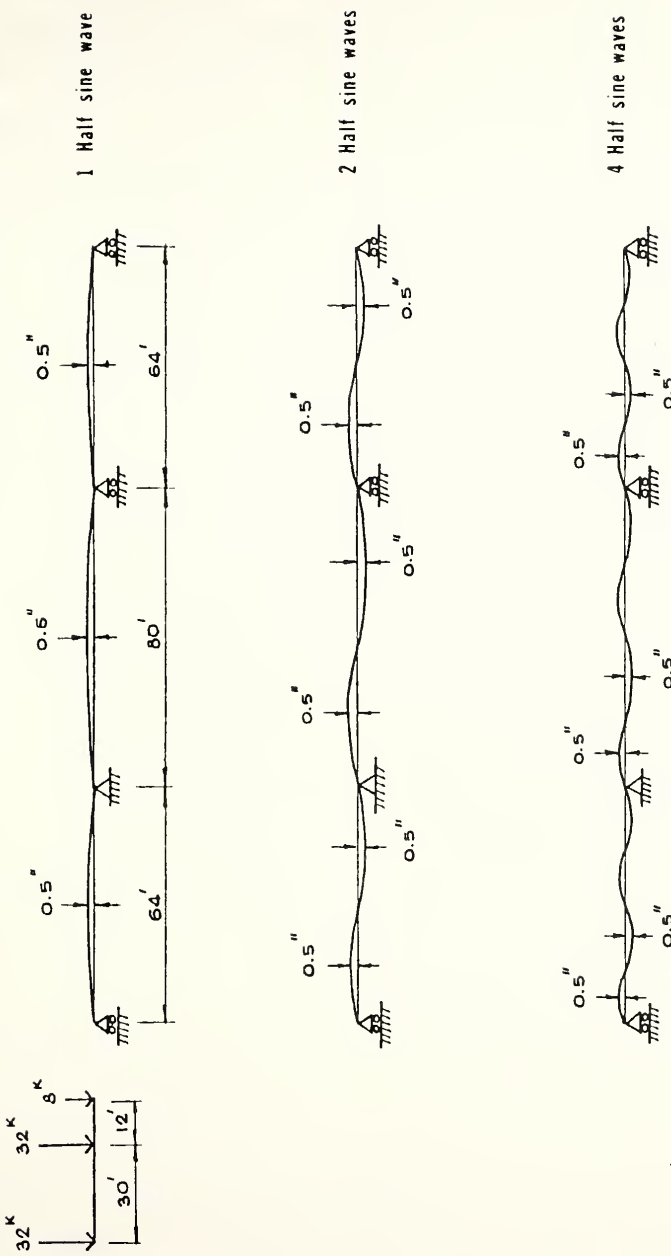


Figure 4.16 Model of Three Span Bridges with Rough Surface

assumed to be the same. In this study, two parameters representing the surface roughness are investigated: the number of half sine waves and the amplitude of roughness.

The effect of different numbers of half sine waves on bridge accelerations are investigated while keeping the peak amplitude of half sine waves constant. The bridge model is a 64 ft. - 80 ft. - 64 ft. damped B.P.R. bridge. The vehicle model has HS 20-44 loading, smoothly moving type with the speed of 60 m.p.h. The peak amplitudes of roughness used are kept constant at 0.5 in. All remaining parameters are considered to be the same as before.

The maximum accelerations at the nodes are evaluated by using from zero to 12 half sine waves. The results are listed in Table 4.16 and shown graphically in Figure 4.17. It can be seen that the accelerations for the number of half sine waves ranging from 0 to 2 are nearly constant. These accelerations increase sharply and attain the maximum for four half sine waves and gradually decrease for more than four half sine waves. The magnitudes of accelerations for four half sine waves are very much greater than those for the level surface condition. This can be explained in Figures 4.18-1 and 4.18-2 which shows the histories of interacting forces of the second axle and accelerations at mid-center span respectively. In

Table 4.16 Maximum Accelerations of Three Span Continuous Bridges  
Due to Different Numbers of Half Sine Waves

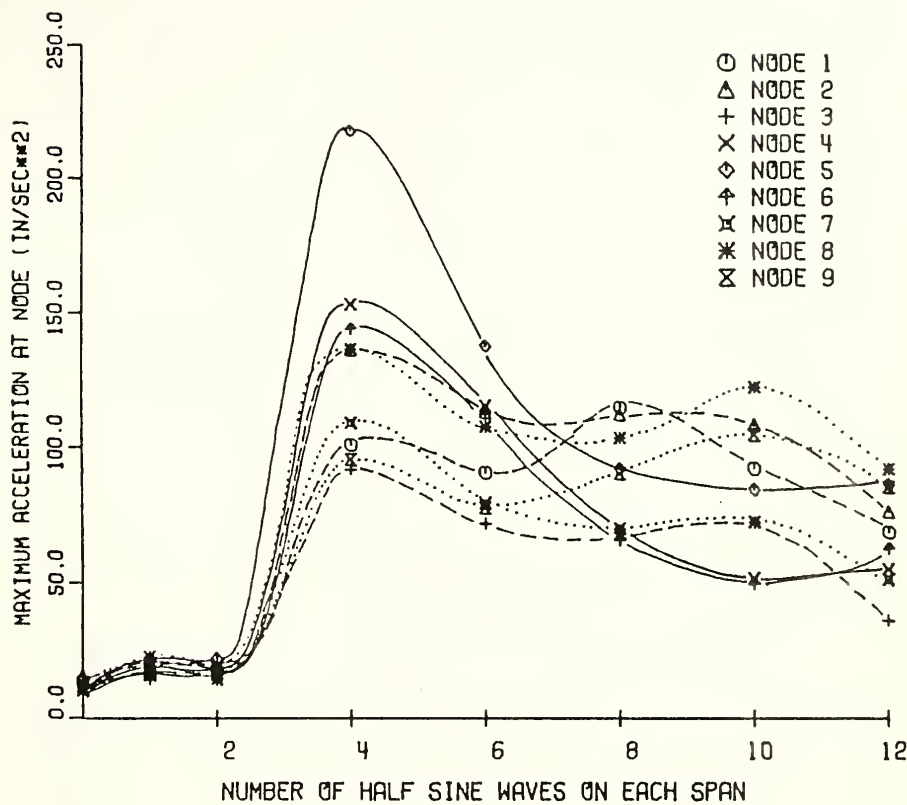
64-80-64 B.P.R. Bridge       $n = 4$        $m = 4$        $c/c_r = .02$       Rough Surface  
HS 20-44 Loading 60 m.p.h.      Smooth Vehicle       $\mu = 0.15$   
Amplitude of Roughness = 0.5 inch

Node	Maximum Acceleration (in/sec <sup>2</sup> )					
	NS* = 0	x/L <sub>b</sub>	NS = 2	x/L <sub>b</sub>	NS = 4	x/L <sub>b</sub>
1	13.30	0.23	-17.79	0.86	-100.87	1.10
2	15.61	0.22	-18.83	0.85	-136.02	1.10
3	-13.00	0.32	-14.00	0.05	-91.77	1.10
4	10.65	0.29	16.38	0.73	-152.92	1.03
5	11.49	0.30	-21.93	0.79	-217.47	1.02
6	10.59	0.20	-15.50	0.78	-143.79	1.16
7	9.96	1.07	-14.28	0.27	-108.81	0.95
8	13.24	0.59	18.63	0.67	-136.34	0.95
9	-11.53	0.33	16.75	0.22	-95.31	0.94

\* NS = Number of Half Sine Waves

Table 4.16, cont.

Node	Maximum Acceleration (in/sec <sup>2</sup> )						
	NS = 8	x/L <sub>b</sub>	NS = 10	x/L <sub>b</sub>	NS = 12	x/L <sub>b</sub>	NS = 16
1	-114.74	0.32	-92.11	0.36	68.62	0.77	-44.48
2	-111.95	0.32	-108.19	0.35	76.14	0.77	-42.62
3	66.26	1.19	72.30	0.39	-35.79	0.81	41.68
4	-67.85	0.53	-51.63	0.78	54.95	0.77	72.85
5	-91.89	0.46	84.31	0.81	86.06	0.70	-56.01
6	65.67	0.57	-49.50	0.63	-62.52	0.74	-82.74
7	-69.94	0.46	72.44	0.88	-51.24	1.03	-42.68
8	103.44	0.42	-122.19	0.85	-91.96	0.88	-62.21
9	90.32	0.42	104.60	0.88	-85.29	0.88	-57.65



64-80-64 BPR BRIDGE    C/CR=0.02    N=M=4    ROUGH    SURFACE  
 HS 20-44    SMOOTH VEHICLE    60 MPH

Figure 4.17 Effect of Surface Roughness on Acceleration

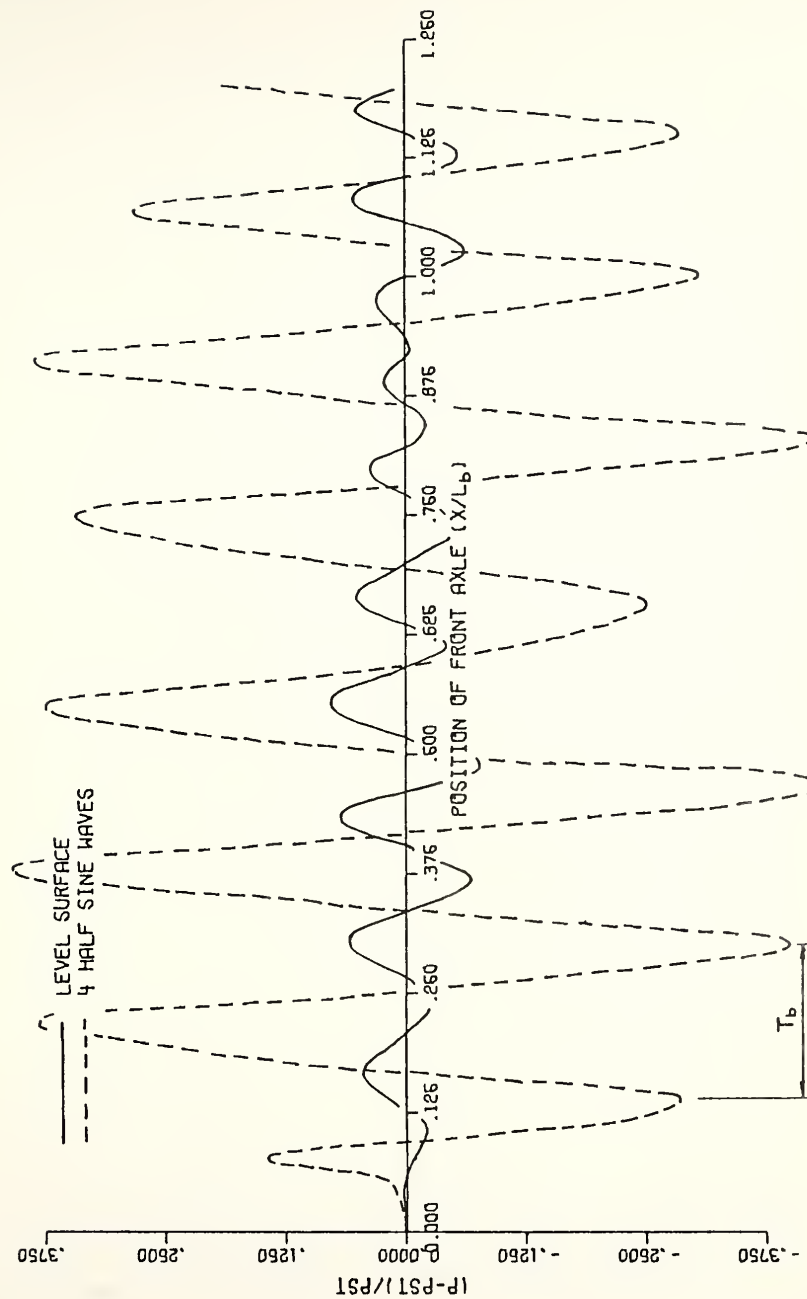


Figure 4.18-1 History Curves for Interacting Force Due to Surface Roughness

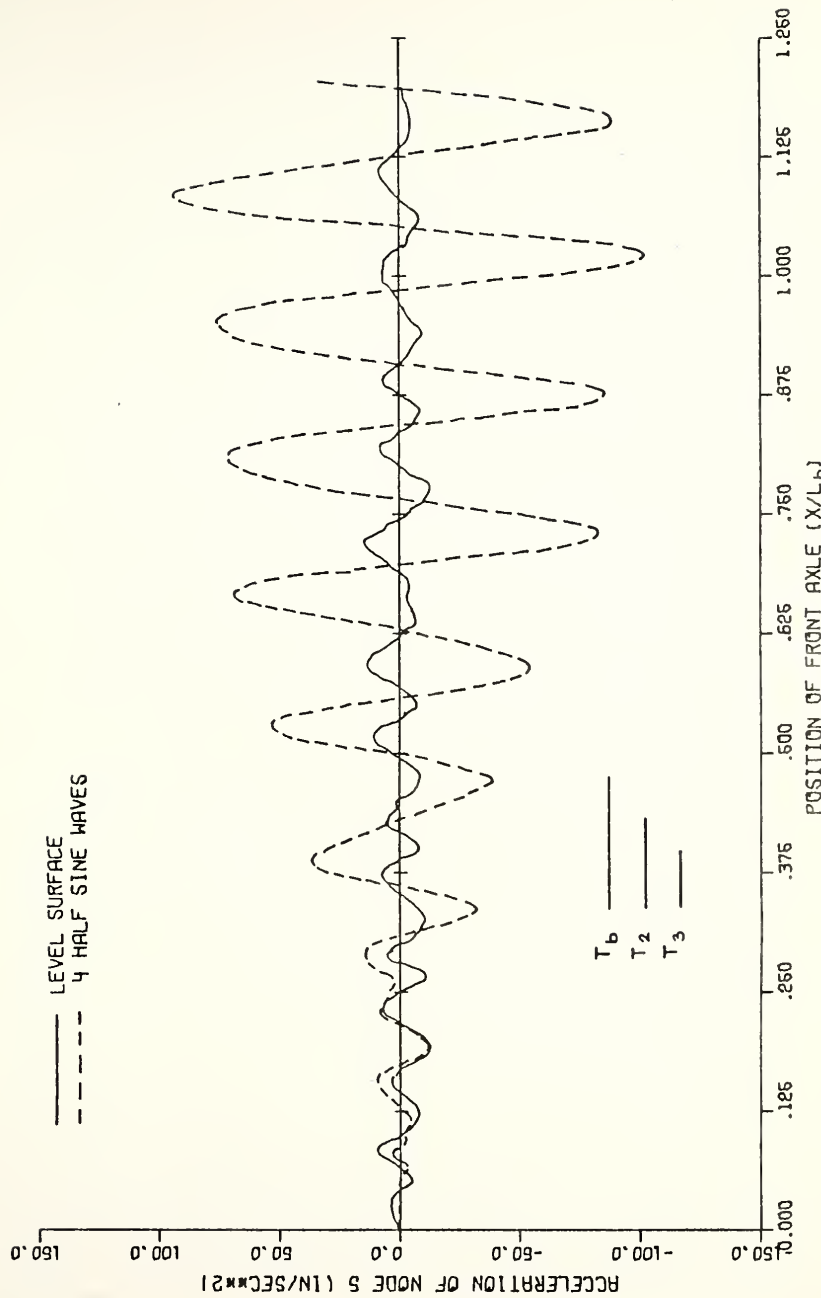


Figure 4.18-2 History Curves for Acceleration as Affected by Surface Roughness

each figure, the results obtained by using the level surface condition and four half sine waves are compared.

It can be seen that the period of the oscillation of interacting force for the value of four half sine waves is coincident with the second natural period of the bridge and resonance between the bridge and the vehicle occurs. The results show that the acceleration of the bridge increases indefinitely although the vehicle is leaving the bridge. On the other hand, the period of the interacting force for the level surface bridge is less than the period of the fundamental frequency of the bridge and the period of the corresponding acceleration at mid-center span corresponds to the lowest three natural periods of vibration of the bridge. Resonance does not occur in this case.

Table 4.17 and Figure 4.19 show the effects of the roughness amplitude on acceleration. The numerical acceleration results are obtained by using amplitudes of roughness which range from 0.0 to 1.0 inch. The number of half sine waves is kept constant and the remaining parameters are the same as before. Two different numbers of half sine waves are selected and classified into two cases. In case A, the two half sine waves are selected, which do not affect the acceleration of the bridge, while in case B, four half sine waves are used, which have most effect.

Table 4.17 Maximum Accelerations of Three Span Continuous Bridges  
Due to Different Amplitudes of Surface Roughness

64-80-64 B.P.R. Bridge     $n = 4$      $m = 4$      $c/c_r = .02$     Rough Surface  
HS 20-44 Loading    60 m.p.h.    Smooth Vehicle

Case A) Number of Half Sine Waves = 2

Node	Maximum Acceleration (in/sec <sup>2</sup> )					
	$A^* = 0.0$	$x/L_b$	$A = 0.25$	$x/L_b$	$A = 0.50$	$x/L_b$
1	13.30	0.23	-17.48	0.56	-17.79	0.86
2	15.61	0.22	-19.19	0.56	-18.33	0.85
3	-13.00	0.32	13.96	0.60	-14.00	0.05
4	10.65	0.29	13.32	0.29	16.38	0.73
5	11.49	0.30	-17.17	0.64	-21.93	0.79
6	10.59	0.30	-12.89	0.63	-15.50	0.78
7	9.96	1.07	-14.51	0.41	-14.28	0.27
8	13.24	0.59	19.80	0.75	18.63	0.67
9	-11.53	0.33	-16.96	0.42	16.75	0.22
					21.13	0.66
						25.33
						0.66

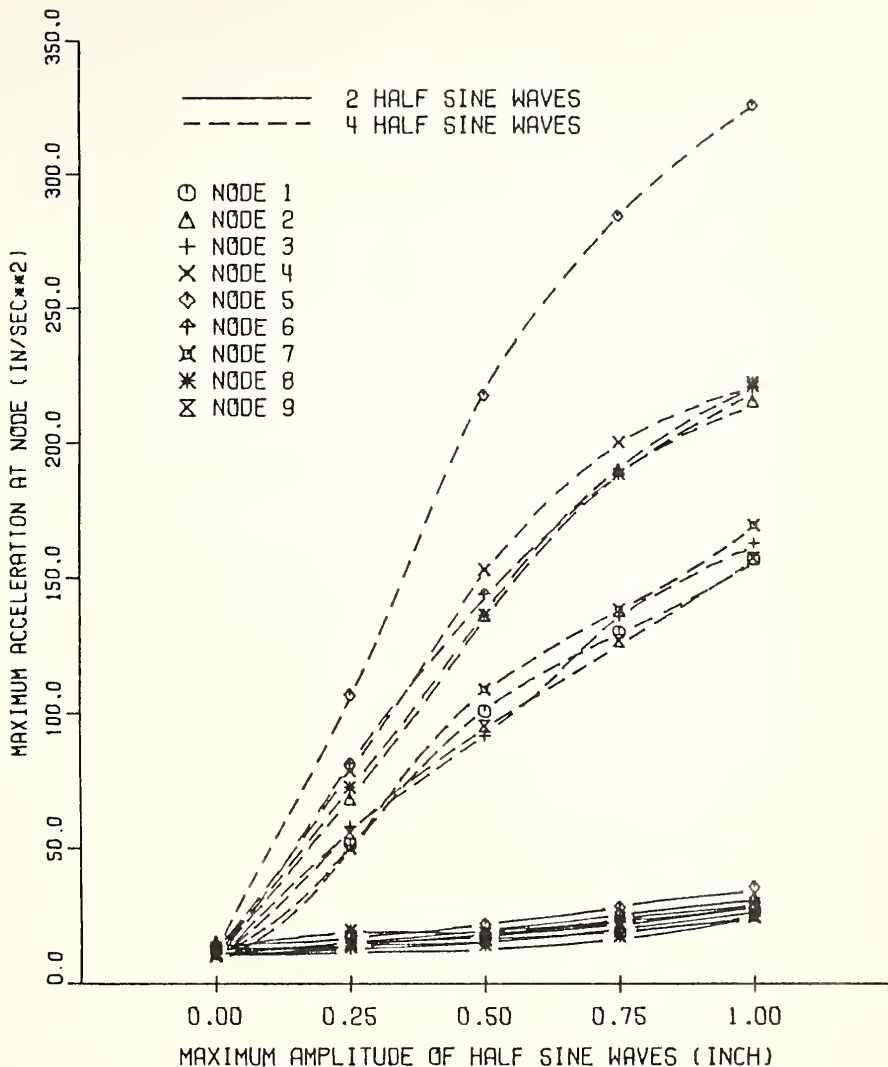
\*  $A$  = Amplitude of Surface Roughness in Inch

Table 4.17, cont.

Case B) Number of Half Sine Waves = 4

Node	Maximum Acceleration (in/sec <sup>2</sup> )					
	A = 0.0	x/L <sub>b</sub>	A = 0.25	x/L <sub>b</sub>	A = 0.50	x/L <sub>b</sub>
1	13.30	0.23	-51.70	0.95	-100.87	1.10
2	15.61	0.22	-68.28	1.09	-136.02	1.10
3	-13.00	0.32	-58.09	1.09	-91.77	1.10
4	10.65	0.29	-78.60	1.02	-152.92	1.03
5	11.49	0.30	-106.89	1.01	-217.47	1.02
6	10.59	0.30	-81.35	1.15	-143.79	1.16
7	9.96	1.07	-49.98	0.93	-108.81	0.95
8	13.24	0.59	-72.66	0.93	-136.34	0.95
9	-11.53	0.33	-55.85	0.94	-95.31	0.94

A = 0.75	x/L <sub>b</sub>	A = 1.00	x/L <sub>b</sub>
-130.04	1.11	-156.84	1.10



64-80-64 BPR BRIDGE    C/CR=0.02    N=M=4    ROUGH    SURFACE  
HS 20-44    SMOOTH VEHICLE    60 MPH

Figure 4-19 Effect of Amplitude of Roughness on Acceleration

It can be seen from the results that accelerations for the two half sine waves are almost constant regardless of the amplitude of roughness while the accelerations for the four half sine waves gradually increase for larger values of the amplitude. This is in good agreement with the results presented in Article 3.5 for simple span bridge. Comparing the two parameters which represent the surface roughness, one can see that the effect of roughness amplitude on acceleration depends upon the number of half sine waves. The amplitude affects the acceleration only if the number of half sine waves does.

It should be remembered that these results were obtained for only this kind of bridge and vehicle models with given velocity. However, it can be seen at this stage that the surface roughness of the three span continuous bridge is the most important parameter that affects the acceleration.

## CHAPTER V

## ACCELERATION STUDIES OF TWO SPAN CONTINUOUS HIGHWAY BRIDGES

5.1 General

The accelerations of two span continuous highway bridges as affected by the important parameters are reported in this chapter. The bridge was idealized as a two span continuous flexible beam subjected to the moving three-axle vehicle with constant velocity. The method of analysis and the description of the computer program used have been presented in Articles 2.3.3 and 2.3.4 respectively. The numerical results of accelerations investigated at the concentrated masses of the bridge are in dimensional form so that it will be convenient to compare these results with the suggested acceleration criteria for human response.

As in the previous chapter, the parameters affecting the acceleration can be classified into the following four groups:

- a) Solution parameters.
- b) Bridge parameters including the span length and the girder flexibility.
- c) Vehicle parameters including the axle spacing and the vehicle speed.

- d) Initial conditions of vehicle and bridge including the initial oscillation of the vehicle and the surface roughness of the bridge.

Throughout this chapter, the bridge is considered to be an I-beam type composed of steel girders and a reinforced concrete deck with non-composite section. It has a prismatic cross section and equal span lengths. Damping is considered in both the bridge and vehicle. The bridge and vehicle models are referred to in Figures 2.15 and 2.11 respectively. The computed accelerations of the bridge occur at the specified concentrated masses and the maximum acceleration value together with the corresponding front axle position at that time are considered.

The natural frequencies of two span continuous bridges can be evaluated by substituting the values of  $\lambda_j$  obtained from Figure 4.1 into Eq. (4-1). Most of the vehicle parameters were obtained from the information for typical vehicles presented in Table 4.1.

## 5.2 Solution Parameters

Table 5.1 shows the convergence of the acceleration at mid-right span due to the various values of the number of integration steps. The acceleration is evaluated at the different positions of the front axle of the vehicle on the bridge. The bridge model used has two 80 ft. spans, with a damping factor of 0.02 and a level bridge

Table 5.1 Accelerations at Mid-Right Span of Two Span Continuous Bridge Obtained by Using Different Numbers of Integration Steps

80-80 Span Length Bridge 36WF170 Girders n = 4 c/c = .02  
Level Surface HS 20-44 Loading 60 m.p.h. Smooth Vehicle

$x/L_b$	Acceleration at Mid-Right Span (in/sec <sup>2</sup> )					
	N = 600	N = 1000	N = 1600	N = 1800	N = 2000	N = 2200
0.1	-2.154	-2.204	-2.222	-2.221	-2.225	-2.224
0.2	1.196	0.852	0.713	0.719	0.700	0.705
0.3	5.768	5.707	5.668	5.677	5.652	5.654
0.4	0.257	-0.021	-0.097	-0.123	-0.123	-0.103
0.5	1.556	0.753	0.324	0.402	0.303	0.377
0.6	-0.993	-0.474	-0.330	-0.347	-0.332	-0.383
0.7	6.153	5.704	5.591	5.529	5.509	5.448
0.8	-13.957	-14.032	-14.353	-14.302	-14.383	-14.216
0.9	5.877	7.136	7.635	7.519	7.640	7.551
1.0	-3.503	-4.705	-5.358	-5.253	-5.401	-5.246
1.1	8.551	9.396	9.204	9.222	9.175	9.252
1.2	3.812	4.324	4.667	4.633	4.662	4.504

surface. The vehicle model is a three axle smooth vehicle with HS 20-44 loading travelling at 60 m.p.h. By considering the accelerations obtained by using from 600 to 2200 integration steps, one finds that the 2000 integration steps is sufficient for the stability of the solutions.

The other solution parameter to assure the accuracy of results is the number of mass concentrations. It was suggested by Huang<sup>(29)</sup> that the results obtained from the bridge model with  $n = 4$  were sufficiently accurate and the natural periods of this model were close to those of the continuous beam. Therefore the value of  $n = 4$  will be used for the bridge model throughout this chapter.

### 5.3 Bridge Parameters

#### 5.3.1 Effect of Span Length

Table 5.2 shows the characteristics of the two span bridge models with three different span lengths, 60 ft. - 60 ft., 80 ft. - 80 ft. and 100 ft - 100 ft. The cross section of the bridge model is shown in Figure 5.1(a). The bridge is of I-beam type consisting of six wide-flange steel girders and a 7.5 inch thick concrete deck. The bridge has a roadway width of 44 ft. and is designed for HS 20-44 loading.

Figure 5.1(b) shows the single beam with the mass concentrations representing the two span bridge models

Table 5.2 Maximum Accelerations of Two Span Continuous Bridges with Different Span Lengths

6 Girder Bridge 44 ft. Roadway Width n = 4 c/c<sub>r</sub> = .02  
 Level Surface HS 20-44 Loading 60 m.p.h.  
 Smooth Vehicle

Span Length (ft)	Girder	I* (in <sup>4</sup> )	w <sub>b</sub> <sup>†</sup> (k/ft)	f <sub>b</sub> <sup>††</sup> (cps)	T <sub>b</sub> (sec)
60-60	33WF118	55200	5.46	3.53	0.28
80-80	36WF170	82800	5.77	2.36	0.42
100-100	36WF245	116400	6.22	1.73	0.58

Node	Maximum Acceleration (in/sec <sup>2</sup> )					
	60-60	x/L <sub>b</sub>	80-80	x/L <sub>b</sub>	100-100	x/L <sub>b</sub>
1	-18.20	0.71	-15.39	0.48	-15.87	0.50
2	24.68	0.38	-18.34	1.15	-13.94	1.17
3	17.87	0.38	-15.47	0.50	-12.14	0.47
4	17.86	0.51	16.52	0.44	11.82	1.10
5	25.86	1.16	19.82	0.43	-17.12	0.83
6	-21.37	0.84	15.88	0.45	-14.35	0.85

\* I is total moment of inertia of cross section.

† w<sub>b</sub> is weight per linear length of right span.

†† f<sub>b</sub> is fundamental natural frequency of bridge.

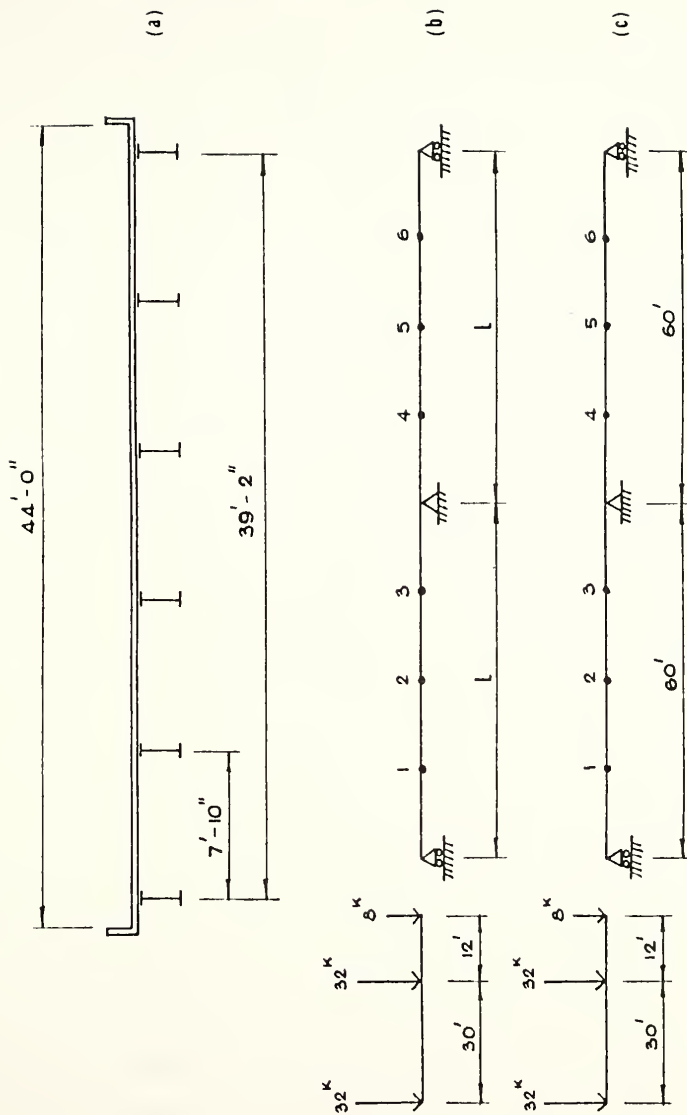
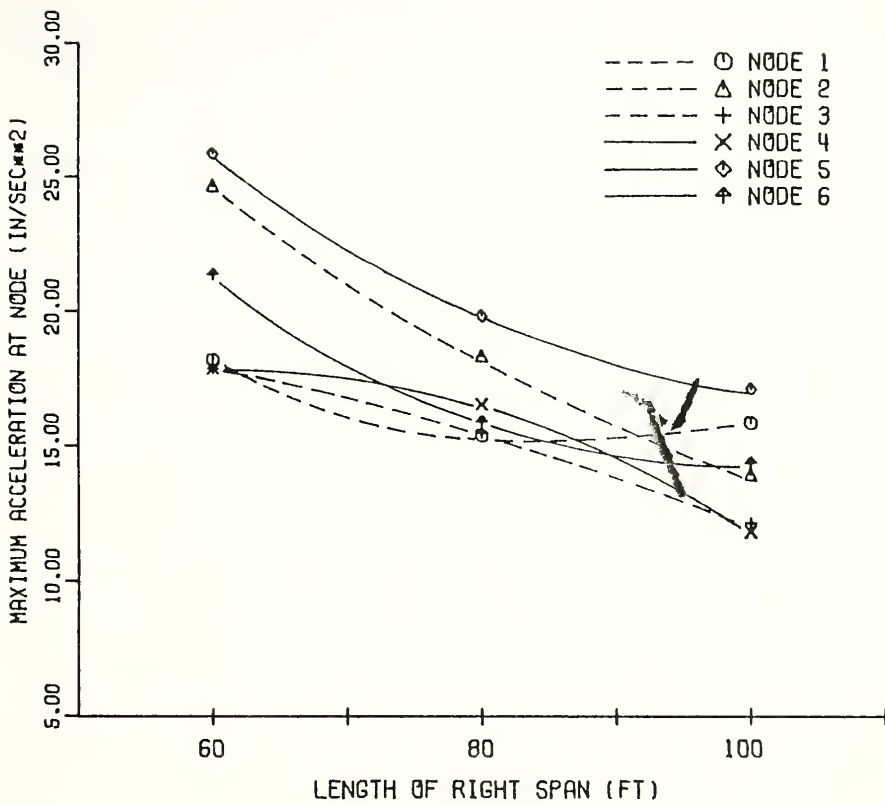


Figure 5.1 Two Span Bridge and Vehicle Models

described above. Also shown is the vehicle model with IIS 20-44 loading and smooth moving condition. It is also assumed that the bridge has a level surface and the vehicle travels at a constant speed of 60 m.p.h. Bridge properties for different span lengths and the remaining vehicle parameters are listed in Tables 5.2 and 4.1 respectively. It should be remembered that the bridge and vehicle models shown are not the complete models used in the analysis. Figures 2.15 and 2.11 show the complete models.

Maximum accelerations at the concentrated masses or nodes are evaluated by using bridge models with different span lengths and are listed in Table 5.2. The corresponding position of the front axle as the maximum acceleration occurred is also shown. These results are plotted in Figure 5.2. It can be seen that the accelerations increase for the shorter spans. This is in agreement with the results of simple span and three span continuous bridges in Articles 3.3.1 and 4.3.1 respectively. It can be noted that the magnitudes of accelerations of the two span bridges are about 1.5 times larger than those of three span bridges for equal span length. In order to compare the accelerations of the two span bridges with those of the simple span bridges, the single axle load is used as the vehicle model for the two span bridges. The results further discussed in Article 5.4.1 indicates that the accelerations of the two span bridges due to single axle



SPAN RATIO = 1.0    LEVEL SURFACE    C/CR=0.02    N=4  
HS 20-44    SMOOTH VEHICLE    60 MPH

Figure 5.2    Effect of Span Length on Acceleration

load are 1.5 times larger than those due to three axle vehicle. For equal span length and the same single axle load as the vehicle model, it can be seen that the accelerations of the two span bridges are still less than those of the simple span bridges.

It is also noted that the accelerations of the two midspan nodes are greater than those of other nodes.

Figure 5.3 shows the history curves of the accelerations of the two midspan nodes. The periods of both accelerations correspond to the lowest three natural periods of vibration of the bridge. The maximum accelerations of nodes 2 and 5 occur when the center of gravity of the total load is either on the mid-left span or on the mid-right span.

### 5.3.2 Effect of Girder Flexibility

Figure 5.1(c) shows the bridge model used for the study of accelerations as affected by using different values of girder stiffness. The bridge has two 60 ft. spans with a damping factor of 0.02 and a level bridge surface. The remaining parameters are considered to be the same as before. Four different girder sections are used to evaluate the acceleration at each node. The properties of each section were obtained from the information given in Reference 42 and listed in Table 5.3. The 33WF118 is supposed to be the proper design section of this bridge model.

Table 5.3 Maximum Accelerations of Two Span  
Continuous Bridge Obtained by Using  
Different Girder Flexibilities

60-60 Span Bridge    n = 4     $c/c_r = .02$     Level Surface  
HS 20-44 Loading    60 m.p.h.    Smooth Vehicle

Girder	$I_{xx}$ ( $\text{in}^4$ )	W (k/ft)	A ( $\text{in}^2$ )	$f_b$ (cps)	$T_b$ (sec)
33WF118	5900	.118	34.8	3.53	0.28
30WF116	4930	.116	34.2	3.34	0.30
30WF99	4000	.099	29.1	3.18	0.31
27WF84	2830	.084	24.8	2.94	0.34

Node	Maximum Acceleration ( $\text{in/sec}^2$ )							
	33WF118	$x/L_b$	30WF116	$x/L_b$	30WF99	$x/L_b$	27WF84	$x/L_b$
1	-18.20	0.71	15.81	0.40	21.59	0.40	22.54	0.40
2	24.68	0.38	21.23	0.39	24.51	0.39	21.70	0.39
3	17.87	0.38	15.84	0.38	20.90	0.38	-23.06	0.55
4	17.86	0.51	-19.39	1.11	22.87	0.53	28.78	0.54
5	25.86	1.16	-22.96	0.86	-26.79	0.88	26.99	0.53
6	-21.37	0.84	-20.99	0.87	-23.99	0.88	25.75	0.51

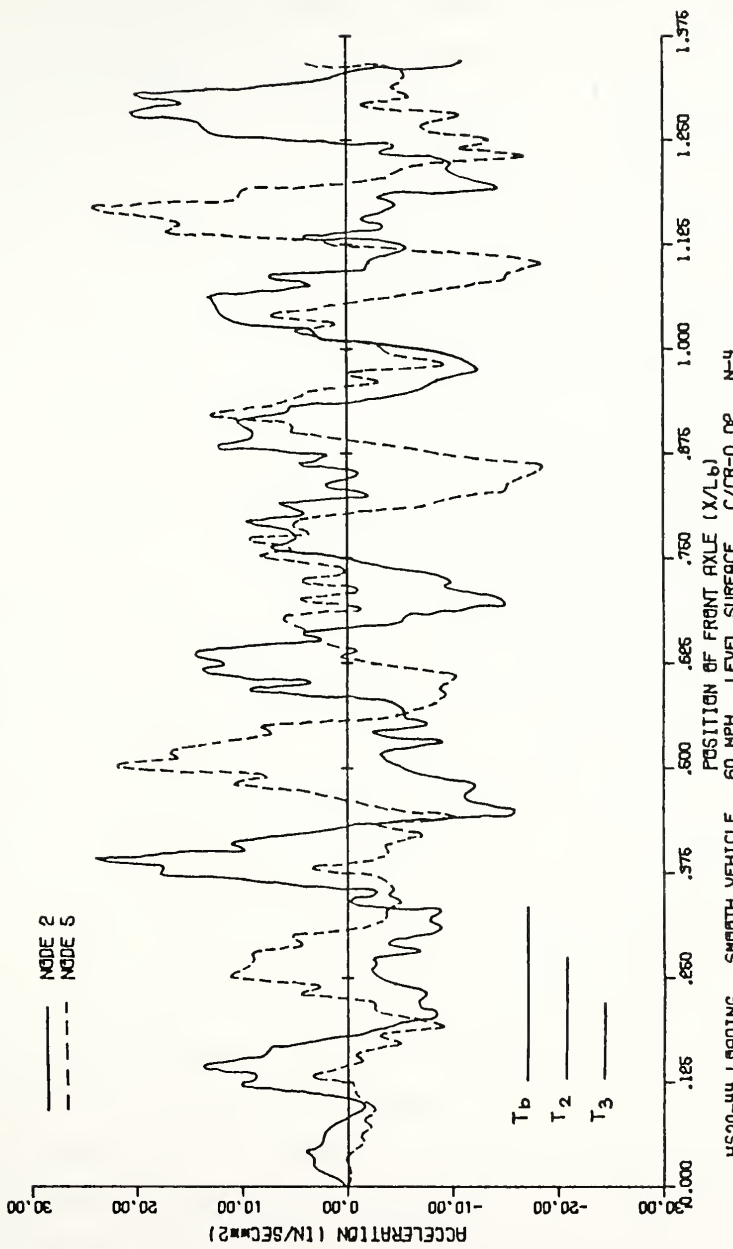


Figure 5.3 History Curves for Acceleration of 60-60 Span Bridge

Maximum accelerations at nodes evaluated by using the four different girder sections are listed also in Table 5.3 and are plotted as a function of girder moment of inertia in Figure 5.4. As might be expected, the results show that the increased flexibility of girder does not affect the overall acceleration level of the bridge appreciably although the moment of inertia of girder was reduced more than half of the original value.

#### 5.4 Vehicle Parameters

##### 5.4.1 Effect of Number of Axles and Axle Spacing

Figure 5.5 shows the typical vehicle models with different number of axles. The details describing the parameters of typical vehicles were given in Table 4.1. The bridge model and the remaining parameters are the same as in Article 5.3.2. All typical vehicles are assumed to be smoothly moving with a constant speed of 60 m.p.h. The maximum accelerations at nodes subjected to different typical vehicles are compared in Table 5.4 and shown in Figure 5.6. As might be expected, the magnitudes of acceleration for two axle and three axle typically are about the same but they are about two-thirds of the magnitudes for single axle loads.

Table 5.5 and Figure 5.7 show the effect of vehicle axle spacing on bridge accelerations. The vehicle model has the HS 20-44 loading with the practical values of axle

Table 5.4 Maximum Accelerations of Two Span Continuous Bridges Subjected to Different Numbers of Axles of Vehicle

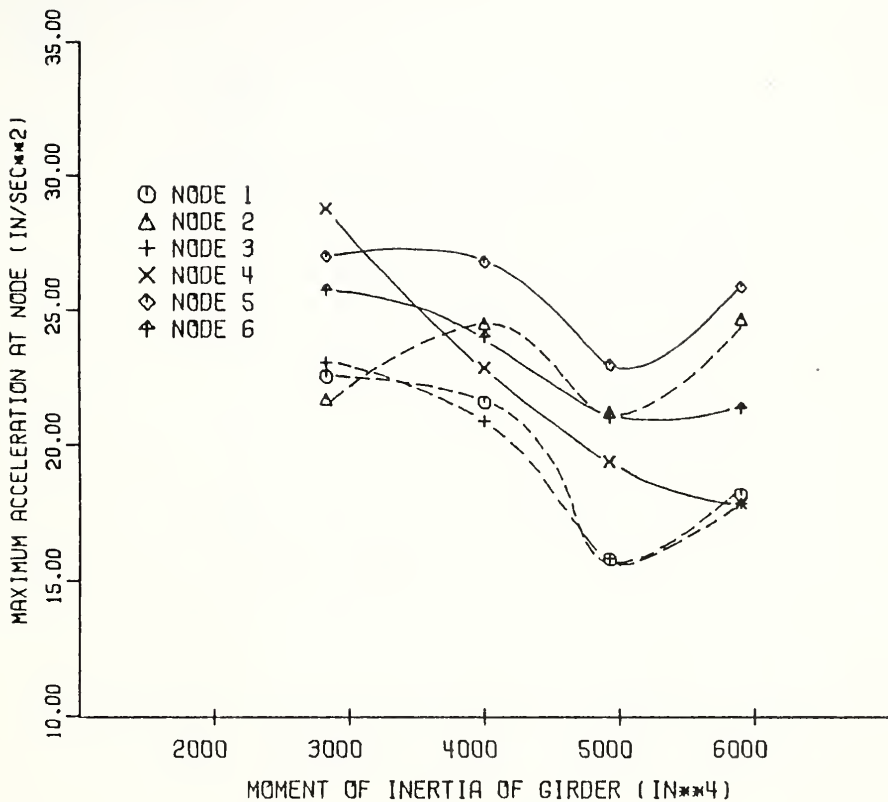
60-60 Span Bridge 33WF118 Girders n = 4 c/c<sub>r</sub> = .02  
Level Surface Smooth Vehicles 60 m.p.h.

Node	Maximum Acceleration (in/sec <sup>2</sup> )					
	3-Axle	x/L <sub>b</sub>	2-Axle	x/L <sub>b</sub>	1-Axle	x/L <sub>b</sub>
1	-24.41	0.46	-24.31	0.36	-28.73	0.19
2	-23.15	0.44	-23.80	0.34	31.75	0.04
3	-21.58	0.43	-21.11	0.33	29.57	0.03
4	-17.81	0.35	17.73	0.32	26.43	0.16
5	17.68	1.13	19.26	1.03	30.89	0.15
6	-18.60	0.79	-17.74	0.69	28.88	0.14

Table 5.5 Maximum Accelerations of Two Span Continuous Bridges Subjected to Vehicles with Different Axle Spacings

60-60 Span Bridge 33WF118 Girders n = 4 c/c<sub>r</sub> = .02  
Level Surface 72 kips Total Load 3-Axle  
60 m.p.h. Smooth Vehicle

Node	Maximum Acceleration (in/sec <sup>2</sup> )							
	l <sub>2</sub> = 20 ft	x/L <sub>b</sub>	l <sub>2</sub> = 25 ft	x/L <sub>b</sub>	l <sub>2</sub> = 30 ft	x/L <sub>b</sub>	l <sub>2</sub> = 35 ft	x/L <sub>b</sub>
1	-24.41	0.46	-23.18	1.17	-18.20	0.71	15.93	0.40
2	-23.15	0.44	28.54	1.25	24.68	0.38	15.52	0.41
3	-21.58	0.43	-21.81	0.48	17.87	0.38	-13.14	1.19
4	-17.81	0.35	20.16	1.13	17.86	0.51	-14.24	1.11
5	17.68	1.13	28.68	1.14	25.86	1.16	17.23	0.54
6	-18.60	0.79	-22.02	0.83	-21.37	0.84	-17.22	1.29



60-60 SPAN BRIDGE    6 GIRDERS    LEVEL SURFACE    C/CR=0.02    N=4  
HS 20-44    SMOOTH VEHICLE    60 MPH

Figure 5.4 Effect of EI on Acceleration

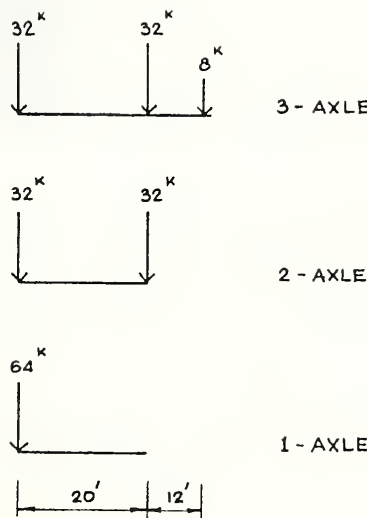
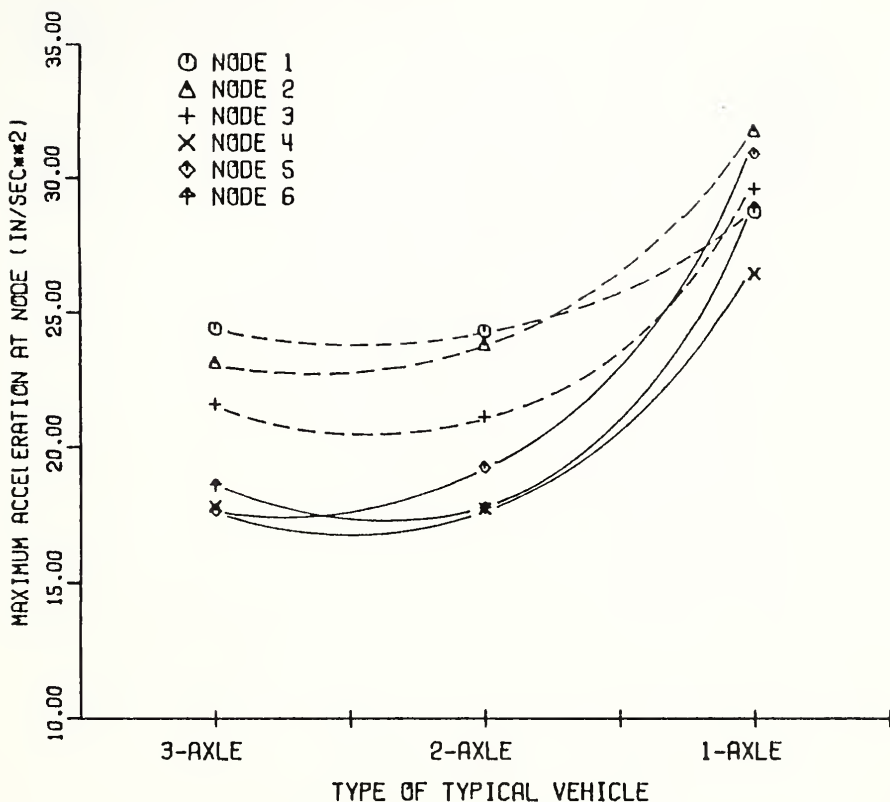
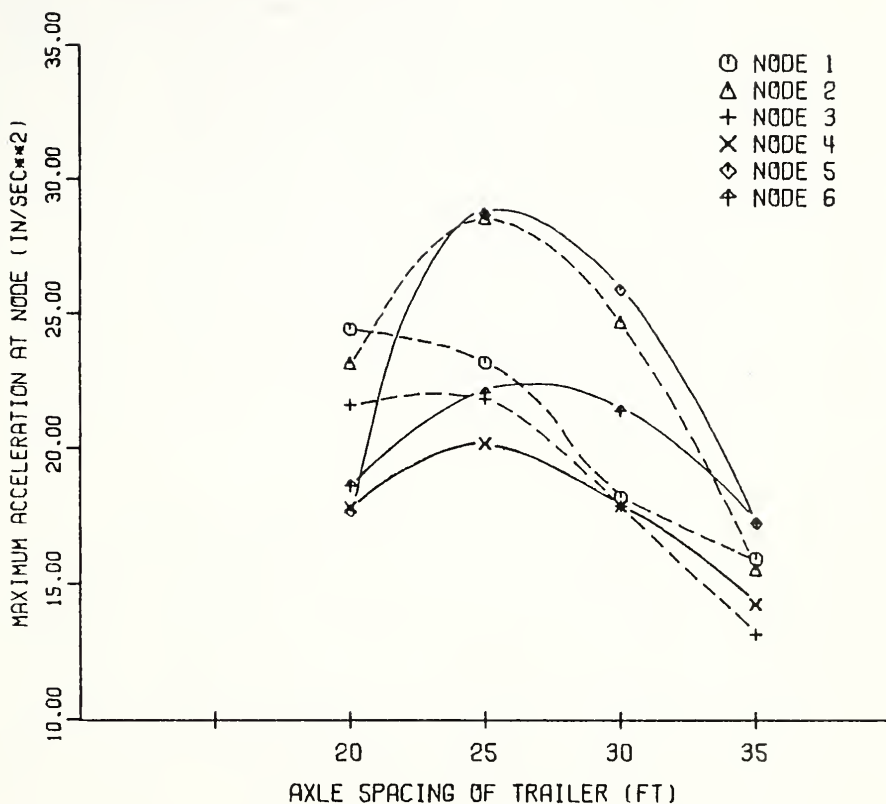


Figure 5.5 Vehicle Models with Different Numbers of Axles



60-60 SPAN BRIDGE    6 GIRDERS    LEVEL SURFACE    C/CR=0.02    N=4  
TYPICAL SMOOTH VEHICLES    60 MPH

Figure 5.6 Effect of Number of Axles on Acceleration



60-60 SPAN BRIDGE    6 GIRDERS    LEVEL SURFACE    C/CR=0.02    N=4  
 3-AXLE SMOOTH VEHICLE    60 MPH    AXLE SPACING OF TRACTOR = 12 FT

Figure 5.7 Effect of Axle Spacing on Acceleration

spacing of trailer varied from 20 ft. to 35 ft. The axle spacing of the tractor is kept constant at 12 ft. All remaining parameters are considered to be the same as before. From the results shown, the magnitudes of accelerations are largest when the axle spacing is equal to 25 ft., or in non-dimensional form, the axle spacing ratio has the value of 0.42. The axle spacing ratio in this case is the ratio of the axle spacing to the length of either span of the two span bridge. The value of 0.42 is in good agreement with the results presented in Article 4.4.2, where three span bridge has maximum accelerations for an axle spacing ratio between 0.37 to 0.43.

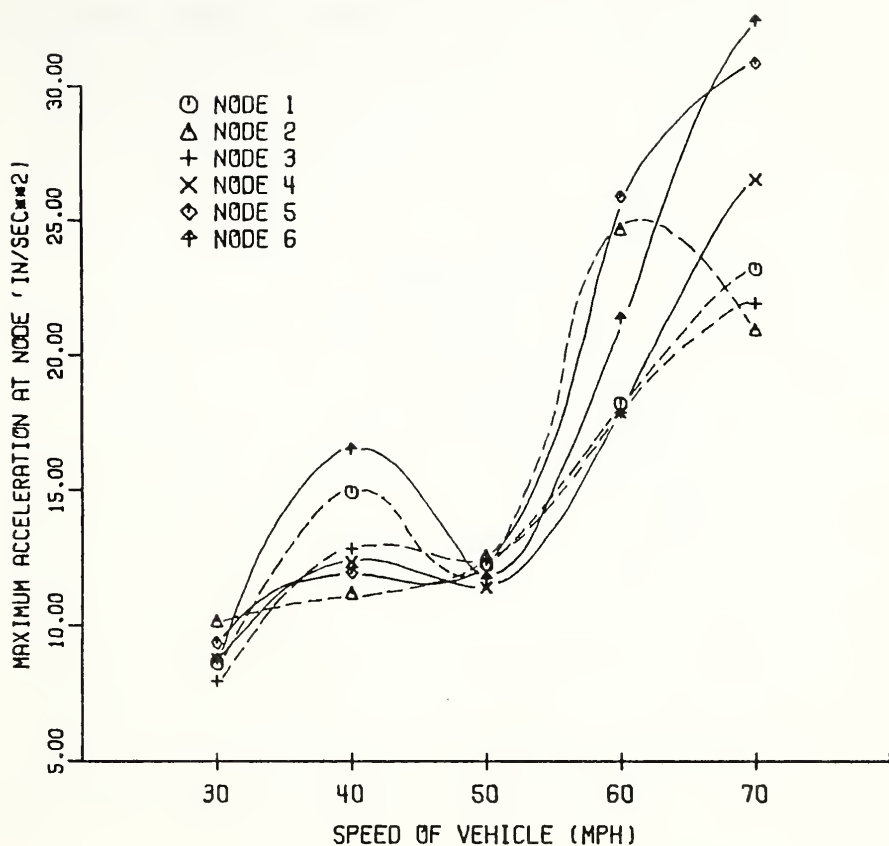
#### 5.4.2 Effect of Vehicle Speed

Table 5.6 and Figure 5.8 show the effect of vehicle speed on acceleration of the two span continuous bridge. The bridge model was shown in Figure 5.1(c) and has the same parameters as before. The vehicle model has HS 20-44 loading and is smoothly moving. The vehicle speed ranges from 30 m.p.h. to 70 m.p.h. Generally, the accelerations of the bridge increase for increased values of speed. However, the accelerations of nodes 1 and 6 decrease for the speed of 50 m.p.h. It is believed at this stage that they were influenced by the other parameters such as the period of oscillation of interacting force and the period of the bridge itself.

Table 5.6 Maximum Accelerations of Two Span Continuous Bridges Due to Different Vehicle Speeds

HS 20-44 Loading  
HS 20-44 Brading  
Bridge Girders  
Smooth Vehicle

Node	Maximum Acceleration (in/sec <sup>2</sup> )									
	30 mph	x/L <sub>b</sub>	40 mph	x/L <sub>b</sub>	50 mph	x/L <sub>b</sub>	60 mph			
1	8.61	1.17	14.92	1.19	12.26	0.35	-18.20	0.71	23.20	0.41
2	10.16	0.36	11.20	0.70	12.58	0.13	24.68	0.38	-20.94	0.50
3	7.95	0.36	-12.83	0.49	-12.46	0.49	17.87	0.38	-21.91	0.54
4	8.74	1.11	12.33	1.12	11.39	0.23	17.86	0.51	-26.50	0.93
5	9.35	0.42	11.94	1.11	-12.23	1.28	25.86	1.16	-30.84	1.21
6	-8.76	1.19	16.51	1.10	-11.71	0.92	-21.37	0.84	-32.42	1.21



60-60 SPAN BRIDGE    6 GIRDERS    LEVEL SURFACE    C/CR=0.02    N=4  
HS 20-44    SMOOTH VEHICLE

Figure 5.8 Effect of Speed of Vehicle on Acceleration

#### 5.4.3 Effect of Frequency Ratio

The maximum accelerations evaluated by using the different values of frequency ratio are shown in Table 5.7 and Figure 5.9. The frequency ratio is the ratio of vehicle frequency to the natural frequency of the bridge. In this study, the frequency ratio is considered to be in the range between 0.5 and 2.0, the bridge model used is two 60 ft. spans and has a fundamental natural frequency of 3.53 cps. The vehicle frequency is the tire frequency of rear axles. It is assumed that the vehicle oscillates on its tires only and the coefficients of friction of suspension springs have the value of infinity. The vehicle has HS 20-44 loading, and is smoothly moving at a constant speed of 60 m.p.h. Generally, the magnitudes of accelerations at the nodes are about the same for all values of frequency ratio although the accelerations of midspan nodes for  $f_v/f_b = 1.0$  increase slightly. It may be concluded that the accelerations of the bridge are not materially affected by the frequency ratio.

### 5.5 Initial Conditions of Vehicle and Bridge

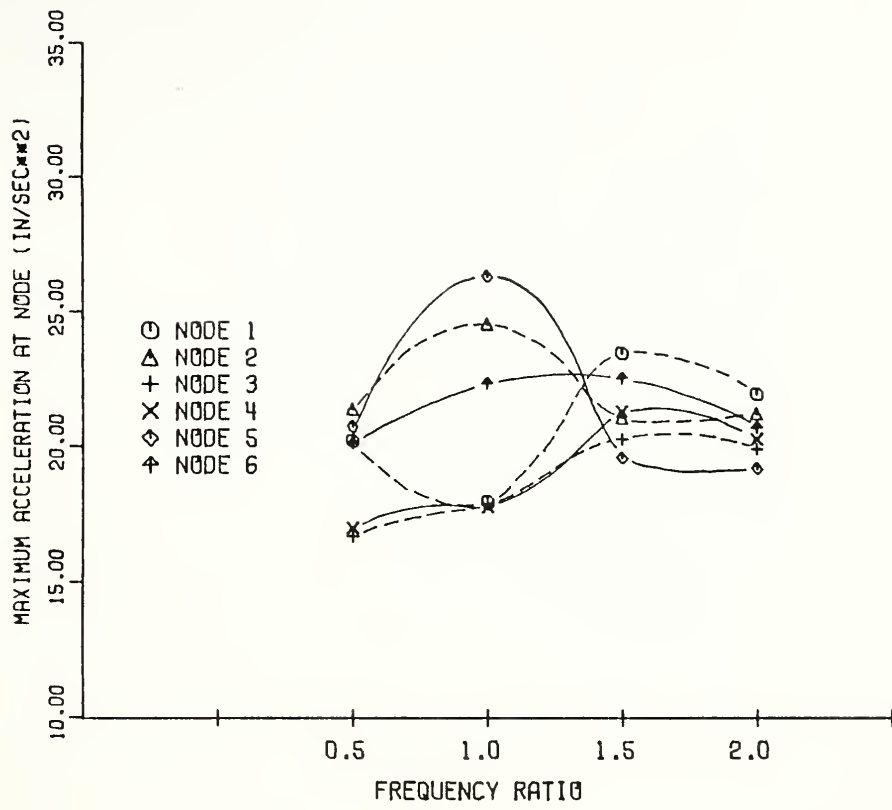
#### 5.5.1 Effect of Initially Oscillating Vehicle

As previously explained in Article 4.5.1, the vehicle usually has an initial oscillation due to approach pavement irregularities and a possible discontinuity at the abutment. The parameters representing the initial oscillation are

Table 5.7 Maximum Accelerations of Two Span Continuous Bridges Obtained by Using Different Frequency Ratios

60-60 Span Bridge      33WF118 Girders       $n = 4$        $c/c_R = .02$       Level Surface<sup>e</sup>  
 HS 20-44 Loading      60 m.p.h.      Smooth Vehicle      The Tire Spring is Only Active  
 $\mu = \infty$

Node	Maximum Acceleration (in/sec <sup>2</sup> )					
	$f_v/f_b = 0.5$	$x/L_b$	$f_v/f_b = 1.0$	$x/L_b$	$f_v/f_b = 1.5$	$x/L_b$
1	-20.20	0.46	17.93	0.37	-23.45	1.17
2	21.36	0.38	24.52	0.38	21.04	1.25
3	-16.66	0.47	17.83	0.38	-20.25	1.15
4	16.98	1.30	17.76	0.51	-21.27	1.26
5	-20.71	0.98	26.29	1.16	19.56	0.50
6	20.09	0.65	22.31	1.15	22.49	1.11



60-60 SPAN BRIDGE    6 GIRDERS    LEVEL SURFACE    C/CR=0.02    N=4  
HS 20-44    SMOOTH VEHICLE    60 MPH  
TIRE SPRING IS ONLY ACTIVE

Figure 5.9 Effect of Frequency Ratio on Acceleration

classified as the amplitude of initial force variation  $C_i$ , the initial phase angle  $\theta_i$ , and the initial coefficient of friction  $\mu_i$ . The results of the three span bridges in Article 4.5.1 showed that the bridge acceleration was not affected by initial phase angles and initial coefficients of friction. It is believed that the accelerations of the two span bridges are also not affected by these two parameters because the method of analysis for the two span bridges is similar to that for three span bridges. Therefore, the amplitude of the initial force variation  $C_i$ , is the only parameter studied here.

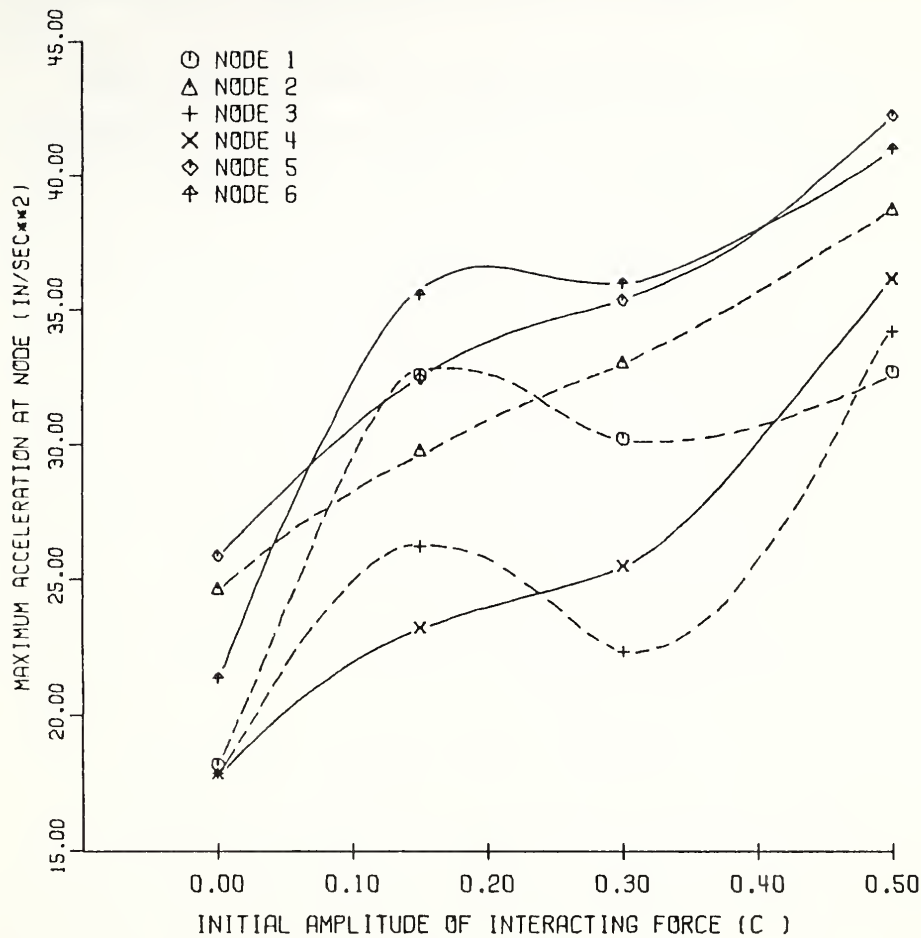
As in the study of the three span bridges, the amplitudes of initial force variation  $C_i$ , are assigned to have the values of 0.0, 0.15, 0.30 and 0.50. The maximum accelerations at the nodes obtained by using different values of  $C_i$  are shown in Tabel 5.8 and Figure 5.10. The bridge is the same as before and the vehicle model has HS 20-44 loading with initial oscillation and a constant speed of 60 m.p.h. The values of  $C_i$  are considered to be the same for each axle. The initial values of the frictional force and phase angle for each axle are all taken equal to zero.

It can be seen from the results that the maximum accelerations increase for the larger amplitude of initial oscillation. For the values of  $C_i$  equal to 0.15 and 0.50, the magnitude of maximum acceleration of all nodes increases

Table 5.8 Maximum Accelerations of Two Span Continuous Bridges Subjected to Vehicle with Different Initial Amplitudes of Oscillation

60-60 Span Bridge      33WFl8 Girders       $n = 4$        $C/c = .02$       Level Surface  
 HS 20-44 Loading      60 m.p.h.      Initially Oscillating Vehicle

Node	Maximum Acceleration (in/sec <sup>2</sup> )					
	$C_i = 0$	$x/L_b$	$C_i = 0.15$	$x/L_b$	$C_i = 0.30$	$x/L_b$
1	-18.20	0.71	-32.58	1.17	-30.22	0.97
2	24.68	0.38	-29.80	1.16	33.06	1.25
3	17.87	0.38	-26.21	1.15	-22.34	1.19
4	17.86	0.51	23.22	0.46	-25.50	1.07
5	25.86	1.16	-32.45	1.30	-35.35	0.85
6	-21.37	0.84	-35.56	1.29	-35.97	0.84



60-60 SPAN BRIDGE    6 GIRDERS    LEVEL SURFACE    C/CR=0.02    N=4  
 HS 20-44    OSCILLATING VEHICLE    60 MPH

Figure 5.10 Effect of Initially Oscillating Vehicle  
on Acceleration

respectively 1.3 and 1.5 times larger than those for  $c_i = 0$ .

Table 5.9 and Figure 5.11 show the effects of initial phase angle difference of the 50% initially oscillating vehicle on bridge accelerations. It is assumed that the vehicle has  $\theta_1 = \theta_2 = 0^\circ$  and  $\theta_3$  ranges from  $0^\circ$  to  $180^\circ$ . All remaining parameters are the same as before. The results show that the magnitudes of accelerations are about the same for all values of phase angle difference except the accelerations of some nodes are larger for the values of phase angle difference equal to  $90^\circ$  and  $150^\circ$ , due to the behavior of interacting forces. It can be noted that the magnitudes are still below  $50 \text{ in/sec}^2$  which does not affect the human response according to Reference 5.

#### 5.5.2 Effect of Surface Roughness of Bridge

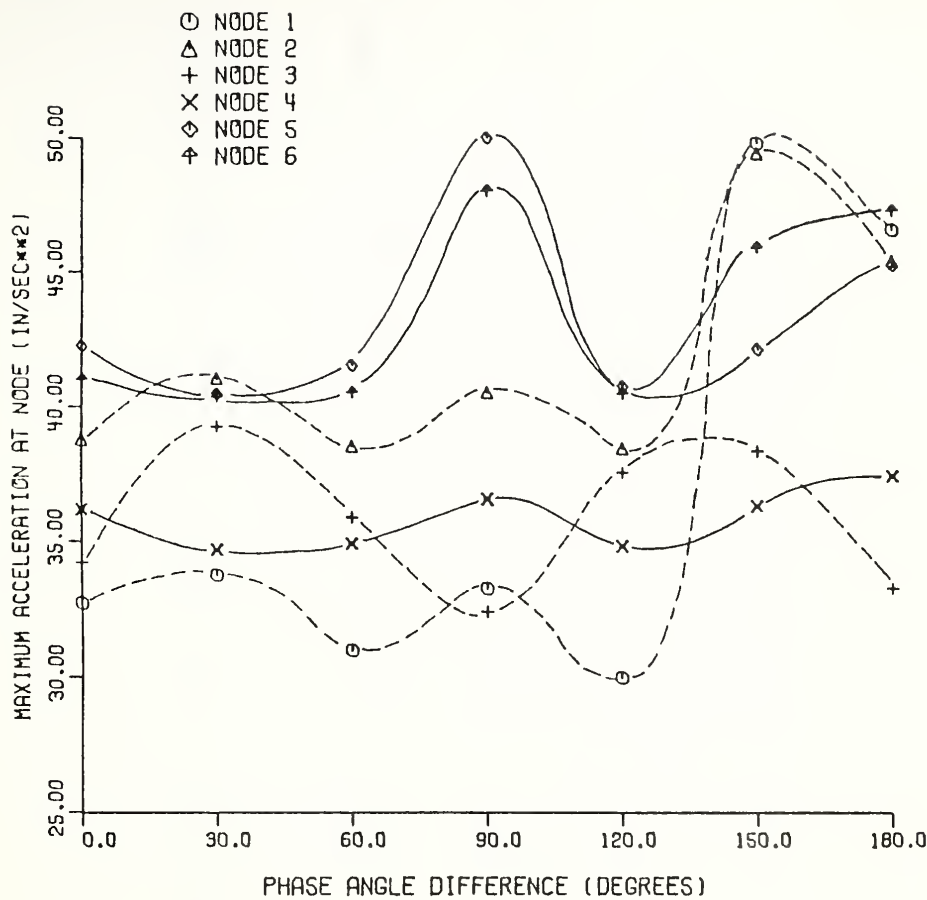
As previously explained in Article 4.5.2, the number of half sine waves and the roughness amplitudes are the two parameters assumed to represent the surface roughness of highway bridge. In Figure 5.12 are shown the profiles of bridge models having one, two and four half sine waves. The peak amplitudes of half sine waves are kept constant at 0.5 in. The bridge model is 60 ft. - 60 ft. span bridge. The vehicle model has HS 20-44 loading and is smoothly moving at a speed

Table 5.9 Maximum Accelerations of Two Span Continuous Bridges Subjected to 50% Initially Oscillating Vehicle with Varied Phase Angle Differences

60-60 Span Bridge 33WF118 Girder  $n = 4$   $c/c_r = .02$   
 Level Surface HS 20-44 Loading 60 m.p.h.  
 Oscillating Vehicle  $C_i = 0.50$   $\mu_i = 0$   $\theta_1 = \theta_2 = 0^\circ$   
 $\Delta\theta = \theta_2 - \theta_3$

Node	Maximum Acceleration (in/sec <sup>2</sup> )							
	$\Delta\theta = 0^\circ$	$x/L_b$	$\Delta\theta = 30^\circ$	$x/L_b$	$\Delta\theta = 60^\circ$	$x/L_b$	$\Delta\theta = 90^\circ$	$x/L_b$
1	32.72	1.29	-33.74	0.54	30.97	1.29	33.24	0.62
2	38.79	1.30	-41.03	0.52	38.50	1.30	40.50	1.27
3	-34.21	0.52	-39.26	0.52	-35.87	0.52	-32.39	1.19
4	36.18	0.51	-34.67	0.40	-34.88	0.40	-36.54	0.40
5	42.25	0.50	-40.44	0.41	41.51	0.50	49.94	0.50
6	41.00	0.49	-40.34	0.42	-40.50	0.42	48.00	0.49

Node	Maximum Acceleration (in/sec <sup>2</sup> )							
	$\Delta\theta = 120^\circ$	$x/L_b$	$\Delta\theta = 150^\circ$	$x/L_b$	$\Delta\theta = 180^\circ$	$x/L_b$		
1	29.98	1.29	-49.77	0.54	46.55	0.62		
2	38.42	1.30	49.40	0.61	45.39	0.63		
3	-37.52	0.52	38.32	0.60	33.25	0.38		
4	-34.79	0.40	-36.27	0.40	-37.40	0.40		
5	-40.71	0.41	-42.10	0.41	45.23	0.50		
6	-40.45	0.42	45.90	0.49	47.28	0.49		



60-60 SPAN BRIDGE 6 GIRDERS LEVEL SURFACE C/CR=0.02 N=4  
HS 20-44 50 PERCENT INITIAL OSCILLATION

Figure 5.11 Effect of Initial Phase Angle Difference on Acceleration

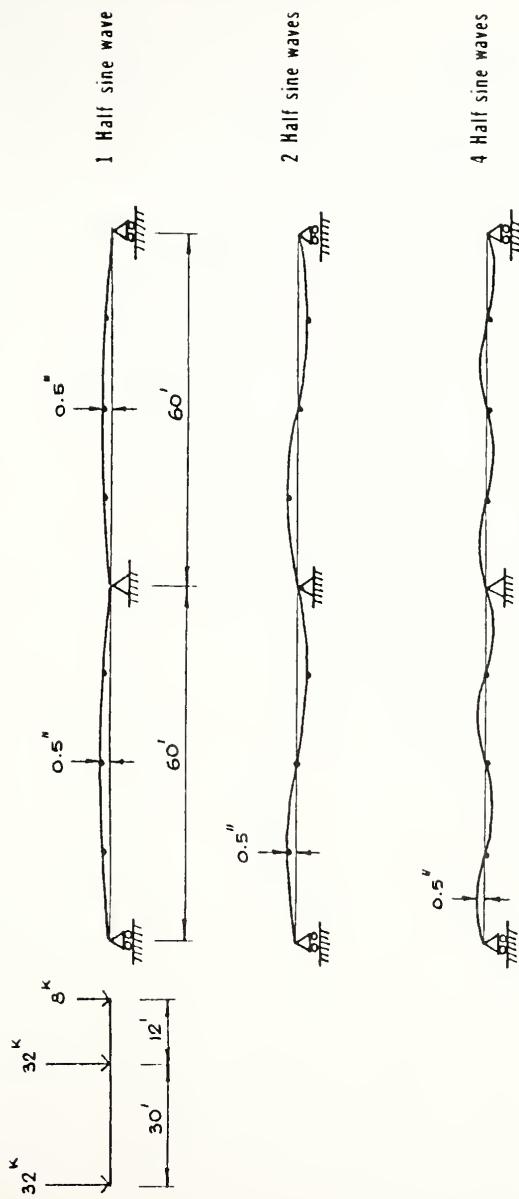


Figure 5.12 Two Span Bridges with Rough Surface

of 60 m.p.h. All remaining parameters are the same as before.

The maximum accelerations at the nodes are evaluated by using the number of half sine waves varied from 0 to 10. The results are listed in Table 5.10 and shown graphically in Figure 5.13. The results are similar to those of the three span bridge in such a way that the accelerations are maximum for the value of 4 half sine waves. It can be explained in Figure 5.14-1 and 5.14-2 which shows the histories of accelerations at mid right span and of interacting forces of the second axle respectively. In each figure, the results obtained by using the level surface condition and four half sine waves are compared.

It can be seen that the interacting force of the vehicle is influenced by the surface roughness. Its magnitude and period of acceleration have been changed. The period of oscillation of the interacting force for the value of four half sine waves is coincident with the fundamental natural period of bridge. Therefore, resonance between the bridge and the vehicle occurs. The magnitudes of accelerations are much larger than the suggested value of  $100 \text{ in/sec}^2$  and this result can cause the unpleasant condition to the bridge users.

Table 5.11 and Figure 5.15 show the comparison of the effect of varied amplitude of roughness on acceleration

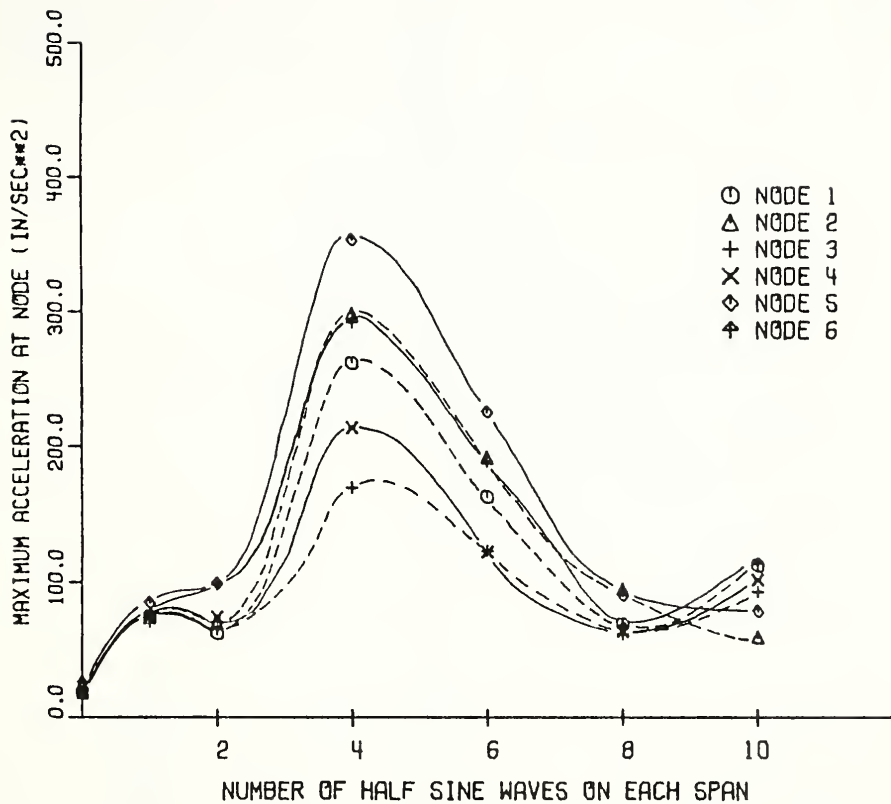
Table 5.10 Maximum Accelerations of Two Span Continuous Bridges Due to Different Numbers of Half Sine Waves

60-60 Span Bridge 33WF118 Girders  $n = 4$   $c/c_r = .02$   
 HS 20-44 Loading 60 m.p.h. Smooth Vehicle  
 Amplitude of Roughness = 0.5 inch

Node	Maximum Acceleration (in/sec <sup>2</sup> )							
	NS* = 0	x/L <sub>b</sub>	NS = 1	x/L <sub>b</sub>	NS = 2	x/L <sub>b</sub>	NS = 4	x/L <sub>b</sub>
1	-18.20	0.71	74.93	1.29	-62.47	1.12	261.57	1.30
2	24.68	0.38	74.41	1.30	-70.74	0.86	-298.01	0.98
3	17.87	0.38	70.50	1.31	-65.16	1.10	169.64	1.05
4	17.86	0.51	73.51	1.18	-74.12	0.97	-213.59	0.86
5	25.86	1.16	85.16	1.18	-99.27	0.98	353.05	1.17
6	-21.37	0.34	73.95	1.16	-98.47	0.99	291.74	1.17

Node	Maximum Acceleration (in/sec <sup>2</sup> )					
	NS = 6	x/L <sub>b</sub>	NS = 8	x/L <sub>b</sub>	NS = 10	x/L <sub>b</sub>
1	162.59	1.26	69.01	0.37	112.10	0.69
2	191.39	1.25	-94.69	0.49	-59.02	0.47
3	-122.79	0.51	-61.43	0.48	-92.72	0.52
4	122.23	1.24	63.38	1.19	101.45	1.05
5	-224.94	1.31	90.25	1.03	78.38	1.03
6	-188.14	1.32	66.15	1.02	113.47	1.02

\* NS = Number of Half Sine Waves



60-60 SPAN BRIDGE    6 GIRDERS    C/CR=0.02    N=4  
 HS 20-44    SMOOTH VEHICLE    60 MPH    ROUGH SURFACE

Figure 5.13    Effect of Surface Roughness on Acceleration

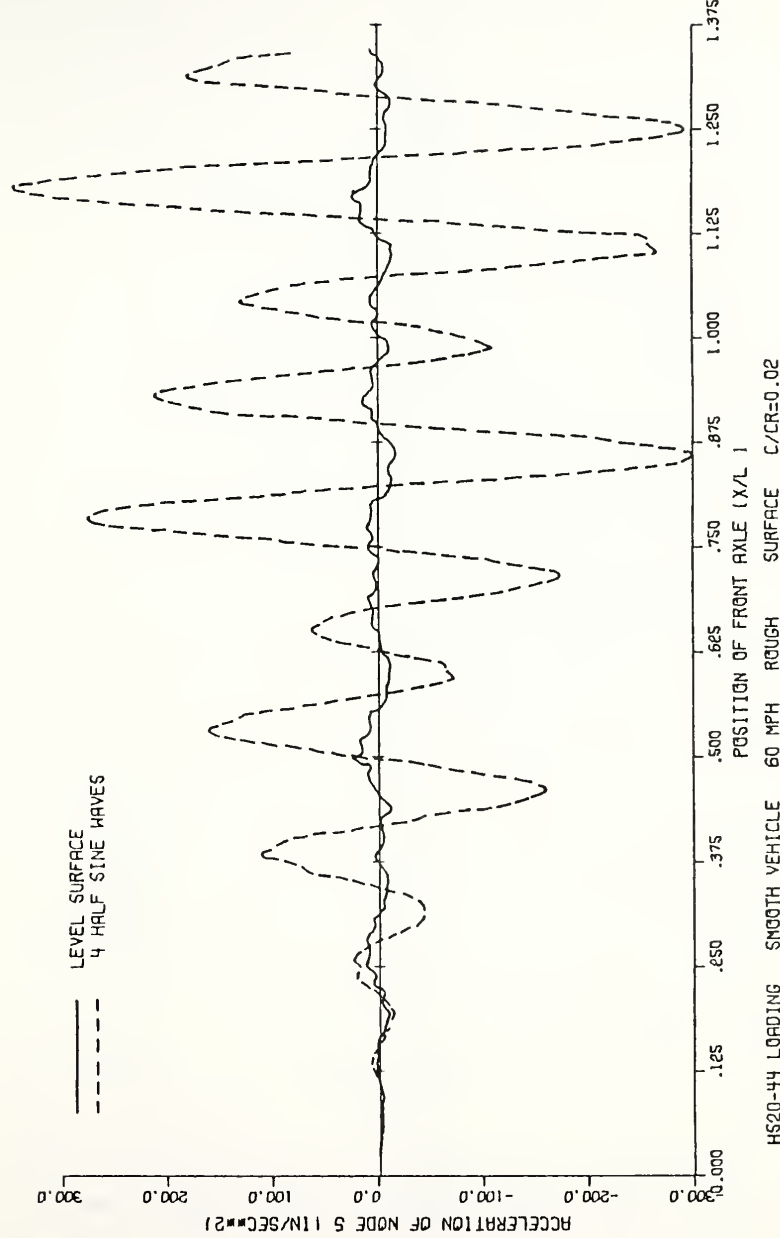


Figure 5.14-1 History Curves for Acceleration is Affected by Surface Roughness

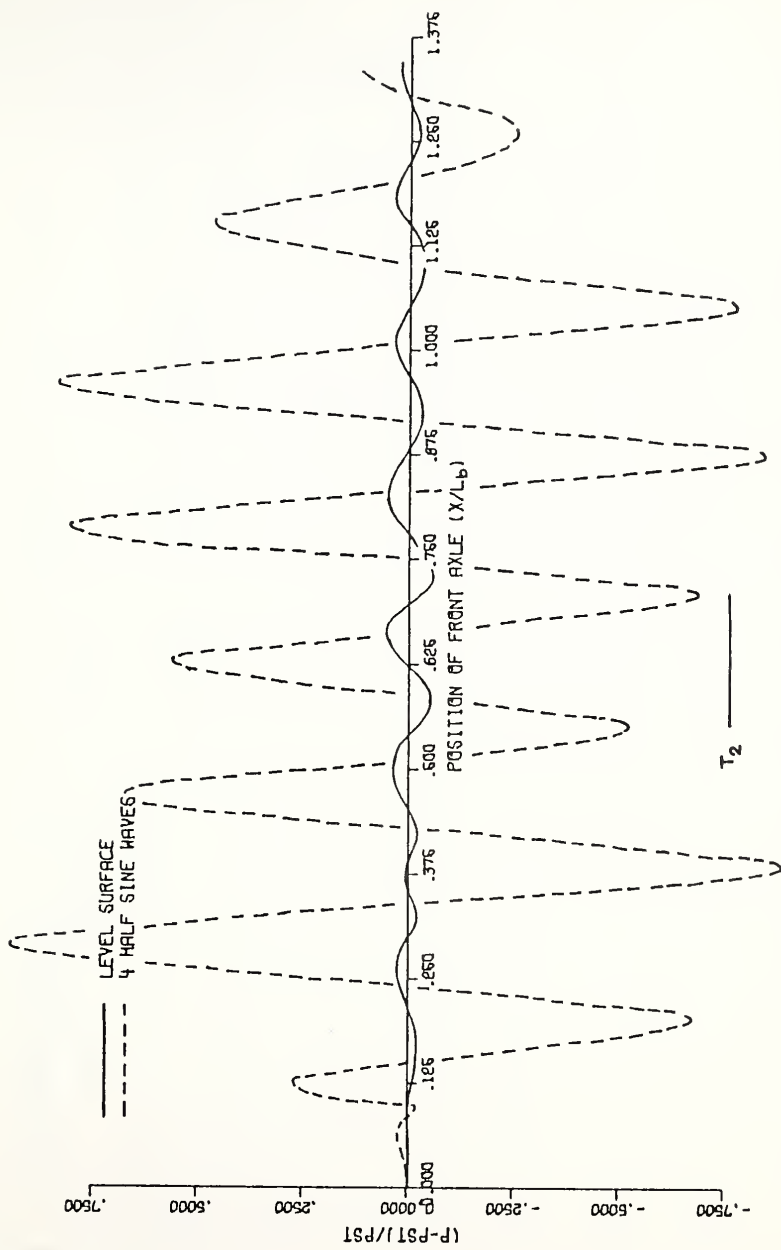


Figure 5.14-2 History Curves for Interacting Force Due to Surface Roughness

Table 5.11 Maximum Accelerations of Two Span Continuous Bridges Due to Different Amplitudes of Surface Roughness

60-60 Span Bridge      33WF118      n = 4      c/c<sub>r</sub> = .02      Roughness Surface  
 HS 20-44 Loading      60 m.p.h.      Smooth Vehicle

Case A) Number of Half Sine Waves = 2

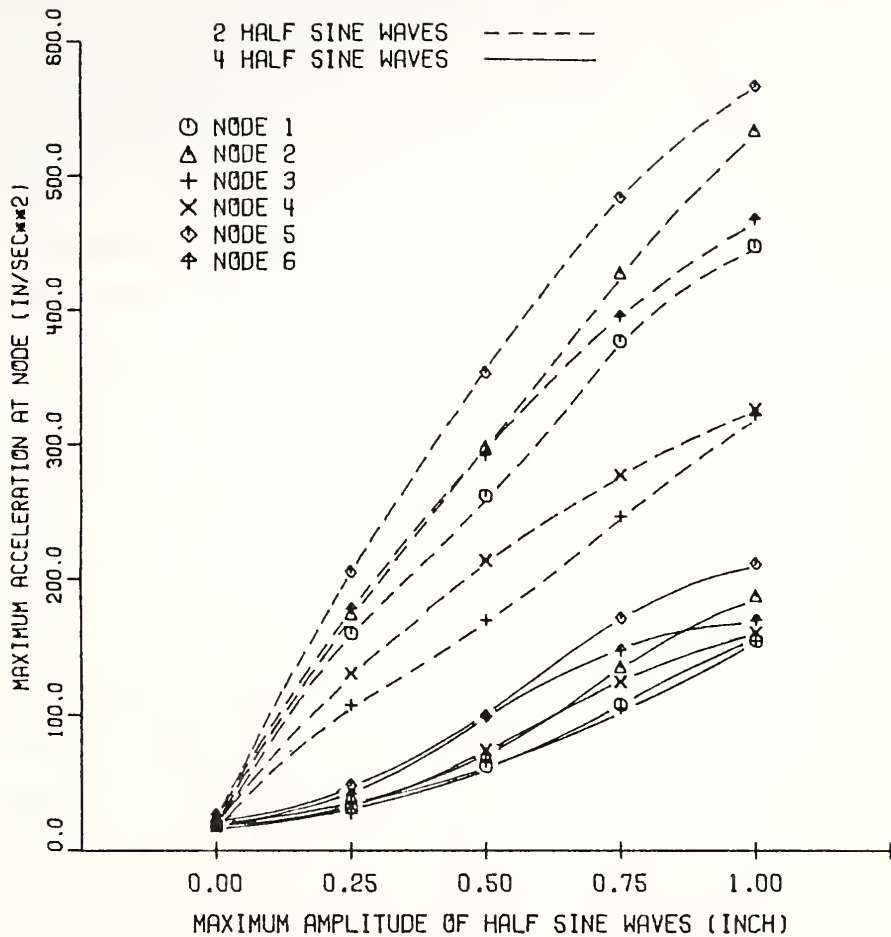
Node	Maximum Acceleration (in/sec <sup>2</sup> )					
	A* = 0.0	x/L <sub>b</sub>	A = 0.25	x/L <sub>b</sub>	A = 0.50	x/L <sub>b</sub>
1	-18.20	0.71	31.75	0.52	-62.47	1.12
2	24.68	0.38	-40.22	1.34	-70.74	0.86
3	17.87	0.38	26.99	1.26	-65.16	1.10
4	17.86	0.51	32.99	1.13	-74.12	0.97
5	25.86	1.16	48.10	1.14	-99.27	0.98
6	-21.37	0.84	-41.09	0.96	-98.47	0.99

\* A = Amplitude of Roughness in Inch

Table 5.11, cont.

Case B) Number of Half Sine Waves = 4

Node	Maximum Acceleration (in/sec <sup>2</sup> )					
	A = 0.0	x/L <sub>b</sub>	A = 0.25	x/L <sub>b</sub>	A = 0.50	x/L <sub>b</sub>
1	-18.20	0.71	-159.85	0.98	261.57	1.30
2	24.68	0.38	174.69	1.29	-298.01	0.98
3	17.87	0.38	107.27	0.65	169.64	1.05
4	17.86	0.51	-130.59	0.86	-213.59	0.86
5	25.86	1.16	205.26	1.17	353.05	1.17
6	-21.37	0.84	177.91	1.17	291.74	1.17
					395.21	1.18
					467.37	1.18



60-60 SPAN BRIDGE    6 GIRDERS    C/CR=0.02    N=4  
HS 20-44    SMOOTH VEHICLE    60 MPH    ROUGH SURFACE

Figure 5.15 Effect of Amplitude of Roughness on Acceleration

for two different cases of number of half sine waves. In case A, two half sine waves are selected, which slightly affects the acceleration of bridge, while in case B, the four half sine waves are used, which has the most effect. In both cases, the nodal accelerations are obtained by using the amplitude of roughness in the range from 0.0 to 1.0 in. It can be seen from the results that the maximum accelerations increase for the larger value of roughness amplitude. The amount of increase in magnitudes of acceleration for four half sine waves is larger than that of two half sine waves. It may be concluded that the amplitude of roughness affects the acceleration only if the number of half sine waves does.

One can see that these results for two span bridge are similar to those of simple span and three span bridges. The only difference among the three is the magnitude. The magnitude of acceleration is largest for simple span bridge and least for three span bridge. It is also seen that the effect of surface roughness seems to be the most important variable in terms of bridge accelerations.

CHAPTER VI  
SUMMARY AND CONCLUSIONS

6.1 Summary

The effects of the major parameters on the accelerations of highway bridges have been investigated and compared to the acceleration criteria for human response. Three different types of highway bridges were investigated: simple span, two span continuous and three span continuous bridges. Major parameters selected include the parameters related to the bridge, to the vehicle and the initial conditions of bridge and vehicle. The numerical data presented are derived from a theory in which the bridge is idealized as a plate continuous over flexible beams for simple span bridges and as a continuous beam with concentrated point masses for multi-span bridges. The vehicle has been represented as a sprung single load consisting of two wheels for the simple span bridge model and as a sprung load unit having one, two or three axles with a suspension system for multi-span bridges.

Most of the bridge parameters used were obtained from the information of Standard B.P.R. bridges<sup>(41)</sup> while the values of vehicle parameters came from manufacturers' data and test reports.<sup>(2) (22) (29)</sup> Because of the very

large number of variables involved and the considerable computer time required for a solution, it was impractical to obtain solutions for all possible combinations of the variables. For the above reason, one parameter was varied at a time to investigate its effect. The results of the investigation are shown in the form of history curves of the response, tables and graphs.

The principal results of the study of simple span bridge are summarized as follows:

a. Standard B.P.R. bridges with different span lengths were investigated and the maximum accelerations of each beam was obtained. The results show that the acceleration of the bridge decreases for longer span lengths and the accelerations of the exterior beams tend to be larger than those of interior beams.

b. For two different cases of the transverse position of load on the bridge, over the edge beam and over the center beam, the width variations of the bridge model do not affect the accelerations appreciably.

c. The increased flexibility of beams does not have much effect on the accelerations. The results show that the maximum acceleration increases approximately by 20 percent when the moment of inertia of beam is reduced nearly 40 percent.

d. The variations of the transverse position of load have an effect on the acceleration distribution among the beams. Generally, the acceleration of an edge beam is greater than that of an interior beam.

e. The bridge acceleration obtained by using a single wheel load is approximately 10 percent greater than that by using two wheels, regardless of the transverse position of load on the bridge.

f. By using the combination of two variables, the flexibility of beam and transverse position of a single load, it was confirmed that the increased flexibility of girder did not have much effect on accelerations as long as the moment of inertia of the beam section was not reduced more than 35 percent of the standard size.

g. The speed of vehicle affected the acceleration of the bridge. The accelerations were greater for the higher speeds.

h. The surface roughness of the bridge was idealized as a series of continuous half sine waves along the span length with equal amplitude for each wave. The accelerations of the bridge as affected by the variation of the number of half sine waves and also the amplitudes of roughness were studied. Generally, the acceleration of the bridge with a rough surface was greater than that of the bridge with a level surface condition. It was shown that the effect of the number of half sine waves caused the bridge

to vibrate severely if the period of the interacting force was influenced by the roughness was equal to one of the natural periods of bridge. The results also showed that the amplitude of roughness had an effect on acceleration only if the number of half sine waves did. Finally, the acceleration increased for larger roughness amplitude.

i. By comparing the amplitudes of acceleration obtained in this study to the suggested value of 100 in/sec<sup>2</sup> as the criteria for pedestrian discomfort. It was shown that the maximum accelerations of the simple span bridges were generally larger than the suggested value.

For the study of three span and two span continuous highway bridges, the following is a brief summary of the principal results:

a. Throughout the study, the spans were kept in the ratios of 4:5:4 for three span bridges and equal spans for two span bridges. Both bridge types had a damping factor of 0.02 and three concentrated masses on each span. The results showed that the accelerations increased for shorter span lengths. Additionally, the accelerations at the middle of any span were more important and had greater amplitude than the accelerations at other points of that span.

b. The increased girder flexibility, the frequency ratio and the span ratio did not materially affect the bridge accelerations.

c. Generally, the bridge accelerations were greater for the heavier vehicles. For the two vehicles with the same total load, the one which had fewer axles caused greater accelerations. The axle spacing of trailer for three axle vehicle did not have much effect on accelerations although the acceleration was greatest for the values of axle spacing ratio ranging between 0.37 to 0.43.

d. The vehicle speed did have an effect on accelerations, with higher speeds, causing greater bridge accelerations.

e. The effect of initial vehicle oscillations due to the bridge surface irregularities or the sharp discontinuity at the approach pavement was investigated. The initial oscillations included the amplitude of initial force variation, the phase angle difference between the axles and the initial value of the frictional force.

Generally, the bridge accelerations when subjected to the initially oscillating vehicle were about 1.5 times larger than the accelerations of the bridge when subjected to the smooth vehicle. The higher the amplitude of irregularities at the approach, the greater was the acceleration. The initial phase angle difference and the initial

frictional force did not have much effect on the acceleration.

f. The surface roughness of bridge was idealized as a series of continuous half sine waves in order to compare the results to those obtained for simple span bridges. Each span was considered to have an equal number of half sine waves. The accelerations of the bridge with a rough surface were greater than those of the bridge with a level surface condition. The bridge can severely vibrate when the period of the interacting force influenced by the roughness is equal to one of the natural periods of vibration of the bridge. Finally, the amplitude of roughness had an effect on acceleration only if the number of half sine waves did and the acceleration increased for larger roughness amplitude.

g. The magnitudes of accelerations as affected by bridge and vehicle parameters for a level surface condition were less than the suggested value of 100 in/sec<sup>2</sup>. The only parameter having an effect approaching the criteria for human response for multi-span highway bridges was the bridge surface roughness.

## 6.2 Conclusions

For simple span bridges, the amplitudes of accelerations which psychologically disturb the pedestrian were predominately affected by the span length of the bridge,

the weight and speed of the vehicle, and the surface roughness. The parameters that provided the minor effects were the girder flexibilities and the transverse position of load. For two and three span continuous bridges, the magnitudes of accelerations were larger than the recommended limit of comfort only when the surface roughness of the bridge was taken into account. High strength steel girders could therefore be used for highway bridges since the effect on the bridge accelerations was relatively insignificant.

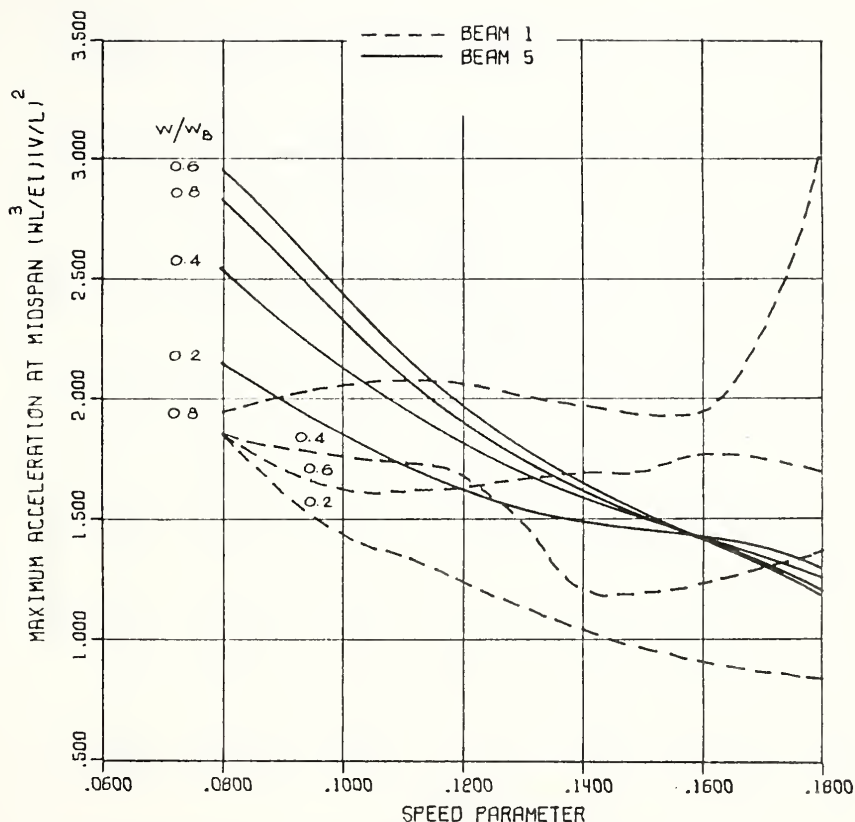
From the information presented in this study, a basis for design regulating the satisfactory vibration characteristics for human comfort can possibly be established. The design procedure would appear in the form of estimating the values of maximum accelerations produced under the most unfavorable but likely combinations of parameters involved. The major parameters such as the speed of vehicle, the span length and the natural frequency of vibration of bridge were combined in the nondimensional form of speed parameter  $\alpha$ . This parameter was expressed in the form:

$$\alpha = \frac{vT_b}{2L}$$

where  $v$  is the speed of vehicle,  $T_b$  is the fundamental period of vibration of bridge and  $L$  was either the length of the simple span bridge, or the length of center span of

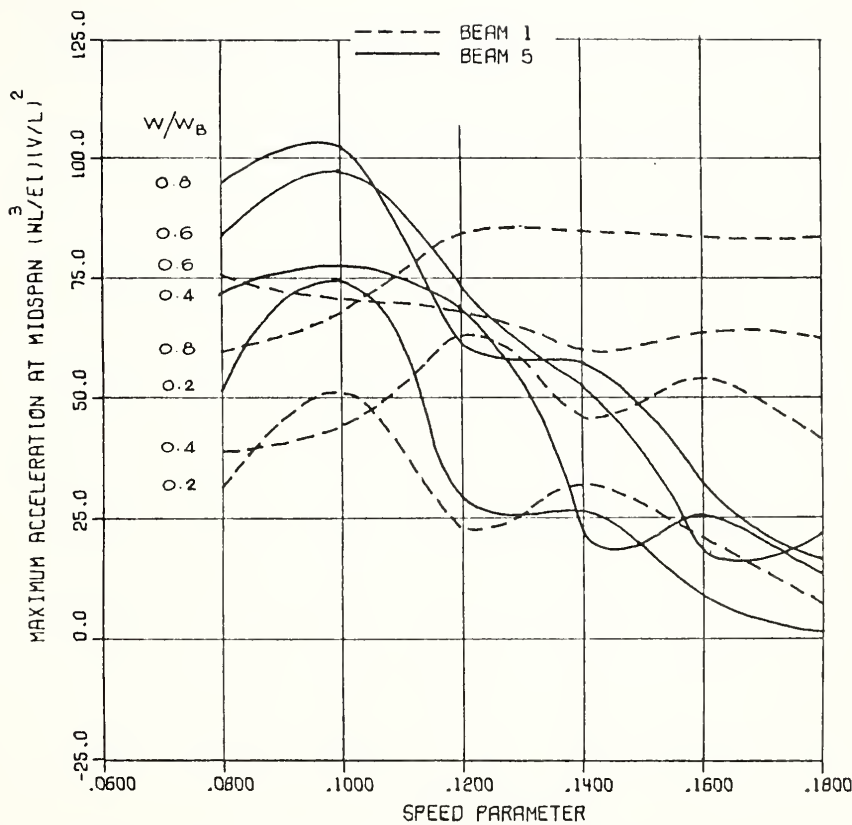
the three span continuous bridge, or the length of either span of the two span continuous bridge. Some examples of the prediction of acceleration of highway bridges as a function of speed parameter and weight ratio are shown in Figures 6.1 and 6.2. The weight ratio is the ratio of the weight of vehicle to the weight of bridge.

Further study is recommended to investigate the effect of surface roughness which was the most important parameter in producing an adverse effect on human response. The measured profiles of various bridges in the field are needed for better correlation in this regard. A basis for design to control the vibration characteristics within the comfort level should also be further studied and proposed for bridge design specifications. Other types of highway bridges should be investigated, such as the cantilever-type, since many test reports<sup>(14) (18) (20)</sup> show that this type produces the most adverse effects.



5 GIRDER BRIDGE SIDE RATIO=0.8 FREQUENCY RATIO=1.0  
TWO WHEELS OVER BEAM 1 LEVEL SURFACE

Figure 6.1 Acceleration of Simple Span Bridge with Level Surface



5 GIRDER BRIDGE SIDE RATIO=0.8 FREQUENCY RATIO=1.0  
TWO WHEELS OVER BEAM 1 ROUGH SURFACE

Figure 6.2 Acceleration of Simple Span Bridge with Rough Surface

## BIBLIOGRAPHY

## BIBLIOGRAPHY

1. Standard Specification for Highway Bridges, American Association of State Highway Officials, 10<sup>th</sup> Edition, Washington, D.C., 1969.
2. "Tractor-Trailer Ride", Technical Board of Society of Automotive Engineers, Inc., 485 Lexington Ave., New York, N.Y., May, 1956.
3. ASCE Committee on Deflection Limitations of Bridges, "Deflection Limitations of Bridges", Journal of the Structural Division, ASCE, Vol. 84, No. ST3, May, 1958.
4. Veletsos, A. S. and Huang, T., "Analysis of Dynamic Response of Highway Bridges", Journal of the Engineering Mechanics Division, ASCE, Vol. 96, No. EM5, October, 1970.
5. Wright, R. N. and Walker, W. H., "Vibration and Deflection of Steel Bridges", Engineering Journal, American Institute of Steel Construction, Vol. 9, No. 1, January, 1972.
6. Wright, D. T. and Green, R., "Human Sensitivity to Vibration", Report No. 7, Department of Civil Engineering, Queen's University, Kingston, Ontario, February, 1959.
7. Wise, J. A., "Dynamics of Highway Bridges", Highway Research Board, Proceedings, 1953.
8. Biggs, J. M., "Vibration Measurements on Simple-Span Bridges", Highway Research Board, Bulletin 124, 1956.
9. Scheffey, C. F., "Dynamic Load Analysis and Design of Highway Bridges", Highway Research Board, Bulletin 124, 1956.
10. Edgerton, R. C. and Beecroft, G. W., "Dynamic Studies of Two Continuous Plate-Girder Bridges", Highway Research Board, Bulletin 124, 1956.
11. Hayes, J. M. and Sbarounis, J. A., "Vibration Study of Three Span Continuous I-Beam Bridge", Highway Research Board, Bulletin 124, 1956.

12. Foster, G. M. and Ochler, L. T., "Vibration and Deflection of Rolled-Beam and Plate-Girder Bridges", Highway Research Board, Bulletin 124, 1956.
13. Biggs, J. M., "The Vibration of Simple Span Highway Bridges", Journal of the Structural Division, ASCE, Vol. 83, March, 1957.
14. Ochler, L. T., "Vibration Susceptibilities of Various Highway Bridge Types", Journal of the Structural Division, ASCE, Paper 1318, July, 1957.
15. Looney, C. T. G., "High Speed Computer Applied to Bridge Impact", Journal of the Structural Division, ASCE, Vol. 84, September, 1958.
16. Hulsbos, C. L. and Linger, D. A., "Dynamic Tests of a Three-Span Continuous I-Beam Highway Bridge", Highway Research Board, Bulletin 279, 1960.
17. Fleming, J. F. and Romualdi, J. T., "Dynamic Response of Highway Bridges", Journal of the Structural Division, ASCE, Vol. 87, October, 1961.
18. Nebraska Department of Roads Bridge Design Section, "Dynamic Test of Two Cantilever Type Deck Steel Girder Bridges", August, 1961.
19. Linger, D. A. and Hulsbos, C. L., "Dynamic Tests of a Three-Span Continuous I-Beam Highway Bridge", Highway Research Board, Bulletin 339, 1962.
20. Wen, R. K. and Toridis, T., "Dynamic Behavior of Cantilever Bridges", Journal of the Engineering Mechanics Division, ASCE, Vol. 88, August, 1962.
21. Wen, R. K. and Veletsos, A. S., "Dynamic Behavior of Simple-Span Highway Bridges", Highway Research Board, Bulletin 315, 1962.
22. "The AASHO Road Test, Report 4 - Bridge Research", Highway Research Board Special Report, No. 61D, 1962.
23. Rowe, R. W., "Vibration in Bridges", Concrete Bridge Design, Chapter 13, London, 1962.
24. Mason, A. F. and Duncan, M. A. G., "Composite Steel and Concrete Bridge Construction in Southern Rhodesia", Institution of Civil Engineers, Proceedings, London, April, 1962.

25. Fenves, S. J., Veletsos, A. S. and Siess, C. P., "Dynamic Studies of Bridges on the AASHO Road Test", Highway Research Board Special Report 71, National Academy of Sciences, Washington, D.C., 1962.
26. Fenves, S. J., Veletsos, A. S. and Siess, C. P., "Dynamic Studies of the AASHO Road Test Bridges", Highway Research Board Special Report 73, National Academy of Sciences, Washington, D.C., 1962.
27. Linger, D. A. and Hulbos, C. L., "Dynamic Load Distribution in Continuous I-Beam Highway Bridges", Highway Research Record, No. 34, 1963.
28. Oran, C. and Veletsos, A. S., "Analysis of Static and Dynamic Response of Simple-Span, Multigirder Highway Bridges", Civil Engineering Studies, Structural Research Series No. 221, Univ. of Illinois, Urbana, Illinois, July, 1961.
29. Huang, T., "Dynamic Response of Three Span Continuous Highway Bridges", Ph.D. Thesis, Univ. of Illinois, Urbana, Illinois, 1960.
30. Nieto-Ramirez, J. A. and Veletsos, A. S., "Response of Three-Span Continuous Highway Bridges to Moving Vehicles", Civil Engineering Studies, Structural Research Series No. 276, Uni. of Illinois, Urbana, Illinois, January, 1964.
31. Eberhardt, A. C., "A Finite Element Approach to the Dynamic Analysis of Continuous Highway Bridges", Ph.D. Thesis, Univ. of Illinois, Urbana, Illinois, 1972.
32. Wright, D. T. and Green, R., "Highway Bridge Vibrations, Part II", Ontario JHRP, Report No. 5, Ontario, Canada, May, 1964.
33. Lee, J. A. N., Brown, R., Windover, L., "Highway Bridge Vibrations III, Cantilever-Type Structures", Ontario JHRP, Report No. 39, Ontario, Canada, January, 1966.
34. Csagoly, P. F., Campbell, T. I. and Agarwell, A. C., "Bridge Vibration Study", The Engineering Research Branch of the Ministry of Transportation and Commerce, Ontario, September, 1972.
35. Newmark, N. M., "A Method of Computation of Structural Dynamics", Journal of the Engineering Mechanics Division, ASCE, Vol. 85, July, 1959.

36. Veletsos, A. S. and Newmark, N. M., "Natural Frequencies of Continuous Flexural Members", ASCE, Proceedings, July, 1955.
37. Lin, T. Y., "A Direct Method of Moment Distribution", ASCE Transactions, Vol. 102, 1937.
38. Lenzen, K. H., "Vibration of Steel Joist-Concrete Slab Floors", Engineering Journal, AISC, July, 1966.
39. Janeway, R. N., "Vehicle Vibration Limits to Fit the Passenger", SAE National Passenger Car and Production Meeting, Detroit, 1948.
40. "Highway Bridge Field Tests in the United States, 1948-70", A Journal of Highway Research, Public Roads, Vol. 36, No. 12, February, 1972.
41. "Standard Plans for Highway Bridge Superstructures", U.S. Department of Commerce, Bureau of Public Roads, 1968.
42. AISC, "Manual of Steel Construction", 7<sup>th</sup> Edition, New York, 1970.
43. Winter, G., Urquhart, L. C., O'Rourke, C. E. and Nilson, A. H., "Design of Concrete Structures", 7<sup>th</sup> Edition, 1964.



COVER DESIGN BY ALDO GIORGINI